From Neurons to Newtons

Neurocomputational Issues of Voluntary Movement

Nielsen, Bjørn Gilbert

Publication date:
2001

Document Version
Publisher's PDF, also known as Version of record

From Neurons to Newtons

Neurocomputational Issues of Voluntary Movement

Bjørn Gilbert Nielsen

A dissertation submitted in partial fulfillment
of the requirements for the degree of

Doctor of Philosophy

at the Technical University of Denmark,
Department of Physics
December 2001

Supervisor of Dissertation:
Prof. Rodney M.J. Cotterill

Contents

List of Figures

List of Tables

Symbols and Abbreviations

Typesetting symbols

- Glossary entries are indicated with a superscripted dagger (†)
- Literature references are indicated with superscripted numbers.
- Footnotes are indicated with superscripted letters.
- Some animations and high resolution graphics have been included in a CD-ROM that is included with official copies of this work (in the cover envelope). Such items are marked with a superscripted o-dot (⊙).

Anatomical Abbreviations

DELA : DELtoideus, Acromial origin

DELS : DELtoideus, Scapular origin

DELC : DELtoideus, Clavicular origin

PMJC : Pectoralis MaJor, Clavicular origin

TMAJ : Teres MAJor

TRIO : TRIceps lOngum

TRIM : TRIceps Mediale

TRIA : TRIceps lAterale

BILH : BIceps longum (Long Head)

BISH : BIceps breve (Short Head)

BRAD : BRAchioraDialis

BRAC : BRAChialis

PROT : PROnator Teres

ECUL : Extensor Carpi ULnaris

ECRD : Extensor Carpi RaDialis

FCUL : Flexor Carpi ULnaris

FCRD : Flexor Carpi RaDialis

Neurophysiology Abbreviations

AMPA : α-amino-3-hydroxyl-5-methyl-4-isoxazole-propionate

NMDA : N-methyl-D-Aspartate

GABA : γ-aminobutyric acid

ACh : Acetylcholine

LTP : Long-Term Potentiation

LTD : Long-Term Depression

STDP : Spike-Timing Dependent Plasticity

PSP : Post-Synaptic Potential

EPSP : Excitatory Post-Synaptic Potential

IPSP : Inhibitory Post-Synaptic Potential

EPP : End-Plate Potential

Glu : Glutamate

Gly : Glycine

Abstract

This thesis describes the elements that form part of a comprehensive neuromuscular simulation system centered around control of the human arm. The resulting computational system necessarily covers many fields of study, and spans several orders of magnitude: From the molecular level where muscle proteins generate forces, to the macroscopic levels where overt arm movements are voluntarily controlled within an unpredictable environment by legions of neurons firing in orderly fashion. An extensive computer simulation system has been developed for this thesis, which *at present* contains a neural network scripting language for specifying arbitrary neural architectures, definition files for detailed spinal networks, various biologically realistic models of neurons, and dynamic synapses. Also included are structurally accurate models of intrafusal and extrafusal muscle fibers and a general body-centered mechanical physics simulation system in which a realistically scaled human arm with accurate muscle origin-insertion points was modelled.

At the molecular level, a novel hypothesis regarding the origin of muscle force is proposed. It is concluded that within the framework laid out by the sliding filament theory, the conformational entropy of the individual myosin molecules has a central role to play in the total force production of the sarcomere. All in all, much emphasis has been given in this thesis to develop a highly detailed model of human muscle. The final muscle fiber model accounts for a variety of phenomena, ranging from the force-velocity and force-length relationships, to tetanic fusion, "catch-like" effects and the distinctions between fast and slow muscle fiber types. Furthermore the model incorporates sufficient neuromuscular information as to permit orderly recruitment of motor units, exponential motor-unit size distributions and gradual force increases.

Also included in the computational model was a mathematical model of an important class of sensory receptors known as muscle spindles which report to the central nervous system on the length and contraction velocity of the innervated muscles. From the simulations it was concluded that the dynamic range of the modelled spindles, as they responded to fusimotor input, was such that it was possible to maintain constant activity levels in the primary and secondary afferents. Further theoretical analysis of this spindle model revealed that an explicit function may be derived which expresses the force that the spindle contractile elements must produce to exactly counter spindle unloading during muscle shortening. This information was used to calculate the corresponding "optimal" γ-motoneuronal activity level. For some simple arm movement tasks, this permits the derivation of a signature activation pattern which in principle may be used to identify such cells in vivo by monitoring spinal activity during tasks that are similar.

Finally, at the level of neural systems, a novel role is proposed for the corticomotoneuronal (CM) cells, which form an important class of motor cortical cells, and which have been shown to have strong correlations with movement. Based on extensive computer simulations it is suggested that these cells might be partially responsible for activating the fusimotor systems according to preprogrammed voluntary movements. The upshot of this is, that CM cells might be responsible for cancelling the reafference that inevitably accompanies any voluntary movements, thus improving the signal-to-noise ratio of spindle afference. To do this, CM cells would have to partake in a complex attractor cortical network where horizontal connectivity allows the system to produce stable and spatiotemporally extended patterns of activity that correspond to the sequential activation of muscles during well-learnt voluntary movements, and to the associated reafference cancelling signal.

Dansk Resumé

Titel: Fra Neuroner til Newtons – Neurocomputationelle elementer af voluntær bevægelse.

Denne afhandling beskriver de elementer som indgår i et omfattende neuromuskulær simulerings-system hvis primære fokus er kontrol af den humane arm. Det resulterende computationelle system spænder nødvendigvis over flere studieområder og størrelsesordener: Fra det molekylære niveau, hvori muskel proteiner genererer krafter og til de makroskopiske niveauer hvor hele armbevægelser er underlagt viljen, båret af tusindvis af neuroner som aktiveres i bestemte mønstre. Et omfattende computerbaseret simulerings-system er blevet udviklet, og indeholder p.t. et fuldt skalérbart "script" baseret neuralt netværk til hvilken definitions filer er blevet udarbejdet med henblik på simulering af rygmarvens neurale netværk. Derudover indgår også i systemet mulighed for at implementere flere forskellige slags neuron modeller, samt dynamiske synapse modeller. Ydermere indgår strukturelle modeller af intrafusale og ekstrafusale muskel fibre samt en generel mekanisk-fysisk simulerings-system, med hvilken en model over den humane arm blev implementeret.

På det molekylære plan, fremsættes en ny hypotese vedrørende kraft produktion i musklerne. Det konkluderes at den komformationelle entropi spiller en afgørende rolle i dette henseende, indenfor de rammer som sættes af "sliding-filament" teorien. Der bliver i denne afhandling lagt stor vægt på at udvikle en så detaljeret model af den humane stribede muskulatur som muligt. Den resulterende model redegør for en lang række fænomener, rækkende fra kraft-hastigheds og kraft-længde relationerne, til tetanisk fusion, "catch-like" effekten og forskellene mellem hurtige og langsomme muskelfibre. Desuden indlemmes i modellen også tilstrækkelig neuromuskulær information til at kunne tillade rekruttering af muskelfibre efter størrelse, en eksponential fordeling af muskelfiber størrelser samt gradvise forøgelse af kraften.

Tillige inkluderes en matematisk model over muskelten-cellerne, en vigtig gruppe af sensoriske celler som rapporterer til centralnervesystemet om ændringer i muskel længde eller hastighed. Af simulationerne konkluderes det, at disse cellers dynamiske rækkevidde, under respons fra fusimotorisk input, kunne opretholde en situation hvori de primære og sekundære afferente fibres aktivitet bibeholdt deres aktiveringsniveau. Efterfølgende analyse af modellen viser, at det er muligt at finde et simpelt udtryk for den kraft med hvilken de intrafusale muskelfibre skal påvirke den centrale region af muskeltenen for at modstå deaktivering forårsaget af aflastning ved muskel sammentrækning. Denne information blev brugt til at udregne den "optimale" γ-motoneuronale aktiverings niveau. For visse simple armbevægelser, tillader dette en udledning af kendetegnende aktiverings mønstre, som i princippet skulle kunne bruges

til at identificere sådanne celler *in vivo*, ved at iagtage aktiviteten i rygmarvsneuronerne under adfærds-opgaver som ligner det modellerede.

Til slut fremlægges en hypotese omhandlende de corticomotoneuronale (CM) celler, som udgør en vigtig gruppe af neuroner i den motoriske del af hjernebarken, og som har vist sig at have stærke korrelationer til bevægelse. På baggrund af omfattende computersimuleringer foreslås det at disse celler kan være delvist ansvarlige for at aktivere det fusimotoriske system i henhold til præprogrammerede voluntære bevægelser. Udfaldet af dette er, at CM cellerne i teorien kunne være ansvarlige for at medvirke til en annulering af den reafferens som nødvendigvis opstår under bevægelse. Herved medvirkende til at forbedre støj-signal forholdet i den primære og sekundære afferens. For at dette kan ske, må CM cellerne være en del af en kompleks cortical attraktor netværk hvori horizontal konnektivitet formodentlig spiller en rolle i produktionen af stabile og spatiotemporalt udstrakte aktivitetsmønstre, svarende til den sekventielle aktivering af muskler under udførelsen af voluntære bevægelser og til det derved associerede reaferens annulerende signal.

Acknowledgements

First I wish to thank my supervisor, Prof. Rodney Cotterill for his unending support and enthusiasm for this project. It has certainly been many very inspiring years under his guidance.

Also, I would like to extend my thanks to the staff at the Department of Physics, who have worked very hard to keep things running smoothly at the institute (while we students were just having fun doing research...).

Thanks also to Salim Abdali at QUP for proofreading the first draft of this thesis, very helpful indeed. Also thanks to Masami Tatsuno at RIKEN for proofreading and commenting on chapter 7, and for the many hours of fruitful conversation we've spent together.

I also wish to thank the organizers of the "EU Advanced Course in Computational Neuroscience" for putting together a "dream-team" of researchers to teach Computational Neuroscience to a bunch of students from all over the world. This is certainly a praiseworthy initiative.

My most heartfelt thanks go to Elizabeth, my wife and muse. Your love has been my guiding light through many a dark hour. Thank you also for helping me design beautiful conference posters and for designing the cover of this thesis (which is so nice, it makes me want to buy this book...).

My warmest thanks go to my family, new and old, for all their love and support. It is to them that I dedicate this work.

Part of this research was supported by ITE ApS.

Chapter 1

General Introduction

Chapter Summary

This chapter is intended as a general overview of this thesis, emphasizing the primary research problems and goals that will be pursued, the suggested hypotheses and the methodology used. As a help to the reader, a chapter overview of the whole thesis is also provided.

Every moving organism owns some sophisticated machinery which can transform energy into precisely directed forces. In nature, many different strategies have arisen to this effect, and sometimes it seems as if the ability to move like no other being has been one of the major driving forces in the arms race of evolution. Almost all the forces that can be derived from classical physics are well represented in the strategies evolved for producing motive force. Identifying and describing these forces is very challenging indeed, and has resulted in the birth of *biomechanics*, a branch of science existing at the threshold between biology and mechanical engineering (see Alexander[5] for a comprehensive introduction to the topic of biomechanics).

In some cases the energy transformation is very direct and the resultant force vector is easy to predict given the current activity of the machinery. For example, when a squid contracts the muscles surrounding its water filled mantle cavity, energy originating from the breakdown of ATP (adenosine triphosphate) is transformed into hydrodynamic forces as muscle contraction reduces the volume of the mantle cavity, and the resulting increase in pressure causes the expulsion of water through a funnel tube (see e.g. Alexander[5]). The direction of the resultant thrust vector can easily be deduced from the position of the funnel and the geometry of the squid's body. Thus so far the causality between muscle activity and direction of motility seems straightforward, but that is only in appearance because the squid's actual direction of movement will depend on other forces too, such as those caused by the position and movement of its own tentacles and the drift caused by external water currents, etc.

As with the squid, the movement of organisms depends on the accurate positioning of structures pertaining to the organism proper through the control of the relevant internal forces. The purpose of such movement is to achieve some goal by means of correct application of forces to the external world. Thus, biological movement in reality depends on the appropriate handling and control of forces pertaining to at least three distinct domains: 1) The intrinsic forces related to the structures being moved (pseudopodia, flagella, tentacles, arms, trunk, etc.), 2) The reaction forces from the environment which are correlated with intrinsic force production, and 3) Extrinsic forces which are not correlated with the organism's motion. Distinguishing between these three sources of force is one of the essential functions that the central nervous system (CNS) must do before appropriate forces can be produced to place the limbs at goal specified positions. Essentially this means that all goal-oriented intrinsic forces must be computed from the sensory stimuli which arise as a consequence of the movement itself.

How does the system distinguish between the different force sources during movement? As will be argued in a later section, it seems that some degree of reafference cancellation is necessary for the system to do this distinction, and in this thesis such a role has been attributed to the γ-motoneuron in its modulation of the muscle spindle's sensitivity (see chapter 10).

Given the extreme complexity of the problems inherent in movement, it should come as no surprise that a large fraction of the brain is concerned with generating motion. However, the present work is aimed at identifying and understanding only some of the causal relations existing between neural activity in different regions of the CNS and biomechanical action from the (surely biased) perspective of computational systems-neuroscience. Particular emphasis will be given to the most basic motor control systems, especially the spinal cord and that part of its cortical input which originates in corticomotoneuronal cells.

1.1 Towards a Hypothesis

This is a thesis about computational methods applied to an integrative physiology of movement in such a way as to (hopefully) increase our understanding of a very complex multidisciplinary subject: vertebrate movement. As might be expected, the subject of movement has been studied with great success for many years and from many different directions (see chapter 2). But more often than not, these approaches span only one or perhaps two strata of the organizational levels of the system, and it is then assumed that the remaining strata above and below probably are organized so as to conform to the studied strata. In a highly competitive research environment, a strategy of extreme specialization of course leads to immediate results, but it also means that a whole field of study is left without strong integrative theories and laws like those discovered in physics. In the preface to his book "I of the vortex", Llinas has stated this preoccupation very eloquently[158]:

> Most neuroscientists feel that two orders of magnitude above and below one's central focus is "horizon enough" and that anyone attempting four orders above and below is reckless. However, there are some who attempt such a dangerous dynamic range. They probably

> know that the risk of failure is the price of synthesis, without which there are only fields of dismembered parts.

My aim with this work will of course be much less than to propose grand unifying theories of movement physiology; but I certainly do intend to take some steps in the direction which I believe will bring us closer, namely along the "reckless" path of multi-level functional integration. Therefore, rather than limiting this work to only one field of study, I have tried to integrate the computationally most accessible elements of various fields of study residing at very different levels, but all of which are deeply related to vertebrate movement, and all of which lie neatly on a path connecting the activity of the brain and spinal cord to the overt movement of complex organisms. Such an approach of course limits the breadth to which each level of the physiological hierarchy may be treated, but that is a small price to pay if the end result yields a continuous, unbroken and biologically realistic line from the activity of neurons to the production of newtons.

With this work I wish to argue in favour of a hypothesis, in which some special aspects of voluntary behaviour are directly controlled by the corticomotoneuronal (CM) cells in primary motor cortex. Through dynamic adaptation and self-organization via horizontal connections within the cortical mantle itself, CM cells create activation patterns which are necessary for the generation of physically well-balanced slow voluntary movements. Although simply stated, further elaborations on this idea require the development of a large number of results which may corroborate it. Such results I will attempt to obtain by creating an extensive computer simulation of the causal chain, starting from CM cells connecting monosynaptically to spinal motoneurons (MN) which connect to muscles which return positional and velocity feedback to the MNs, finally producing forces that pull a skeleton to new positions.

1.2 Methodology

There are still many technical difficulties involved in simultaneously measuring cortical, spinal and muscular activity in individual neurons and cells during various tasks; even identifying particular species of neurons is quite challenging, and sometimes impossible *in vivo* due to neuron size, density or interneuronal similarity. In addition to these technical difficulties, there are many ethical issues which must be satisfactorily solved prior to doing experiments on living creatures. In particular, it is not ethically acceptable to have long-term multi-electrode insertions in the brains of living humans solely for experimental purposes (at least not with current electrode technology which requires the skull to be opened). Brain and spinal electrode insertions during surgical procedures are performed routinely as part of the localization of dysfunctions, which opens a narrow window for direct experimentation on the human brain (one famous case being the identification of the sensorimotor homunculus by Penfield and Rasmussen[211]). However, the results of such experiments might be unpredictably affected by the dysfunctions that motivated the operation. Furthermore, the patient is in a highly vulnerable situation so the time window for experimentation is necessarily very narrow. These ethical and technical problems do somewhat limit the range of possibilities for studying the central nervous system in humans, and forces us to use only non-invasive techniques such as PET, fMRI,

SPECT and TMS, or to base our assumptions on results gained from a different species.

For this thesis computer simulation has been chosen as the primary method for studying the system, a method which, pitfalls and dangers notwithstanding, does indeed permit a full description at all levels of the system. If done with care, computer simulation may be used to test hypotheses and to identify the critical parameters of the system. And by following a "biology first" principle in the design of the simulation, where biological structures and functions are replicated as faithfully as possible, a meta-analysis of the functioning system becomes possible. This allows for the discovery of new properties which for technical reasons might not yet be directly measurable *in vivo*, and the postulation of novel hypothesis, both of which may subsequently be tested with real experiments[a].

For example, it has been suggested by Georgopoulus and co-workers [79,81] that the motor cortex controls movement with a population coding strategy. But how does such a code translate into movement in the spinal cord?, is the code perhaps really an epiphenomenon [233] related to the organization of the nervous system, rather than a control strategy *per se*?, and is the observed rotation of the population vector in certain experiments involving mental rotation [80] a consequence of processing within primary motor cortex (M1) itself, or is it a faithful reflection of the input to M1?. These are very hard questions to answer in a direct experimental setup as it would require simultaneously recording activity in the motor cortex, brainstem, spinal cord and muscles during specific tasks. It is not within the scope of this thesis to answer these particular questions arising from Georgeopoulus work. What *is* within the scope of this thesis is to determine how a limited group of neurons in the motor cortex (particularly the corticomotoneuronal cells) which have been shown to have specific task dependent activation patterns [67], may communicate with pools of neurons in the spinal cord to produce muscle synergies that yield stable, balanced and yet sufficient forces for a given movement of the human arm. To this end, an extensive computer simulation system has been developed for this thesis, which *at present* contains a neural network scripting language for specifying the neural architecture, various realistic models of neurons (based on the works of Hodgkin-Huxley [108], Morris and Lecar [195], and Wilson [274]), dynamic synapses [263,262], definition files for detailed spinal networks [31], structurally accurate models of muscle forces (force-velocity [107] and force-length [176] relationships in individual muscles, and origin–insertion points in skeleton at systems level [7,206]), and of the activation of spinal motor units [105,189,32], and finally it also consists of a completely general body-centered mechanical physics simulation system.

1.3 Main Contributions of this Thesis

Once in possession of a realistically scaled and structurally accurate neuromusculoskeletal simulation system, there are virtually hundreds of ideas and

[a] To avoid overextending the predictions of the models, the correct way to proceed when dealing with computer simulations is this: If experimental data has brought knowledge about a given system to some level, x, then a computer simulation of such system including all information up to x may take us to $x + \Delta x$, where Δx is a short range prediction of what should be expected in the next experiment. No further predictions should be made prior to actually performing the next experiment aimed at evaluating the accuracy of Δx.

hypothesis that can be tested and explored. However, due to the high level of exigency that should be imposed on any such simulation system with respect to accounting for experimental data, only small steps should be attempted, as was discussed in the previous section. The four most important contributions in this work are the following:

- It is proposed that muscle force at the sarcomeric level has its origin in the conformational entropy of the myosin molecule, and therefore the forces at the individual actin-myosin bonds should be described using the Worm-Like Chain[168] model of entropic elasticity in combination with the properties of parallel spring arrays. A novel mathematical model of muscle force is derived based on this idea, which turns out to be a derivation from first principles of Hill's famous force-velocity relationship[107]. Although not directly related to the study of motor control *per se*, there is general agreement in the field that structurally accurate while computationally efficient models of striate muscle are very much needed, particularly for large-scale neuromuscular simulations. With this work I hope to have contributed with such a model.

- A hypothesis regarding the function of γ-motoneuronal modulation of the muscle spindles is strongly endorsed, based on the simulation results from a computational model of a simplified neuromuscular system. Analysis of the simulation data lend support to the idea that γ-motoneuron activity might be essential for cancelling *expected* stimuli rather than only for programming servo-controlled equilibrium positions of the limbs. From the simulations it is concluded that the best performance of a movement is obtained when spindle reafference is cancelled by γ activity, thereby allowing for a relatively pure and "noise-free" detection of unexpected loads, which then may be compensated for correctly.

- As an extension to the previous item, a novel hypothesis is proposed linking motor-cortical activity directly to muscle action. The absolutely simplest and most direct connection linking cortex and muscle starts at the corticomotoneuronal (CM) cells in primary motor cortex. These cells have been shown[65,40] to innervate cell populations in the spinal cord monosynaptically, and have been positively correlated with post-spike facilitation (PSF) of electromyographic (EMG) activity as measured by electrode insertions in muscle. A strong case can therefore be made in favour of the idea that these cells are essential for some aspects of voluntary cortical motor control[40]. But given the many different types of activity patterns observed in such cells[39,67], what exactly *is* their role? In the last chapters of this thesis it will be argued that some of the activity patterns observed in CM cells *in vivo* during simple "ramp-hold" tasks, share some features with those optimal activity patterns of static and dynamic γ-motoneurons that would be required for reafference cancellation in the spindle as inferred from the neuromusculoskeletal computer simulation.

And last but not least:

- This thesis presents the theoretical counterpart of what has become a very detailed computer program for simulation of the human arm and its immediate spinal control systems. The resulting program is relatively easy

to use, to customize and to include in other programming environments, which makes it a highly useful research tool because it may serve as a test-bed for a variety of human arm movement hypotheses (see chapter 2), many of which have so far only been evaluated with severely simplified arm simulation systems.

1.4 Overview of Thesis

This thesis is divided into twelve chapters, each of which may be considered as an independent unit with methods and results intrinsic to that chapter only, but which should nevertheless be seen in association with the remaining chapters. Chapter 2 is a short review of some important results in the field of motor control. In it various topics will be discussed, such as the equilibrium point hypothesis (α and λ versions), forward internal models, optimization theories and the origin of the bell-shaped velocity profile of straight hand movements. In chapter 3 the basic elements are presented for creating a computational model of biomechanical systems, and the resulting general physics simulation system is introduced. In chapter 4, a novel model of sarcomeric force production is derived, which is empirically and structurally accurate, and which directly links muscle contraction phenomena with entropic forces in the myosin-actin interactions. Chapter 5 presents a brief review of neuronal dynamics with emphasis on finding models that support different types of spiking behaviour. A simple modification to previous neuron-models is seen to account for the Henneman effect observed in spinal motoneurons. Computational models of synaptic dynamics and spike-time dependent learning will be reviewed in chapter 6. Neurons are perhaps most interesting when part of networks, so chapter 7 is dedicated to give a small glimpse into the dynamics of abstract networks of recurrent artificial neurons. In chapter 8 a simplified account of neural networks in the spinal cord is presented, and a brief introduction to a few aspects of motor cortical neurons is provided. In chapter 9, the muscle models developed in chapter 4 will come together with parts of the spinal networks developed in chapter 8 in order to provide an accurate account of force production in whole muscles. This chapter comes almost as a preamble to chapter 10 which emphasizes the role of spindles, and in particular the role of γ-motoneuron activity for reafference cancellation. In chapter 11 a simulation of the human arm during some simple tasks is given. This simulation is based on the models and experimental data presented in all the previous chapters. Finally, chapter 12 will recapitulate all the results in an attempt to give a consistent picture of the long road from neurons to newtons.

That is a lot of ground to cover for a single monograph, especially considering that the subject matter contained in each chapter easily could be expanded into many books. The scope of study at each level has therefore necessarily been limited to the absolute minimum motor control system which still includes all levels from cortex to muscle. I should add, that the primary purpose of this report of course is to present the main results of my research, but almost as important is the fact that this report should serve as documentation to the extensive simulation environment that has been developed to get those results in the first place. Rather than giving a step by step tour through more than 12000 lines of programming code comprising roughly 50 different tailor-made object classes, it seems much more useful to present all the theoretical background

and insights in a programming independent way. The main advantage of this approach is the complete transparency that one obtains: everyone can see what has gone into the works and may therefore easily verify the results. The major disadvantage being the increase in size and the necessity for a perhaps tedious repetition of basic material.

Chapter 2

Trends and perspectives in motor control theory

Chapter Summary

Some of the most influential ideas in the field of motor control had their origins in the early work of Sherrington, and are briefly reviewed in this chapter together with some more recent accounts. The aim of this chapter is thus to set up the theoretical framework upon which the rest of this thesis will be based. The aim is also to make a clear statement as to why it is necessary to have highly detailed models of the systems (arms, legs, etc.) that are supposedly controlled using one or several of the reviewed methods.

Progress in the field of motor control theory has been difficult due to the fact that extraordinarily simple experimental observations often require exquisitely complex mathematical-physical-physiological models and interpretations. And it is also very common to find several competing theories that perfectly explain different aspects of the same data, but which are structurally unrelated and sometimes even essentially incompatible with each other. An example in point being the observation that during ordinary voluntary reach-to-grab tasks, the hand follows a straight trajectory with a single peaked velocity profile [190]. Among the proposed theoretical explanations for this simple observation one finds high level planning of virtual equilibrium point trajectories [24], the formulation of highly sophisticated biomechanical optimization schemes [89], the speculation that perhaps percolation or diffusion dynamics in 2-dimensional networks may be required [86], or even the more mundane observation that perhaps it is the geometrical and physical properties of the arm itself that cause this behaviour rather than any particular neuromuscular plan [97] (see chapter 11). Some of these issues will be reviewed in the following sections, however, before doing so it is useful to review some of the basic principles.

2.1 Foundational issues

Descartes was of the opinion that reflexes were the result of hydraulic forces originating in the brain's ventricles as a response to stimuli, and producing muscle force by inflating the muscles[50]. Although this idea later turned out to be completely wrong, Descartes should at least be credited with being among the first to attempt a truly mechanistic description of the muscle reflex. Following in the mechanistic tradition, Sir Charles Scott Sherrington is considered by many to be one of the founding fathers of modern neurophysiology, mainly due to his extensive experimental work on reflexes which he saw as an integrated activity of the nervous system (for his work he received the Nobel prize for physiology or medicine in 1932). The notion that stimulating one set of muscles is accompanied by simultaneous inhibition of the antagonist muscles is sometimes referred to as "Sherrington's law", and essentially forms the functional basis of the myotactic unit[159] (see chapter 8).

2.1.1 Springy Muscles – The Tonic Stretch Reflex

In the early 20^{th} century, Sherrington discovered that the rigidly extended hindlimbs of decerebrate cats would oppose flexion, first with a phasic increase in extension force, shortly followed by a tonic plateau. Thus, a muscle with proper spinal connections will respond to any lengthening with an attempt to contract. These stretch reflexes are a consequence of the increased positive feedback to the α motoneuron resulting from the increased activity of spindle afferents in the extensor muscle (see also chapter 10). Steady-state muscle spindle activity will only have significant modulatory influence on α-motoneurons which are already active[93], not being strong enough to bring α-motoneurons to threshold. However, in decerebrate cats the α-motoneurons innervating extending muscles are tonically active, which is why Sherrington was able to elicit stretch reflexes in these animals.

One immediate consequence of this stretch reflex is that there will be a very clear monotonically increasing force-length relationship in intact muscles: The more the muscle is stretched, the greater will be the contractile force reflexively opposing this stretching, just like a spring. Varying the level of tonic α-motoneuron activity shifts the position of the force-length curves but without changing the slope at near maximal stretching[64], and so force-length curves associated with different α-motoneuron activities do not cross each other. See figure 2.1 As it turns out, this property of the force-length curves is one the reasons that the tonic stretch reflex forms the foundation for several very influential general theories of motor control, namely those which rely on the spring-like properties of innervated motor-units to move the limbs to some equilibrium position, i.e. where the flexing and extending muscles are in balance[61].

2.1.2 Equilibrium point hypothesis

In physics, equilibrium is used to denote a state in which all the forces and moments affecting a system balance out. When in equilibrium, a system will remain indefinitely in that state unless perturbed. If the equilibrium is stable, small perturbations will not affect the system significantly, as the system will just return to the equilibrium position. But if unstable, any perturbation,

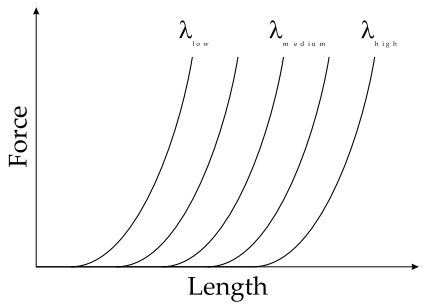

Figure 2.1: Force-Length invariant properties of muscle. The figure shows force-length curves for different thresholds of the tonic stretch reflex, λ.

however small will cause the system to move away from equilibrium. In motor control theory, an equilibrium point (EP) corresponds to a coordinate in the system's state-space where all the forces are in balance[61]. It is in this sense that many researchers[25,199,146] have adopted this concept to propose a simplifying motor control strategy. Basically, the idea is that the CNS generates a (temporarily constant) control signal which by activation of the spring-like muscles will bring the controlled system to a stable EP that corresponds to the control activity. This is like using a control signal to set the stiffness of a simple damped mass-spring system: after a transient oscillation the system will reach its new stable EP. If the controlled plant is a multi-jointed rigid body system connected by spring-like actuators (see chapter 3), then the control signal will be an activation vector which imposes a stiffness on each of the actuators. To avoid persistent oscillatory modes (a limit cycle), the actuators of the system must of course be damped appropriately.

To simplify matters a bit when working with multi-jointed systems like the human arm, it is useful to consider only the position of the endpoint (e.g. the hand, or a fingertip). If the system is in stable equilibrium when the endpoint is at a certain position $\boldsymbol{r} = \boldsymbol{r}_{EP}$, then any perturbation away from EP, $\boldsymbol{r} = \boldsymbol{r}_{EP} + \Delta r$, will set in motion reaction forces which will try to bring the endpoint back to the EP, $\boldsymbol{r}_{EP}$ (although not necessarily via the same route as the initial displacement). A natural consequence of this is that, for every displacement of the endpoint within the limb's workspace, a force vector exists which if applied at the endpoint exactly counters the re-equilibration force, thus maintaining the endpoint at the displaced position. This is equivalent to stating that within the limb's workspace there exists a force field which affects the endpoint pushing it towards equilibrium.

In a nice set of experiments done by Bizzi and co-workers[24,85] it was shown that force-fields like the one just described, actually do exist in frogs, and can easily be measured. To do this, a frog was immobilized at the pelvis, its spinal cord was laid bare and electrically stimulated with a microelectrode (or chemically with N-methyl D-aspartate) so as to activate the frog's leg muscles (see experimental details in Bizzi et al.[24], Giszter et al.[85], also reviewed in Bizzi et al.[22], Shadmehr[243]). Using a force sensor attached to the ankle, a force field like the one just described was created by recording the force during stimulus induced movement as a function of the leg's starting position. Four important results came out of these experiments:

- The resulting force field has a point at which the force vectors vanish, corresponding to the equilibrium point.
- Different stimulation sites in the spinal cord generate different force fields, i.e. force fields with different positions for the equilibrium point.
- Stimulating two sites simultaneously generates a force field that resembles the vectorial sum of the force fields corresponding to independent stimulation of each of the two sites.
- The force fields are time dependent.

Further experimental observations[85,23] have led these groups to propose a "virtual trajectory" used for more complicated limb positioning tasks, in which the limb follows a temporal sequence of equilibrium points.

These are technically quite impressive experiments with far-reaching consequences, and the underlying notion of equilibrium points seems to account for much of the data. Nevertheless, the results of these groups are perhaps not entirely surprising: constant input to a system composed of damped springs will inevitably move towards an equilibrium (as discussed by van der Helm and van Soest[266]). The EP hypothesis leaves open the issue about how the controller for such a system should be configured in order to create the necessary muscle synergies. The old engineering concept of load compensation by servo-control has been the central tenet for some very influential motor control models [154,180], which by far pre-date the EP hypothesis, but are nevertheless somewhat dependent on it.

2.1.3 Movement Invariants: Straight path movement with Bell-shaped velocity profiles

Even a simple task like reaching for an object involves the production of muscle forces with complex spatiotemporal dynamics. In particular one very simple experiment performed by Morasso[190] illustrates this. In this experiment subjects were asked to reach out with their hands from an initial starting position to different target positions. The conclusion was simply that the nervous system selects motor activations for this task which bring the hand from start to goal along a straight path, and with a bell-shaped (single-peaked) velocity profile. An almost explosive development of hypotheses has resulted from this observation, ranging from low level physical explanations to high level control theories and computational strategies. These experiments have been extended to multi-joint movements in space, however the results remain similar[191].

Based on this result it could be argued that the brain plans movements in world coordinates rather than body coordinates, perhaps attempting to simplify the transport path. Such a simplification comes at a cost, namely that in order to perform a straight path hand movement, the joint angles must change in a very specific non-linear manner. A schematic rendering of this is shown in figure 2.2. Notice that in most directions of movement there is a non-linear relation between the angles, θ_1 and θ_2, and sometimes there is even a reversal in the direction with which an angle changes. (The angles are calculated from the inverse kinematic relation derived in section 3.1.2). Thus, in order to generate straight hand transport paths, the central nervous system is forced to generate

activation patterns in the muscles which cause the joint angles to change in a rather complicated non-linear way. Explaining this observation has been yet another central issue in motor control theory.

2.1.4 Control engineering terminology

Motor control theories are often framed in control engineering terms (for a neurobiologically relevant review see Narendra[201], Miall[183], Miall and Wolpert[184], Carpenter[36]), where a distinction is made between the following parts of the system:

- Controller: Sends motor commands to the controlled object. Different sources of state information, such as input from internal, external and reference state sensors may be used in order to specify appropriate motor commands.
- Plant: Controlled object which acts on the environment, thereby changing the values of the controlled variables.
- Controlled variables: Subset of state variables which are affected directly by the plant's action.
- Reference variables: Subset of state variables which specify the goal state for the system, usually by comparing their values with those of the corresponding input variables.
- Input variables: Subset of state variables which the controller and plant use to compute and generate appropriate output.

The two most important classes of control, termed feedback and feedforward control are distinguished, respectively, by the presence or absence of input variables that are affected by the plant's action. A suitable combination of feedback and feedforward components within a controller is necessary to attain flexibility, precision and load compensation during a positioning task. An important class of such controllers is based on correcting positioning errors by comparing the reference variables with some of the input variables and generating appropriate responses, such systems are also known as servo controllers.

Insofar as the discussion only concerns general strategies for control, these divisions are quite useful and permit easy communication of some central concepts. In a biological context, however, some of these terms should preferably be used only when the underlying structures have already been completely specified thus permitting an unambiguous labelling of the structures, otherwise one runs the risk of overestimating the capabilities of biological structures. For example, even though it definitely is possible to train a neural network using the backpropagation algorithm[230] in such a way as to take on the role of the controller for positioning a multi-limbed manipulator[129], this does not entail that biology works like that. It might be good robotics to solve a problem in such a fashion, but it is certainly not good biology to claim (without hard and uncontrovertible proof) that the neural networks in the brain do e.g. backpropagation of error. Our control systems 'need to bear some systematic relation to the realities of biology and psychology if they are to tell us anything about natural, intelligent organisms' (from Scutt and Damper[240], p. 221).

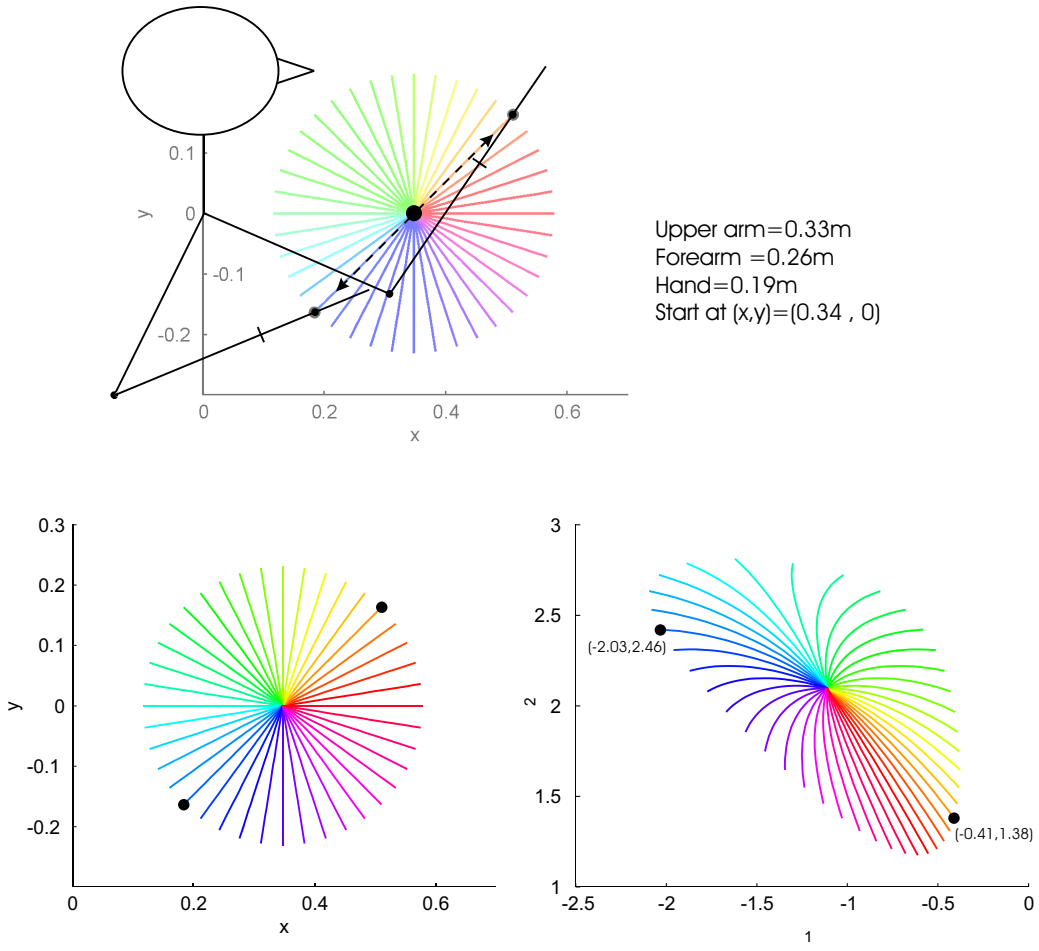

Figure 2.2: Required joint angle variations for straight hand transport paths. The upper graph shows a schematic representation of the task (horizontal planar movement, as seen from above) which consists of moving the hand from the central position and out along one of the straight lines. Lower left graph shows the hand position (in the xy-plane), and the lower right graph shows the corresponding joint angles (θ_1 and θ_2). Different directions are colour coded for direct comparison between hand positions and corresponding joint angles.

In biology, and particularly in neurophysiology, feedforward and feedback connections sometimes have special names due to their particular function or the type of information they carry. In this thesis the following terms will be useful:

- Afference: Neural signals resulting from activity in sensory neurons and impinging on the CNS.
- Efference: Neural signals originating in the CNS and impinging on effector systems (essentially muscles).
- Efference copy: An exact copy of the efference signals, but impinging somewhere within the CNS itself.
- Exafference: Signals from the environment that act on the sensory organs (light, pressure, temperature, etc.).
- Exefference: Signals originating in the effector systems of the organism, and acting on the environment (vibrating vocal cords, mechanical forces of moving limbs, etc.).
- Reafference: That part of afference that results as a direct consequence of efference. Reafference will have a combination of sources, so it is necessary to distinguish between exteroceptive reafference (associated with the activation of sensory receptors that are attuned to events in the environment, e.g. hearing your own voice), and proprioceptive reafference (associated with sensory receptors that are attuned to events within the organism itself, e.g. activity changes in joint receptors and in type Ia, Ib, II spindle afference).

Of these, reafference poses a special and very hard problem as it directly interferes with the stimulus-response causality that otherwise applies for most of these signal pathways. Sensory receptors are highly independent from the rest of the nervous system and seem designed to convey a highly reliable estimate of the variables to which they are attuned (temperature, pressure, velocity, etc.). But they are also "source-blind", that is, they are unable to distinguish between different sources of the measured variables, be they internal or external. They just respond to their appropriate stimuli regardless of what caused the stimuli. So, for example, how does a system distinguish own vocalizations from external voices given the fact that in both cases the sensory exafference comes through the same channel, namely the ears?. How do the voltage sensitive organs of the electric eel distinguish between the potentials across the electric eel itself, the response potentials in the environment and the potentials of other eels?, and more to the topical point of this thesis: How does the spindle organ in muscles distinguish between externally imposed changes in muscle length, length changes that are a consequence of other muscles moving, and length changes that arise from the muscle itself contracting?. This last question is the major driving force for producing this thesis, and the simple answer might come as a surprise: It doesn't have to make the distinction because reafference is centrally cancelled via the γ-motoneuronal system, so all a muscle spindle ever registers are externally imposed changes in muscle length that may be used for load correction or for reprogramming the task execution parameters. This ties in

perfectly with the idea that the fusimotor system is concerned with feedforward servo-assistance of the muscle system.

2.2 Control theories

Some of the most influential theories of motor control are deeply rooted in the concept of equilibrium points and at least one of them, the γ-model, actually precedes the modern EP formulation by several decades. Other theories, or rather principles, hold that the problem of motor control is one of optimization, where the system should find the best solutions according to some optimality criterion. Gradient ascent methods have also been proposed, particularly within the context of finding optimal state-space trajectories that a motor control system might follow to position a limb. It will be fruitful to review the main arguments pertaining to each type of approach.

2.2.1 The γ control model

Far ahead of their time Sherrington and Liddell [154] were proposing a servo-like, load compensating function for the tonic stretch reflex, but it was Merton and co-workers [180,56] who properly developed this idea to a theory of motor control. According to Merton, the activity in γ-motoneurons was essential because it directly affects the sensitivity of the muscle spindle, and thereby is involved in setting the resting length of the spring-like muscle. Thus, if we have a high level of activity in a given γ-motoneuron, then the contractile elements of the corresponding spindle will stretch the central region of the spindle, increasing type Ia and type II spindle afference (see chapter 10). The increased afference will augment the activity of the α-motoneuron pool until the additional contraction thus produced brings the muscle to a length which corresponds to the γ-motoneurons activity level. Once there, any perturbations to the muscle length will be countered by an increase (the tonic stretch reflex) or decrease of contractile force (according to the force-length curves mentioned earlier).

In short, the γ-motoneuron sets the target position for the servo controller. Merton's idea is very compelling, general and seemingly simplifies the problem of motor control significantly, but alas, it is also wrong. There is at present no experimental evidence with which to fully validate this version of Merton's servo controller (discussed in Latash [146] and Carpenter [36]). Three problems with the model are of particular importance: The fact that experimentally measured gains of the tonic muscle reflex are not as high as required for length regulation [172,146]; there is no evidence indicating that γ efference by itself can recruit α motoneurons via Ia afference; and the fact that γ-motoneuronal activity does not usually *precede* α-motoneuron and EMG activity [265].

2.2.2 The α control model

As reviewed in a previous section, experiments on frogs showed that microstimulation at certain locations in the spinal cord will cause the frog's leg to move to a certain position and stay there [25]. This effect is stable even for deafferented animals, i.e. animals where no sensory input enters the spinal cord, which led Bizzi and co-workers [22] to the conclusion that pure α-motoneuron activity is

sufficient for limb control. They proposed that the muscle synergy associated with a given equilibrium position could be invoked by precisely setting the activities of an α-motoneuron pool in the spinal cord. Needless to say, this is a very artificial model in that it completely ignores the important contribution of the tonic stretch reflexes to movement, without which the gain of the system would not be sufficient to load compensate. See Feldman[62] and Latash[146] for an thorough analysis and criticism of the α-model.

2.2.3 The λ control model

Still within the explanatory paradigm of servo-control systems, equilibrium points and force-fields, resides the λ-model[62,146]. The debacle of the γ and α control models as originally formulated was, respectively, the failure to include quantitative aspects of activation, and the failure to include relevant physiological structure. The λ-model does not suffer from such problems because it completely leaves open the question of *how* things are physiologically implemented, and instead focuses on *what parameters* are controlled[146]. In the λ-model, emphasis is again given to the tonic stretch reflex, and the existence of some invariant characteristics of muscle, in particular the family of force-length curves produced by imposing different activation levels of α-motoneurons. As noted earlier, these curves are non-intersecting smooth and monotonically increasing functions, indicating that very simple control signals in principle would be sufficient to attain all possible positions. Based on these facts, Feldman[61] proposed to use the length threshold of the tonic stretch reflex, indicated by λ, as the centrally controlled variable. Thus λ indicates the length at which the tonic stretch reflex becomes active, thereby shifting the force-length curves exactly like the force-length invariants. Recent additions to this model[63] have tried to link the λ control signal to a subthreshold depolarization of the α-motoneurons (thus increasing their sensitivity).

2.2.4 Internal Model Controllers

In the ideal case without transmission delays, the servo-control strategy would be optimal in that it would perfectly correct positioning and load errors. In reality, however, the transmission delay around the spinal-musculo-spinal loop in humans is in the range from 10 to 30 ms, which means that the corrective servo command always will be delayed with respect to the disturbance causing it. It is well known from physics that a system having strong feedback loops with long transmission delays will be intrinsically unstable, which for a servo-controller means that the position error will almost always be under- or overcorrected. This can lead to strong oscillations (tremor) where the hand oscillates around a position, or it may lead to position errors caused by undershooting or overshooting the target.

Preoccupation with these issues has led researchers to propose different strategies by which the feedback delays might be reduced or removed altogether. Such ideas are often based on determining the forward and inverse dynamics of a system and are deeply rooted in the field of robotics, but hold a strong position in biological motor control theory due to the fact that the proposed controller architectures often superficially resemble structures in the brain, or are sometimes even inspired by them. In the field of robotics an extensive mathematical

formalism has been developed to handle the positioning of kinematic chains (see section 3). Within this formalism the problems inherent in motor control are very easy to define explicitly, and solutions can often be found readily. Thus, in some simple situations it is possible to specify all the relevant forward and inverse equations needed to control a manipulator precisely to a given position. The forward dynamics equations are only ever useful if the controller needs to make predictions about where the manipulator will move if a particular set of joint torques is applied, or if the system is a simulation without a physical counterpart. To correctly position a manipulator it is more useful to know the inverse equations because then it is simply a question of specifying the end-effector's goal position, and the inverse dynamical equations will provide target values for the torques that should be produced by the joint actuators in order to move the endpoint to the right position.

Although this is perfectly realizable in artificial systems, there are several hindrances to applying this strategy in biological systems. First of all is the question of whether the the central nervous system may be assumed to contain a fully detailed internal forward or inverse model of the body's dynamics. And if such an internal model exists, it should be noted that the dynamical properties of an organism's moving appendages will change as a result of growth, damage or due to changing environmental requirements so this model should be adaptive. Furthermore, there is the question of representation: How can such a model be implemented within the restrictions imposed by neural tissue? And the question of complexity: How much detail is required in the model?

2.2.5 Optimization hypothesis

Although not evident at first, there is quite a big strategic difference between studying movement in single-jointed limbs vs. multi-jointed structures. The difference resides in the fact that multi-jointed kinematic chains suffer from Bernstein's problem[18], which means that it is not yet clear how to uniquely specify the muscle forces that will accurately position the limb. Through the years several attempts have been made to find solutions to Bernstein's problem, some of these will be reviewed in what follows. Rather than trying to identify the control parameters *per se*, many researchers have instead focused on discovering the motor control strategies that the brain might use when specifying the parameters[70,264,136,184,110]. Based on ideas about evolution and survival ability, it has been proposed that the motor system might try to maximize some fitness function. It is assumed that this fitness function would be related to one or several of the controlled variables such as limb velocities, accelerations, torques [264], jerk (the third time derivative of position)[70], limb position error[68], etc. Framed in this way motor control problems will have an optimal solution which can be directly expressed with objective functions. It is not yet clear whether the brain actually does seek out such optimal objective functions (e.g. by training the cerebellum), or whether it takes a more pragmatic approach and uses some simple heuristics in combination with the limb's inertia and "springiness" (laws of nature) that it gets for free (for a thorough and lucid discussion of this issue, see Greene[97]). In any case, to be valid the analytic expressions resulting from solving the objective functions should describe some experimentally identified features of the movement, usually the hand trajectory and velocity profiles. There are many optimization strategies which might be applied to

the problem of motor control, but in the following I shall only consider two of the most promising, namely the *maximum smoothness theory* proposed by Flash and Hogan [70] and the *minimum torque change model* proposed by Uno and co-workers [264]. In a way these two models are closely related in that they both consider jerkiness, but in different coordinate frames: Where the maximum smoothness theory proposes using the time derivative of the end-effectors acceleration (it could thus well be called a minimum force change model), the minimum torque change model in essence considers using the time derivative of the joint angular acceleration. These similarities notwithstanding, there are fundamental differences between the two.

Maximum smoothness

Presumably the best way to simplify the sensory task of tracking and correcting errors of a moving end effector like the hand is to make the movement as smoothly as possible [110]. This would have the additional advantage of minimizing the requirements for a hand trajectory planning and prediction system [71]. By expressing the objective function for the hand positioning problem in cartesian coordinates it is possible to maximize smoothness by minimizing jerkiness, that is by minimizing the following expression [70]:

$$C_J = \int_0^{t_f} \left(\left(\frac{d^3x}{dt^3} \right)^2 + \left(\frac{d^3y}{dt^3} \right)^2 \right) dt \tag{2.1}$$

where t_f is the duration of movement in the xy plane. The analytical expressions derived using this criterion [70] reproduce some of the principal movement invariants of the end effector, in particular the single-peaked velocity profile and the straight hand trajectories. Curved trajectory movements, or movements where obstacle-avoidance is required may also be described in the maximum smoothness paradigm by specifying a number of "via"-points through which the hand must pass.

Minimum torque change model

Instead of considering the time derivative of the end-effector's linear acceleration, Uno and co-workers [264] consider the time derivative of the joint angular accelerations (angular acceleration being related to torque according to equation 3.14 in chapter 3). It was reported in Uno et al. [264] that this model can account for the same movement invariants as the maximum smoothness theory, but with the added advantage that the minimum torque change model is better suited to find solutions to motor control tasks which are ill-posed due to actuator or kinematic redundancy (see chapter 3). In a planar manipulator with m torque inducing actuators the following expression should be minimized [264]:

$$C_\tau = \frac{1}{2} \int_0^{t_f} \sum_{i=1}^{m} \left(\frac{d\tau_i}{dt} \right)^2 dt \tag{2.2}$$

where t_f is the duration of the movement, and τ_i is the torque induced by the i^{th} actuator.

It should be noted that this model includes the dynamic aspects of the multi-jointed movement, and not only the kinematics of the endpoint. In addition,

the joint-based reference frame adopted in this model permits a straightforward reformulation of the objective function, C_τ, to be dependent on some of the underlying torque inducing processes such as muscle tensions or motoneuron activities. Thus an objective function can be formulated for a minimization of the muscle tension change [264] which takes into consideration that joint torques are generated not by one but by several muscles, and in addition accounts for the experimentally observed triphasic muscle activities characteristic of fast movements. Still compatible with the minimum torque change model, a minimum motor command change model has been proposed [135] which penalizes rapid changes in the motoneuronal firing rates. The experimentally observed simplicity of corticomotoneuronal activations during ramp-hold tasks [39] gives this last model some indirect support. And finally, from an evolutionary point of view, it would make sense to assume that the strategies that have evolved for motor control are of such a nature that they minimize the overall energy requirements of the system. This energy-minimization issue is also compatible with torque minimization because the work done by a torque, τ, on a rotating system turning through a small angle, $d\theta$, is $dW = \tau d\theta$ (see e.g. Tipler [261]), so minimizing torque will also reduce energy requirements.

2.2.6 Hyperspatial labyrinths

In a sense, the task that must be solved by the CNS during voluntary positioning of the limbs is reminiscent of the problem to be solved when getting from start to goal in a labyrinth. Let me explain. The task when trying to solve a typical "brain-teaser" labyrinth in two dimensions consists of drawing a continuous line that effectively connects the "start" and "goal" positions while avoiding contact with the constraining "walls" of the labyrinth. Other constraints may apply, such as the requirement for finding the shortest route through the labyrinth, or the route with fewest turns, etc. In any case, the solution is a simple 2-dimensional trajectory cris-crossing the labyrinth's plane. As will become apparent in chapter 3, the complexity of correctly positioning a limb is related to the degrees of freedom (DOFs) of the limb, the number of available constraints and the dimensionality of the task (hand positioning requires 6 DOFs, but the human arm has 7 DOFs available). If one lets each of a limb's DOFs be represented by a single variable in a coordinate system, then the human arm exists in a 7-dimensional limb-space, and the act of moving the hand from a position, A, to a different position, B, can essentially be represented as a continuous trajectory within this 7-dimensional system. In this context, the presence of external constraints such as obstacles in the environment, and internal constraints such as joint excursion limits, may be represented as regions or "blobs" within limb-space (much as the holes in a cheese) through which the limb's trajectory may not move. These constraints are conceptually similar to the walls of a labyrinth, and thus the task of moving a limb is the task of solving a high dimensional labyrinth. Some of these constraint blobs may of course be removed by reorienting the arm, but that will require whole body movements (or a broken arm). In a sense, performing a well learned motor task is perhaps akin to traversing a labyrinth where guiding arrows have been provided at the junctions. Sometimes disturbances and constraints will invalidate some of the usual pathways, forcing the system to come up with alternate solutions. A way out of such a *cul de sac* is to permit movement in yet another dimension, out

of the labyrinth's plane so to speak, e.g. by invoking other body movements.

By using this labyrinthine formalism one opens this type of problems to an array of well-established path-finding and energy minimization techniques. Although this could be highly useful from a robotics point of view, it might not be biologically relevant because of the involved algorithms. Furthermore, it should be noted, that there is a marked computational difference between having a bird's eye overview of a labyrinth's layout and actually being inside a labyrinth. In the former case the route may be planned beforehand and the solution is quite transparent, at least if compared to the latter case where it becomes an exploratory task rather than a planning task. It may be argued that the eye performs similar exploratory movements while scanning the bird's eye view of the labyrinth, however, it still has the advantage of being able to localize several landmarks at once and observe how they are positioned with respect to each other (not to mention that it even knows in which general direction to search for the exit!).

From a biological point of view, the most important objection to this type of methods (many of which are in fact used in robotics), may be levelled at the underlying assumption that limbs are controlled directly through their DOFs. These DOFs are thus assumed to be identical to the set of state variables that some subsystem in the CNS uses as input to generates the appropriate torques at the limb's joints. Although there is nothing wrong with this tenet *per se*, to be of any biological relevance, a strong case should be made to argue that these state variables are actually the ones that the CNS uses.

Activity percolation in topographically ordered neural networks

As a case in point related to the previous discussion, consider the implicit assumptions of Glasius et al.[86,87], Yang and Meng[283] and Yang and Meng[284], who model 'real-time collision-free path planning of robot manipulators'[284] by topologically ordering a neural network along different dimensions of a defined state space. That is, a number of neurons, N, are organized in a 2 dimensional grid that corresponds to the environment or state space that has to be explored. Despite some important differences in the detailed implementation used by these authors (in particular the use of Hopfield networks[86] vs. the use of shunting equations for defining the neuronsYang and Meng[283]), the networks are essentially identical. In Yang and Meng[283], each neuron represents a particular 2d coordinate within the grid and thus a position in the environment (or state space), and each neuron provides excitatory input only to its closest neighbours (the complexity of the network thus scaling linearly with N, a very efficient feature). Obstacles in the environment are represented by imposing strong inhibition onto the neurons that are positioned at the appropriate grid-points, whereas the target position has a strong excitatory input. By imposing a gradient ascent algorithm, the robot or manipulator may follow a trajectory through this 2-dimensional space directly from the starting position to the goal position, with guaranteed success and following the (metrically) shortest route. Depending on the particular parameters represented by the neurons (cartesian coordinates corresponding to a labyrinth or joint angles of a 2-link manipulator), it is thus possible to solve a complicated path-planning problem with what

essentially comes down to a gradient ascent method [a]. This is a quite remarkable feat of neural computation, but it is not entirely clear yet whether such a mechanism has any biological relevance in the present context. There will be a bit more to say about these topics in a later chapter (section 8.4.1), after some of the structures and functions involved in voluntary motor control have been properly identified and investigated.

2.3 On the need for neuromusculoskeletal modelling systems

A point of criticism often levelled at attempts to understand nature by creating simple models and/or computer simulations of various phenomena can be condensed in the following sentence (heard at a conference): 'a computer simulation of a hurricane is *very* different from a real hurricane'. The reply to this remark should be: 'True, but it nevertheless helps us understand the real thing at a much deeper level than otherwise possible because it forces the investigator to first gather all the known experimental parameters, then to organize them systematically and evaluate their relative importance, and finally to link them together according to the various theories that may have been proposed on the subject'.

In view of the large variety of motor control theories that have been proposed along the years, a few of which have been reviewed in this chapter, it is highly relevant to develop structurally accurate models of those systems that are supposed to be controlled as specified in the theories. An accurate test-bed for the many theories is much needed, and it alone merits the investment of much effort into its development. In the following chapters emphasis will be on developing just such a test-bed system, with as many biologically relevant details as possible given the current level of experimental understanding.

[a] Move in the direction where the intensity of some variable is highest. Or in more mundane terms: to find the kitchen, follow your nose...

Chapter 3

Biomechanics – Defining the Problem

Chapter Summary

A brief overview of vertebrate biomechanics is given in this chapter, with particular emphasis on some of the central problems encountered when trying to position multi-jointed limbs. This overview is given in order to appreciate the requirements and constraints that must be imposed on any neural controller pretending to emulate biological reality. Some recent developments will be reviewed and evaluated in the light of neurobiological findings.

The structural stability of all living organisms depends on their ability to correctly produce internal forces that may balance out the external forces imposed by the environment (such as gravity, collisions, osmotic pressure, etc.). Indeed, were it not for the continuous action of muscles and tendons pulling on the skeleton, the human body would immediately collapse under the force of gravity. The central nervous system is prodigious at determining appropriate levels of motoneuron activity that lead to the correct production of muscle forces that are required to position our limbs. So proficient in fact, that the "user" is usually completely "blind" as to the biomechanical complexities that are involved: To all appearances, the limbs position themselves effortlessly and automatically upon command, and even complex sequences of muscle activations leading to behaviours such as grooming or locomotion are effected on auto-pilot.

There is a long tradition in mechanical engineering to study systems composed of multiple rigid bodies linked together at joints of varying geometries and affecting each other and the environment with torques and forces. In the context of robotics, such systems are often referred to as multi-jointed manipulators, and a vast theoretical framework has been developed to their study. By adopting this theoretical framework for the study of vertebrate movement, it

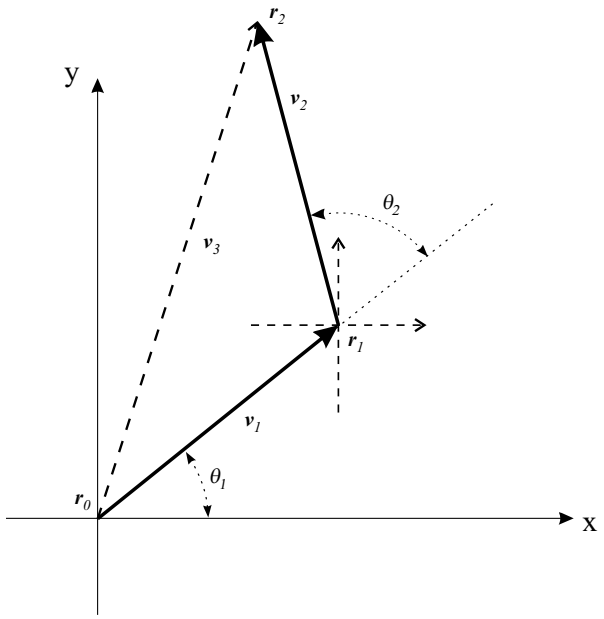

Figure 3.1: Geometrical nomenclature of a 2-link planar manipulator.

becomes possible to make a very clear analysis of the problems that the central nervous system must solve in order for us to move. In what follows I will therefore provide a brief introduction to the topics of kinematics and dynamics as they are related to the problem of human arm movements.

3.1 Skeletal kinematics

According to some accounts[94] there are, on average, 206 bones in the normal human skeleton (approx. 270 separate bones at birth, many of which subsequently fuse together during adolescence). A majority of these have skeletal muscle tissue attached to them, and are thus participant in the production of internal forces within the body and on the goal defined application of forces to the environment. The scope of the present work is limited to the study of human arm movements, so we need only consider 2-linked, or at most 3-linked manipulators in 3d space, but the mathematical formalism used to describe such systems generalizes very well to more complex n-linked manipulators.

The simplest non-trivial example of a multi-jointed rigid body system is the 2-link planar manipulator, as represented in figure 3.1. This system corresponds to a human arm if one only includes the shoulder ($\boldsymbol{r}_0$) and elbow ($\boldsymbol{r}_1$) joints, and if it is assumed that the arm only can perform planar movements. It is worthwhile to consider this simplified system with some detail, not only because it is fully solvable (in contrast to systems with more than two links), but because of the large number of physiological experiments that have been done involving simple planar arm movements, which gives a good basis for comparisons and understanding.

3.1.1 Forward kinematics of a 2-link planar manipulator

It is relatively straightforward to work out the equations that specify the position of the manipulator's endpoint (corresponding to the wrist) if the angles of the limbs with respect to world coordinates are specified in advance. Following the nomenclature used in figure 3.1, let $\boldsymbol{r}_0$, $\boldsymbol{r}_1$ and $\boldsymbol{r}_2$ be the position vectors of the shoulder, elbow and wrist joints respectively. Also let the upper arm be represented by the vector $\boldsymbol{v}_1 = \boldsymbol{r}_1 - \boldsymbol{r}_0$, while the forearm is given by $\boldsymbol{v}_2 = \boldsymbol{r}_2 - \boldsymbol{r}_1$. If the upper arm is at an angle θ_1 with respect to horizontal, and the forearm is at an angle θ_2 with respect to the upper arm, then the forward kinematics limb positioning equation is:

$$\begin{aligned}
\boldsymbol{r}_2 &= \boldsymbol{r}_0 + \boldsymbol{v}_1 + \boldsymbol{v}_2 \\
\boldsymbol{r}_2 &= \boldsymbol{r}_0 + \begin{bmatrix} |\boldsymbol{v}_1| \cdot \cos(\theta_1) \\ |\boldsymbol{v}_1| \cdot \sin(\theta_1) \end{bmatrix} + \begin{bmatrix} |\boldsymbol{v}_2| \cdot \cos(\theta_1 + \theta_2) \\ |\boldsymbol{v}_2| \cdot \sin(\theta_1 + \theta_2) \end{bmatrix} \\
\boldsymbol{r}_2 &= \boldsymbol{r}_0 + \begin{bmatrix} \cos(\theta_1) & \cos(\theta_1 + \theta_2) \\ \sin(\theta_1) & \sin(\theta_1 + \theta_2) \end{bmatrix} \cdot \begin{bmatrix} |\boldsymbol{v}_1| \\ |\boldsymbol{v}_2| \end{bmatrix}
\end{aligned} \tag{3.1}$$

3.1.2 Inverse kinematics of a 2-link planar manipulator

In practice, the joint angles are seldom known in advance, and it is instead the endpoint position that is given. This could be the case during a transportation task such as: Move the hand from position $\boldsymbol{r}_A$ to position $\boldsymbol{r}_B$. Such a situation demands the solution of the inverse kinematic problem, that is: find the joint angles such that the endpoint moves to the correct position. Given the simplicity of the forward problem, it would be natural to assume that the inverse problem would be equally simple. Unfortunately the inverse problem is not as straightforward, and in some cases it is even intractable, the problem being that the same endpoint might be reached for many different sets of joint angles.

In the 2-link planar case, the joint angles may be found by using a helping vector, $\boldsymbol{v}_3$ which joins the shoulder to the wrist. It is assumed that the endpoint position, $\boldsymbol{r}_2$, is given, and also that the shoulder position, $\boldsymbol{r}_0$, is known. For all points inside the workspace, $\mathbb{W}$, of the manipulator (i.e. $\boldsymbol{r}_2 \in \mathbb{W}$, see figure 3.2), one may find the angle, θ_1, of the upper arm with respect to the horizontal axis, as well as the angle, θ_2, between the upper arm and the forearm using the following equations:

$$\begin{aligned}
\theta_1 &= \theta_3 \pm \alpha_2 \qquad (3.2) \\
&= \arctan\left(\frac{(\boldsymbol{r}_2 - \boldsymbol{r}_0) \cdot \boldsymbol{e}_y}{(\boldsymbol{r}_2 - \boldsymbol{r}_0) \cdot \boldsymbol{e}_x}\right) \pm \arccos\left(\frac{|\boldsymbol{v}_1|^2 + |\boldsymbol{v}_3|^2 - |\boldsymbol{v}_2|^2}{2 \cdot |\boldsymbol{v}_1| \cdot |\boldsymbol{v}_3|}\right) \\
\theta_2 &= \pi - \alpha_3 \qquad (3.3) \\
&= \pi - \arccos\left(\frac{|\boldsymbol{v}_1|^2 + |\boldsymbol{v}_2|^2 - |\boldsymbol{v}_3|^2}{2 \cdot |\boldsymbol{v}_1| \cdot |\boldsymbol{v}_2|}\right)
\end{aligned}$$

where $\boldsymbol{e}_x$ and $\boldsymbol{e}_y$ are unit vectors aligned to the x- and y-axis, respectively. It may be seen from these equations (notice the $\pm$ sign of equation 3.2) and the diagram in figure 3.1, that even when solving for the joint angles in the simple 2-link PM there exists the problem of deciding on which side of the shoulder-wrist line the elbow should be (i.e. upper-left or lower-right on figure 3.1), as both solutions are correct but yield very different limb positions. In 3d space the

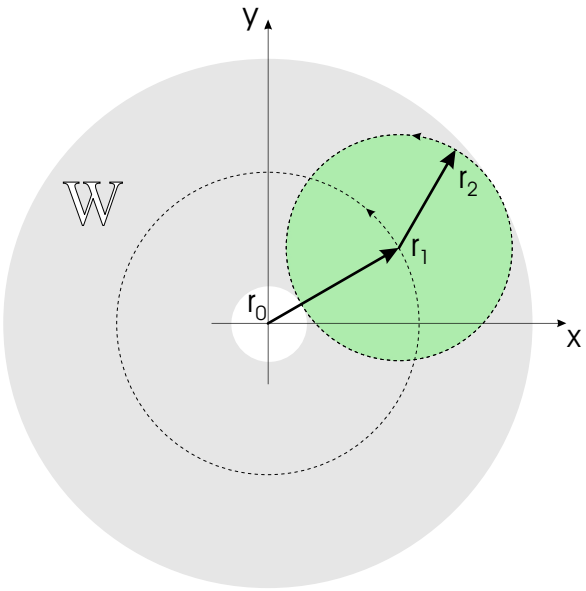

Figure 3.2: The workspace of a 2-link planar manipulator is here represented as the gray area. See text for details.

situation becomes more difficult even for the 2-link case: the shoulder-wrist line becomes a rotationally symmetric axis around of which the elbow joint position may rotate.

Equation 3.1 can easily be generalized to describe any n-link planar manipulator:

$$\begin{aligned} \boldsymbol{r}_n &= \boldsymbol{r}_0 + \boldsymbol{v}_1 + \boldsymbol{v}_2 + \ldots + \boldsymbol{v}_n \qquad (3.4) \\ \boldsymbol{r}_n &= \boldsymbol{r}_0 + \\ & \begin{bmatrix} \cos(\theta_1) & \cos(\theta_{1,2}) & \ldots & \cos(\theta_{1,n}) \\ \sin(\theta_1) & \sin(\theta_{1,2}) & \ldots & \sin(\theta_{1,n}) \end{bmatrix} \cdot \begin{bmatrix} |\boldsymbol{v}_1| \\ |\boldsymbol{v}_2| \\ \vdots \\ |\boldsymbol{v}_n| \end{bmatrix} \end{aligned}$$

where $\theta_{i,j}$ is used as a short-hand notation to represent the sum of angles from the i^{th} to the j^{th} link. In this case the inverse kinematical problem is non-solvable from an analytical point of view because we only have two equations, but n unknown variables. This of course does not mean that no solutions exist, quite the contrary: for $n > 2$ there potentially exists an infinite number of chain configurations which have the endpoint at $\boldsymbol{r}_n$, see also section 3.1.4.

3.1.3 Generalized forward kinematics

A much more general expression for the kinematics of a multi-jointed structure in 3d space may be obtained if one uses coordinate frame transformation matrices. These matrices are used to transform a given position defined in one coordinate system to the equivalent position in a different (rotated) coordinate system, and

have the form:

$$\boldsymbol{R} = \begin{bmatrix} \cos\theta_{xx'} & \cos\theta_{xy'} & \cos\theta_{xz'} \\ \cos\theta_{yx'} & \cos\theta_{yy'} & \cos\theta_{yz'} \\ \cos\theta_{zx'} & \cos\theta_{zy'} & \cos\theta_{zz'} \end{bmatrix} \tag{3.5}$$

where $\theta_{ij'}$ indicates the angle between the i^{th} axis of the base system and the j^{th} axis of the rotated system. For example, if we know a position $\boldsymbol{r}$ in the base reference frame, its position, $\boldsymbol{r'}$, in the rotated frame will be:

$$\boldsymbol{r'} = \boldsymbol{R} \cdot \boldsymbol{r} \tag{3.6}$$

One can go in the opposite direction by inverting the matrix (i.e. simply transposing it if orthogonal) and multiplying it by the coordinate in the rotated frame. There are several ways to explicitly represent a kinematic chain regardless of how many links or dimensions it contains. For simplicity it may be assumed that the proximal joint of the k^{th} limb is positioned at the origin of a local coordinate system and that the position of the link's distal end within this k^{th} coordinate system is given as $\boldsymbol{r}'_k$. Then the endpoint position of a kinematic chain with n links may be found as:

$$\begin{aligned} \boldsymbol{r}_n &= \boldsymbol{v}_1 + \boldsymbol{v}_2 + ... + \boldsymbol{v}_n \\ \boldsymbol{r}_n &= \boldsymbol{R}_1^T \cdot \boldsymbol{r}'_1 + \boldsymbol{R}_2^T \cdot \boldsymbol{r}'_2 + ... + \boldsymbol{R}_n^T \cdot \boldsymbol{r}'_n \end{aligned} \tag{3.7}$$

where $\boldsymbol{R}_k^T$ is the transposed rotation matrix corresponding to the k^{th} limb. Except for the trivial case where $k = 1$, there is no explicit way to find unique solutions to the inverse kinematical problem (given endpoint find link configurations) because the number of parameters when $k > 1$ is larger than the number of available equations, as was the case for the n-link planar manipulator.

3.1.4 Intractability of kinematic chains: Bernstein's problem

A very simple way to determine whether a kinematic chain has none, one or several possible solutions to a given positioning problem involves finding the mobility of the chain, i.e., the total number of degrees of freedom (DOF's) of the chain. Considering each link separately, notice that at least six variable coordinates are necessary to unambiguously position an unconstrained free-floating rigid body in 3d space: three position coordinates and three orientation coordinates. Such an object is said to have 6 DOF's. The task of a kinematic chain might be to bring such an object into the correct position and orientation, in which case the chain must have at least 6 DOF's. If the chain has less DOF's than required for the task, then it will be impossible for it to attain a configuration in which the object is positioned correctly. On the other hand, if the chain has more DOF's than required for the task (redundant DOF's), then there is an infinite number of chain configurations which solve the task, and the problem becomes choosing one of the configurations according to some optimality criterion. The problem of configuring kinematic chains with redundant DOF's has become known as Bernstein's problem, after the Russian physiologist Nicholai A. Bernstein (1896-1966) who first identified it [18,287].

To find the mobility of a kinematic chain it is useful to notice that strong interlink couplings or constraints will limit the ways in which the chain is allowed to move, as will also externally imposed constraints. The chain might for example be firmly attached at one or several points (resulting in open or closed chains respectively). Also the joints might constrain motion to one (revolute joints), two (as the temporomandibular joint), or three DOF's (spherical joints). With this in mind, the total mobility, $\mathcal{M}$, of a kinematic chain can be found by using Gruebler's formula (modified from Zatsiorsky[287]):

$$\mathcal{M}_{chain} = 6(N-k) + \sum_{i=1}^{k} \mathcal{D}_i \tag{3.8}$$

where N is the number of links, k is the number of joints and $\mathcal{D}_i$ is the number of DOF of the i^{th} joint. In an open chain one end is firmly attached (e.g. like an arm attached to an immobilized shoulder), so the number of links is equal to the number of joints and therefore only the summation remains in equation 3.8. Under such conditions the human arm has 7 DOF's: three at the shoulder (spherical joint between scapula and the head of humerus), 1 at the elbow hinge joint between humerus and ulna, 2 at the wrist (between the carpal articular surface of the radius and the carpal bones of the wrist) and finally one DOF related to rotation of the forearm (which for simplicity is sometimes attributed to either the elbow joint or the wrist joint, but in fact is related to the presence of an additional pair of hinge joints positioned proximally and distally between the radius and the ulna, enabling the forearm to twist about its longitudinal axis). Thus the arm has one DOF more than is required to position the hand (6 DOF's required), so even in this simple situation Bernstein's problem makes itself evident as can be verified if you place your hand flat on the table while maintaining the shoulder at a fixed position: What is in this case the optimal position for the elbow joint? Several optimality criteria come to mind: Energy minimization, tension minimization, maximization of manoeuvrability (i.e. avoiding locked or awkward positions), etc.

Using Gruebler's formula, it has been estimated[287] that the mobility of the human body is approximately 244, and if positioning the hand requires 6 DOF's, that leaves us with 238 redundant DOF's for the task (in theory). With so much redundancy the brain has ample opportunity to search for optimal solutions to the positioning task[287]. It should be pointed out here, that for each degree of freedom available to the skeleton, at least two antagonistic muscles will be required to control the relevant movement, so in fact the number of DOF's at the muscular level might even be double that at the skeletal level.

3.2 Skeletal Dynamics

It is now time to add forces and masses to the skeletal kinematical model presented in the preceding sections. The long history of classical mechanics has yielded numerous approaches to solving problems related to dynamics. Depending on the complexity and requirements for the physical model that is being developed, one might use the Newton-Euler method which only considers fundamental forces and moments, or the Euler-Lagrange model which also includes energy considerations. The Euler-Lagrange method permits analysis of

the movement of a constrained system without the difficulties inherent in defining constraint forces (such as joint forces or contact forces at a surface). This is because the Euler-Lagrange approach uses generalized rather than cartesian coordinates, and with a proper analysis of the problem it is possible to specify constraint equations which limit or even remove some of these coordinates. In contrast to this, the Newton-Euler method requires the detailed specification of all constraining forces. There are several advantages and disadvantages one should keep in mind before settling on one or the other method. In particular:

- Extendability of model: How difficult is it to include new elements in the system (an extra limb, an external obstacle, etc.)?
- Explicitness of constraint and contact forces: Is there a reason for which we might want to know exactly the constraint and contact forces, or at least their magnitudes? (characterizing the wear and tear of joint surfaces causing arthritis might be one reason)
- Computational efficiency.

In the present case, I will be using the Newton-Euler approach because it has better extendability within the context of generalized physics simulation systems, and because we do have some interest in fully specifying the joint forces and constraints in that their continuous evaluation during model performance permits us, amongst other things, to control that the simulation is producing realistic joint forces.

3.2.1 Basic Dynamical Model

The equations of motion for a rigid-body spatial manipulator may be expressed in their most general and compact form as:

$$\boldsymbol{T} = \boldsymbol{I}(\boldsymbol{\theta}) \cdot \boldsymbol{\alpha} + \boldsymbol{C}(\boldsymbol{\theta}, \boldsymbol{\omega}) \cdot \boldsymbol{\omega} + \boldsymbol{G}(\boldsymbol{\theta}) \tag{3.9}$$

where $\boldsymbol{\theta} = [\theta_1, ..., \theta_n]^T$ is the vector of joint angles, $\boldsymbol{\omega}$ is the vector of angular velocities, and $\boldsymbol{\alpha}$ is the vector of angular accelerations. In this equation $\boldsymbol{T}$ corresponds to the torques on each limb, $\boldsymbol{I}(\boldsymbol{\theta})$ corresponds to the inertial components of the movement, $\boldsymbol{C}(\boldsymbol{\theta}, \boldsymbol{\omega})$ represents centrifugal and coriolis terms and finally $\boldsymbol{G}(\boldsymbol{\theta})$ represents gravitational terms. Due to its simplicity and amenability to mathematical analysis, this is the preferred formulation in a wide range of recent investigations[38,75,145,89,238]. Although very innocent looking, this equation does indeed expand to many pages of equations if its components are spelled out explicitly, even in the case of a 2-link planar manipulator (see for example the derivations provided in Cesari et al.[38] or in Frolov et al.[75]).

All its virtues notwithstanding, in this work I will not use equation 3.9 for modelling the arm, but will instead now focus my efforts on developing a completely general rigid-body physics simulator into which different skeleton-tendon-muscle configurations (not even necessarily chain-like) may be inserted (as if into a virtual theater of physics). And even if the main thrust in this thesis is on models of the arm, a multi-purpose physics simulator is more useful when it comes to applications, or if focus shifts to more complex skeletal structures, such as the shoulder or ankle, or even whole body simulations. These reasons more than warrant the extra effort invested into making a general physics solver.

Movement of a single rigid body in space is fully specified by the following set of equations:

$$\begin{aligned} \frac{d\boldsymbol{x}}{dt} &= \frac{1}{m} \cdot \boldsymbol{p} \\ \frac{d\boldsymbol{p}}{dt} &= \boldsymbol{F} \\ \frac{d\boldsymbol{L}}{dt} &= \boldsymbol{\tau} \\ \frac{d\boldsymbol{R}}{dt} &= \boldsymbol{\omega}^* \cdot \boldsymbol{R} \end{aligned} \tag{3.10}$$

where m is the mass of the object, $\boldsymbol{x}$ is the position of the center of mass (COM) in an inertial "world" frame, $\boldsymbol{p}$ is the linear momentum, $\boldsymbol{L}$ is the angular momentum and $\boldsymbol{R}$ is the orientation tensor for the object with respect to the inertial frame. Forces and torques affecting the object at its COM are represented by $\boldsymbol{F}$ and $\boldsymbol{\tau}$ respectively. The only remaining variable is the angular velocity matrix, $\boldsymbol{\omega}^*$, which is defined by the following expression[279,16]:

$$\boldsymbol{\omega}^* = \begin{bmatrix} 0 & -\omega_z & \omega_y \\ \omega_z & 0 & -\omega_x \\ -\omega_y & \omega_x & 0 \end{bmatrix} \tag{3.11}$$

construed, as a convenient way to find the time derivative of the orientation tensor, by rearranging the elements of the angular velocity vector, $\boldsymbol{\omega}$, which is defined by:

$$\boldsymbol{\omega} = \boldsymbol{I}^{-1} \cdot \boldsymbol{L} \tag{3.12}$$

where the inertia matrix, $\boldsymbol{I}$ may conveniently found using the relation:

$$\boldsymbol{I} = \boldsymbol{R} \cdot \boldsymbol{I}_{Body} \cdot \boldsymbol{R}^T \tag{3.13}$$

in which $\boldsymbol{I}_{Body}$ simply is the inertia body tensor.

Two additional expressions are useful to know during interactions with other objects, but are not essential for describing movement in the free floating rigid body, these are the linear acceleration $\boldsymbol{a}$ and the angular acceleration, $\boldsymbol{\alpha}$:

$$\begin{aligned} \boldsymbol{a} &= \frac{1}{m} \cdot \boldsymbol{F} \\ \boldsymbol{\alpha} &= \boldsymbol{I}^{-1} \cdot \boldsymbol{\tau} \end{aligned} \tag{3.14}$$

Although these equations almost go without introduction as they are so well known in physics, some comments are nevertheless necessary. These equations fully describe movement of a rigid body in a simple and straightforward manner and are easily implemented in a computer simulation. The real challenge is to find a representation of the forces and torques which correspond nicely with what is found in the vertebrate skeleton. In particular, it is important to specify the way in which muscles produce force, and to specify the attachment points at which they are going to affect the system. Also it is necessary to identify and compute the joint forces (ligament forces) that hold the limbs together. Finally it is necessary to specify each limb's mass, dimensions and inertia tensor.

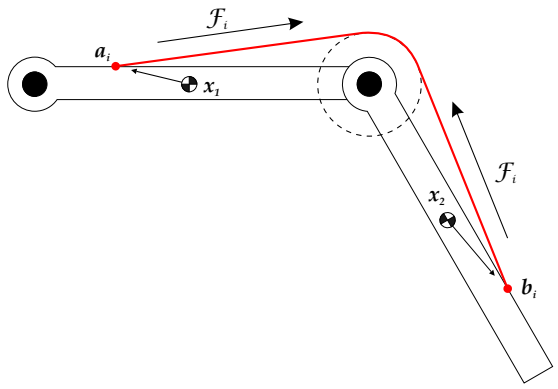

Figure 3.3: Example of muscle lines of action (see text for details).

3.2.2 Muscle forces and torques

In a later section an empirically accurate and structurally based model of striate muscle force will be derived, but for the time being let us assume that we already have such a model, $\mathcal{F}_k$, which represents the total magnitude of the force produced by the k^{th} muscle, and which is a function of muscle length, $\mathcal{L}_k$, muscle contraction velocity, $\mathcal{V}_k$, and the level of neuromuscular activation, $\mathcal{A}_k$. (see equation 9.4 in section 9.4 for the full model). The muscle will be pulling with equal force on the attachment points but along different lines of action determined by the geometrical configuration of the muscle and limbs (see diagram on figure 3.3). The force applied to the attachment point $\boldsymbol{p}_{ik}$ on the i^{th} limb by the k^{th} muscle may be expressed as:

$$\boldsymbol{f}_{ik} = \mathcal{F}_k \cdot \boldsymbol{n}_{ik} \tag{3.15}$$

where $\boldsymbol{n}_{ik}$ is the normal vector corresponding to the line of action.

Any force that is applied to a rigid body will also produce a torque except if the force is applied directly at the COM. The moment arm associated with the k^{th} muscle, $\boldsymbol{h}_{ik}$, is a vector pointing from the center of mass of the i^{th} limb to attachment point on that limb pertaining to the k^{th} muscle, $\boldsymbol{p}_{ik}$. With this, the torque, $\boldsymbol{\tau}_{ik}$, produced by the k^{th} muscle around the i^{th} limb's COM may be calculated directly:

$$\boldsymbol{\tau}_{ik} = \boldsymbol{h}_{ik} \times \boldsymbol{f}_{ik} \tag{3.16}$$

while the total force transmitted to the i^{th} limb's COM is simply $\boldsymbol{f}_{ik}$. If we have a set of muscles, $\{k\}$ attached to the i^{th} limb, then the total resulting torque on this limb is simply the sum of the torques produced by each individual muscle, and the total resulting force at the COM will likewise be the sum of all contributions from individual muscles:

$$\begin{aligned} \boldsymbol{\tau}_i &= \sum_{\{k\}} \boldsymbol{h}_{ik} \times \boldsymbol{f}_{ik} \\ \boldsymbol{f}_i &= \sum_{\{k\}} \boldsymbol{f}_{ik} \end{aligned} \tag{3.17}$$

3.2.3 Joint forces and ligaments

Even in the absence of active muscle forces, the skeleton is held together and protected against damage by complicated mechanical structures. Joints and ligaments are passive with respect to force production in that they only produce force as a reaction to externally imposed limb configurations. Ligaments are made of collagen and elastin, and act as elastic bands holding together the limbs against pulling forces, while the cartilage and synovial fluids at the joint junctions acts as a Voigt elements against inter limb contact forces (reducing damage caused by friction or sudden loads). For some applications it is relevant to identify each and every individual force component at the joint, mapping out all ligaments, their elasticity and damping coefficients and the volumetric damping/elastic effects at synovial joints. This would be the case if we were studying the effect of varying loads on the wear and tear on the joints (ergonomics, prosthetics), or perhaps to specify optimal training exercises for arthritic patients, or other similar subjects. In the present case, we are only concerned with joint forces insofar as they maintain structural stability in the arm. In the lack of precise quantitative data specifying the geometry and elastic coefficients of ligaments and joints, there are two good ways to proceed: 1) Absorb all joint force contributions into a simple damped elastic element with a non-zero resting length, 2) Calculate directly the forces necessary to hold the arm together during movement. After trying both I have opted for the second option mainly because of increased stability and numerical reliability.

To find the joint forces it is useful to break the joint accelerations up into a radial component that is parallel to the line from the center of mass of the link to the attachment point, and a tangential component that is perpendicular to this.

$$\begin{aligned} \boldsymbol{a}_i &= \boldsymbol{a}_{i-1} - \underbrace{\boldsymbol{v}_{i-1} \times \boldsymbol{\alpha}_{i-1} + \boldsymbol{r}_{C,i-1} \times \boldsymbol{\alpha}_i}_{Tangential} \\ &\quad - \underbrace{\boldsymbol{\omega}_{i-1} \times (\boldsymbol{v}_{i-1} \times \boldsymbol{\omega}_{i-1}) + \boldsymbol{\omega}_i \times (\boldsymbol{r}_{C,i-1} \times \boldsymbol{\omega}_i)}_{Radial} \end{aligned} \tag{3.18}$$

where $\boldsymbol{v}_i$ is the limb vector as defined in section 3.1, and $\boldsymbol{r}_{C,i-1}$ is a position vector from the center of mass of the i^{th} limb to its proximal joint. The total force, $\boldsymbol{J}_i$ required to maintain the i^{th} limb attached to the $(i-1)^{\text{th}}$ joint is thus:

$$\boldsymbol{J}_i = \boldsymbol{a}_i \cdot m_i \tag{3.19}$$

resulting in the following torque on the limb:

$$\boldsymbol{\tau}_i = \boldsymbol{r}_{C,i-1} \times \boldsymbol{J}_i \tag{3.20}$$

These should simply be added to the current total torque and force on the limb, and thus concludes the mechanical treatment of multi-jointed limbs.

3.3 Anthropometry

To produce a mechanically realistic model of the human arm, it is necessary to quantify some of the model parameters such as the limb's inertial properties (the I_{body} matrix), mass, length, muscle attachment points, pinnation angles

and physiological cross-sectional area (PCA). Fortunately much of the needed data is readily available from various sources (e.g. Winter[279]), and with some approximations the remaining parameters may be determined directly from the data. Of course the data will usually be an average over a larger population, so what we essentially will be modelling is a "standard" human arm. Some of the most important parameters required by the model are summarized in table 3.1.

The most difficult mechanical parameter to determine for a limb is perhaps its inertia body tensor, but there are several good algorithms for doing so, one of which only requires geometrical information about the surface of the limb. Suppose that the surface geometry of an object with homogeneous density has been converted into an equivalent polygonal mesh. Then it is possible to identify whether any given point is within or outside the volume by using the "Odd-man-in" algorithm, which essentially works on the assumption that any ray projecting out from a point within the volume of interest will *always* have to cross an odd number of surface polygons. The object should now be bounded by a box which is subsequently subdivided into N volume elements. Each and every volume element within the box is now tested with respect to whether it resides inside the volume of the object, or outside. By adding up all the volume elements that tested positive a good estimate of the total volume of the object is obtained, and the center of mass may also be determined. Furthermore, if the density (assumed homogeneous) is known then the total mass may also be found. Let the i^{th} volume element with mass μ_i have its center positioned at $\boldsymbol{r}_i$ then the center of mass for the whole object, $\boldsymbol{c}$, will be:

$$\boldsymbol{c} = \frac{1}{N} \sum_i \boldsymbol{r}_i \tag{3.21}$$

and the total mass of the object becomes:

$$m = \sum_i \mu_i \tag{3.22}$$

To calculate the body inertia tensor, the center of mass should initially be at the origin of the coordinate system within which the object is defined, so in the case that $\boldsymbol{c} \neq \boldsymbol{0}$, the object should be translated by an amount $-\boldsymbol{c}$.

The inertia tensor has the form[279]:

$$\boldsymbol{I} = \begin{bmatrix} I_{xx} & -D_{xy} & -D_{xz} \\ -D_{yx} & I_{yy} & -D_{yz} \\ -D_{zx} & -D_{zy} & I_{zz} \end{bmatrix} \tag{3.23}$$

where I_{xx}, I_{yy} and I_{zz} are moments of inertia in the x, y and z axes, respectively, and the remaining components are the products of inertia, or deviation moments. When the center of mass has been properly positioned at the origin, the inertia tensor of the object equals:

$$\boldsymbol{I}_{body} = \sum_i \begin{bmatrix} \mu_i \cdot (r_{iy}^2 + r_{iz}^2) & -\mu_i \; r_{ix} \; r_{iy} & -\mu_i \; r_{ix} \; r_{iz} \\ -\mu_i \; r_{iy} \; r_{ix} & \mu_i \cdot (r_{ix}^2 + r_{iz}^2) & -\mu_i \; r_{iy} \; r_{iz} \\ -\mu_i \; r_{iz} \; r_{ix} & -\mu_i \; r_{iz} \; r_{iy} & \mu_i \cdot (r_{ix}^2 + r_{iy}^2) \end{bmatrix} \tag{3.24}$$

where r_{ij} is the distance from the j^{th} axis to the i^{th} volume element. The methods presented here are universally applicable in the sense that any object

	Upper Arm	Forearm	Hand
Mass fraction	0.028	0.016	0.006
Length fraction	0.186	0.146	0.108
COM fraction	0.436	0.430	0.506
Density [kg/l]	1.07	1.13	1.16

Table 3.1: Summary table of normalized anthropometric data used for simulations. The mass fraction times total body mass yields the mass of corresponding limb. In a similar vein, the length fraction times the total body height yields the length of the corresponding limb. The distance from the proximal joint to the center of mass of the limb may be found by multiplying the COM fraction times the total length of the limb. All data from Winter[279].

	Upper Arm	Forearm	Hand
Proximal radius [m]	0.054	0.038	0.15
Distal radius [m]	0.042	0.028	0.15
Flatness	1.1	1.3	3
Volume [l]	2.8	1.25	0.43
Mass [kg]	2.98	1.41	0.5

Table 3.2: Parameters used for dynamic simulation of human arm calculated for a person measuring 1.9 m in height and weighing 90 kg.

can be processed to yield its inertial tensor, as long as the surface of the object is known, as well as the density of the object. In the case of the human arm, precise surface information can be gained from MRI scans. Delimiting bone surfaces and skin surfaces independently would yield the best results, but would require each link in a limb to be composed of two physically distinct model objects: A bone model and a tissue model. In the present case, however, such a level of detail is not necessary as we are looking for general rules of motor control and not specific physical details of the limbs. Anyway, for the sake of generality of the results, the model has to be based on an average human, and not on the specifics of any particular individual. A more fruitful approach is therefore to generate simplified models of the arm based on some of the average human values presented in table 3.1, because then once the motor control model is up and running, we may freely vary several critical parameters (such as the total height and weight of the person whose arm is simulated, see table 3.1) to test for generality. Note, that at any time we may return to include as precise a model of the arm as we care to simulate, all the equations and calculations will be the same.

From a dynamics point of view, a good approximation to the human arm for a person measuring 1.90 m in height and weighing 90 kg will have parameters similar to those listed in table 3.2. Unless otherwise noted, these parameters are assumed throughout the rest of this thesis.

Before ending this chapter and moving on to the determination of muscle force models *per se*, there are two additional topics which need attention: The characterization of the moment arms of upper extremity muscles which depend on the muscle attachment geometry, and the specification of physiological cross-sectional area and pinnation angles for muscle.

Muscle	Origin	Insertion	Actions
Deltoid	Clavicle, acromion process, spine of scapula	Deltoid tuberosity	Extension, flexion and abduction of humerus
Biceps, long head	Supraglenoid tuberosity	Radial tuberosity and ulna	Elbow flexion and hand supination
Biceps, short head	Coracoid process	Radial tuberosity and ulna	Elbow flexion and hand supination
Brachial muscle	Inferior 2/3 of anterior surface of humerus	Ulnar tuberosity	Elbow flexion
Brachioradial muscle	Lateral humerus	Styloid process of radius	Elbow flexion
Triceps, long head	Infraglenoid tubercle	Olecranon	Extension of forearm and shoulder adduction
Triceps, lateral head	Lateral and proximal to radial sulcus on posterior humerus	Olecranon	Extension of forearm
Triceps, medial head	Medial and distal to radial sulcus on posterior humerus	Olecranon	Extension of forearm

Table 3.3: Main flexion and extension muscles in human arm.

3.3.1 Muscle attachment geometry

There are approximately 30 muscles involved in arm control, and these may be subdivided into several functional groups depending on whether they flex, extend, supinate, pronate, rotate, abduct, or adduct the limb onto which they insert. Also, muscles may span over one or more joints, and may have widely distributed origin and insertion areas. As a first approximation only flexor and extensor muscles of the arm will be considered, and will assume point-like origins and insertions. The principal flexor and extensor muscles of the human arm are listed in table 3.3. For the computer model it is necessary to be more specific than just listing the relevant muscles: the coordinates for the muscle attachment points are required. At present we do not need to be very precise about the exact coordinates, as long as they are within a reasonable range, but it is important that the computational model allows for easily including better data when available. A very simple but general coordinate system is used to pinpoint the locations of muscle attachment points. In the previous section the COM and inertia tensor of a rigid body object were found. It was suggested that the object should be positioned so that the COM coincided with the origin of a coordinate system. If that is done, then it is possible to orient the object so that its inertia tensor only contains diagonal elements. Although that is useful from a mechanical point of view, it is not strictly necessary, and actually for the present purposes it is much more useful to orient the body so that its anatomical directions coincide with the chosen coordinate system. The following should apply:

- COM at origin
- positive x-axis points to anterior regions
- positive y-axis points to medial regions
- positive z-axis points to proximal regions

Figure 3.4 shows approximate normalized distances along the z-axis from the COM to the different attachment regions in the humerus, radius and ulna. Similar schemes may be created for the hand and scapula, and also for the remaining axes. Other coordinate systems are of course equally valid (see e.g. Nijhof and Kouwenhoven[206] for a coordinate scheme centered in the humeral head) and it is easy to make transformations between them, but for the present general physics solver system, a body-centered coordinate system like the one adopted here is best.

3.3.2 PCSA and pinnation angle

Assuming sufficient structural rigidity in narrower regions of a muscle, it seems obvious that the cross-sectional area of a muscle at its widest point determines the maximal force that a muscle can produce. Nevertheless this is not necessarily the case, unless "widest point" always is defined according to the direction of muscle fibers and not to the overall muscle geometry. It turns out that in many muscles, the direction of muscle fibers (the fibre line of action) is at an angle to the force axis of the muscle (the muscle line of action). This angle is the *pinnation* angle of the muscle, θ, and can be used to find the physiological cross-sectional area (PCSA) of the muscle given the muscle's total length, l, mass, m, and density, δ, with the formula[279]:

$$PCSA = \frac{m \cdot \cos\theta}{\delta \cdot l} \tag{3.25}$$

In non-pinnate ($\theta = 0$) muscle the PCSA can be used to estimate directly the number of muscle fibers which are in parallel with the muscle's line of action. In pinnate muscle the PCSA has a slightly different meaning: it gives the cross-sectional area that a non-pinnate muscle should have to be equivalent to the pinnate muscle. In either case, the PCSA gives a measure of the maximum force that may be produced by a muscle, and the total number of sarcomeres in a cross-section may easily be found using myological data (see, e.g. table 4.1). Typical PCSA values are listed in table 3.4 together with the average muscle fiber lengths.

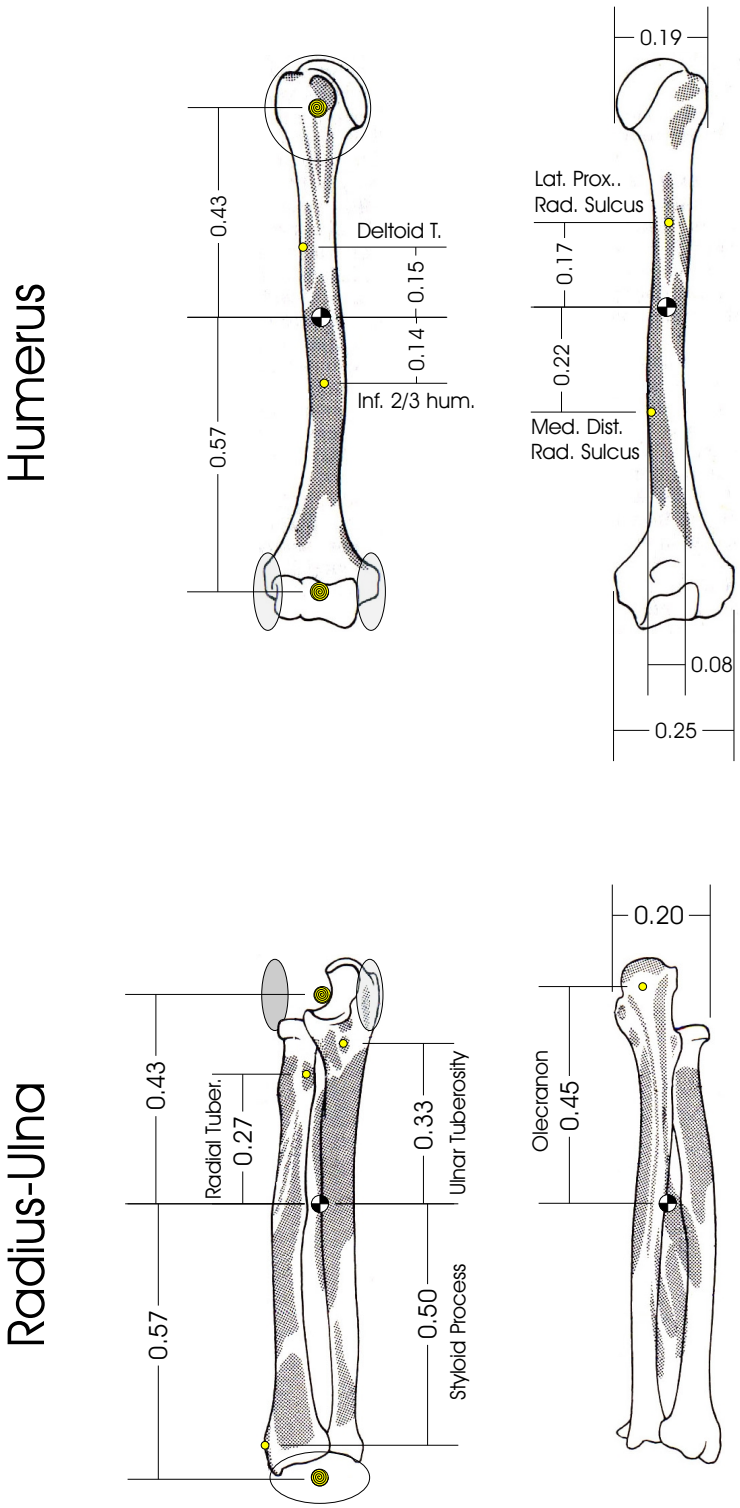

Figure 3.4: Origin and insertion point positions for various muscles, normalized to total link length of limbs (from proximal to distal joint center). In the case of wider attachment areas, the position refers to the center of the distribution. Refer to table 3.3 for the relevant muscles.

Muscle	**Abbrev.**	**Fiber Length [cm]**	**PCSA [cm^2]**
Deltoideus, acromial origin	DELA	(7.4)	13.5
Deltoideus, scapular origin	DELS	(9.6)	3.9
Deltoideus, clavicular origin	DELC	(8.1)	4.5
Pectoralis Major, clavicular origin	PMJC	(11.2)	5.2
Teres major	TMAJ	(6.8)	5.8
Triceps longum	TRIO	12.7	6.7
Triceps mediale	TRIM	9	6.1
Triceps laterale	TRIA	9.3	6.0
Biceps longum	BILH	11	2.5
Biceps breve	BISH	12.5	2.1
Brachioradialis	BRAD	19	1.5
Brachialis	BRAC	9.9	7
Pronator Teres	PROT	7	3.4
Extensor Carpi ulnaris	ECUL	(4.5)	3.4
Extensor Carpi radialis	ECRD	(4.5)	5.3
Flexor Carpi ulnaris	FCUL	(4.5)	3.2
Flexor Carpi radialis	FCRD	(4.5)	2.0

Table 3.4: Typical fiber lengths,and PCSA's for selected arm muscles. Data in parenthesis are estimates based on total muscle length. All data was compiled from An et al.[7], Fridén and Lieber[74], Nijhof and Kouwenhoven[206], Murray et al.[198].

Chapter 4

On the entropic origin of muscle force

Chapter Summary

The aim of this chapter is to present a minimal mechanical model of force production in the sarcomere which is compatible with known experimental facts while maintaining a clear connection with the underlying molecular structure. The model draws heavily on the ideas and insights gained from state-of-the-art sliding filament and lever-arm models[118,119,286] and should in part be seen as an attempt to simplify the dynamics of such models for their inclusion in large-scale whole-limb biomechanical and neurocomputational simulations. However there are also some very important distinctions between the models which lead to very different interpretations of the available experimental data. In particular it is concluded that muscle force has its origin in the conformational entropy of the myosin[†] molecule, and therefore the forces at the individual actin-myosin bonds should be described using the Worm-Like Chain model of entropic elasticity[168].

Note: The material in this chapter has been submitted for publication.

As seen in the previous chapter, it is relatively straightforward to include the geometrical aspects of muscle force in a physical model of the arm, simply based on anatomical observations. Historically it has proved much more challenging to actually describe what takes place inside muscles which permits them to produce force, and subsequently to quantify this force. One of the earliest documented and most persistent ideas about muscle force production is attributed to Erasistratus in the 3rd century B.C., who hypothesized that *pneuma* filled

up the muscle in such a way that its diameter increased while simultaneously causing a shortening of the muscle (thus contracting and causing movement) [176]. This idea was finally debunked in the 17th. century by Jan Swammerdamm, who showed that there are no volumetric changes associated with muscle contraction. Several contraction hypotheses ensued, but it took the arrival of the electron microscope to finally settle the issue by the following observation [122,120]: There are filaments in muscle which slide between each other.

4.1 Sliding filament theory

According to the sliding filament and lever-arm model [120,122], muscular force is produced as a result of the deformation or tilting [123] of a myosin head while it is forming a cross-bridge between the myosin† and the actin† filaments. Any movement parallel to the filaments of a myosin head while forming a cross-bridge to actin, will force the filaments to slide among each other and produce tension. The force interaction between thick filaments and thin filaments is thus quite analogous to an array of springs connected in parallel in that a certain number of myosin cross-bridges belonging to a thick filament will be in force-producing contact with an equal number of actin binding sites. All these cross-bridges will be pulling in the same direction, and thus each one of them will contribute with a small fraction of the total tension of the muscle, not unlike the situation that one observes in a tug-of-war (a contest where two opposing teams are pulling on a rope with the purpose of dragging the opponent team over a line).

It is in the characterization of these spring forces and in the specification of the spring-length distributions that the main differences will be found between different muscle force production models. In Huxley-type models of muscle force, linear springs are used in conjunction with complicated spring-length distributions based on Michaelis-Menten type kinetic schemes of actin-myosin bond formation. For such models to account for the different experimentally observed characteristics and dependencies of muscle force, such as Hill's force-velocity curve [107], many free parameters must be estimated, some of which subsequently have been specified experimentally, whilst others still remain as best-fit parameters.

In the present work emphasis will be given to deriving a model in which most parameters (if not all) can be directly verified experimentally, a situation which is attainable if slightly more complex spring forces are used in conjunction with very simple spring-length distributions. As will be shown in a later section, a simple expression can be derived which fully accounts for force production during different lengthening and shortening velocities. But to get there, it will first be necessary to reexamine some of the assumptions underlying sliding filament and lever-arm models, particularly with respect to the mechanical properties (section 4.2) and geometrical relations (section 4.3) that one might expect in muscle.

4.2 The mechanics of parallel spring arrays

The total tension, T_{tot}, produced by a mechanical system comprised of N springs connected in parallel is simply the sum of the partial forces, s_i, produced by

each of the springs in the array (let i be an index to the springs, so $i \in [1, N]$). Spring forces depend on the length of the spring in question, so if we let the length of the i'th spring be represented by x_i, then the force produced by the i'th spring will be $s_i = s(x_i)$. In short:

$$T_{tot} = \sum_{i=1}^{N} s(x_i) \tag{4.1}$$

where s essentially may be any real-valued function. For linear springs like those typically assumed in Huxley-type muscle models we have that $s(x) = k \cdot x$, with k as the spring constant. In section 4.5 some other (non-linear) spring force functions will be explored.

In the general case the spring lengths need not necessarily be distributed evenly within an interval, but may instead be clustered into groups whose group members share a particular length. If we let m represent the total number of such clusters, each of which shall be identified using the index j, then the total tension produced by the system can formally be expressed as:

$$\begin{aligned} T_{tot} &= n_1 \cdot s(x_1) + n_2 \cdot s(x_2) + \ldots + n_j \cdot s(x_j) + \ldots + \\ &\quad + n_{m-1} \cdot s(x_{m-1}) + n_m \cdot s(x_m) \\ T_{tot} &= \sum_{j=1}^{m} n_j \cdot s(x_j) \end{aligned} \tag{4.2}$$

where n_j indicates the number of springs with length x_j, that is the number of springs belonging to the j'th cluster. The number n_j should really be considered a function of x_j, so that $n_j = n(x_j)$. In principle, $n(x_j)$ can have values ranging from $n(x_j) = 0$, when no springs have the corresponding length, and up to $n(x_j) = N$ when all the springs have the same length (only one cluster). Because the total number of springs still is N, the following relationship must hold:

$$\sum_{j=1}^{m} n(x_j) = N \tag{4.3}$$

It is helpful to assume that the spring-length clusters are spread out evenly within the permitted interval $x \in [a, b]$ so that each corresponds to a subinterval of size $\Delta x = (b - a)/m$. An expression for the spring-length corresponding to a given cluster, j, would then become:

$$x_j = j \cdot \Delta x = j \cdot \frac{b - a}{m} \tag{4.4}$$

From this it follows that within a finite interval $x_j \in [a, b]$, we may write:

$$0 \leq a = x_1 < x_2 < ... < x_j < ... < x_{m-1} < x_m = b < \infty \tag{4.5}$$

If all the springs in the array are allowed to shorten a distance $\Delta x = (b - a)/m$, the system will have generated the following amount of work:

$$W_{\Delta x} = T_{tot} \cdot \Delta x = \sum_{j=1}^{m} n(x_j) \cdot s(x_j) \Delta x \tag{4.6}$$

Table 4.1: Summary table of geometric regularities in sarcomeres of striate muscle.

Property	**Symbol in text**	**Value**
Actin Binding Site Separation	l_{act}	~ 5.3nm
Myosin Head Separation	l_{myo}	~ 43nm
Relative M-A displacement	δ_{MA}	~ 0.6nm
Length of A-band†	l_A	$\sim 1.67\mu$m
Length of H-band	l_H	$\sim 0.25\mu$m
Length of overlap zone in sarcomere	$l_{lap} = l_A - l_H$	$\sim 1.42\mu$m
Rotational symmetry	C_{rot}	~ 6
Thick filament radius	r_{thick}	~ 20nm
Thick filament cross-sectional area	$a_{thick} = \pi r_{thick}^2$	~ 1256 nm^2
Sarcomere radius	r_{sarc}	~ 500nm
Sarcomere cross-sectional area	$a_{sarc} = \pi r_{sarc}^2$	$\sim 7.8 \cdot 10^5$nm^2
No. thick filaments pr. sarcomere	$n_{ts} = a_{sarc}/a_{thick}$	~ 625
No. sarcomeres pr. $1cm^2$ muscle	$n_{sm} = 10^{14} nm^2/a_{sarc}$	$\sim 1.3 \cdot 10^8$
No. filaments pr. $1cm^2$ muscle	$n_{filaments} = n_{sm} n_{ts}$	$\sim 8 \cdot 10^{10}$
Myosin heads pr. 1/2-sarcomere	$N_{tot} \sim 0.5 \cdot n_{ts} \cdot C_{rot} \cdot l_{lap}/l_{myo}$	$\sim 6 \cdot 10^5$

At the limit where $m \gg 1$, we observe that $\Delta x \to 0$, and given that the springs have lengths which are bounded to an interval in the way shown in equation 4.5, it becomes evident that equation 4.6 is a Riemann sum, and therefore the total work done by the system when contracting a small step, Δx, may be found according to the following integral:

$$W_{\Delta x} = \int_a^b n(x) \cdot s(x) \cdot dx \tag{4.7}$$

Using this result, a simple integral expression may be found for the total tension in the system, namely:

$$\begin{aligned} T_{tot} &= \frac{1}{\Delta x} \cdot W_{\Delta x} \\ &= \frac{1}{\Delta x} \cdot \int_a^b n(x) \cdot s(x) \cdot dx \\ &= \frac{m}{b-a} \cdot \int_a^b n(x) \cdot s(x) \cdot dx \end{aligned} \tag{4.8}$$

After proper specification of $n(x)$ and $s(x)$ and selection of upper and lower integration bounds, equation 4.8 becomes similar in essence to Huxley's model of force production in muscle[118].

4.3 Geometry of the sliding filaments

A large number of microscopy studies of muscle have established that there are some very consistent regularities in the molecular structure of muscle even to the extent that some regions seem quasi-crystalline in nature. Some of these regularities are summarized in table 4.1, and are represented schematically in figure 4.1.

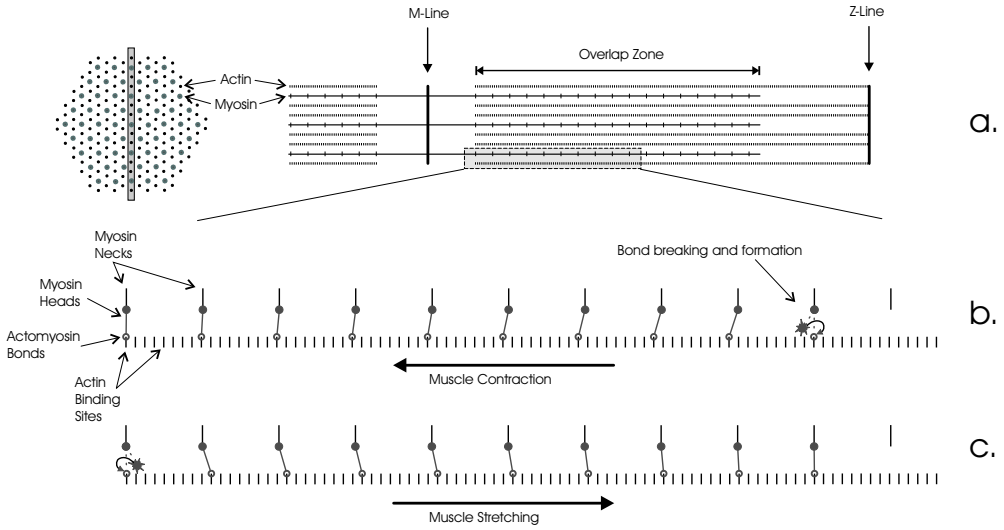

Figure 4.1: Sarcomeric structure and the origin of the relative actin-myosin binding site displacement (δ_{MA}, see text)$^{\odot}$. a) Schematic representation of sarcomeric structure (approximately drawn to scale) corresponding to the plane of section shown in the diagram to the left. b) Relative displacement of myosin and actin binding sites along a filament during contraction. See also figure 4.2I. for further details. c) Relative displacement of myosin and actin binding sites along a filament during stretching. See also figure 4.2II. for further details. In this highly schematic figure it should be noted that a gradual increase (decrease) of cross-bridge tilting angle is observed in b) and c) as one moves from left to right along a filament. A more realistic picture would allow "holes" in this sequence where no bonds have formed, and in a situation close to isometric conditions (e.g. slow contraction turning into slow stretching) perhaps even cross-bridges tilting in directions opposite to the general flow would be observed (perhaps smoothing the force-velocity discontinuity found at $v = 0$).

There are 6 myosin head series around a thick filament, where each consecutive series is displaced by approximately 14.3nm and rotated by 60 degrees with respect to the previous series. Along any one series, myosin heads are located at equal intervals of roughly $l_{myo} \sim 43$nm. If we only look at one of the 6 myosin head series (corresponding to the plane of section shown in the upper part of figure 4.1) then it may be observed that for every 43 nm that one advances along a thick filament (corresponding to the myosin head separation) we shall find that 8 A-sites have been passed plus a small extra displacement δ_{MA}. If we assume that the A-sites are positioned at intervals of $l_{act} \sim 5.3$nm this extra displacement may be found as follows:

$$\begin{aligned} \delta_{MA} &= l_{act} \cdot \left(\frac{l_{myo}}{l_{act}} - \texttt{trunc}\left(\frac{l_{myo}}{l_{act}} \right) \right) \\ &= l_{act} \cdot \left(\frac{l_{myo}}{l_{act}} - 8 \right) \sim 0.6nm \end{aligned} \tag{4.9}$$

where the $\texttt{trunc}(x)$ function simply removes the decimal part of the argument. Supposing that the first myosin neck region (MN-region) is perfectly aligned with an A-site, then the second MN-region along the filament will be offset by the distance $\delta_{MA} \sim 0.6nm$ with respect to the nearest A-site to the left, the third MN-region will be offset by $2 \cdot \delta MA$, the fourth by $3 \cdot \delta MA$, and so on. This is shown schematically in the lower part of figure 4.1. If we continue along the filaments, then after passing 9 MN-regions, the nearest A-site will be within a distance of 0.1 nm, and allowing for experimental error in the measurement of A- and MN-region distances one could easily accept that a full period has been completed after ∼9 MN-regions. In any case there can at most be approximately 16 MN-regions within the 710 nm run corresponding to the myosin head covered zone in one half sarcomere (i.e. within $L_{lap}/2$ nm, corresponding to the overlap zone in figure 4.1) so any periodicity longer than this would not fit within the allotted space. In conclusion, the minimum length difference between two bonded myosin "springs" belonging to the same periodic series on a thick filament will necessarily be $\delta_{MA} \sim 0.6nm$. If a whole thick filament with its 6-fold symmetry is considered we should obtain that the minimum value for δ_{MA} becomes less than 0.6nm because of the 14.3nm shifts between myosin series and the variations in alignment between the 6 corresponding actin filaments.

These geometrical considerations seem to indicate that in a fully activated muscle (i.e. one in which all possible cross-bridges have formed) strict geometrical constraints will be imposed on the myosin spring length distribution at the level of the individual thick filament, and in particular at the level of a single myosin series along a filament. At this level of magnification the spring-length distribution appears to be *flat*, which means that within a single period of a myosin series along a thick filament there exists exactly one cross-bridge for each possible (discrete) length.

It should be noted however that the individual myosin springs still can have any length whatsoever within the allowable interval but only if the filaments are aligned differently, e.g., following a sliding motion of the thick and thin filaments. Also, it should be noted that different thin filaments across the sarcomere cannot be expected to be perfectly aligned to each other with respect to their actin binding sites, and neither can perfect alignment be expected from the thick

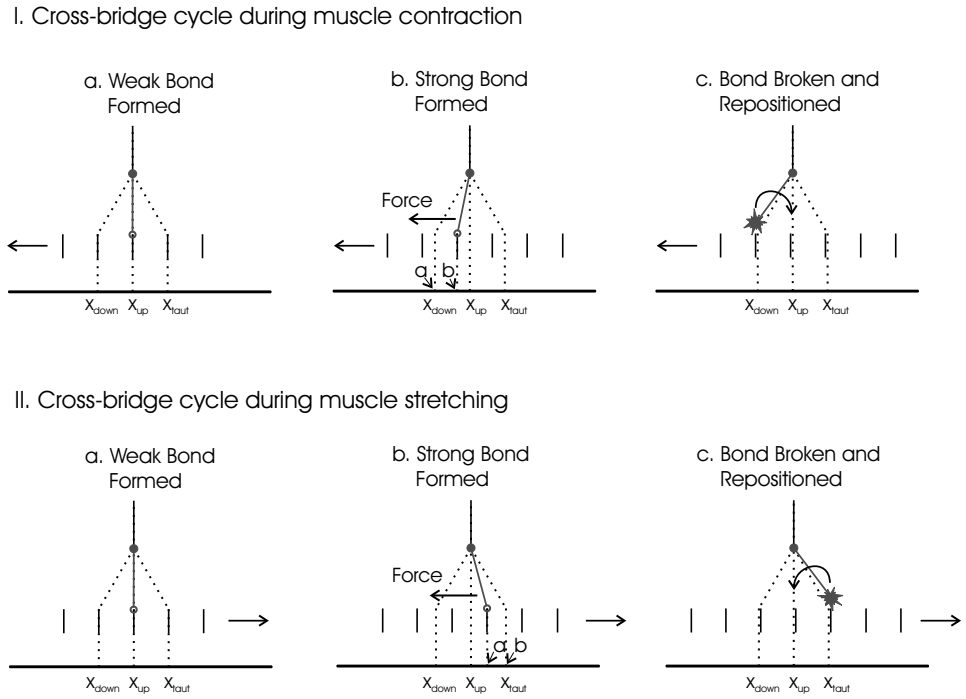

Figure 4.2: Cross-bridge cycle during muscle contraction (I) and stretching (II). For a detailed explanation see text in sections 4.4.1 and 4.4.3 respectively. The definitions of x_{down}, x_{up} and x_{taut} may be found in section 4.4.4

filaments. Given the small critical distances involved ($\sim 5.3nm$ between actin binding sites), it would not be surprising to find that, within such a short range, both thin and thick filaments are more or less randomly distributed longitudinally. So even though the single myosin series in a thick filament is severely constrained geometrically, a sufficiently large sample of fully activated thin and thick filaments would probably contain an almost continuous range of myosin spring lengths even without the sliding.

The consequences of these geometric constraints on force production depend mainly on the underlying assumptions regarding the dynamics of cross-bridge formation and the assumed effects of sliding filament velocity. In a later section (section 4.5) the possibility of a continuous range of myosin spring lengths will be used to invoke a special case related to the parallel spring force derivations of section 4.2, a case in which the number of spring length subintervals (the number m of clusters) is equal to the total number of springs, $m = N$, i.e. all springs are different and $n = 1$ (according to equation 4.3).

4.4 The cross-bridge cycle revisited

Several authoritative reviews already exist on the topic of cross-bridge cycling [78,112,216,193,212,114], so it might seem superfluous to review this topic yet again, but it is necessary in order to extract some of the features which are important

for the minimal structural model that is being advocated in this work. Also, in most previous reviews (except Proske and Morgan[216]) priority has been given to muscle contraction, while stretching muscle only has been mentioned cursorily, but because muscle force dynamics during stretching should also be encompassed by any model of muscle, three different situations will be emphasized separately in the following presentation: Contraction ($v > 0$), isometric activation ($v = 0$), stretching ($v < 0$).

4.4.1 Contraction ($v > 0$)

1. Immediately after a force producing stroke, the unbound myosin head quickly moves back to its equilibrium position which is at $x = 5.3$nm. In this stage the myosin head will be oriented perpendicularly to the thick and thin filaments (Lymn and Taylor's 90° conformation[164], Holmes' "up" conformation[111]), and will be in almost perfect alignment with an actin binding site (which was dragged there during the previous stroke), see diagram in figure 4.2Ia. The ATP binding site will be occupied by an ADP.P_i complex, thus favouring the "up" conformation of the myosin head[111] and allowing weakly binding myosin-actin interactions to take place.

2. Given the closeness of the myosin's active site to the actin binding site when in the "up" state, weak interactions (perhaps stereospecific[111]) may take place forming a weakly bonded cross-bridge, as hinted in figure 4.2Ia., but only if the tropomyosin block on the actin binding sites has been removed by an appropriate concentration of Ca^{2+}. Weak binding is reckoned to bring stronger bond forming hot-spots into better alignment (e.g. by gradually increasing contact area[220]). The probability that such a weak bond will become sufficiently stable to turn into a strong bond might depend on the sliding velocities of the filaments: The faster the sliding the lower is that probability.

3. Once a stronger bond is formed the power stroke begins when P_i is released from the ADP.P_i complex[220]. This power stroke probably occurs because some regions of the myosin undergo certain transformations which bring the protein into different energetically stable configurations which are favoured when only ADP is bound to the ATP binding site, thus producing the characteristic "tilting", "rocking" or "rowing" motion of the myosin head. This tilting motion increases the tension within the actomyosin complex in a direction parallel to the actin and myosin filaments. This situation is represented schematically in figure 4.2Ib.

4. If a sufficient number of cross-bridges within the muscle is recruited in this force producing step, then the tension will be sufficient to overcome the load imposed on the muscle, and the filaments will slide between each other shortening the muscle, and bringing the myosin head into Lymn and Taylor's 45° state[164] or Holmes' "down" state[111]. This will drag the bound actin site towards $x = x_{down}$, as defined by the coordinate system shown in figure 4.2, at which point the actomyosin tension goes to zero (the tension being a spring-like force which depends on the length of the spring, see section 4.2).

5. At some point during this contraction, but probably towards the end, the ADP will be released from the ATP binding site. The strong actomyosin bond is very stable and will remain bonded until a new ATP molecule binds to the corresponding site thus weakening the actomyosin bond. Hydrolysis of the newly bound ATP into an ADP.P_i complex favours a myosin configuration in the "up" position, and the myosin head therefore returns to the equilibrium position as soon as the weakened actomyosin link is broken. This weak bond breaking might be accomplished through a combination of the continuing contraction of the muscle (which will keep separating the myosin neck site from the actin site, see figure 4.2Ic.) and the tensile stress produced by the reconfiguration of the myosin to its stable ADP.P_i bound "up" state. Since the total distance that the filaments were displaced during this process corresponds exactly to the distance between actin binding sites, the system is now back at step 1.

4.4.2 Isometric activation ($v = 0$)

Essentially like the muscle shortening cycle, except that in step 4 it will be impossible for the filaments to slide so the actin binding site will remain at whatever distance x it had when the isometric load was imposed. Even though no mechanical work is done during isometric contractions, energy is certainly being used, so ATP hydrolysis must be taking place. This is why it must be assumed that ADP may become unbound in step 5 even before a full working stroke has been accomplished. A new ATP molecule is then bound causing changes in the myosin and weakening the actomyosin bond (the myosin now having a different energetically favourable configuration). The question now remains as to whether this weakened interaction is still sufficiently strong to maintain the myosin head in its "down" or "tilted" position when no additional sliding movement (sliding tension) is taking place, but given that the newly bound ATP might have become hydrolyzed forming an ADP.P_i complex for which a non-tilted configuration is most energetically favourable. If the weakened actomyosin interaction is stable under these circumstances and if P_i is released promptly then the "weak tilted" bond may again grow into a "strong tilted" bond (without myosin head movement) continuing the force production until the ADP is again released, at which point the cycle repeats, a continuous supply of ATP being necessary to maintain tension. On the other hand, if the weak bond is too feeble to maintain the tilted position, then the myosin head, when bound to an ADP.P_i complex, will spring back to its equilibrium position where it must remain unbound to actin because the nearest potential actin binding site is actually the one just released (according to the geometry of the system, se e.g. figure 4.2), and energy would be required for it to move back into the tilted state. So unless P_i release at the "up" position permits the myosin head to attain the "down" or "tilted" configuration *irrespective* of whether myosin is bound to actin or not, this second option would produce no force because the actomyosin link cannot be reestablished, and the muscle would have to yield.

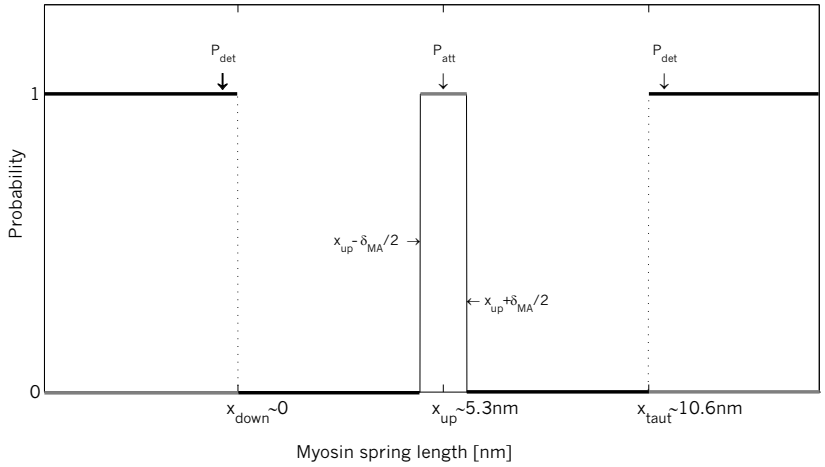

Figure 4.3: Simplified model of cross-bridge attachment and detachment probabilities as a function of myosin spring length.

4.4.3 Stretching ($v < 0$)

To begin with, this situation is like the muscle shortening cycle (see figure 4.2IIa.), but steps 3, 4 and 5 change fundamentally because the load imposed on the muscle will be larger than the tension currently produced by the muscle. This means that the myosin heads will not be allowed to move towards the "down" conformation but will instead be stretched into a "taut" state (for which $x > x_{up}$), provided the strong actomyosin bond withstands the additional strain (see figure 4.2IIb.). It is unclear what happens in this situation with the ADP.P$_i$ complex which to begin with would be bound to the ATP site (starting in step 3), but it might actually remain bound in which case the following scheme would apply: At some point the tensile stress produced by stretching the muscle becomes so large that it forcibly breaks the actomyosin bond (as hinted in figure 4.2IIc.), and when this happens the myosin-head will return to its most energetically favourable configuration which, given that ADP.P$_i$ is still bound, means the non-tilted "up" conformation. The system is then essentially back at step 1, which means that a link to actin might be formed, and the cycle may repeat without adding ATP. However, it might also be possible that the myosin heads sometimes "overshoot" the equilibrium position, where they release their ADP, and subsequently rebind ATP which is then hydrolyzed to the "up"-seeking ADP.P$_i$-bound myosin complex.

4.4.4 The bare essentials

The following is an attempt to give a simplified mechanically oriented description of the just reviewed cross-bridge cycle at different velocities which ties in well with the analysis made in sections 4.2 and 4.3. Because it is a mechanical treatment, emphasis will be on the position of the myosin heads and their potential for force production in different situations. The model assumes that the force producing interaction between thick and thin filaments can be modelled as a parallel spring array or a tug-of-war, and the conformational changes oc-

curring in the actomyosin complex are directly associated with changes in the length of the springs in this array.

First of all it should be noted that there are three critical myosin head positions involved in the reduced cross-bridge cycle, and these are defined as follows:

x_{down} Myosin bond release point. This corresponds to the most energetically favourable position of the myosin head when the ATP-site on actomyosin is empty or only bound to ADP (the "down" position). The actin-myosin bond transforms from a strong to a weak bond if an ATP molecule binds to actomyosin, at which point the myosin heads might release their hold on actin. In the present model $x_{down} = 0$ and is by definition the origin of the coordinate system which measures the myosin spring length, which means that the total spring force here becomes $s(x_{down}) = 0$.

x_{up} Myosin bond creation point. This corresponds to the most energetically favourable position of the myosin head when an ADP.P_i complex is bound to it (the "up" position). In this state the myosin hot-spot and the passing actin binding sites can come into perfect apposition thus giving optimal conditions for bond formation. Shortly after actomyosin bonding, P_i is released and the power stroke begins with an initial spring force defined as: $s(x_0) = s(x_{up} - x_{down}) = s(x_{up})$. Typically $x_{up} = 5.3$nm because this corresponds to the step size at which myosin moves along an actin filament[139].

x_{taut} Myosin bond breaking point. The maximum attainable length by the myosin cross-bridge beyond which the actomyosin bond will be forcibly broken due to the tension imposed on the bond. After bond-breaking the myosin head will swing back to x_{up}. Current experimental estimates set x_{taut} in the range 10 to 15nm[29].

There are also several critical time constants involved in cross-bridge cycling, two of which are essential for the TOW-model and are defined as follows:

τ_{weak} Weak-bonding time constant, related to the actin-myosin confrontation time that is required for a weak bond to form and stabilize.

τ_{strong} Strong-bonding time constant, related to the time delay that exists between the formation of a stable weak bond and the release of P_i from the ADP.P_i complex associated with the initiation of the power stroke.

And finally there is the dependency of the attachment/detachment dynamics to the myosin head position. One of the basic assumptions of Huxley's original model[118] is that the rate of cross-bridge formation and breaking depends on the position of the myosin binding site with respect to the actin binding site. In the two-stage model[119] high rates of cross-bridge formation are assumed to occur only when the position, x, of the M site with respect to the A site, is within a limited interval of width d. Outside of this interval there is a high rate of detachment. Other recent models[100,286] are based on similar assumptions, and also work with a varying distribution of myosin spring lengths. The spring forces in these models are assumed to depend linearly on length.

In a similar vein, the present model also assumes that cross-bridges have a high attachment probability within an interval and a low attachment probability

outside, but in the present case this interval is very narrow (of width $\sim \delta_{MA}$ in figure 4.3) and centered around x_{up}. This means that all myosin springs start out with the length $x_{up} \pm \frac{1}{2}\delta_{MA}$, and the only way in which their length can change is by filament sliding. Once formed, the cross-bridge remains stable as long as the myosin spring length stays in the working interval $x \in [x_{down}, x_{taut}]$ within which the detachment probability is close to zero. Outside the working interval the detachment probability is close to one (almost certain detachment). A direct consequence of this approach is that the shortest possible power stroke is of length $x_{up} \sim 5.3$nm, which indeed seems to be the case at least in some experimental preparations[139]. These probability relations are schematized on figure 4.3. The view presented here differs somewhat from views stating that cross-bridges are continuously attaching and detaching at high rates, but is well in accordance with recent optical-tweezer experiments which show relatively long-lasting (1-100ms) attached states for the S1 myosin-actin bond, as can be inferred from the long lasting reductions in the variance of brownian motion during the attached state[268].

4.4.5 Cross-bridge formation vs. sliding velocity

As stated previously, it seems reasonable to assume that a certain latency is associated with the attachment and detachment processes related to cross-bridge formation. The actin-myosin confrontation time that is required for formation of weak-bonds, τ_{weak}, sets an upper limit to the speed with which the thick and thin filaments can slide over each other while still permitting cross-bridge formation. If the sliding speed is too high, cross-bridges will simply not have time to form (this reasoning applies to muscle contraction and stretching alike). The total available time for weak-bond formation (call it t_{avail}) can be found from the sliding velocity if it is assumed that weak-bond formation requires that the distance between actin and myosin active sites is less than a critical "weak-interaction" distance, δ_{weak}. From this the total time that the actin-myosin binding sites are within interacting range of each other (i.e. the time it takes for the actin binding site to traverse the interaction range of the myosin head) can be found as follows:

$$t_{avail} = \frac{2 \cdot \delta_{weak}}{|v|} \tag{4.10}$$

The coefficient, 2, stemming from the fact that the interaction window will have a width equal to $2 \cdot \delta_{weak}$. Note that the absolute velocity is used, because the possibility of actin-myosin interaction is assumed symmetric in both directions (contraction and stretching). The usual convention (see e.g. McMahon[176]) is to let the sliding velocity, v, be positive ($v > 0$) during contraction, and negative ($v < 0$) during stretching in a reference frame given by the muscle fiber.

At the maximal contraction velocity the minimum available time for weak-bond formation under contraction can be found:

$$t_{min} = \frac{2 \cdot \delta_{weak}}{v_{max}} \tag{4.11}$$

For simplicity, it may be assumed that the minimum available interaction time is

related to the actin-myosin confrontation time through a single constant, thus:

$$\tau_{weak} = \kappa \cdot t_{min} = \kappa \cdot \frac{2 \cdot \delta_{weak}}{v_{max}} \tag{4.12}$$

where κ currently is an arbitrary constant, but which at some point could be determined experimentally (κ is important in determining the yielding velocity during stretching, but is otherwise relatively innocuous).

The probability that a weak bond will *not* form because of insufficient time is proportional to the ratio between the required time and the time available, τ_{weak}/t_{avail}, the less time that is available the higher will be the probability that the bond is "missed". Alternatively, this means that the probability that the bond actually forms, p_{bond}, can be defined as:

$$p_{bond} = 1 - \frac{\tau_{weak}}{t_{avail}} \tag{4.13}$$

which when substituting with equations 4.10 and 4.12 becomes:

$$p_{bond} = 1 - \frac{\kappa \cdot \frac{2 \cdot \delta_{weak}}{v_{max}}}{\frac{2 \cdot \delta_{weak}}{|v|}} = 1 - \kappa \cdot \frac{|v|}{v_{max}} \tag{4.14}$$

If we let N_{tot} be the total number of myosin heads in a given segment of the sarcomere, then the number of fully formed cross-bridges, N_{cb}, will depend on the bond formation probability:

$$N_{cb} = p_{bond} \cdot N_{tot} \tag{4.15}$$

As stated in previous sections and shown in figure 4.3 the present model assumes that once formed the cross-bridge will remain bonded until sliding brings the cross-bridge to one of its unbinding positions x_{down} or x_{taut}, this means that the actual number of force producing cross-bridges at any time is identical to N_{cb}. We may then conclude that the total number of cross-bridges that are available for force production at any given time depends only on the instantaneous sliding speed of the muscle filaments (and is independent on sliding direction) . This, of course, is under the assumption that the muscle is fully activated (i.e., sufficient amounts of Ca^{2+} is present intracellularly to displace the tropomyosin from the actin binding sites on the actin filament).

4.4.6 Velocity dependent spring length distribution interval

According to the cross-bridge cycling scheme presented earlier, there will be a time delay, τ_{strong}, which lasts from the formation of a stable weak bond until the release of the P_i from the ADP.P_i complex usually associated with the initiation of the power stroke. When actin and myosin filaments slide among each other during continuous elongation or shortening of the muscle, existing cross-bridges will be affected by a tensile stress which might cause changes in their configuration length. Seen in combination with the time delay, τ_{strong}, this means that from the moment that a weak bond has formed until force is actually produced by the cross-bridge a lapse of time will pass during which the length of the corresponding "myosin-spring" will be changing but without doing any work.

After the delay, the myosin-spring will start producing force corresponding to whatever length it was pulled to during the delay. The displacement induced by sliding will have the net effect of changing the distribution of myosin-spring lengths depending on the sliding velocity's magnitude and direction.

The total filament displacement, dx, that is possible within the delay time τ_{strong} when filaments are sliding at a fixed velocity v is:

$$dx = -\tau_{strong} \cdot v \tag{4.16}$$

where the negative sign indicates that contraction ($v > 0$) is associated with a shortening of the myosin-springs whereas stretching ($v < 0$) is associated with lengthening myosin-springs (see section 4.3). For the maximal contraction velocity, v_{max}, we get:

$$|dx_{max}| = \tau_{strong} \cdot v_{max} \Leftrightarrow \tag{4.17}$$

$$\tau_{strong} = \frac{|dx_{max}|}{v_{max}} \tag{4.18}$$

If we substitute this expression into equation 4.16 the following simple relationship between velocity and filament displacement is obtained:

$$dx = -|dx_{max}| \cdot \frac{v}{v_{max}} \tag{4.19}$$

where dx_{max} as a first simplification may be set equal to the maximal possible displacement during contraction (i.e. from x_{up} to x_{down}). Finally, given that all myosin-springs start out with a length of x_{up}, the effective initial length, x_{eff}, of the springs when force production starts will be determined by the following relationship:

$$x_{eff} = x_{up} + dx = x_{up} - \frac{v}{v_{max}} \cdot (x_{up} - x_{down}) = x_{up} \cdot (1 - \frac{v}{v_{max}}) \tag{4.20}$$

The permitted spring-length interval ($x \in [a, b]$) which is so essential for muscle force production according to the present model (see section 4.2) can now be specified precisely:

$$x \in [a, b] = \begin{cases} [x_{down}, x_{eff}] & \text{during contraction} \\ [x_{eff}, x_{taut}] & \text{during stretching} \end{cases} \tag{4.21}$$

4.5 TOW-model of muscle

The underlying assumption permeating this work is that muscle force is produced by a number of "myosin" springs connected in parallel and with lengths distributed evenly within some interval, all springs pulling in the same direction. As the spring lengths vary, so will the force produced by each individual spring, but the resultant parallel spring array may be considered as a single unit producing force according to equation 4.8. All in all, force production in the model presented here slightly resembles force production during a Tug-Of-War (TOW) contest (hence the name), where each individual athlete is pulling on a rope with varying strength, and where the total force produced by one team is the sum of the forces produced by the team members (all cooperatively pulling in the same direction).

Recalling the geometrical constraints found at the level of individual actin and myosin filaments (section 4.3) it seems plausible that along a single thick filament, the lengths of the myosin-springs will be distributed evenly within an interval $x \in [a, b]$. As shown in section 4.4.6, this interval is dependent on filament sliding velocity, and is specified exactly by equation 4.21. Also, after the analysis presented in section 4.4.5 it seems plausible that sliding velocity will affect the number of cross-bridges that may be recruited to produce force according to equation 4.15. And finally, given that small variations in the alignment of actin filaments within a sarcomere may well be expected, it might be supposed that all the myosin-springs within a sarcomere have different lengths, and hence an almost continuous distribution of spring-lengths within the working interval ($x \in [a, b]$) is possible. This final assumption permits us to consider the special case where the number of clusters and the number of springs is equal, $m = N$, and according to equation 4.3 this allows us to set $n = 1$. All considered, the following force production function for one sarcomere emerges:

$$T_{sarc} = \frac{N_{cb}}{b-a} \cdot \int_a^b s(x) \cdot dx \tag{4.22}$$

where N_{cb} can be found from equation 4.15 (if we let N_{tot} be the total number of myosin heads in the given sarcomere half), and where the interval $[a, b]$ is determined from equation 4.21. As before, $s(x)$ is the length dependent spring force and ideally its profile should be determined by experiment, e.g. by setting up an optical tweezer experiment designed to pull on a single cross-bridge. Although the force-length dependency in the spring force function often is assumed to be linear, recent "protein pulling" optical tweezer experiments do seem to lend support to non-linear models. In the following sections different force-length dependencies will be investigated: linear (section 4.5.1), power function (section 4.5.3) and Worm-Like Chain (WLC) model based (section 4.5.2). These different models are compared during contraction on figure 4.7.

4.5.1 Linear spring forces

A very common assumption in muscle-force models is that the force-length relationship at the cross-bridge's myosin spring is linear [121]. Although there is no *a-priori* reason to assume such linearity other than to keep the mathematics simple, there does seem to be at least some experimental evidence in favour of the linearity assumption (see e.g. figure 3c. in Molloy et al. [188]), a fact which should taken into consideration in any proposed force-length models.

In a linear force-length model, force is simply defined as the length of the spring, x, times a spring constant, k_{cb}:

$$s(x) = k_{cb} \cdot x \tag{4.23}$$

Integrating this function over the interval $x \in [a, b]$ according to equation 4.22 yields the following sarcomeric tension:

$$\begin{aligned} T_{sarc} &= \frac{N_{cb}}{b-a} \cdot \int_a^b k_{cb} \cdot x \cdot dx \\ &= \frac{1}{2} \cdot k_{cb} \cdot N_{cb} \cdot (b+a) \end{aligned} \tag{4.24}$$

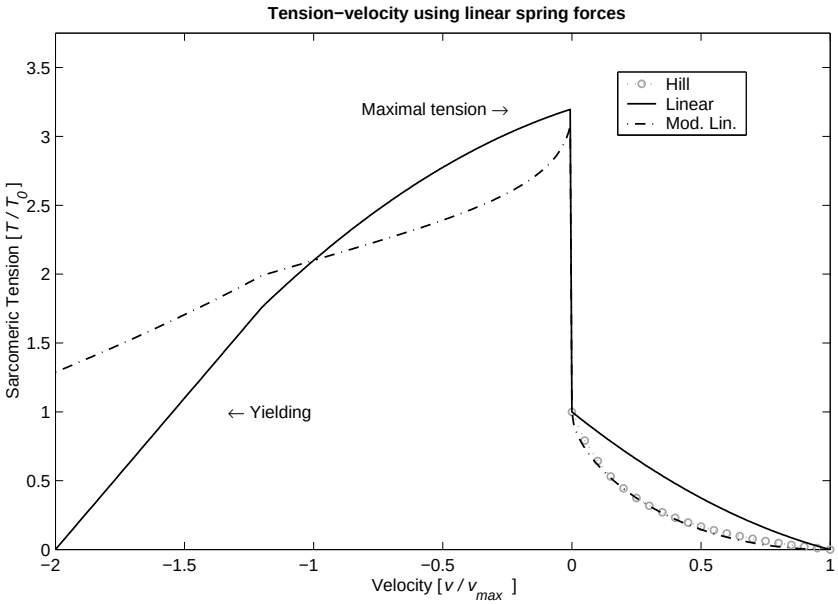

Figure 4.4: Linear force-length model. The force-velocity relationship in the TOW-model when using equation 4.24. The figure shows both the direct linear derivation and the modified linear model (in which a different cross-bridge formation probability is used that depends on the square root of velocity).

This function is plotted in figure 4.4 in conjunction with the following version of Hill's force-velocity relation (adapted from McMahon[176]):

$$T_{Hill} = \frac{(1-v)}{(1+4\cdot v)}; \tag{4.25}$$

It should be noticed in figure 4.4, that even though the individual spring's force-length relationships are linear, the parallel spring array produces a slightly non-linear force-velocity relationship which is comparable to the Hill relation. If one insists on using linear spring forces, a better fit can be obtained if one accepts the use of a slightly more complicated (non-linear) velocity dependence of the myosin cross-bridge formation probability, i.e. instead of using equation 4.14 one could use:

$$p_{bond} = 1 - \kappa \cdot \left(\frac{|v|}{v_{max}}\right)^{\alpha} \tag{4.26}$$

where α is an arbitrary constant (a good fit is obtained if $\alpha = 0.5$ and $\kappa = 1$ during contraction and $\kappa = 0.5$ during stretching, see figure 4.4). At present it is unclear whether such a dependence of the cross-bridge formation probability on the square root of the sliding velocity is warranted from a biological perspective.

Even without these additional modifications on the cross-bridge formation probability, the simple linear model is capable of reproducing several of the most important experimentally observed features of the force-velocity relationship:

- During contraction force decreases non-linearly as a function of velocity and the force becomes zero for $v = v_{max}$[107].

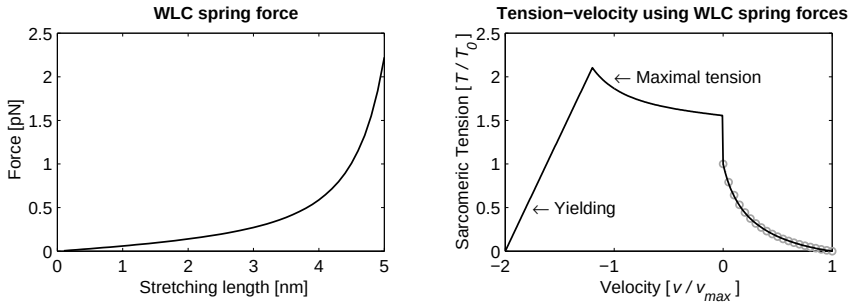

Figure 4.5: WLC (entropic elasticity) force-length model. The force-velocity relationship in the TOW-model when using equation 4.28, with $\kappa = 0.5$, $T = 310K$, $A = 20$Å, $L = 5.95$nm during contraction and $L = 13.27$nm during stretching.

- A discontinuity is present at $v = 0$ [142]
- The maximal force is approximately $3T_0$, where T_0 is the isometric tension when $v = 0$ (should be $1.8T_0$ according to Katz [134]). Theoretically the maximal force will be: $T_{max} = T_0 \cdot (x_{taut} + x_{up})/(x_{up} + x_{down})$.
- Yielding during fast stretching (described in McMahon [176]).

The isometric force in one sarcomere using the linear force model with $k_{cb} = 5.6 \cdot 10^{-4}$N/m amounts to $T_0 = 9 \cdot 10^{-8}$N if the parameters from table 4.1 are used, which for a whole muscle means an isometric force of approximately 11.7N/cm^2.

4.5.2 WLC model and entropic elasticity

As reviewed in section 4.4, most current thinking about the structural origin of force in the myosin-actin cross-bridge associates this process with conformational changes of the involved proteins (see e.g. Rayment et al. [220] and Rayment et al. [219]). Such changes in proteins are usually associated with changes in the conformational energy of their structure, and they are often accompanied by the formation and breaking of bonds (particularly hydrogen bonds) and the repositioning of hydrophobic pockets. Any work done on a protein will thus be used to overcome the energy barriers imposed by such bonds. Conversely, any work done by the protein will originate from transitions between energy states within the structure. The complexity of determining these energy transitions in a protein is closely related to the problem of determining the secondary and tertiary structure of a protein directly from the amino-acid sequence and certainly remains one of the major areas of research of the "post-genomic" era. Even so, some major advances have been made on quantifying the forces involved in protein folding and unfolding, and it is to this research we now must turn in order to identify what the author believes to be a more realistic expression for the force-length relationship in the myosin-actin cross-bridge, namely the worm-like chain (WLC) force model.

Recent technical advances have allowed experimenters to perform well-controlled stretching experiments on a wide range of macromolecules, particularly DNA

[248,35] and several different proteins (e.g. titin[137,171,247], and tenascin[207]). This is usually done by firmly attaching one end of the macromolecule to a fixed surface, while the other end is attached to a small moveable bead (manipulated magnetically or by optical tweezers) or to the cantilever of an atomic force microscope. (Attachment is accomplished by using substances which bind specifically to the investigated protein.) By pulling on one end of the molecule and then registering the force required to do so, very precise force-extension curves can be obtained. These curves are usually composed of a series of increasingly high force "peaks" appearing as the elongation proceeds (see figures in Oberhauser et al.[207], Smith and Radford[247]): initially the tension increases during elongation because of the energy barriers holding the molecule together, until a critical tension is reached at which point the least mechanically stable region of the molecule "unfolds" (as the energy barrier has been overcome for that region) and the tension plummets to zero[247]. Continued elongation will stretch the next "weakest region" towards its critical tension, and so on until the molecule has been completely extended.

The force-extension profile observed at the sub-critical force range pertaining to each folded region can be derived by observing that the work done when stretching a polymer essentially goes into reducing the conformational entropy of the structure. A statistical-mechanical analysis of the force-extension relationship in macromolecular chains is thus possible and has been given in a seminal paper by Marko and Siggia[168]. They base their analysis on the Worm-Like Chain (WLC) model (in which the linear elasticity of a thin rod is used to model the energy required for conformational fluctuations in a macromolecular chain), and they provide the following force-extension interpolation formula to summarize some of their results:

$$s(x) = \frac{k_B \cdot T}{A} \cdot \left(\underbrace{\frac{x}{L} - \frac{1}{4}}_{\text{linear}} + \underbrace{\frac{1}{4(1-\frac{x}{L})^2}}_{\text{non-linear}} \right) \tag{4.27}$$

where k_B is Boltzmann's constant, T is the temperature, A is the "persistence length" and L is the length of the "unfolded" polymer chain (the reader is referred to Marko and Siggia's paper[168] and references therein for an in-depth treatment of these variables). In what follows it will be claimed that this equation is also well suited as a model of the myosin-actin cross-bridge's force-length relationship.

Strictly speaking equation 4.27 was derived as a force-extension model for relatively rigid and straight macromolecules like DNA (where $L \gg A$), so one may question its validity in more complicated situations. Given its successful application in the sub-critical force ranges of more complicated polymers where α-helices and β-sheets are affected by the tensile forces[137,207,171,247], it does not seem so far-fetched to assume that a similar force-extension relationship might apply in the case of myosin-actin cross-bridges: The myosin filament's neck and head regions are assumed to undergo some energetically favourable (entropy increasing) conformational changes during the power stroke, so any load (stretch) counteracting this change will effectively go into reducing the conformational entropy of the myosin's neck and head regions thus giving rise to the entropic elasticity described by equation 4.27.

An altogether different difficulty with the WLC force model in the context of myosin-springs is that at first sight it might seem impossible to reconcile

the force-length relationship expressed by equation 4.27 with the commonly assumed linearity in myosin-springs. Closer inspection of equation 4.27 reveals that it actually encompasses both linear terms and non-linear terms which are dominant in different regions of the stretching variable x, so the requirement for linearity in the force-length relationship of individual myosin-springs can actually be met under some circumstances (e.g. small x or large L).

Integrating the WLC force-extension function over the interval $x \in [a, b]$ according to equation 4.22 yields the following sarcomeric tension:

$$\begin{aligned} T_{sarc} &= \frac{N_{cb}}{b-a} \cdot \int_a^b \frac{k_B \cdot T}{A} \cdot \left(\frac{x}{L} - \frac{1}{4} + \frac{1}{4(1-\frac{x}{L})^2} \right) \cdot dx \\ &= D \cdot \int_a^b \left(\frac{x}{L} - \frac{1}{4} + \frac{1}{4(1-\frac{x}{L})^2} \right) \cdot dx \\ &= D \cdot \left(\frac{b^2-a^2}{2 \cdot L} - \frac{1}{4} \cdot (b-a) + \frac{L}{4} \cdot \underbrace{\left(\frac{1}{1-\frac{b}{L}} - \frac{1}{1-\frac{a}{L}} \right)}_{\text{Hill-like terms}} \right) \end{aligned} \quad (4.28)$$

where D is defined as:

$$D = \frac{N_{cb}}{b-a} \cdot \frac{k_B \cdot T}{A} \quad (4.29)$$

The sarcomeric force-velocity function expressed by equation 4.28 has been plotted in figure 4.5, from which it seems that the WLC-based force model in combination with the parallel spring array that has been proposed in the present TOW model seems to be capable of reproducing the different features of the force-velocity relationship during stretching and contraction to a remarkable degree of precision. The presence of "Hill-like" terms in equation 4.28 means that an *exact* fit can be made to Hill's force velocity relationship (equation 4.25) during contraction. During stretching the model reproduces the yielding that is observed for high stretching velocities [176], the discontinuity at zero velocity [142] and the maximal tension of approximately $1.8T_0$ that has been observed experimentally [134,239]. (The reader is strongly encouraged to compare figure 4.5 with figure 6 in Scott et al. [239]).

The isometric force in one sarcomere using the WLC model amounts to $T_0 = 3.5 \cdot 10^{-7}$N if the parameters from figure 4.5 and table 4.1 are used, which for a whole muscle means an isometric force of approximately 45N/cm^2 (cross-sectional area). It should be noted, that the magnitude of the force depends strongly on the persistence length, A, while the form of the force-velocity curve depends on the other parameters. A persistence length of $A = 20$Å is used here, corresponding to the persistence length for titin according to Kellermayer et al. [138].

4.5.3 Power function force models

For the sake of completeness, one final section will be dedicated to exploring the properties of the TOW-model, when power functions are used to describe myosin-spring forces, thus:

$$s(x) = k_{cb} \cdot x^n \quad (4.30)$$

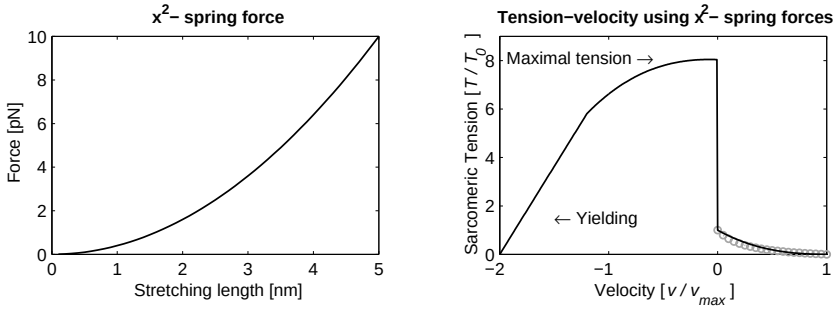

Figure 4.6: Power function force-length model. The force-velocity relationship in the TOW-model when using equation 4.31.

Integrating this function over the interval $x \in [a, b]$ according to equation 4.22 yields the following sarcomeric tension:

$$\begin{aligned} T_{sarc} &= \frac{N_{cb}}{b-a} \cdot \int_a^b k_{cb} \cdot x^n \cdot dx \\ &= \frac{k_{cb}}{n+1} \cdot \frac{N_{cb}}{b-a} \cdot (b^{n+1} - a^{n+1}) \end{aligned} \tag{4.31}$$

which for $n = 1$ reduces to equation 4.24. For $n = 2$ equation 4.31 becomes:

$$T_{sarc} = \frac{k_{cb}}{3} \cdot \frac{N_{cb}}{b-a} \cdot (b^3 - a^3) \tag{4.32}$$

This function is plotted in figure 4.6, and like the linear and WLC models, it shows all the required characteristics for a muscle contraction model: Hill-dynamics during contraction, discontinuity at $v = 0$, yielding at high stretching velocities, and the existence of a maximal tension (which in the present case gives a severe overestimate, $T_{max} = T_0 \cdot (x_{taut}^3 + x_{up}^3)/(x_{up}^3 + x_{down}^3) \sim 9 \cdot T_0$). The isometric force in this case cannot be found directly as the spring constant, k_{cb}, is not explicitly known.

4.6 Are sarcomeric forces entropic in origin?

The muscle force model presented in this chapter is based on the observation that cross-bridges along a filament generate force independently of each other and therefore the total force produced by a set of cross-bridges which pull in the same direction can be modelled as a parallel array of springs with varying lengths, or as a Tug-of-War contest with team members of varying strength. Although the model draws heavily on the ideas and insights gained from state-of-the-art sliding filament models it was seen to differ from these in several important aspects. Inspection of the molecular geometry of thick and thin filaments in the sarcomere, reveals that there are certain regularities which makes it possible to identify the spring-length distribution that must be used in the spring array. In a fully activated muscle the geometrical constraints existing between actin and myosin filaments will impose a situation where a single line of cross-bridges will have lengths that are evenly spaced out (in steps of size δ_{MA}) within an

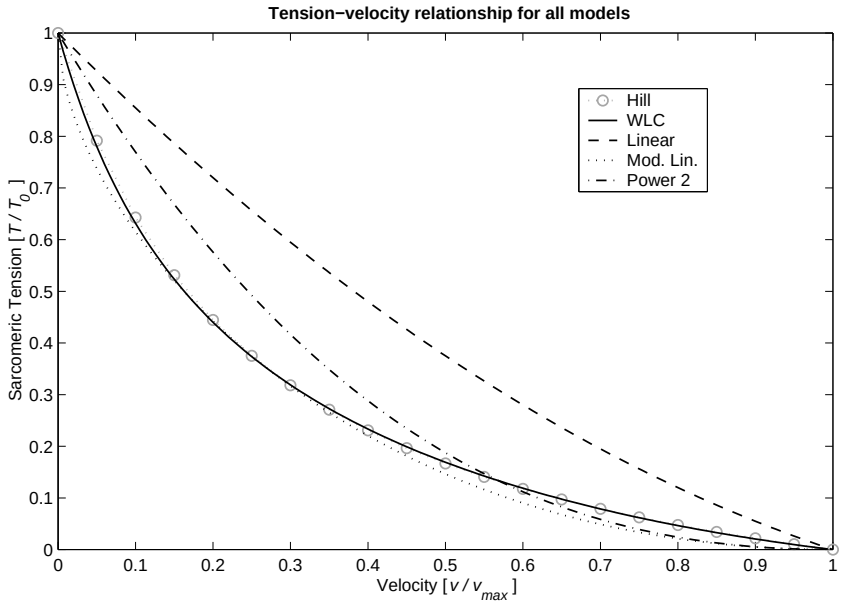

Figure 4.7: This figure shows a direct comparison of all the models and variations of models that have been presented in this work (only contractile forces shown). It should be noted that the best fit to the phenomenological Hill equation is attainable when using WLC myosin-spring forces in association with the TOW model.

interval defined by the minimum and maximum lengths of the myosin-springs at different sliding velocities. The force produced by such a simple system of parallel springs with evenly distributed lengths can be described by a simple integral, namely equation 4.8 which becomes equation 4.22 when calculating sarcomeric tension under the assumptions given in section 4.5.

There are 3 things which must be explicitly defined in order to use this equation: the lower integration bound a, the upper integration bound b and the force-extension function of the investigated myosin-springs. With respect to the integration bounds these turn out to be dependent on the filament sliding velocity in a very simple way, and can be inferred from the cross-bridge cycle. With respect to the force-extension profile of the cross-bridge springs, several functions were investigated: a) cross-bridges as linear springs (the usual assumption), b) cross-bridges as springs with entropic elasticity using WLC models and c) cross-bridges as springs depending on the n'th power of the spring's extension. To validate the different models, these were compared to the force-velocity curve generated by Hill's equation [107]. From this comparison it seems that the best (exact) fit was possible with the WLC force based model, also because this model reproduces other experimentally identified aspects of the force-velocity curve, in particular yielding at high stretching velocity and the existence of a maximum stretching force which has a magnitude twice that of the isometric force.

The fact that the TOW-model yields the best fit to the Hill equation when a WLC force is used, seems to indicate that force production in the myosin-

springs might not, in general, be linearly dependent on extension after all. Force production at the cross-bridge might actually be dependent on the entropic elasticity of the cross-bridge, entropic elasticity being a force that has its origins in the conformational energy of the myosin molecule.

4.7 Completing the sarcomeric force model

The total number of myosin heads that are participating in cross-bridge formation, N_{cb}, will directly affect the force that a sarcomere may produce according to equation 4.28. To derive this equation it was assumed (in section 4.4.5), that N_{cb} only depended on sliding velocity. In fact, the number of cross-bridges that may form during a given contraction depends on two other factors[176,57]: (1) On the intracellular Ca^{2+} concentration (required to unblock the actin binding sites) and (2) on the degree of actin-myosin filament overlap. Regarding the Ca^{2+} concentration, this is related to the activation history of the muscle fiber associated with the firing of the α-motoneuron that innervates the fiber. This is a subject which will have to await a more careful treatment of the relationship between neurons in the spinal cord, the neuromuscular junction and the motor unit, and is therefore deferred to chapter 8 section 9.3. Suffice it to say for now, that all the activation dynamics related to the muscle fibers in a particular motor unit, indexed by i, may be captured in a single variable, $\mathcal{A}_i$ which is defined in equation 9.1.

With respect to the actin-myosin overlap, this is a direct consequence of the filament sliding[90,91]. If a sarcomere is stretched beyond a certain length, the myosin-actin overlap will be gradually reduced until there is no longer any overlap between the actin and the myosin filaments, and consequently no cross-bridges may form (see figure 4.8)[176]. On the other hand, if the sarcomere is shortening, a point will be reached when one end of the actin filaments will touch the M-line, and if the shortening continues beyond this point (at a reduced force), the myosin filaments will collide with the Z-line further reducing contraction force until no further contraction may take place when the actin fiber of one compartment collides with the Z-line of a neighboring compartment [176]. These changes in the maximal isometric force produced by a muscle fiber as the length varies is known as the force-length relationship of muscle[90,91], and it is relatively simple to model this property of muscle. Let ξ be the fraction of myosin heads that are available for cross-bridge formation at different sarcomeric lengths, thus:

$$\xi = \begin{cases} y_A & \text{for } L_{sarc} > x_A \\ y_B + \alpha_{AB} \cdot (L_{sarc} - x_B) & \text{for } x_B < L_{sarc} \leq x_A \\ y_C + \alpha_{BC} \cdot (L_{sarc} - x_C) & \text{for } x_C < L_{sarc} \leq x_B \\ y_D + \alpha_{CD} \cdot (L_{sarc} - x_D) & \text{for } x_D < L_{sarc} \leq x_C \\ y_E + \alpha_{DE} \cdot (L_{sarc} - x_E) & \text{for } x_E < L_{sarc} \leq x_D \\ y_E & \text{for } L_{sarc} \leq x_E \end{cases} \tag{4.33}$$

where L_{sarc} is the total length of the sarcomere (distance between neighboring Z-lines). The constants x_A to x_E indicate the total sarcomeric lengths corresponding to the situations indicated (A. to E.) in figure 4.8, while the constants y_A to y_E similarly correspond to the normalized forces in the different situations. The slopes of the interconnecting lines are indicated by α_A to α_E. All

these constants may be extracted by inspection of experimentally obtained force-length relationships[90,91,176]. The force-length model is represented in figure 4.8 (modified from McMahon[176]), and the features to which the different constants correspond have been marked.

If it is assumed that the muscle activation factor, $\mathcal{A}$ also is normalized (see equation 9.1), then a very simple expression may be given as an estimate of the number of cross-bridges:

$$N_{cb} = p_{bond} \cdot \xi \cdot \mathcal{A} \cdot N_{tot} \tag{4.34}$$

where p_{bond} is defined in equation 4.14, and N_{tot} is the total number of myosin-heads that exist within one-half sarcomere. In a complete model of muscle force including changing muscle lengths and activation levels, this equation should be used instead of equation 4.15 when evaluating the sarcomeric force with equation 4.28.

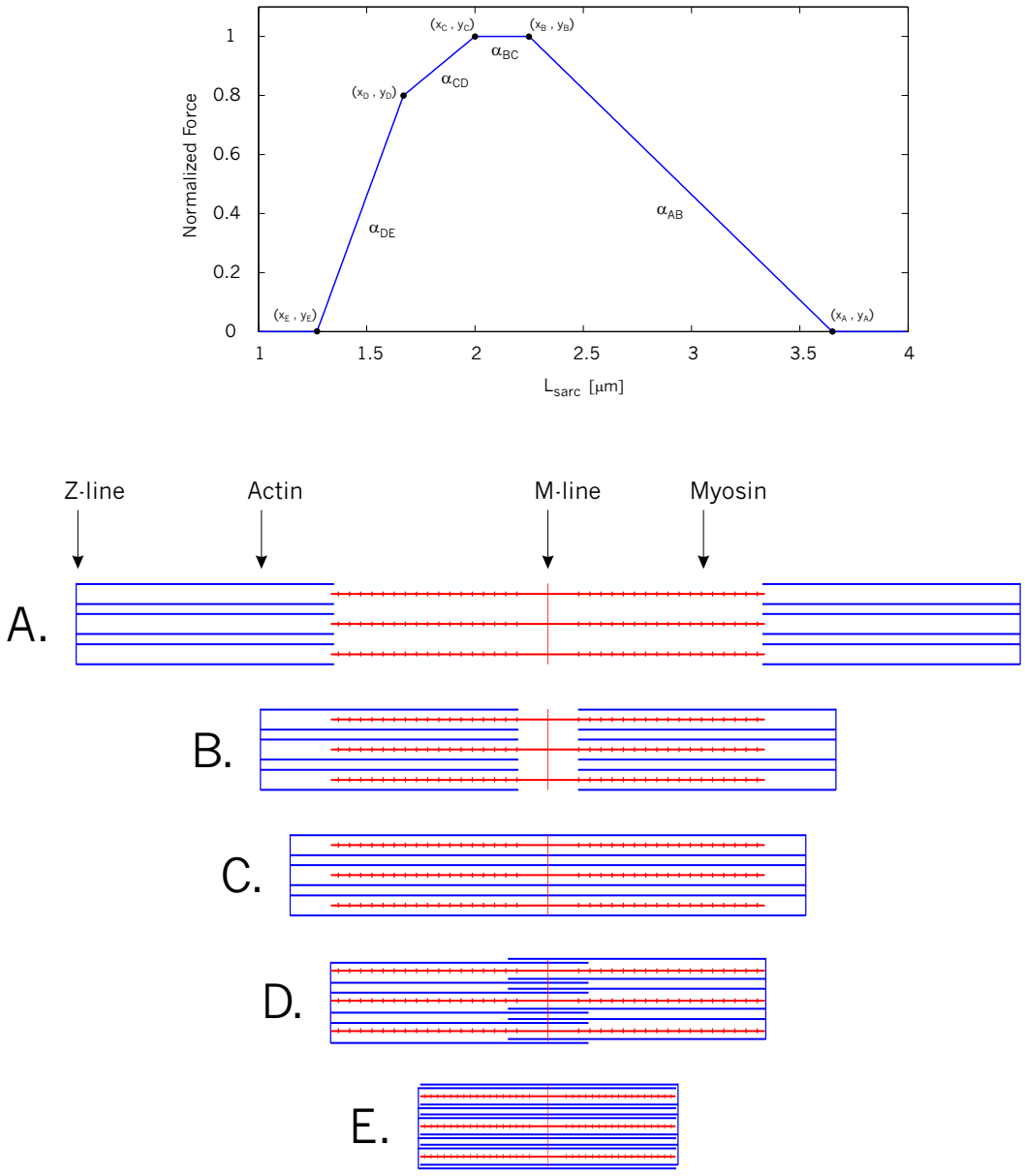

Figure 4.8: Force-length relationship in a muscle fiber. This sarcomere corresponds to a frog's semitendinosus muscle, so in order for it to correspond to human muscle it must be normalized using the optimal sarcomeric length for humans $\sim 2.8\mu$m, reported by Walker and Schrodt[269] (corresponding to situation B. in the figure). See also Murray et al.[198], Lieber and Fridén[156]. (Redrawn and adapted from McMahon[176])

Chapter 5

Neurodynamics

Chapter Summary

Various mathematical models of neuronal dynamics are reviewed in this chapter. Emphasis will be on finding models which combine four important properties within the context of large scale neural network models: Biological validity, generality, computational efficiency and ease of customization. Under these criteria, the best model tested turns out to be a neocortical neuron model developed by Wilson [274], which was therefore adopted in this thesis.

The need to increase the size of neural network simulations in order to account for increasingly complex stages of information processing in the brain, such as sensory processing or motor control, has made simplification of the underlying neural dynamics an issue of major importance. But this simplification should not be at all costs, since much can be gained by maintaining a certain level of biological realism, especially with respect to the explanatory power of our models. As the work reviewed in this section shows, it is relatively simple to create a neuron model that accounts for much physiological data quite nicely, without requiring too much complexity in the model. Needless to say, such models are ideal for the study of large scale neural networks, but more importantly these simplifications force us to ask the neurophysicist's primary question: What are the *bare essentials* of neural activity?.

5.1 Mathematical models of neural spike generation

Ever since the *neuron doctrine* took hold during the 19$^{\text{th}}$ century thanks to the likes of Santiago Ramón y Cajal and Camillo Golgi (who in fact strongly adhered to the *reticular theory*) [218], theorists have tried to develop mathematical models that could account for the properties of neural tissue. The year 1943 saw

Ion	Z	$\frac{[KA]_i}{[mM]}$	$\frac{[KA]_o}{[mM]}$	$\frac{E_{KA}}{[mV]}$
K^+	+1	400	20	$E_K = -75mV$
Na^+	+1	50	440	$E_{Na} = +55mV$
Cl^-	-1	52	560	$E_{Cl} = -60mV$
A^-	-1	385	–	–

Table 5.1: Typical concentrations and steady state potentials for the squid axon. Data from Koester[141]

a breakthrough in the neuromodelling area with the classical "McCulloch–Pitts" neuron[174], which even if very simplified and abstract did show some important properties of neuronal networks in relation to their information processing abilities. An even more important breakthrough occurred in 1952, when Hodgkin and Huxley published a paper in which they provided a full mathematical model of the neuron's action potential[108]. This model is still the standard by which other candidate models are evaluated. But the basis of it all is a property first identified by Du-Bois Raymond in the late 19^{th} century, namely the existence of a voltage difference across the neuronal membrane.

5.1.1 The Resting Membrane Potential

The *steady state* or *resting* potential across the neural membrane depends on various factors, but primarily it arises from the balance of forces between a voltage gradient and a chemical (osmotic) gradient affecting the traversing ions. The voltage gradient is maintained mainly by:

- Activity of the Na-K pump, which performs the electrogenic ATP dependent task of moving 3 sodium ions out of the cell while moving 2 potassium ions into the cell.
- Large intracellular anions which are unable to pass the membrane bilayer, and thus passively maintain an electric gradient.

The normal steady state potential for most neurons is experimentally found to be approximately $-70mV$ (negative *intracellularly* by definition), but can vary with as much as $\pm 20mV$ depending on the particular type of neuron. The steady state potential existing across a cellular membrane where only one ionic species is involved can be found using Nernst's equation if the steady state concentration is known intra- and extracellularly.

$$E_{KA} = \frac{RT}{FZ_{KA}} \ln\left(\frac{[KA]_o}{[KA]_i}\right) \tag{5.1}$$

Typical concentrations and steady state potentials for the squid axon are given in table 5.1 (data from Koester[141]).

Finding the actual resting membrane potential of a neuron requires the use of the so called *constant field*, or *Goldman, Hodgkin and Katz* equation, which also takes into consideration the permeability of the different ionic species through the neural membrane:

$$V_m = \frac{RT}{F} \ln\left(\frac{P_K[K^+]_o + P_{Na}[Na^+]_o + P_{Cl}[Cl^-]_i}{P_K[K^+]_i + P_{Na}[Na^+]_i + P_{Cl}[Cl^-]_o}\right) \tag{5.2}$$

At rest, the following permeability ratios have been found experimentally[109]:

$$P_K : P_{Na} : P_{Cl} = 1 : 0.04 : 0.45 \tag{5.3}$$

Using these permeability values in the GHK equation gives the previously mentioned resting membrane potential of $-70mV$.

5.1.2 The Action Potential

Some ion-channels have opening dynamics that depend directly on the voltage gradients across the membrane. Their opening probability is a function of the membrane potential. This happens due to voltage dependent conformational changes of their proteinic structure. At the resting membrane potential, both channels are usually closed, but a slight depolarization of the membrane (e.g., induced by applying positive current intracellularly), the opening probability of these channels change:

- The Sodium channel is very sensitive to the membrane potential. Its opening probability increases drastically almost immediately after reaching a sufficient level of depolarization (approx. $20mV$ above rest). Shortly after opening, the Na^+ channels close again, and remain closed for as long as depolarization lasts.

- The Potassium channel opens shortly after the Na^+ channel, and stays open for as long as the membrane is depolarized.

The opening and closing of voltage gated ion-channels leads to drastic changes in the permeability ratios for the involved ionic species, e.g., at the peak of the action potential it is found that:

$$P_K : P_{Na} : P_{Cl} = 1 : 20 : 0.45 \tag{5.4}$$

Note that, compared with the permeability situation at rest, the Na_+ permeability has increased ~ 500 fold. Given the concentration gradients of sodium and potassium at rest (see table above), opening of the sodium channel leads to a massive influx of Na^+ ions, thus further depolarizing the cell (a *positive feedback loop*), whereas opening of the potassium channel will lead to an efflux of K^+ ions, thereby leading to a repolarization of the membrane (a *negative feedback loop*).

5.1.3 Electrically Equivalent Circuit of a Neuron Membrane

To summarize all these insights and results it has proven very useful to rephrase them in the form of an electrical circuit analog model of the neural membrane. Here the electrical analog of an ion-channel is a serial coupling between a conductance (ion-permeability) and a battery (Nernst potential), and the analog of the bilayer membrane is a capacitor. The whole circuit would consist of a parallel coupling of one capacitor (C_m), and several conductances (ion-channel specific: g_{Na}, g_K, g_{Cl}).

The current flowing through the membrane, I_m, can at any time be found using the membrane equation:

$$\begin{aligned} I_m &= I_{capacitance} + I_{ion} && (5.5) \\ I_m &= C_m \frac{dV_m}{dt} + \\ &\quad + g_{Na}(V,t)(V - E_{Na}) + \\ &\quad + g_K(V,t)(V - E_K) + \\ &\quad + g_{Leak}(V - E_{Leak}) && (5.6) \end{aligned}$$

5.1.4 Hodgkin and Huxley's equations

A heroic effort by Alan Hodgkin and Andrew Huxley in 1952, led to a full phenomenological description of the voltage dependency of the ion-channel conductances[108]. They proposed a model where the ion-channel conductances were controlled by the gating functions n, m and h:

$$\begin{aligned} g_K &= n^4 \overline{g}_K && (5.7) \\ g_{Na} &= m^3 h \overline{g}_{Na} && (5.8) \end{aligned}$$

Where $\overline{g}_K$ and $\overline{g}_{Na}$ represent the maximal conductances of the K^+ and Na^+ channels respectively, and the n, m and h functions are defined by:

$$\begin{aligned} \frac{dn}{dt} &= \alpha_n(1-n) - n\beta_n && (5.9) \\ \frac{dm}{dt} &= \alpha_m(1-m) - m\beta_m && (5.10) \\ \frac{dh}{dt} &= \alpha_h(1-h) - h\beta_h && (5.11) \end{aligned}$$

Here $\alpha_n, \beta_n, \alpha_m, \beta_m, \alpha_h$, and β_h are empirically determined functions of the membrane potential (for a full account see Johnston and Wu[128]):

$$\begin{aligned} \alpha_n(V) &= 0.01(-V+10) / \left(e^{\frac{(-V+10)}{10}} - 1\right) && (5.12) \\ \beta_n(V) &= 0.125 e^{\frac{-V}{80}} && (5.13) \\ \alpha_m(V) &= 0.1(-V+25) / \left(e^{\frac{(-V+25)}{10}} - 1\right) && (5.14) \\ \beta_m(V) &= 4 e^{\frac{-V}{18}} && (5.15) \\ \alpha_h(V) &= 0.07 e^{\frac{-V}{20}} && (5.16) \\ \beta_h(V) &= 1 / \left(e^{\frac{(-V+30)}{10}} - 1\right) && (5.17) \end{aligned}$$

Basically this means that n and m are activation functions for K^+ and Na^+ ion-conductances respectively, while h is a deactivation function for the Na^+ ion-conductance.

Hodgkin and Huxley went on to prove that solving these equations actually leads to dynamics similar to the experimentally observable action potentials[108]. This they did using a mechanical calculator!

5.1.5 FitzHugh-Nagumo equations

Probably the simplest equations attempting to describe neural dynamics were proposed by FitzHugh[69] and Nagumo[200]:

$$\frac{dV_m}{dt} = 10\left(V - \frac{V^3}{3} - R + I_{input}\right) \tag{5.18}$$

$$\frac{dR}{dt} = 0.8(-R + 1.25V + 1.5) \tag{5.19}$$

The version presented here was adapted from Wilson[275].

5.1.6 Rinzel's simplifications of the HH equations

Hodgkin and Huxley's set of equations can be much simplified, and Rinzel[224] noted that the m function reaches its equilibrium value for most values of V so rapidly that it can be set to its equilibrium value at infinity, which is:

$$m_\infty(V) = \frac{\alpha_m(V)}{\alpha_m(V) + \beta_m(V)} \tag{5.20}$$

Thus $m(V) = m_\infty(V)$ can be substituted directly into the membrane equation. Furthermore, Rinzel noted that the time course and equilibrium values for the functions h and n permit the following approximation to be made:

$$h = 1 - n \tag{5.21}$$

So that equation 5.11, describing h, can be eliminated. Using these approximations, the neuron model can now be simplified as follows[224,274]:

$$\begin{aligned} C_m\frac{dV_m}{dt} &= I - \overline{g}_{Na}m_\infty(V)^3(1-R)(V-E_{Na}) - \\ &\quad -\overline{g}_K R^4(V-E_K) - g_{Leak}(V-E_{Leak}) && (5.22)\\ \frac{dR}{dt} &= \frac{1}{\tau_R(V)}(-R + G(V)) && (5.23)\\ \tau_R(V) &= 1 + 5e^{\left(\frac{-(V+60)^2}{55^2}\right)} && (5.24) \end{aligned}$$

Where $G(V) = R_\infty(V)$, which is a function that describes the equilibrium value of the recovery function $R(V)$. This model is actually quite similar to the neuron model proposed by Morris and Lecar[194]:

$$\begin{aligned} C_m\frac{dV_m}{dt} &= I - \overline{g}_{Ca}m_\infty(V)(V-E_{Ca}) - \\ &\quad -\overline{g}_K w(V-E_K) - g_{Leak}(V-E_{Leak}) && (5.25)\\ \frac{dw}{dt} &= \phi\frac{1}{\tau_w(V)}(w_\infty(V) - w) && (5.26)\\ m_\infty(V) &= 0.5[1 + \tanh((V-V_a)/(V_b))] && (5.27)\\ w_\infty(V) &= 0.5[1 + \tanh((V-V_c)/(V_d))] && (5.28)\\ \tau_w(V) &= 1/\cosh((V-V_c)/(2V_d)) && (5.29) \end{aligned}$$

where V_a, V_b, V_c, and V_d are arbitrary parameters (Rinzel and Ermentrout[225] use: $V_a = -1.2, V_b = 18, V_c = 2, V_d = 30$).

One final simplification (before proceeding to more complex dynamics) can be accomplished with the appropriate selection of the Na^+ equilibrium activation function $m_\infty(V)$, and of the equilibrium value of the recovery function $R_\infty(V)$. Wilson proposes to use a simple polynomial fit[275]:

$$C_m \frac{dV_m}{dt} = I - m_\infty(V)(V - E_{Na}) - R(V - E_K) \tag{5.30}$$

$$\frac{dR}{dt} = \frac{1}{\tau_R(V)}(-R + R_\infty(V)) \tag{5.31}$$

$$m_\infty(V) = a + bV + cV^2 \tag{5.32}$$

$$R_\infty(V) = d + eV + fV^2 \tag{5.33}$$

where a, b, c, d, e and f are arbitrary constants selected to fit a set of data.

5.2 Model Predictions

All of the above models were specifically created to reproduce in the simplest possible way the dynamics of spike generation, and as such have only necessitated the inclusion of two voltage-gated ion-channels. But even in their simplest form, the spike generation models presented so far permit us to make some predictions which have been experimentally confirmed, such as the appearance of *repetitive firing*, *neural hysteresis*, *post inhibitory rebound excitation*, *depolarization block*, and *bistability*.

5.2.1 Repetitive Firing

Using linear stability analysis on the above systems of equations it is possible to find some parameter domains for which the models undergo a transition from having an asymptotically stable point attractor to having stable limit cycles. It can be shown that there are several ways in which transitions to repetitive firing can occur, as summarized by Ermentrout[58]:

1. Hopf Bifurcation (Class II neurons): Oscillations with a finite initial frequency proportional to $Im\{\lambda\}$ appear at some threshold value. This is not very common in cortical neurons, but the squid axon belongs to this class.

2. Saddle-node limit cycle bifurcation (Class I neurons): Oscillations can appear at zero frequency, which is more common for mammalian neurons.

3. Homoclinic bifurcation: Similar to Class I neurons.

5.2.2 Neural Hysteresis

One of the more striking predictions arising from the presented neural models is the appearance of hysteresis in the spiking response of neurons[44,223,19]. This prediction was soon followed by experimental verification in the giant axon of the squid. This prediction of hysteresis was based on a stability analysis of the equations, which shows that for certain parameters, the system will go through a subcritical Hopf bifurcation. A consequence of this is that it becomes possible to terminate a spike train if the neuron is depolarized in exactly the right moment.

This was predicted by Rinzel[223] and later experimentally confirmed by Guttman *et al.*[101].

5.2.3 Post Inhibitory Rebound (Anodal Break Excitation)

In their seminal paper from 1952, Hodgkin and Huxley described and numerically confirmed a phenomenon they observed in the squid axon which they called *anodal break excitation*. Under some circumstances, they observed, it is possible to make a neuron fire using a brief hyperpolarizing pulse! This, of course, is very counterintuitive since usually hyperpolarization is associated with deactivation of the neuron's membrane. PIR spike generation occurs because sudden release of hyperpolarization immediately moves the equilibrium point of the system while the systems trajectory is left in a region of phase-space where spikes are normally generated.

5.3 Neural response dynamics in neocortex

Some properties of neurons cannot directly be accounted for using the simplified models introduced before, they require more advanced models, often involving the addition of several specialized ion-channels to do the job. Physiologically it has been found that neurons sometimes contain more than a dozen different types of ion-channels, all specialized for modifying the ionic environment of the neuron in special ways, and the task for the neuron modeler is now to find the minimum set of ion-channels that can account for as many different types of neuron responses as possible. Several successful attempts in this direction have been made[225,274]. There are at least 4 types of neural response dynamics in cortex that should be accounted for, and they are (as classified in Connors and Gutnick[43], Gray and McCormick[96]):

- Regular Spiking Neurons: Begin firing at a high rate, but within 100ms rate is lowered due to spike frequency adaptation.
- Fast Spiking Neurons: Have firing rates in the 400-800 Hz range, and show no frequency adaptation.
- Continuously Bursting Neurons: Produce periodic short bursts of activity for as long as stimulation is present.
- Intrinsic Bursting Neurons: Start with a burst containing 2-6 spikes, but after a pause become tonic.

To account for these dynamics, it has been found useful to add at least two more ion-channels to the standard models[225]: an extra depolarizing Ca^{2+} channel and a Ca^{2+} sensitive hyperpolarizing K^+ channel.

5.3.1 Simplified model of human neocortical neurons

In a recent article, Wilson[274] proposes a minimal model of the neocortical neuron which *does* account for the four previously mentioned types of neural response dynamics (RS, FS, IB, and CB). His model includes an extra depolarizing I_T current based on a Ca^{2+} channel with activity $T(V)$, and an after-hyperpolarization current I_{AHP}, based on a Ca^{2+} sensitive hyperpolarizing K^+

channel with activity $H(V)$.

$$\begin{aligned} C_m \frac{dV_m}{dt} &= I - m_\infty(V)(V - E_{Na}) - R(V - E_K) \\ &\quad -g_T T(V - E_{Ca}) - g_H H(V - E_K) \quad (5.34) \\ \frac{dR}{dt} &= \frac{1}{\tau_R}(-R + R_\infty(V)) \quad (5.35) \\ \frac{dT}{dt} &= \frac{1}{\tau_{Ca}}(-T + T_\infty(V)) \quad (5.36) \\ \frac{dH}{dt} &= \frac{1}{\tau_{CaK}}(-H + 3T) \quad (5.37) \\ m_\infty(V) &= a + bV + cV^2 \quad (5.38) \\ R_\infty(V) &= d + eV + fV^2 \quad (5.39) \\ & \quad (5.40) \end{aligned}$$

where $a = 17.8$, $b = 47.6$, $c = 33.8$, $d = 1.24$, $e = 3.7$, and $f = 3.2$

Accounting for Neocortical Dynamics

Regular and fast spiking neurons: Simulation with this model leads to the conclusion that the "magnitude of spike frequency adaptation can be controlled by the parameter g_H" in equation 5.34 "from none up to a point where firing ceases entirely". The time constant τ_R appears to be essential for the control of the spike width, and it permits shifting from the RS state to the FS state simply by reducing it, e.g. from 4.2 to 1.5 ms.

Continuously Bursting Neurons: With appropriately selected parameters, the model permits CB dynamics. Why this is so can be seen if the Na^+ contribution, represented by m_∞, is removed. It appears that under the right conditions a Hopf bifurcation can occur solely based on the I_T and I_{AHP} currents. This means that it is now the spikes generated by the Ca^{2+} ion-channel that drive the bursting.

Intrinsic Bursting Neurons: With appropriately selected parameters, IB dynamics can also be demonstrated by the Wilson's model. Following a similar analysis as for the CB neurons, it can be shown that in the parameter range where IB dynamics appear, the system's steady state is an asymptotically stable spiral point, suggesting that the I_T and I_{AHP} mediate a heavily damped oscillation.

5.4 High level effects of low level dynamics

5.4.1 Short Term Memory

The last topic in this review will be a brief look at a possible neurodynamical mechanism that accounts for the existence of so called *memory cells*, believed to be the neural correlate of working memory[76]. An often used experimental task for studying short-term, or working memory is the *delayed matching to sample* task. The task is as follows:

1 A brief sample stimulus is shown (e.g., a red light).

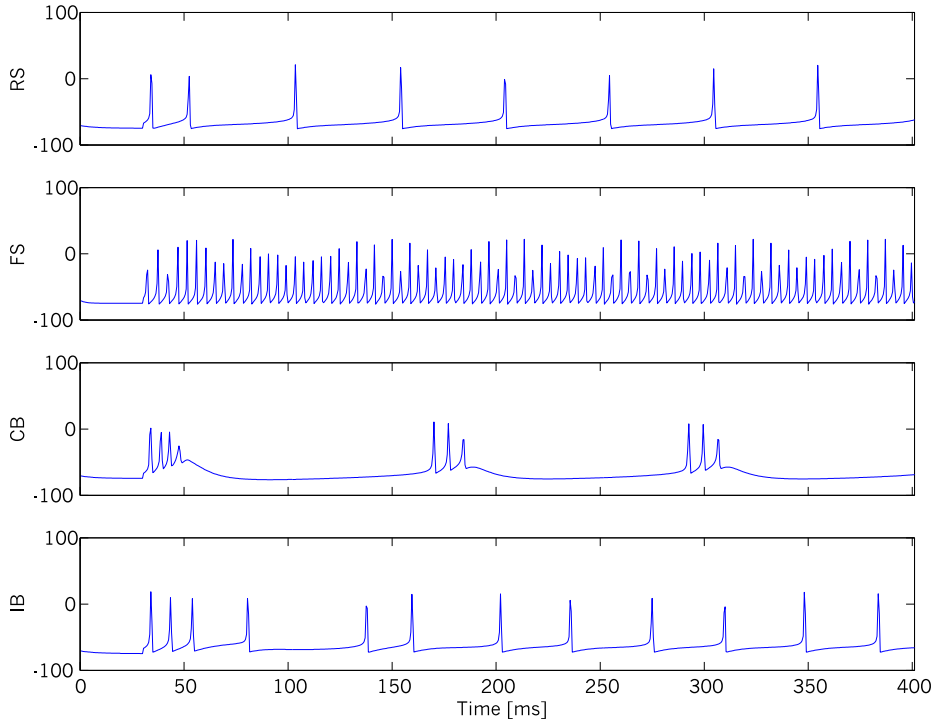

Figure 5.1: Spiking patterns for different parameter regimes of Wilson's model of neocortical neurons. The 4 different spiking patterns, RS, FS, CB and IB are readily identified.

2 After a variable delay, a signal is given prompting the experimental subject to select amongst two or more target samples, one of which is identical to the initial sample stimulus (e.g., a red and a green light).

In the *delayed matching to sample*, the correct response is to select the identical sample after the delay. In a very similar setup called *delayed* non-*matching to sample* the correct response is to select the *new* sample. Some neurons in the inferotemporal cortex of awake and behaving monkeys doing the matching task respond specifically to the presentation of a particular stimulus (e.g., a red sample), *even during the intervening delay*, indicating that activity of such neurons corresponds to a *memory trace* of recent events (e.g., the identity of the initial sample).

In principle, there are several plausible activation scenarios which would account for such *memory neurons*. The trivial solution of course being that it receives activation from elsewhere. Given the fact that during the delay the target stimulus is not present, this is probably not the case. A more intriguing solution involves the existence of bistable neurons, that is neurons that are either firing repetitively or remain completely quiet. Such neurons can be moved from one state to the other simply by giving a small stimulation at an appropriate time. An even more advanced solution involves setting up a two neuron network with reciprocal positive feedback. Consider the network[275]:

$$\frac{dV_1}{dt} = \frac{1}{\tau}\left(-V_1 + \frac{a(bV_2)^2}{c^2 + (dV_2)^2}\right) \tag{5.41}$$

$$\frac{dV_2}{dt} = \frac{1}{\tau}\left(-V_2 + \frac{a(bV_1)^2}{c^2 + (dV_1)^2}\right) \tag{5.42}$$

where a, b, c and d are arbitrary parameters.

With appropriately selected parameters, such networks can be shown[275] to have 3 steady states (by finding intersections between the isoclines). Closer analysis reveals cases where two such states can be asymptotically stable nodes, while the third is a saddle node. If one of the asymptotically stable nodes is at $E_1 = 0$ and $E_2 = 0$ and the other is at $E_1 > 0$ $E_2 > 0$, the network will be either quiet or active with a finite frequency, as required for explaining memory neurons.

5.4.2 Henneman's size principle

Most contemporary models of neural spiking are neuron size invariant because the equations have been normalized with respect to surface area by appropriate selection of the dimensions pertaining to constants and variables. Thus capacitances and ionic conductances are thus usually specified pr. cm^2, reflecting the assumption that ionic channels exist at certain densities in the neural membrane. In most cases this approach is quite appropriate because no distinction is necessary concerning the *size* of the neuron. But at least in one case this size invariance becomes problematic, namely during the orderly recruitment of motoneurons in the spinal cord with increasing input strength. Henneman and co-workers have observed that neurons with low conduction velocities (CV) start spiking earlier than neurons with high CV's during ramp increases of input to these neurons[105]. This effect has been attributed to the physical size of the

neurons simply because CV is proportional to the axonal diameter, which again is proportional to the neuron's size.

One very simple way to overcome this limitation of size invariant neuron models is to specify input currents (synaptic or electrode) as currents pr. neuron area (cm^2), just like all the other ionic currents of the neuron. This necessitates the addition of a scaling factor to the input current. The rationale for this is the following: assuming that the total number of neurotransmitter gated ionic channels within a synaptic junction is constant regardless of postsynaptic neuron size, then the absolute number of positively charged ions entering postsynaptically during synaptic activity will also be constant. But if the postsynaptic neuron's surface area increases, the charge density of the ionic species will decrease accordingly, thus limiting the postsynaptic effect of the synaptic current. This can easily be captured in a scaling factor, ϱ:

$$\varrho = \frac{A}{r_{pn}^2} \tag{5.43}$$

where r_{pn} is the radius of the postsynaptic neuron (squared instead of cubed because most ionic mobility occurs at the neuron's surface and not in the bulk volume), and where A is an arbitrary constant. The synaptic input current may now be specified as follows:

$$I_{syn} = \varrho \cdot \bar{g}_{syn} \cdot (V_m - E_{syn}) \tag{5.44}$$

where E_{syn} is the reversal potential for the synapse, and $\bar{g}_{syn}$ is the specific conductance of the synapse.

A different approach is to assume that small synapses impinge on large neurons and that large synapses impinge on small neurons. This could have exactly the same scaling effect as before, but to my knowledge this has not been verified experimentally.

5.5 Dynamic range of Wilson's neocortical neuron model

In order to optimize the functional customization of the neuron models that are used for simulating different regions of the nervous system, it is necessary to specify the working range of the used neuron model. As shown in section 5.3.1, Wilson's model of neocortical neurons[274] is very versatile with respect to showing different firing patterns. As a mathematical model of neuron firing, this model is quite flexible. Therefore, although the model was originally intended for simulating neocortical neurons, there is no a priori reason to discard its use for other types of neurons as long as the firing patterns and frequency ranges correspond to the neuron to be simulated. This is a pragmatic approach to the complex issue of deciding which neuron models to use for different neuron populations: Simply choose one model of sufficient versatility and adapt its parameters to the case at hand. From a biological point of view, such a step might seem rather drastic and perhaps even criticizable, because the features that specifically identify a neuron species might be lost, such as the particular form of the spike, or some other such feature. However important it is to characterize and model the specific features of a particular neuron's activity

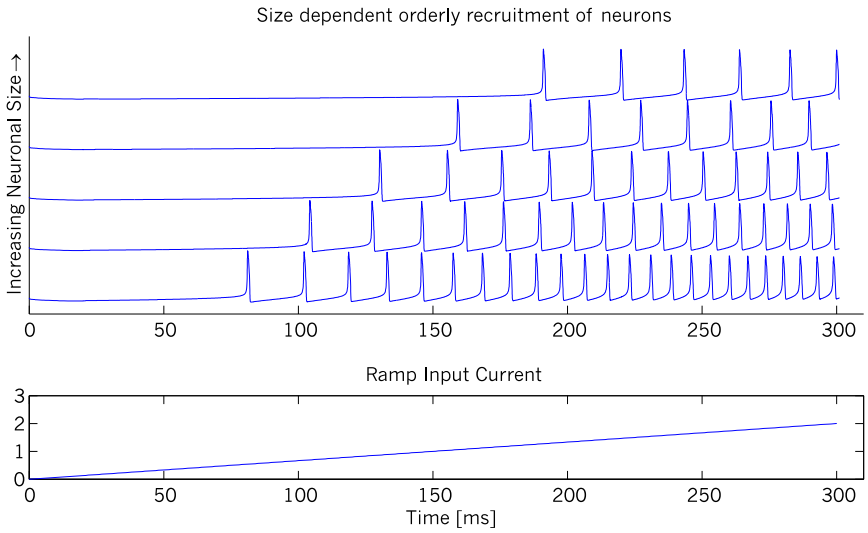

Figure 5.2: This figure shows the orderly recruitment of neurons with varying sizes, also known as Henneman's size principle.

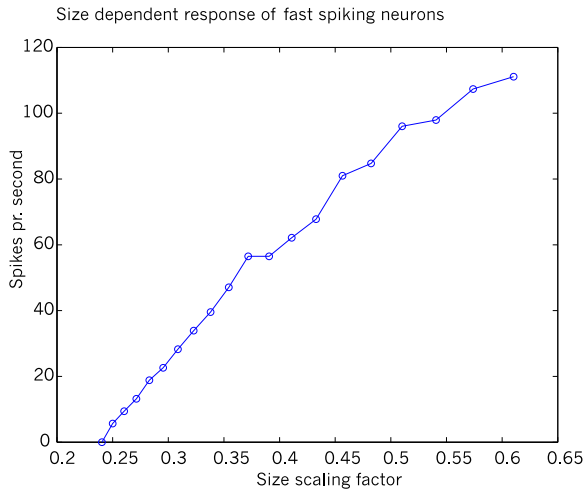

Figure 5.3: Spiking frequency of a FS neuron as a function of the size scaling variable, ϱ, in response to a constant synaptic input conductance

by analyzing all of its biophysical parameters (variety of ionic channels, time constants, etc.), such a level of detail is unnecessary for the present purposes. (In the simulation program the possibility that more detailed models will be tested at some point has been taken into account by imposing a very high level of modularity in its design.) Figures 5.5 and 5.4 show the frequency-response of the four modelled neuron species as a function of synaptic input conductance. This information may be used for scaling the network to match the frequency range of a given neuron species with known afference.

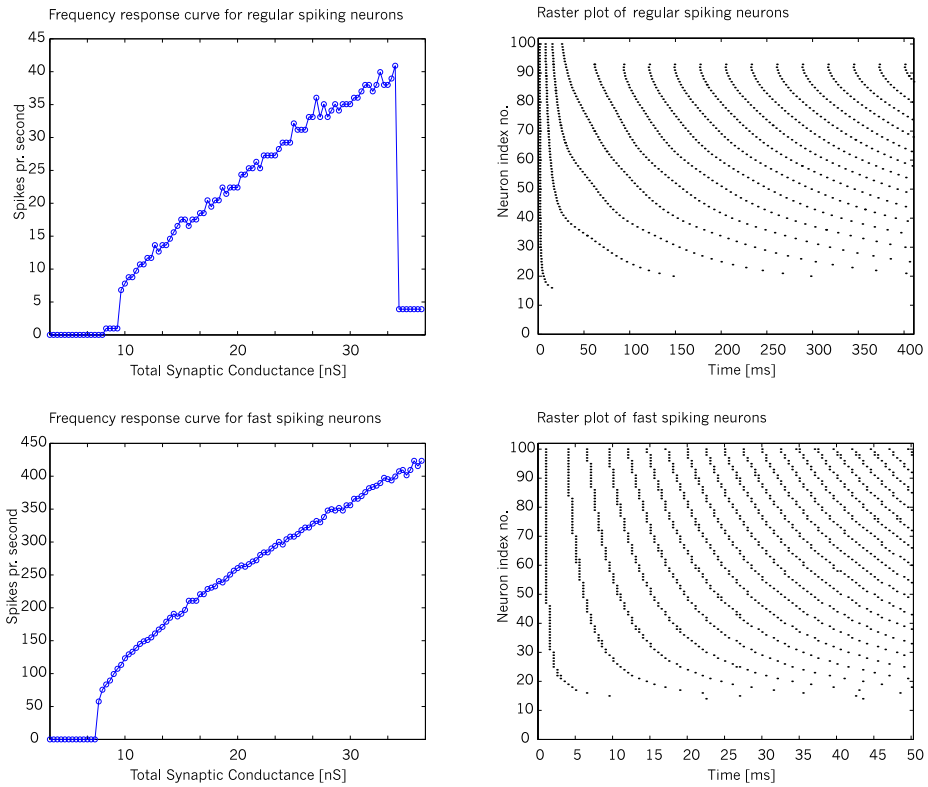

Figure 5.4: The two graphs to the left show the firing rate of regular (upper) and fast (lower) spiking neurons as a function of total synaptic conductance. To the right are shown the corresponding raster plots of 100 neurons (indexed along y-axis) receiving different input currents ($I_{input} = -g_i \cdot (V_m)$), where higher index numbers, i, relate to larger input conductances ($g_i = 40 \cdot i/100$). Each point corresponds to a spike event (membrane potential $V_m > 0$). The size scaling factor was $\varrho = 0.51$. Notice that for input conductances below a certain lower threshold, the neurons are inactive, and for currents above a high threshold, the neurons are not continuously active, but only fire a couple of times after which they remain inactive. See figure 5.5

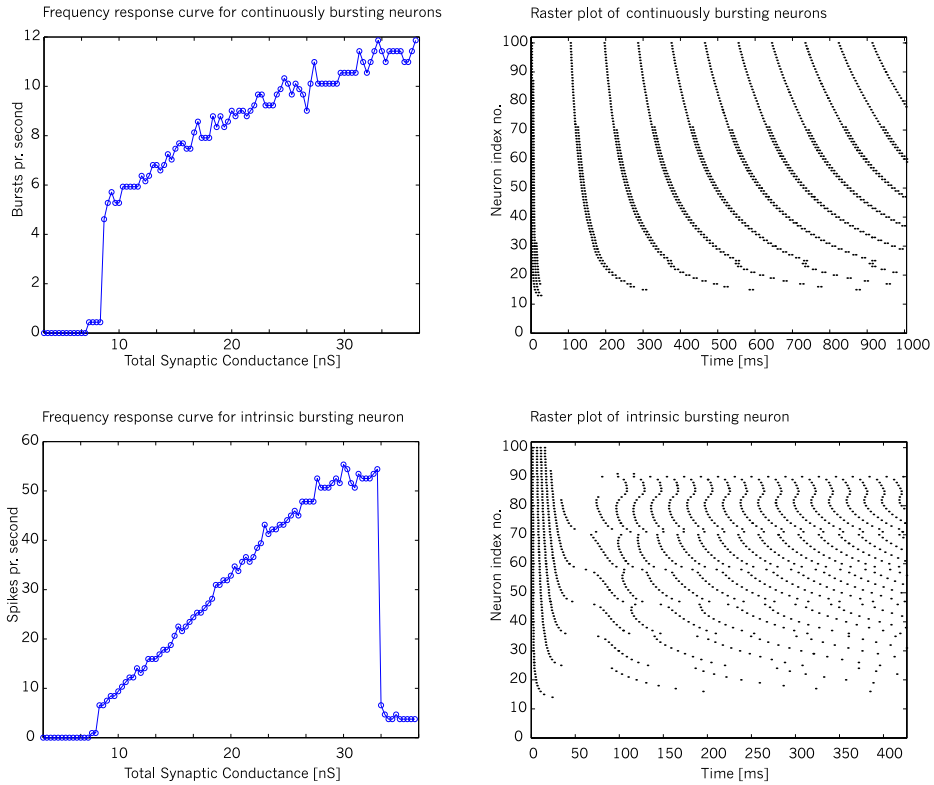

Figure 5.5: The two graphs to the left show the firing rate of continuously (upper) and intrinsic (lower) bursting neurons as a function of total synaptic conductance. To the right are shown the corresponding raster plots of 100 neurons (indexed along y-axis) receiving different input currents ($I_{input} = -g_i \cdot (V_m)$), where higher index numbers, i, relate to larger input conductances ($g_i = 40 \cdot i/100$). Each point corresponds to a spike event. The size scaling factor was $\varrho = 0.51$ Notice that for input conductances below a certain lower threshold, the neurons are inactive, and for currents above a high threshold, the neurons are not continuously bursting. See also figure 5.4

Chapter 6

Synaptic dynamics

Chapter Summary

This chapter is intended as a brief summary of recent experimental and theoretical results related to synaptic activity. The material presented herein should be seen in extension to chapter 5, and is provided with the usual emphasis on biological realism and computational efficiency. Some of the synaptic algorithms (particularly the dynamic synapse formalism) that are reviewed herein will be used directly for the network simulations in chapters 8 to 11.

Communication between neurons is mediated by the synapses, which are specialized structures making up the axon's terminals. It has been estimated that each and every neuron in the vertebrate nervous system produces on the order of 10^4 synapses with which it connects to other neurons. It turns out that there are several ways in which to classify synapses, e.g. according to the neurotransmitters they use, to the effects they produce at the post-synaptic site, to whether they are chemical or electrical, etc. In this review focus will primarily be on chemical synapses of the directly gated variety, as these have turned out to be the most ubiquitous in the vertebrate nervous system. In these, the arrival of an action potential to the synaptic terminal causes Ca^{2+} channels in the presynaptic plasma membrane to open, resulting in an influx of Ca^{2+} ions. There is ample evidence indicating that this Ca^{2+} influx is the key event which precipitates a long series of biochemical cascades inside the synapse finally leading the release by exocytosis of neurotransmitter into the synaptic gap. The details of this fascinating process of neuronal communication have been long under way, starting with the pioneering works of Sherrington [246], Fatt and Katz [59] and Eccles [53] (for an introduction see Kandel et al. [133], Kandel and Siegelbaum [132], Kandel and Schwartz [130]). In recent years there has been much concern about the neurocomputational role of short-term synaptic plasticity [288], which is a rapid presynaptic change of the synaptic efficacy occurring within milliseconds of the arrival of a spike, and which lasts a few seconds and changes the

postsynaptic potentials with up to several hundred percent of the initial value.

6.1 Mathematical models of the synapse

Several mathematical models have been developed to account for the detailed flows of chemicals within the synapse, giving good insight into the internal workings of the synapse, but such models are much too detailed for our present purposes. If we allow ourselves to ignore most of the biochemical details of synaptic transmission, and focus only on the overt phenomenological (physiological) electrical effects of such transmission, it is possible to simplify the mathematical description tremendously without loosing track of our main objective, which is to identify computationally efficient models of synaptic transmission.

The three synaptic workhorses in the central nervous system are the AMPA (α-amino-3-hydroxyl-5-methyl-4-isoxazole-propionate), the NMDA (N-methyl-D-Aspartate), and the GABA (γ-aminobutyric acid) receptor type synapses. Through these the vast majority of communication in the central nervous system is mediated.[133,130]. In the periphery one primarily finds ACh receptor type synapses of the nicotinic variety as these are used at all neuromuscular junctions[59,60,132]. Common to all these synaptic types is that the postsynaptic receptors are directly linked to an ion channel which opens upon binding of neurotransmitters. Such synapses may therefore be described using the same type of approach as was used for studying neuron activity in chapter 5.

6.1.1 The Reversal Potential

One very important difference between the opening of ion channels in the axon during an an action potential, and the opening of post-synaptic ionic channels in a directly gated chemical synapse is in the value of the reversal potential for the involved channels and the time dependent variations of the conductance. By definition the reversal potential is reached when the ionic currents through a channel balance out. For channels selective to a single ionic species, the reversal potential is identical to the Nernst potential for the particular ion. The current, I_{ion}, flowing through an ion selective channel is given by:

$$I_{ion} = g_{ion} \cdot (V_m - E_{ion}) \tag{6.1}$$

where g_{ion} is the channels conductance with respect to the ion in question, V_m is the membrane potential and E_{ion} is the Nernst potential for the particular ion. This relationship was used in chapter 5 in connection with the membrane equation, eq. 5.5, and is simply Ohm's law. Opening an ion channel will always result in an ion current which will bring the membrane potential towards the ion's Nernst potential, i.e. until the current balance through the channel is zero.

In the case of synaptic ion channels, these are often permeable to multiple ions simultaneously, and the reversal potential, E_{RP}, is then the membrane potential at which the sum of currents of all the permeating ionic species, I_{RP}, becomes 0:

$$I_{RP} = \sum_i g_i \cdot (E_{RP} - E_i) = 0 \tag{6.2}$$

Synapse Type	Ion Channel	Reversal Potential	Peak Conductance
AMPA	K^+, Na^+	$E_{AMPA} = 0$ mV	$G_{AMPA} < 2$ nS
NMDA	K^+, Na^+, Ca^{2+}	$E_{NMDA} = 0$ mV	$G_{NMDA} < 2$ nS
ACh	K^+, Na^+	$E_{ACh} = 0$ mV	$G_{ACh} = 5$ mS
GABA	Cl^-	$E_{GABA} = -60$ mV	$G_{GABA} < 2$ nS

This expression can be rewritten as:

$$E_{RP} = \frac{\sum_i g_i \times E_i}{\sum_i g_i} \tag{6.3}$$

Initially the ionic conductances for a synapse under study will not be known, so in practice the reversal potential for a given synapse is best found experimentally by clamping the post-synaptic membrane at various membrane potentials and measuring the current flowing through the open synaptic channel. Surprisingly, such a procedure yields a very simple dichotomy of most directly gated synapses: Those with strongly negative reversal potentials and those with reversal potentials at 0mV (see table 6.1.1). It thus seems as if synaptic variability is more related to time dependent conductance dynamics than to any particular ionic species. Table 6.1.1 lists the reversal potentials for a few different synaptic types as they have been measured experimentally, and the relevant ionic species (data from Kandel and Siegelbaum[132], Kandel and Schwartz[130]). In connection with the previously mentioned dichotomy, synapses are usually classified as excitatory if their activity tends to depolarize the post-synaptic cell towards firing threshold ($E_{RP} >\sim -50mV$), while inhibitory synapses are those which have the opposite effect ($E_{RP} <\sim -50mV$). Note that all excitatory synapses have a reversal potential at 0mV whereas inhibitory synapses channels have negative reversal potentials.

To be valid, this classification is based on the assumption that the post-synaptic neuron is at its resting membrane potential when the synaptic activation occurs, which will of course most often be the case given that an action potential has a much shorter duration than the intervening refractory period. In reality, the post-synaptic currents resulting from any given synaptic activation depend on the membrane potential at the post-synaptic site, and on the ion species to which the channel is selective.

6.2 The Dynamics of Postsynaptic Potentials

Up till now, only the electrochemical properties of a maximally activated post-synaptic site have been considered, without taking into consideration the large variations in the number of active receptors that may occur as a function of the changing neurotransmitter concentrations in the synaptic gap. As the total current flowing into the postsynaptic cell depends directly on the number of open receptor channels, it is very important to characterize these variations. There

are several pre- and postsynaptic mechanisms which conspire to cause variations of the EPSP or IPSP, the most obvious of which are (for an introduction see Johnston and Wu[128], Purves et al.[217], Destexhe et al.[52]):

- Variations in the opening and closing time constants intrinsic to the receptor molecules.
- Neurotransmitter deactivation in the synaptic gap by enzymes.
- Neurotransmitter deactivation by the postsynaptic receptor.
- Neurotransmitter reuptake through specialized transporters, where the presynaptic site or nearby glial cells reabsorb some of the released neurotransmitter or decay products.
- Variations in the amount of released neurotransmitter at the presynaptic site.
- Variations in the number of receptor molecules.
- Variations in the conductance of receptor channels.

It should come as no surprise that very different time constants would be involved in the dynamics related to each mechanism, but the range covered by these constants is truly astounding: 10 orders of magnitude. From the enzymatic deactivation of neurotransmitters (milliseconds), over short-term changes of presynaptic release (seconds or minutes), to truly long-term variations sometimes requiring permanent structural changes to the synapse (days or years). In what follows focus will stay primarily on the short and medium ranges as it is now widely believed that it is in the fast dynamics that the most important computational properties of neural tissue are expressed. Nevertheless, a brief note will be made also on the long-term range as this is related to the permanent storage of information needed for memory and learning.

6.2.1 Fast Synaptic Dynamics – $\tau \sim 10^{-3}$ s

Measurements of EPSP's and IPSP's at different synapses following a single action potential have been done routinely for many years, and have been modelled with equivalent electrical circuits similar to the ones used for modelling neurons (for an introduction see Kandel and Siegelbaum[132], Kandel and Schwartz[130]). In some investigations these measurements have instead been fitted with very simple exponential functions describing the postsynaptic potential, with time constants ranging from a few milliseconds (AMPA, GABA) to about a hundred milliseconds (NMDA). In voltage-independent receptor channels like the AMPA receptor a very simple model may be used which correctly captures the changes in conductance as a function of time[255,177]:

$$G_{AMPA} = \bar{g}_{AMPA} \frac{t - t_{AP}}{\tau_{AMPA}} \exp\left\{1 - \frac{t - t_{AP}}{\tau_{AMPA}}\right\} \tag{6.4}$$

where $\bar{g}_{AMPA}$ is the peak conductance through AMPA-receptor channels in the synapse ($\bar{g}_{AMPA} \sim 2$ nS), τ_{AMPA} is the AMPA receptors time constant ($\tau_{AMPA} \sim 1$ ms) and t_{AP} is the time of arrival of the presynaptic Action

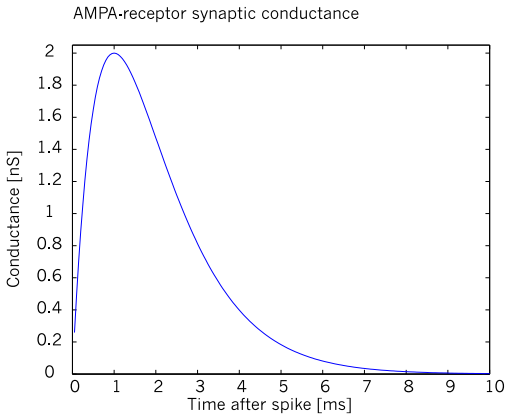

Figure 6.1: The conductance through an AMPA-receptor type synapse as a function of time since spike arrival. This plot is based on equation 6.4

Potential. A similar model applies for GABA'ergic synapses. Equation 6.4 is plotted in figure 6.1.

To account for voltage-dependent receptor channel dynamics as seen in the important glutamatergic NMDA receptor channel[13], a slightly more complex mathematical model is required[125,126,285,177]:

$$G_{NMDA} = \bar{g}_{NMDA} \frac{e^{-(t-t_{AP})/\tau_1} - e^{-(t-t_{AP})/\tau_2}}{1 + \eta[\mathrm{Mg}^{2+}]e^{-\gamma V_m}} \tag{6.5}$$

where $\bar{g}_{NMDA} \sim 1$ nS is the peak conductance through NMDA receptor channels in the synapse, $\tau_1 \sim 40$ ms and $\tau_2 \sim 0.33$ ms are the time constants, $\eta \sim 0.33/$ mM is a scaling constant related to the Mg^{2+} concentration given by $[Mg^{2+}]$ ($\sim 1 - 2$ mM is a typical value)[13], and $\gamma = 0.06/$ mV is a scaling factor related to the postsynaptic membrane potential, V_m. Figure 6.2a shows equation 6.5 plotted as a function of time and postsynaptic membrane potential.

When only single sparsely distributed spikes are considered, these phenomenological models account very well for the conductance changes in the postsynaptic membrane. It turns out, however, that these models are unable to account for the variations associated with the arrival of multiple spikes in close temporal proximity, in which case a wholly different type of model must be invoked due to effects such as neurotransmitter depletion.

6.2.2 Short-Term Synaptic Dynamics – $\tau \sim 1$ s

Resources within a volume as small as that of a synapse will necessarily be limited, affecting the amount of available neurotransmitter, the concentration gradients of calcium, the availability of ATP, etc. This inevitably means that prolonged activation of a synapse will result in a gradual reduction of synaptic output if ever the amount of resources used during activation exceeds the speed of recovery. *Ab initio* one might expect that normal activity in the nervous system would be tuned in such a way as to avoid over-activation of the synapses, preventing a situation where synapses might fall silent due to overexertion and fatigue. Surprisingly, this turns out to be a false tenet, and there is by now much

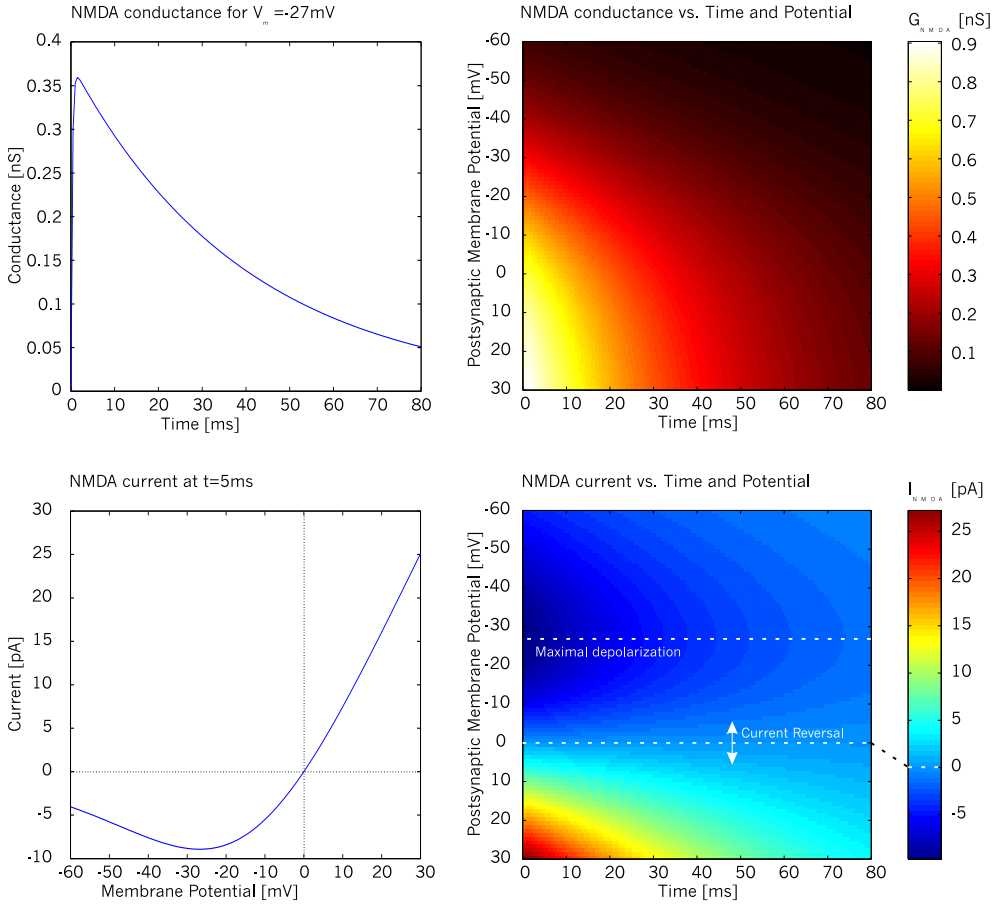

Figure 6.2: Upper Row: NMDA-receptor based conductance as a function of time and postsynaptic membrane potential. As the membrane potential becomes more positive, more current is allowed to flow through the NMDA-receptor channels. Lower Row: NMDA-receptor based current as a function of time and membrane potential. Note that the current reverses when the membrane potential reaches $V_m = 0$ mV, and that maximal postsynaptic depolarization is obtained for $V_m \sim -27$ mV. These plots are based on equations 6.5 and 6.4

experimental evidence supporting the view that synaptic output is extremely variable even on a very short time scale of 10-100 milliseconds [288,263,2,1]. Initially, most evidence was based on invertebrate data, such as habituation in Aplysia, and on a few specialized vertebrate systems like the neuromuscular junction (an early review is given in Zucker [288]). To begin with these results had little influence on neural information processing theory, probably because of the apparently limited number of neuronal types in which it occurred, so at the time Long-Term Potentiation (LTD) and Long-Term Depression (LTD) were seen as the most promising types of synaptic plasticity in the vertebrate brain (see section 6.2.3), and rate coding was ubiquitously accepted as the neural code *par excellence*. Now it is known that even pyramidal neurons in vertebrate cortex have synapses which depress or facilitate within milliseconds, depending on the recent presynaptic activity and on the type of postsynaptic neuron. Thus it has been reported [170] that excitatory synapses between pyramidal neurons are subject to synaptic depression, which is a brief facilitation followed by an extended reduction in efficacy. The story is further complicated by the fact that some synapses seem to be rapidly facilitated on a short-term basis without the subsequent depression, particularly those connecting pyramidal cells with inhibitory interneurons [170]. Based on these experimental results theorists have begun to invoke the notion that perhaps synaptic short-term plasticity has some important computational role in the nervous system [2,166,1]. Recently it has been proposed that synaptic short-term depression may remove signal redundancy [88], may permit the neural implementation of universal non-linear filters [166] or might be involved in dynamic gain control in cortical neurons [2].

There is some evidence that short-term synaptic plasticity is mainly caused by presynaptic events [288,263]. This being so, it must affect all the synapses belonging to a particular neuron simultaneously. For pyramidal neurons one consequence of this might be, that after an initial barrage of excitation to its postsynaptic contacts, the pyramidal cell is rendered functionally inhibitory as it is only its synapses on inhibitory neurons which are facilitated, while its synapses to other excitatory cells are depressed. Without additional experimental evidence, it is difficult to say what computational effects this might have, but one possibility could be that it confers unidirectionality to the flow of activation across a field of neurons.

All in all, current experimental evidence casts some doubts on the biological relevance and explanatory power of any neural information processing system solely relying on slowly changing synaptic "weights" (as those usually invoked for optimal learning in most artificial neural network systems). Short-term synaptic plasticity also poses some difficulties for ideas depending on direct rate coding schemes because the inactivation by depression of synapses will turn any incoming rate into a very compact postsynaptic event, which seems to hint that only the first few spikes in a train are of any relevance to the neural code. This last difficulty may be avoided to some extent by considering small groups, clusters or assemblies of neurons (e.g. cortical microcolumns), which under some circumstances may work as a single functional unit [72] yielding as output an average assembly rate code. It has been proposed that long-range horizontal cortical connections might carry just such signals [73].

Resource distribution models of short-term synaptic dynamics

Several mathematical models have been proposed to account for the observed presynaptic frequency dependent short-term variations[267,153,263,262]. These are all phenomenological models that have to be fitted to the existing experimental data, but one in particular[262] stands out from the rest in that it includes frequency dependent facilitation and depression, both of which will be needed for modelling cortical structures.

In their model, Markram and Tsodyks[263,262] assume that the total amount of neurotransmitter encountered pre- and postsynaptically (including precursors and decay products) is finite due to limited resources, and that it probably remains relatively constant throughout an experiment. This neurotransmitter is subdivided into three different pools depending on the functional state in which the transmitter is encountered:

E : The effective, or active neurotransmitter pool corresponds to that fraction of the neurotransmitter that is currently bound to postsynaptic receptors, causing PSP's.

I : The inactive neurotransmitter pool contains all the neurotransmitter which has become deactivated. It might have been metabolized by enzymes in the synaptic gap, as when acetylcholinesterase breaks ACh into acetate and choline, or perhaps it has been reabsorbed into the presynaptic terminal or into glial cells (as in the glutamate-glutamine cycle). After reabsorption into the presynaptic terminal via specialized transporters the neurotransmitter may be reactivated.

R : The recovered neurotransmitter pool contains all the neurotransmitter which has been reactivated or has been newly synthesized and is now packed into vesicles and ready to be launched back into the synaptic gap upon the arrival of the next action potential.

When an action potential arrives they further assume that it is only a fraction of the total available (recovered, R) neurotransmitter that is released. This fraction is represented by U_{SE}, i.e., the utilization of synaptic efficacy. To describe the whole process, the following kinetic equations were proposed in Tsodyks and Markram[263], Tsodyks et al.[262]:

$$\begin{aligned} \frac{dR}{dt} &= \frac{I}{\tau_{rec}} - U_{SE} \cdot R \cdot \delta(t - t_{AP}) \\ \frac{dE}{dt} &= -\frac{E}{\tau_{inact}} + U_{SE} \cdot R \cdot \delta(t - t_{AP}) \\ I &= 1 - R - E \end{aligned} \tag{6.6}$$

where t_{AP} is the arrival time of an action potential, $\delta(t)$ is the delta function, τ_{rec} is the time constant associated with recovery processes in the synapse, and τ_{inact} is the time constant associated with inactivation of the activated (receptor bound) transmitter. At all times the postsynaptic current associated with presynaptic activity is given as the product between the absolute synaptic efficacy, A_{SE}, and the fraction of effective neurotransmitter, E:

$$I_{ps} = E \cdot A_{SE} \tag{6.7}$$

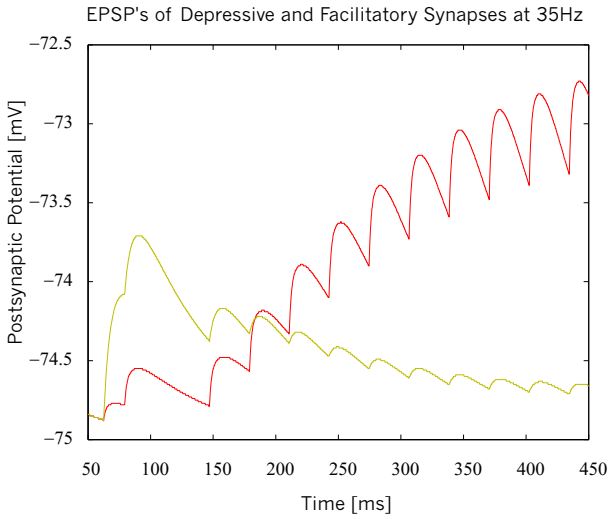

Figure 6.3: EPSP's of depressive (green) and facilitatory (red) synapses during presynaptic stimulation at 35Hz.

It is practical to let A_{SE} be a current in pA, as it can then be included directly into neuron models like the ones presented in chapter 5.

So far this model only accounts for synaptic depression. To include facilitation, Tsodyks, Pawelzik and Markram[262] have proposed to let the utilization of synaptic efficacy, U_{SE}, be time dependent as well. An increase in U_{SE}, they argue, could correspond to calcium accumulation in the presynaptic terminal caused by the arrival of multiple action potentials. To describe this increase in the utilization of synaptic efficacy, the following kinetic scheme was proposed (adapted from Tsodyks et al.[262]):

$$\frac{dU_{SE}}{dt} = -\frac{dU_{SE}}{\tau_{facil}} + \mathcal{U} \cdot (1 - U_{SE}) \cdot \delta(t - t_{AP}) \tag{6.8}$$

where $\mathcal{U}$ determines the amount by which U_{SE} is allowed to increase for every presynaptic spike (the Ca^{2+} accumulation), and τ_{facil} is the time constant associated with this facilitation process.

Collectively, the main output from these equations is the postsynaptic current, I_{ps}. At the postsynaptic soma, this current will first have passed through the dendrites before resulting in a somatic EPSP. This effect may be calculated using a passive membrane model (a simple capacitive membrane with one input current and one leak current)[262], corresponding to a very simple dendrite. The resulting somatic EPSP's of depressive and facilitatory synapses may be seen in figure 6.3 for a presynaptic neuron firing at 35Hz.

Figures 6.4 and 6.5 show some different scenarios involving a simple simulation comprising two neurons interconnected by a single synapse. The neurons can be of any of the four usual types (RS, FS, CB, or IB), modelled using Wilson's model of neocortical neurons (see chapter 5, section 5.3.1). The interconnecting synapse is either of the depressing (figure 6.4) or facilitating type (figure 6.5). Different presynaptic activation frequencies were tested to give an idea of the dynamic range for the synaptic model. Note, e.g., that for high

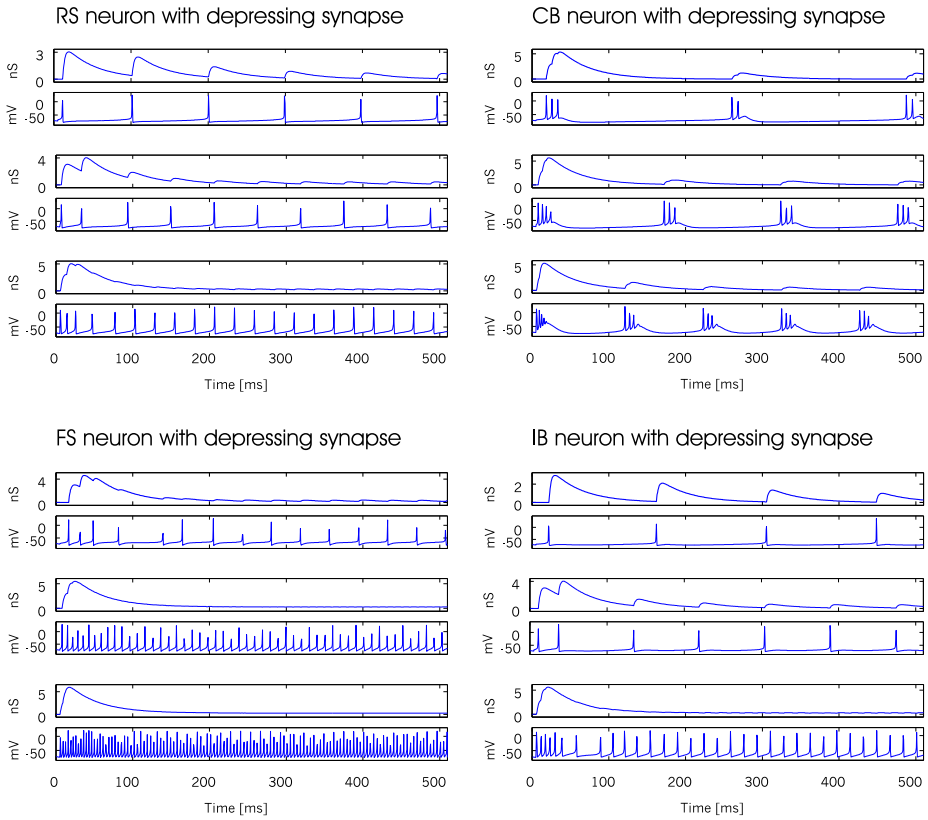

Figure 6.4: The effect of presynaptic neuron type on depressive synapses. Simple simulation involving two neurons that are interconnected with a depressive synapse. The presynaptic neurons can be of any of the four usual types (RS, FS, CB, or IB), modelled using Wilson's model of neocortical neurons (see chapter 5, section 5.3.1)

presynaptic frequencies, the dynamic synapse only responds to the first few spikes in the train, after which the chord conductance falls to a constant value slightly above zero. (Chord conductance is defined[128] as $G_i = I_i/(V_m - E_i)$). Contrast this to the response of a facilitating synapse, which also has an initial increase and subsequently settles at a much closer value to the maximal conductance. In all cases the absolute synaptic current was set to 1nA, so note also that the maximal chord conductance of the depressing synapse is three times larger than for the facilitatory synapse. This should be taken into account when using this model to simulate synapses of known conductance, e.g. by setting A_{SE} appropriately.

6.2.3 Long-Term Synaptic Dynamics – $\tau \sim 10^3$ s

The idea that the interconnecting *corpuscles* between neurons or groups of neurons must undergo some kind of activity dependent, correlational and permanent change in order to establish a memory trace predates the invention by

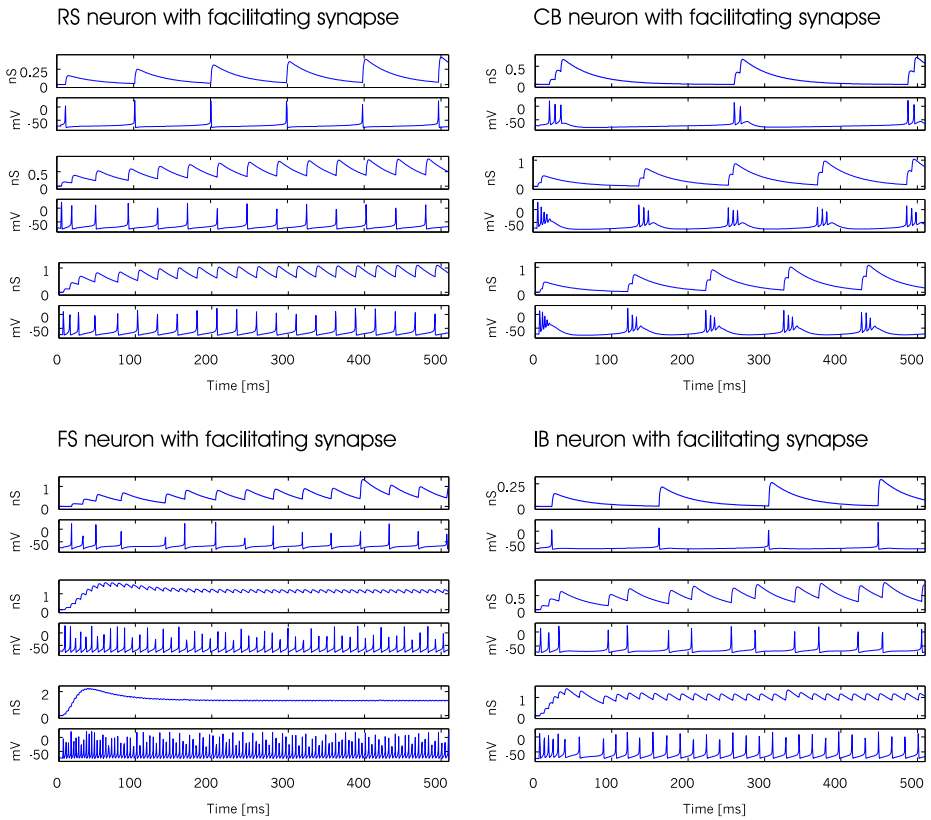

Figure 6.5: The effect of presynaptic neuron type on facilitatory synapses. Simple simulation involving two neurons that are interconnected with a facilitatory synapse. The presynaptic neurons can be of any of the four usual types (RS, FS, CB, or IB), modelled using Wilson's model of neocortical neurons (see chapter 5, section 5.3.1)

Sherrington and Verrell[246,245] of the term *synapse* (nowadays used to refer to said corpuscles). Although often attributed to Hebb[104], this idea was actually already proposed in 1873 by Alexander Bain in his book *Mind and Body*[15,272]:

> We know what are the conditions of making an acquirement, or of fixing two or more things together in memory. The separate impressions must be made together, or flow in close succession; and they must be held together for a certain length of time, either on one occasion or on repeated occasions. Now to each impression, each sensation or thought, there corresponds physically a group or series of nerve-currents; *when two impressions concur, or closely succeed one another, the nerve currents find some bridge or place of continuity, better or worse, according to the abundance of nerve matter available for the transition. In the cells or corpuscles where the currents meet and join, there is, in consequence of the meeting, a strengthened conexion or diminished obstruction–a preference track for that line over lines where no continuity has been established.* Excerpt from Bain[15], page 117, as cited in Wilkes and Wade[272] (italics added).

This came at a time when there was still much dispute about the structure of the nervous system, in particular the neuron doctrine vs. the reticular theory, which may well be the reason that Bain was overheard and it was Hebb who with a firm basis on a widely accepted neuron doctrine, could propose a more neurophysiologically based postulate[104].

There is much variation in the molecular and physiological mechanisms involved in permanently strengthening or weakening postsynaptic potentials, depending on species, neuronal systems and neuronal types (see Raymond et al.[221], Bliss and Collingridge[26], Bailey et al.[14], Andersen and Soleng[9], Lynch[165] for a general overview of this rather extensive topic). It is therefore not possible to give a single account of such mechanisms, but on a general note it should be observed that all samples studied so far share a few features. First of all, long-term plasticity seems to be activation pattern specific: The patterns of pre- and postsynaptic activities that are required to induce long-term plasticity are idiosyncratic to the types of cell in the investigated sample (see reviews in Bliss and Collingridge[26]). Then there is the observation that protein synthesis always seems to be required: Blocking protein synthesis at any level in the chain of events disturbs or completely inhibits long-term plasticity effects[226]. With regard to the primary site within the synapse which is responsible for the plasticity, arguments seem to have finally settled on the parsimonious view that pre- and postsynaptic sites are equally responsible but in different ways (for review see Bliss and Collingridge[26]): Presynaptic increase of neurotransmitter release, and postsynaptic increase of neurotransmitter sensitivity and/or channel conductance.

In the vertebrate nervous system, two types of plasticity have received much attention, namely what has become known as Long-Term Potentiation (LTP) and Long-Term Depression (LTD). LTP was initially observed by Bliss and Lomø[27] in the perforant pathway of the hippocampus. When the perforant fibers were stimulated at high frequency (15Hz for 10 seconds) several times, the amplitude of the EPSP's at the granule cell layer in the dentate gyrus would increase by several hundred percent. This increase in the EPSP's remains stable

for days and even weeks[253], and has under similar circumstances been observed ubiquitously in the vertebrate brain, strongly endorsing the common view that LTP is an important part of memory consolidation. The NMDA receptor (a model of which was presented in section 6.2.1) seems to be a mayor player in the induction of LTP, and the molecular mechanisms involved have been mapped out in great detail[26,14,42]. Three very special attributes of LTP make it the primary candidate for being *the* neurobiological basis of "Hebbian" (Bainian?) learning (see also review in Bliss and Collingridge[26]) as they all have been shown to require coincident pre- and postsynaptic activity:

- Cooperativity: A minimum number of presynaptic axons must be active simultaneously to elicit LTP[27].
- Associativity: If two or more fiber systems impinge on the same neuron, complex interactions occur at the dendritic level permitting that the activity of one system may induce LTP in one of the other systems if the later is active at what would otherwise have been a sub-LTP-threshold activation[17].
- Specificity: Strong stimulation in one of the aforementioned fiber systems will induce LTP in that system but not in the others (unless, of course, the other systems are activated at only slightly subthreshold levels)[17].

Even in systems normally known to undergo LTP, certain pre- and postsynaptic patterns of activity induce a long-lasting *reduction* in the EPSP's, an effect known as Long-Term Depression (LTD). This effect was first discovered by Masao Ito[124,49], and was observed when activity in the parallel fiber system of the cerebellum was followed by activity in the climbing fiber system: Such coincidences resulted in a reduction of the EPSP's associated with parallel fiber activity. It is now known that LTD not only occurs in the cerebellum, but is as common in the vertebrate brain as LTP, although requiring slightly different activation patterns. It has been shown that NMDA receptor activation is a prerequisite for induction of LTD in most of the systems studied[260] (with the important exception of the cerebellum), its involvement in postsynaptic Ca^{2+} dynamics being its main contribution[12,41] to this event. In fact, it seems that the most important activation related factor which determines whether LTD or LTP will be induced at a junction is the postsynaptic Ca^{2+} concentration during the activity: LTP requires a larger postsynaptic depolarization and a greater increase in Ca^{2+} concentration[12] to be induced than does LTD. This observation has led to the ABS learning rule, proposed by Artola, Bröcher and Singer[12], in which potentiating and depressing effects compete (see figure 6.6) based on the postsynaptic potential (or Ca^{2+}-influx). Two thresholds are defined, one for induction of LTD at low postsynaptic potentials, and one for induction of LTP at high postsynaptic potentials. This rule is essentially identical to the BCM rule proposed by Bienenstock, Cooper and Munroe[20], except that the LTD induction threshold in the BCM rule is at zero postsynaptic depolarization (see figure 6.6).

Spike-timing Dependent Plasticity

A rather recent development in the field of study concerned with long-term plasticity is the discovery that the relative timing between pre- and postsynaptic

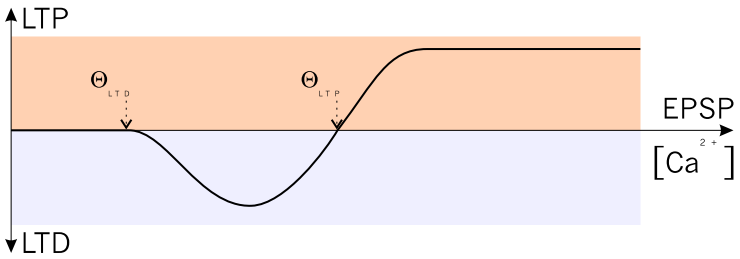

Figure 6.6: Artola, Bröcher and Singer rule for long-term plasticity[12]. At low EPSP there is neither potentiation nor depression of the synapse, until a threshold is reached at Θ_{LTD}, where long-term depression of the EPSP ensues. At increased EPSP values a second threshold is crossed, Θ_{LTP}, where the plasticity now shifts towards potentiation. The BCM rule[20] corresponds to the ABS rule if $\Theta_{LTD} = 0$.

spikes actually determines whether potentiation or depression will take place at the involved pyramidal synapse[152,169,157]. This is really a consequence of the dependence on postsynaptic Ca^{2+} concentration (or EPSP), which led to the ABS plasticity rule (see figure 6.6). To see why consider the following two scenarios:

1. *Presynaptic neurotransmitter release precedes postsynaptic depolarization.* Upon the arrival of a presynaptic action potential, glutamate is released which binds postsynaptically to AMPA and NMDA type receptor channels (reviewed in Kandel and Schwartz[130]). Unless the postsynaptic cell is already strongly depolarized, most current will only flow through the AMPA-type receptor because initially the NMDA receptor will be partially blocked[13] by Mg^{2+}. If the postsynaptic neuron is depolarized sufficiently by this single event, or by other similar events nearby along the dendrite, then the NMDA receptor's ion channel will become unblocked gradually and a large Ca^{2+}-influx will begin, further contributing to the EPSP and leading to LTP induction and a postsynaptic spike.

2. *Postsynaptic depolarization (spike) precedes presynaptic neurotransmitter release.* The NMDA-type receptor will not contribute to the EPSP unless it has been activated by glutamate *and* has been depolarized to a certain level. In the present case the first condition has not been met, so there will be no NMDA-current prior to the arrival of a presynaptic spike. And due to its late arrival, once the presynaptic spike arrives the postsynaptic neuron will already be in the midst of a spike or in the repolarization and refractory phase. An NMDA-receptor based Ca^{2+} current will still enter the postsynaptic cell (the Mg^{2+}block is only fully effective at -80mV[13]), but it will be smaller than in the previous scenario, as can be seen in figure 6.7.

Assume for now that small differences in the postsynaptic Ca^{2+}concentration (resulting from different activation patterns) is the most important factor determining whether LTP or LTD is induced. Then in order for STDP to occur, such differences in Ca^{2+}should be attainable simply by varying the arrival

times of the presynaptic spikes with respect to the postsynaptic spike (or more specifically, with respect to the phase of the postsynaptic membrane potential). In some preparations of pyramidal cells [257,256] action potentials have been observed "backpropagating" from the soma and up into the dendrites. As a first approximation it may therefore be assumed that the postsynaptic potential at a dendrite during or shortly after a postsynaptic spike, is very similar to the actual action potential (at least with respect to its temporal variations). Using this information, a simple simulation comprising two neurons (A and B) connected by a single NMDA-synapse (from A to B) may be used to determine the postsynaptic NMDA-currents when the spike times of A are varied with respect to the spike time of B (the neurons are induced to spike at determined times by simulated current injections). This has been done to yield the results presented in figure 6.7. The NMDA-current is calculated using G_{NMDA} from equation 6.5:

$$I_{NMDA}(t) = G_{NMDA} \cdot (V_m(t) - E_{NMDA}) \tag{6.9}$$

where $V_m(t)$ is the time varying postsynaptic neuron's membrane potential at the location where the NMDA synapse is situated. By integrating the individual NMDA-current profiles with respect to time (essentially calculating the area under the curves in figure 6.7C), one gets the total charge that has entered the postsynaptic cell as a function of the particular pre- and postsynaptic spike times (t_{pre} for the presynaptic spike, and t_{post} for the backpropagated postsynaptic spike). This relationship is shown in figure 6.7D. It should be noticed that if the presynaptic spike arrives before the backpropagated postsynaptic spike, $\Delta t = t_{pre} - t_{post} < 0$, then the total charge entering postsynaptically will be larger than if the presynaptic spike arrives after the postsynaptic backpropagated spike ($\Delta t > 0$). It is well known that the NMDA-receptor channel is most permeable to Ca^{2+}ions [13], so a large fraction of the charge will be based on Ca^{2+}ion flux. It thus seems that spike-timing dependent plasticity (STDP) may depend on the ordinary Ca^{2+}concentration related rules that apply to LTP and LTD induction.

It is also important to notice that the graph in figure 6.7D will be shifted to the *right* by as much as 3-6 ms if one uses the postsynaptic spike times *per se* rather than the backpropagated spike times (i.e. equivalent to resting 3-6ms from the t_{post} used here). This is interesting if compared to some of the reported experiments showing STDP [169], in which it is the postsynaptic spike times *per se* that are used, and which yield a large discontinuity at zero pre- and post synaptic spike delay [1]. This means that the spike backpropagation delay of 5 ms is taken into account by the dynamics of the NMDA-receptor system, so that the temporal correlation learning rules of STDP apply to actual axonal spiking times.

Spike-timing dependent plasticity (STDP) opens up a range of new possibilities with respect to how neurons may interact and what patterns they may learn [1]. The temporal directionality that is implicated by STDP does indeed open up the possibility that networks of neurons may learn spatiotemporal patterns [181,204]. And within the context of this thesis, this is an important property as it allows for the learning and execution of motor programs of higher complexity. As a preamble to some of the final chapters, the topic of spatiotemporal encoding in networks of abstract neurons will be investigated in the following chapter. The exploration will aim at identifying some of the problems that one might

expect from using mechanisms like STDP in densely connected artificial neural networks that are expected to perform many different programmed sequences as response to different simple tonic inputs (e.g. from a "command-like" signal).

6.3 Implementation Related Issues

In order that the here reviewed models of synaptic dynamics may be used to interconnect networks of neurons, there are some issues which must be resolved related to the problem of scaling. As mentioned at the beginning of this chapter, each neuron has in the order of 10^4 synapses, which amounts to 10^{15} synapses in the human brain. Although there is nothing in principle to hinder us from implementing a realistically scaled simulation of the brain by using the equations in this and the previous chapter, at present there is no computer in the world which would be able to run a simulation with so many equations and parameters at a speed which could be considered even marginally practical [a].

To be practical, smaller scale simulations must be designed so as to behave as larger scale systems. In a nutshell, the problem is this: If a neocortical neuron receives 10^4 synapses from other neurons [254], then that is also the minimum number of neurons that must be simulated, the total number of individual synapses thus soaring to at least 10^8. In a realistic simulation the number would be even larger because real cortical tissue is not composed of completely segregated clusters of neurons, but rather of overlapping regions with some long-distance connections interspersed. It has been estimated that a typical pyramidal cell only contributes with $1/100000^{\text{th}}$ of all the synapses present within the region to which it projects [28]. So if one considers the columnar organization of the cortex [196], where each column contains approximately 10^4 neurons, then even if a given pyramidal neuron projected directly back at the column where it resides, only 1000 of its synapses would be on neurons within the column. The remaining 9000 synapses would necessarily be projecting elsewhere (neighbouring or even distant columns via horizontal projections). One should of course take this type of calculations with a "grain of salt", they are only estimates yielding some orders of magnitude we might work with. But if we continue the exercise along this route, it is possible, without loss of generality, to rescale the networks by determining some convergence-divergence ratios and by changing the peak synaptic conductances thus permitting a dramatic reduction in the number of neurons and synapses in the simulation. The only item missing is to figure out the fraction of synapses that normally need to be active to fire a neuron. Fortunately this fraction is known from experiments which have shown that approximately 10-30 active (glutamatergic) synapses are necessary to elicit a postsynaptic spike [210,254], corresponding to 0.1 to 0.3 percent of the synapses.

[a] Even on what IBM claims to be the worlds fastest supercomputer (as of 2001), the 512-node RS/6000SP ASCI White system running at 12.3 teraflops, you would need approximately 80 seconds to update the synapses by a single time step (assuming each synapse takes only one operation, e.g. a simple multiplication). A single millisecond of brain simulation would thus take perhaps 1 hour realtime. Not that bad actually!, but still impractical considering that a cognitive event takes up to 200ms.

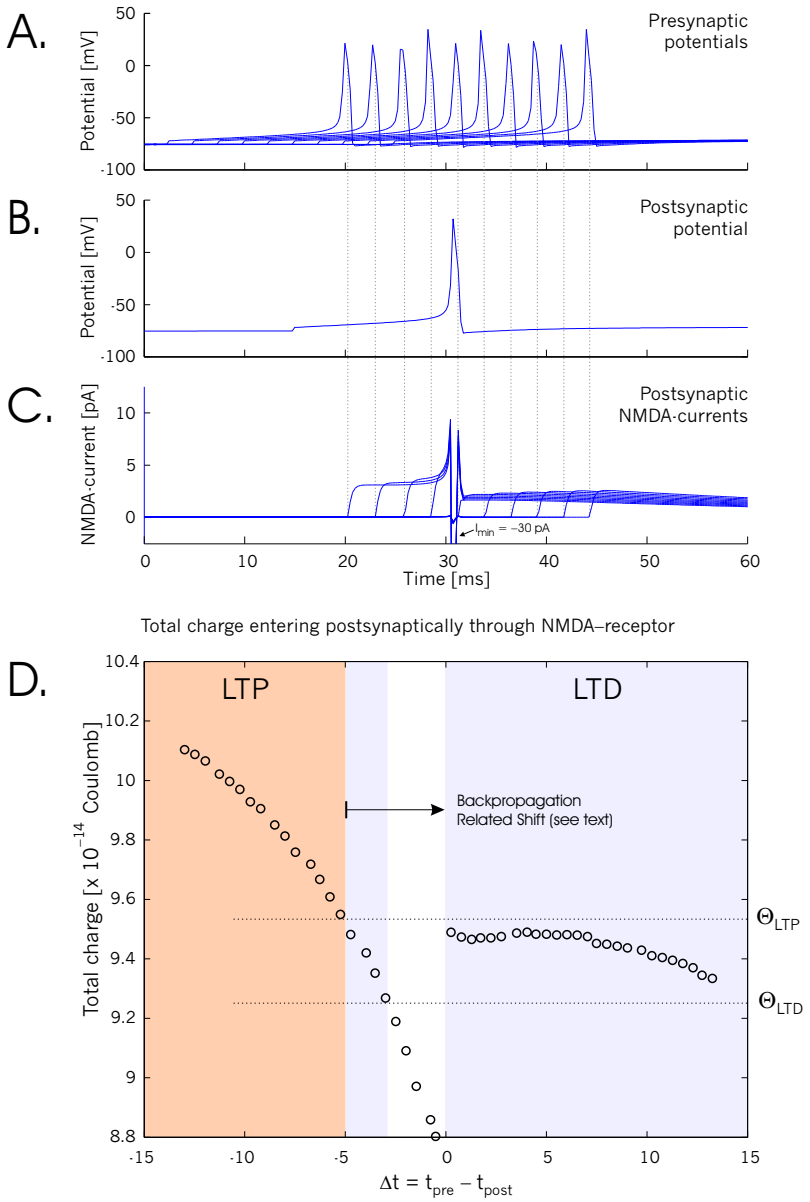

Figure 6.7: Spike-timing dependent currents in NMDA-based receptor channels. A. Presynaptic potentials; B. Postsynaptic potential; C. Postsynaptic NMDA-currents resulting from presynaptic activity arriving at various times before or after postsynaptic activity; D. Total charge entering postsynaptic neuron through NMDA-receptor as a function of the temporal displacement between pre- and postsynaptic activity. See text for further details.

Chapter 7

Abstract neural network dynamics

Chapter Summary

This chapter presents one way in which spike-timing dependent plasticity may be used to affect network dynamics. Although this chapter presents a brief digression from the main line of argument followed in this thesis, it is nevertheless highly relevant to the subject of motor control. The results presented herein might serve as a starting point for developing more advanced neural network models that can learn and recall complex sequences of activation patterns. Such a "dynamics"-learning system would be required to implement the high-level reafference cancellation functions, herein attributed to corticomotoneuronal cells when activating α and γ-motoneurons in predefined spatiotemporal patterns.

Note: The material in this chapter has been submitted for publication.

Neurons receive the main bulk of their input through the dendrites. Until recently it was believed that dendrites only served to increase the receptive surface area of the neurons, and that the only information processing which took place there was summation of the synaptic currents thought to flow passively along the dendrite towards the soma. Such an oversimplified view of the dendrite has been challenged by many authors, who have shown that dendrites have a much wider range of responses to activation. Some dendrites even contain voltage-gated channels which permit dendritic Ca^{2+}-based spikes, generated either locally[237] or as a result of a back-propagating action potential[257,256]. There have been several reviews of these and other findings related to dendritic dynamics[55,241,178,3].

The main view advocated herein is, that differentially activated areas of a dendrite permit the existence of zones with distinct rates of synaptic modification, and that such areas can be individually accessed using a reference signal which localizes synaptic plasticity and memory trace retrieval to certain subregions of the dendrite. It is proposed that the neural machinery required in such a learning/retrieval mechanism could involve the NMDA receptor, in conjunction with the ability of dendrites to maintain differentially activated regions. In particular, it is suggested that such a parcellation of the dendrite allows the neuron to participate in multiple sequences, which can be learned without suffering from the "wash-out" of synaptic efficacy associated with superimposition of training patterns. This is here proposed to be a biologically plausible solution to the stability-plasticity dilemma of learning in neural networks.

Very recent experimental evidence[237] has strengthened the idea that prebinding of glutamate to the NMDA receptor can be invoked as a mechanism to create "hot-spots" on the dendrites. In their paper, Schiller et al. (2000) present evidence showing that basal dendrites in cortical pyramidal cells are able to sustain NMDA-receptor based Ca^{2+} spikes, independently of the activity in neighbouring dendritic branches. This kind of mechanism has been invoked [203] to argue for the existence of independently accessible learning sites, which allow for immediate access to the stored memory traces, as well as posing a novel solution to the stability-plasticity dilemma initially identified by Grossberg[98,99]. This idea is further developed and formalized here, in the context of learning spatiotemporal sequences of patterns, which are particularly sensitive to the stability-plasticity tradeoff. This work is not intended to be a complete formal treatment of a neural network architecture; rather it is a presentation, by way of example, of what is thought to be a neurobiologically plausible method for multiple sequence learning in networks suffering from the stability-plasticity dilemma.

7.1 Creating Synaptic Subsets

A fully recurrent artificial neural network can be trained with a set or sequence of ordered patterns, in such a way that the network associates a given pattern with the next in the sequence. After stabilization of the synaptic weights through training, the learned sequence can be recalled by forcing one of the patterns upon the network, whereupon the network recalls by association the next pattern in the sequence[181,251,6,106]. In this scheme, all the synapses of the network are involved in the storage of the sequence. Thus, for a given pattern sequence, A, a synaptic efficacy matrix, $\mathbf{W}_A$, can be found which enables the network to express the sequence; the dynamical behaviour of the network depends directly on this synaptic matrix.

Supposing now that the network is further trained with a new sequence, B, then the synaptic weights in the network must be modified to accommodate this second succession. The synaptic matrix will reflect these changes and it will gradually differ more and more from the original $\mathbf{W}_A$, converging to a completely different matrix, $\mathbf{W}_B$. In this new state, the network will recall sequence B perfectly, but sequence A will no longer be accessible.

Thus, a tradeoff exists between stability of existing memory traces and the plasticity required to store new information. Nevertheless, it *is* possible to

store multiple sequences in a network of this kind, if the patterns within the sequences are relatively sparse and non-overlapping[251], that is, the patterns must be sufficiently different as to cause no interference between the sequences (e.g. the sequences A-B-C-D-E and M-N-C-O-P would interfere at C). Even if the non-interference and the sparseness requirements can be relaxed a bit and still lead to good results, it would be useful if the specialized synaptic matrices $\mathbf{W}_A$ and $\mathbf{W}_B$ could be kept completely segregated, in order to allow optimum performance even with sequences consisting of dense and overlapping patterns.

A very direct way of accomplishing this would be to allow independent access to different subsets of the network's synapses. Each synaptic subset can then comprise one particular synaptic matrix whose contents can be accessed and modified whenever that particular subset is reactivated. For example, consider the following simple recurrent neural network. Let the activity level h_i of the i'th neuron in a network with N neurons be defined by:

$$h_i = \sum_{j=1}^{N} w_{ij} \cdot f(h_j) \tag{7.1}$$

where w_{ij} is the synaptic weight between neuron j and neuron i, and $f(x)$ is a rate-limiting function (e.g. sigmoidal). As can be seen, all the synapses in the network can influence the activity level h_i of neuron i. It is possible to modify the synaptic influence selectively by including a reference factor, R_{ij}, inside the sum of the above activation function:

$$h_i = \sum_{j=1}^{N} R_{ij} \cdot w_{ij} \cdot f(h_j) \tag{7.2}$$

For simplicity, let the components, R_{ij}, of the reference activity matrix $\mathbf{R}$ have values 1 or 0, depending on whether the corresponding synapse, w_{ij}, should be enabled or disabled, respectively. It should be noted here that the activity level of a synapse *per se* is independent of the reference activity, that is, a synapse may well be fully activated even if the reference component $R_{ij} = 0$. The only thing that happens when setting R_{ij} is that the actual influence of the corresponding synapse on the neuron's activity will be modulated by the reference value. Also, it should be noted that the reference activity matrix should not necessarily be interpreted as affecting synapses on an individual basis: The deeper (neural) meaning of setting $R_{ij} = 0$ is that a particular synapse (w_{ij}) happens *not* to belong to the synaptic subset currently being accessed (in neural terms, the synapse happens to be in an area of the dendrite that is not currently being amplified by NMDA-receptor activity; see section 7.2 for further details).

Given this scheme, it is now possible to individually access a number of different synaptic subsets, $\mathbf{w}_1$, $\mathbf{w}_2$, ..., $\mathbf{w}_q$ from the network's complete synaptic matrix $\mathbf{W}$, simply by defining an equivalent number of different reference activity matrices, $\mathbf{R}_1$, $\mathbf{R}_2$, ..., $\mathbf{R}_q$. Given that the dynamics of a neural network usually depends directly on the particular synaptic set, modulating the influence of synaptic activity on the neurons with a reference activity will also directly influence the dynamics. In particular, it can be inferred that down-modulating the influence of some fraction of the synaptic population will effectively restrict the network's dynamics, to whatever is contained in the remaining synapses. And if these same "emphasized" synapses also were up-modulated by the same

reference activity during learning, then the network's dynamics will express whatever was learned during training as long as that particular reference activation is used. If the reference is changed the synaptic subset will be modified, and thus also the network's behaviour.

7.2 Neural Mechanisms

A neural mechanism which corresponds to the neural network model proposed above could be the following: afferent fibers prime a specific dendritic region by pre-binding glutamate to NMDA-receptors in the region, thus creating potential "hot-spots" of activity. If we start by assuming that this priming reference activity is not in itself sufficient to fully activate the hot-spots, but is only capable of bringing the membrane potential sufficiently close to the NMDA-receptor channel's unblocking potential of $-40mV$, then any additional synaptic activity within a given "hot-spot" can be amplified tremendously if it contributes with sufficient current to overcome the NMDA-receptor's Mg^{2+}-barrier (for further details about the NMDA-receptor see [13,42]). Assuming instead that the priming reference is capable by itself of fully activating a "hot-spot" (e.g. by co-activating AMPA-receptors together with the NMDA-receptors) implies that the reference activity also can function as a trigger to the memory traces stored in that synaptic subset, and not only as an address.

Regardless of how a particular "hot-spot" is activated, synapses within the hot-spot region would have an increased tendency to undergo activity induced modifications (during learning) compared with synapses outside. Furthermore, during normal functioning (e.g., during expression of stored memory traces), such synapses will have a much larger influence on the neuron's response than synapses outside the hot-spot. In the formalism presented above, this would correspond to assigning a reference matrix value of $R_{ij} = 1$ to synapses inside the hot-spot, and a value $R_{ij} \ll 1$ to synapses outside this NMDA-receptor amplified region.

It is proposed that this hot-spot activation mechanism is active both during normal performance of the nervous system and during learning of particular items, so if "hot-spots" are NMDA-receptor dependent, then a prediction of this model would be that NMDA-receptor activity is necessary during learning but also to some extent during expression of the stored memory. There is much experimental evidence indicating that the NMDA-receptor is required at least for some kinds of learning [195,187,167]. Whether the NMDA-receptor is also required during memory recall is still a subject of much debate because experimental evidence has been found in support of NMDA-receptor involvement in recall [167,149], but also in direct conflict with this idea [187]. It seems that the difference in findings might be based on methodological issues related to the experiments [149]. In any case the prediction requirements can be relaxed a bit if "hot-spots" can be maintained independently of the NMDA-receptor, for example by using high-frequency activity in afferent fibres to access the correct storage locations on the dendrites.

Further support of the model presented here is the experimental evidence showing induction of long-term potentiation (LTP) following localized depolarization of a dendritic branch. This suggests that increased activity of neighbouring synapses might induce LTP [17].

7.3 Simulation Results

Some simulations are presented here in support of the points raised in this work. First a model of a neuron with compartmentalized dendrites was simulated using Hodgkin-Huxley type dynamics[108,242], to show that local dendritic potentials are capable of reaching a depolarization of $> -40mV$, and thereby indicating that NMDA-receptor channels in principle can be locally unblocked. A compartmental-model neuron with 258 compartments was generated using a recursive function that calculated the length, radius and tilting angle of the individual compartments in such a way that when connected the outcome resembles the apical dendrite of a pyramidal cell visually as well as electrotonically (by staying within the neurophysiological range of neuron scales and parameter values). The activity of the generated model neuron was simulated by numerically solving the membrane equation for each of the 258 compartments. Neighbouring compartments were linked to each other through series resistances. Voltage gated ion-channels were not relevant for the simulation presented in figure 7.1 where only the pre-spike situation of a passive dendrite was considered. The voltage, V_j, across the passive membrane of the j'th compartment changed according to the following equations (for details about the derivation of the membrane equations see[108,242,282]):

$$\begin{aligned} \frac{dV_j}{dt} &= \frac{1}{C_m} \cdot \left(I_{m_j} - I_{ion_j} - I_{stim_j} \right) \\ I_{m_j} &= I_{j-1,j} - I_{j,j+1} \\ I_{ion,j} &= G_L(V_j - E_L) \end{aligned} \tag{7.3}$$

where C_m is the membrane capacitance ($C_m = 1\mu F/cm^2$), $I_{j-1,j}$ is the current between compartments $j-1$ and j, $I_{j,j+1}$ is the current between compartments j and $j+1$, G_L is the conductance of the passive (leak) channels and E_L is the reversal potential of the passive channels. Synaptic input at selected compartments (asterisks in figure 7.1) was simulated by setting I_{stim_j} to a non-zero value. (For an introduction to compartmental modelling methods see Segev et al. 1998).

A depolarization gradient map of the simulated neuron is shown in figure 7.1. The left branch closest to the soma is the recipient of widely distributed current injections (marked with asterisks), and it can be seen that it reaches a depolarization of up to $-14mV$, independently of the rest of the neuron. Focusing the current injections to a smaller region of the branch would reduce the extent of the hot-spot. A very similar situation has been observed experimentally, as was recently reported by Schiller et al. (2000), where it was shown that basal pyramidal dendrites independently can support NMDA-receptor channel mediated Ca^{2+}-spikes.

To test the model proposed in section 7.1, a fully recurrent neural network

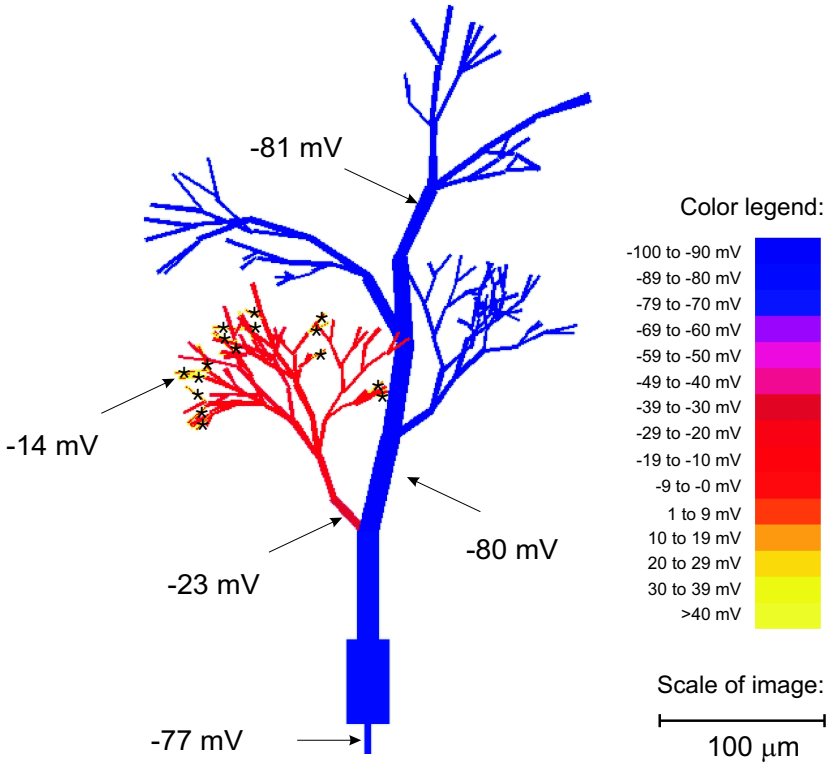

Figure 7.1: Compartmental modelling of the apical dendrite of a pyramidal neuron. Currents injected at sites marked with asterisks ($*$) lead to a localized dendritic membrane depolarization of up to $-14mV$, which exceeds the NMDA-receptor's unblocking threshold of $-40mV$, thus in principle permitting synaptic plasticity at such localized regions.

with $N = 400$ neurons was simulated using the following set of equations:

$$
\begin{aligned}
h_i &= E_i - I_i + \sum_{j=1}^{N} w_{ij} \cdot S_j \cdot R_{ij} \qquad (7.4)\\
\rho_i &= \frac{1}{1 + e^{-\beta(h_i - \theta)}}\\
S_i &= \begin{cases} 1 & \text{with probability } \rho_i \\ 0 & \text{with probability } 1 - \rho_i \end{cases}\\
w_{ij}(t) &= w_{ij}(t-1) + R_{ij} \cdot \Delta w_{ij}(t)\\
\Delta w_{ij}(t) &= \begin{cases} \gamma \cdot (1 - |w_{ij}(t)|) & \text{if } S_j(t-1) = 1 \text{ and } S_i(t) = 1 \\ -\gamma \cdot (1 - |w_{ij}(t)|) & \text{if } S_j(t-1) = 1 \text{ and } S_i(t) = 0 \\ 0 & \text{otherwise} \end{cases}
\end{aligned}
$$

where h_i is the total input to neuron i, E_i is a forced excitatory input, I_i is a stabilizing inhibitory input, N is the number of neurons in the network, $w_{ij}(t)$ is the synaptic efficacy of the connection from neuron j to neuron i at time t, β is a positive constant affecting the slope of the sigmoidal function, θ is a constant affecting the activation threshold, $S_j(t)$ is the activity level of neuron j at time t, γ (where $0 < \gamma < 1$) is a constant affecting learning rate, and R_{ij} is a reference activity with value 0 or 1. Note that changes of synaptic efficacy can only take place when the presynaptic neuron has been active in the previous time step, and note also that the direction of change depends on whether the postsynaptic neuron is currently active (positive change) or inactive (negative change). This also means that synapses that do not change during training also do not have any influence on the dynamics since the presynaptic neuron always was inactive.

Except for the reference activity matrix, these equations are largely equivalent in form and function to those proposed by Metzger and Lehmann (1990) for learning temporal sequences (see Metzger and Lehmann, 1990, for further details about the dynamics of such a system).

During training, a sequence of neural activation patterns was forced upon the network several times. Even though the synaptic weights are initially set to random values between 0 and 1, many of the synaptic weights will converge during the forcing procedure to values which effectively associate the patterns with each other in the specific order in which they were presented. To see the influence of the reference matrix $\mathbf{R}$ on the network's ability to learn sequences, three experiments were performed: 1) The network was trained with one sequence and one reference matrix (with all components set to unity), 2) The network was trained with two sequences but still only one reference matrix, and 3) The network was trained with two sequences and two different reference matrices.

7.3.1 Experiment no. 1: One sequence and one reference

During training of the network in this first experiment, a neural activation pattern $\mathbf{P}_1$ (i.e., a vector containing N elements with values 1 or 0) was forced upon the network for a certain number of updates, after which it was exchanged with a different pattern, $\mathbf{P}_2 \neq \mathbf{P}_1$. This was done for all the patterns in the ordered sequence $\sigma_A = \{\mathbf{P}_1, ..., \mathbf{P}_5\}$ (in these experiments, sequences usually contained 5 different patterns), until most of the involved synapses started converging

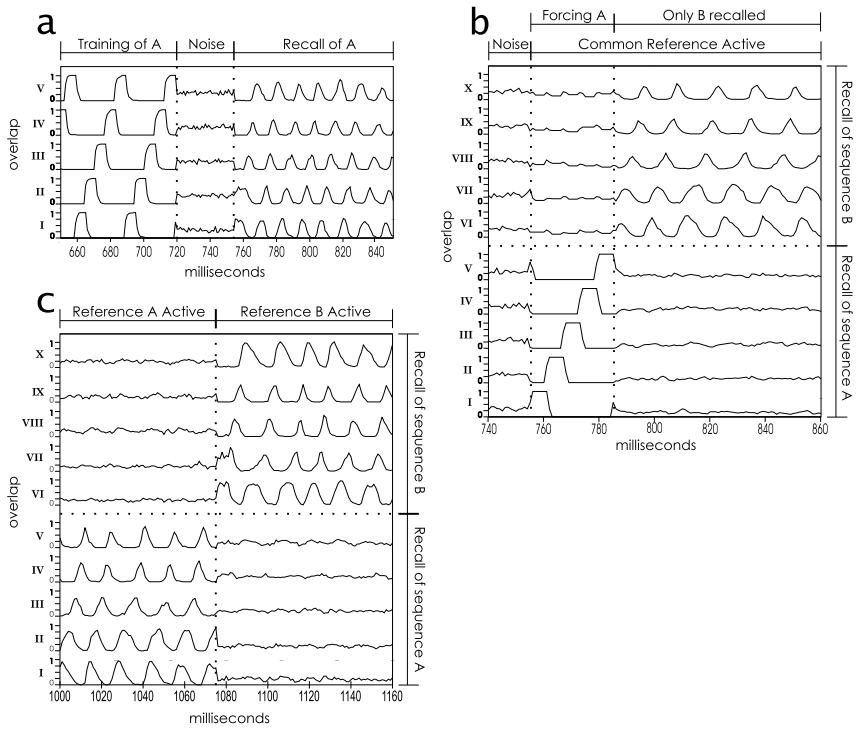

Figure 7.2: Simulation results for experiments no. 1, 2 and 3. The figure shows traces of the overlap value (see equation 7.5) between the network's actual state at some epoch, and the set of templates corresponding to the original patterns in the sequences used to train the network (patterns I-V correspond to sequence A, and patterns VI-X correspond to sequence B). Values close to unity indicate that the network state is currently very similar to one of the stored patterns, whereas values close to zero indicate that the network state is currently very different from the corresponding template pattern. a) Training with one sequence and one reference results in good sequence recall; b) Training with two sequences but only one reference results in a recency effect, where only the last trained sequence can be recalled; c) Training with two sequences and using two references permits storage of both sequences, and each sequence can be recalled individually by using the appropriate reference activity. Note that the shift from one sequence to the other occurred immediately upon changing the reference, indicating that this reference-based network architecture permits very fast access to stored data. See main text for further details.

(see Metzger & Lehmann, 1990, for an explanation of this convergence). All elements in the reference matrix $\mathbf{R}_A$ were set equal to 1, so that all synapses in the network were involved in learning the sequence σ_A.

After training, the network is able to traverse the sequence σ_A with up to 80% correct performance in pattern recall, and respecting the original order of patterns in the sequence. A slightly shorter latency of the patterns was found, but this should have no consequences for the main conclusions in this work. These results can be seen in figure 7.2a.

Recall performance was measured by computing the overlap, Ω_i, between the recalled network state $\mathbf{S}$ and each of the original training patterns $\sigma_A = \{\mathbf{P}_1, ..., \mathbf{P}_5\}$:

$$\Omega_i = \frac{1}{N_{\mathbf{P}_i}} (\mathbf{S} \cdot \mathbf{P}_i) \tag{7.5}$$

where i identifies the training pattern under evaluation, and $N_{\mathbf{P}_i}$ is the total number of active elements (i.e. with activation equal to 1) in the i'th training pattern.

7.3.2 Experiment no. 2: Two sequences and One reference

The already-trained network from section 7.3.1 was now further trained with a new sequence, $\sigma_B = \{\mathbf{P}_6, ..., \mathbf{P}_{10}\}$, but still using the reference matrix $\mathbf{R}_A$. As can be seen from the results in figure 7.2b, this resulted in a situation where the network could recall only the last-presented sequence, in this case sequence σ_B, even if the network was initially forced to go through a complete cycle of sequence σ_A. The network's learning parameters were set so as to permit fast synaptic convergence, so it did not help much to train by shifting between the sequences (i.e., to first train σ_A, then σ_B, then again σ_A, and so on), since this still meant that it was only the last-trained sequence which was stored.

7.3.3 Experiment no. 3: Two sequences and Two references

A third experiment was performed, in which two unequal reference matrices were used, $\mathbf{R}_A$ and $\mathbf{R}_B$. To keep things simple, $\mathbf{R}_A$ was created by first setting all components to 1, and then randomly selecting half of the components and setting them to 0. The second reference matrix, $\mathbf{R}_B$ was generated from $\mathbf{R}_A$ using $\mathbf{R}_{B,ij} = 1 - \mathbf{R}_{A,ij}$ (so that these two matrices were complementary to each other).

Using first $\mathbf{R}_A$, the network was now trained to perform sequence σ_A. After this, $\mathbf{R}_B$ was used while training the network to perform sequence σ_B. Effectively this divided the synaptic population in two equally large partitions, one designated to store the sequence σ_A, and the other specialized for sequence σ_B. As can be seen from the results on figure 7.2c, the network now successfully stores *both* sequences, each of which can be recalled by using the appropriate reference matrix.

7.4 Network Limitations

The experiments presented above prove by way of example that the approach taken is viable, the network indeed becomes able to clearly separate two sequences, but many outstanding questions still remain, in particular: how well does the neural network perform when using this method if the number of sequences (references) is increased?, how well does it respond in the presence of noise or of overlapping reference fields?, how does subdividing the synaptic population affect capacity?. Some of these questions will be addressed next.

7.4.1 Experiment no. 4: Capacity Tradeoff between References and Patterns

To investigate the capacity limitations of this type of network when the number of references (synaptic subsets) is increased, a simulation was performed using a network with 1024 neuron nodes in which the overall network performance (the accuracy of sequence recall) was evaluated as a function of the number of references and the number of patterns pr. reference. Performance was measured by using a simple template matching technique, which is based on the fact that the correct pattern sequence corresponding to a reference activity is known (the training set of patterns). One simply needs to compare the network's activity over time with the correct template over time. Formally, a template vector $\mathbf{x}_{temp}$ of length N can be compared with an output vector $\mathbf{x}_{out}$ of length M, where $M > N$ by sliding a window of width N containing the template vector over the output vector and finding the scalar product between the template vector and the subset of the output vector currently within the sliding window. The maximum value for this sliding dot product corresponds to the best fit between the vectors, and may be normalized with respect to the number of active nodes pr. template pattern, n_{act}, which gives a value ranging from 0 (worst performance) to 1 (perfect template fit). This normalized value is used in the present case as a simple measure of performance. For $i \in [0, M-N]$ we have:

$$Performance = \frac{1}{n_{act}} \cdot max \left\{ \mathbf{x}_{temp}|_0^N \cdot \mathbf{x}_{out}|_i^{i+N} \right\} \tag{7.6}$$

The network's performance was sampled as a function of the number of references (ranging from 1 to 16) and the number of patterns pr. sequence (ranging from 2 to 20 with steps of 2) which yielded a 16×10 performance array. This array is visualized in figure 7.3 wherein the performance indices were translated into a colour code, each point corresponding to a coloured square. Already here it is evident that a trade-off exists between the number of references vs. the number of patterns pr. reference. In order to quantify this trade-off more precisely, contour lines were generated using interpolation of the raw data (i.e., of the 16×10 performance array), and figure 7.3 therefore also shows the iso-performance contour lines corresponding to performance levels of 0.1, 0.5 and 0.9. Each contour line bounds a region within which performance is relatively constant. There seems to be a non-linear relationship between the number of references and the number of patterns pr. reference corresponding to a given level of performance. For the contour line corresponding to a performance level

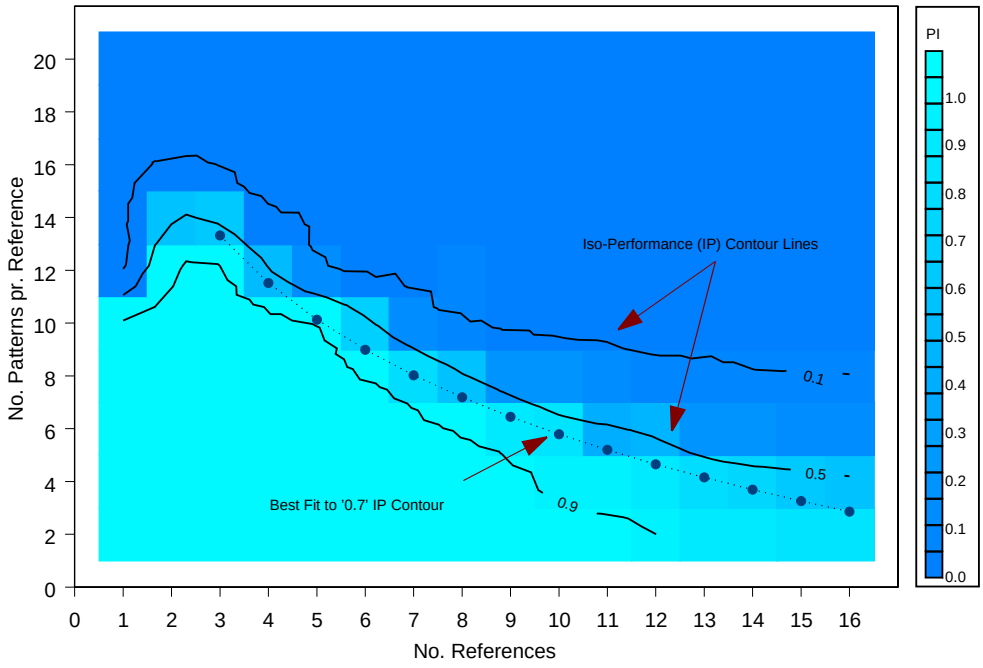

Figure 7.3: Performance as a function of the number of references and the number of patterns pr. reference in a network with 1024 neuron nodes. The resulting simulation data is here represented as coloured squares which are coded according to the colour index (PI) shown at right. A continuous valued contour plot can be derived from the data by interpolation, so that Iso-Performance contour lines may be drawn. (Only 3 contour lines are shown in the plot, corresponding to Iso-Performance indices of 0.1, 0.5 and 0.9). The best fit to the contour line corresponding to a performance index of 0.7 ($\cdot\cdot\bullet\cdot\cdot$) was achieved using the function: $y = -14.22 \cdot \log_{10}(x) + 20.1$, where y is the number of patterns pr. reference and x is the number of references.

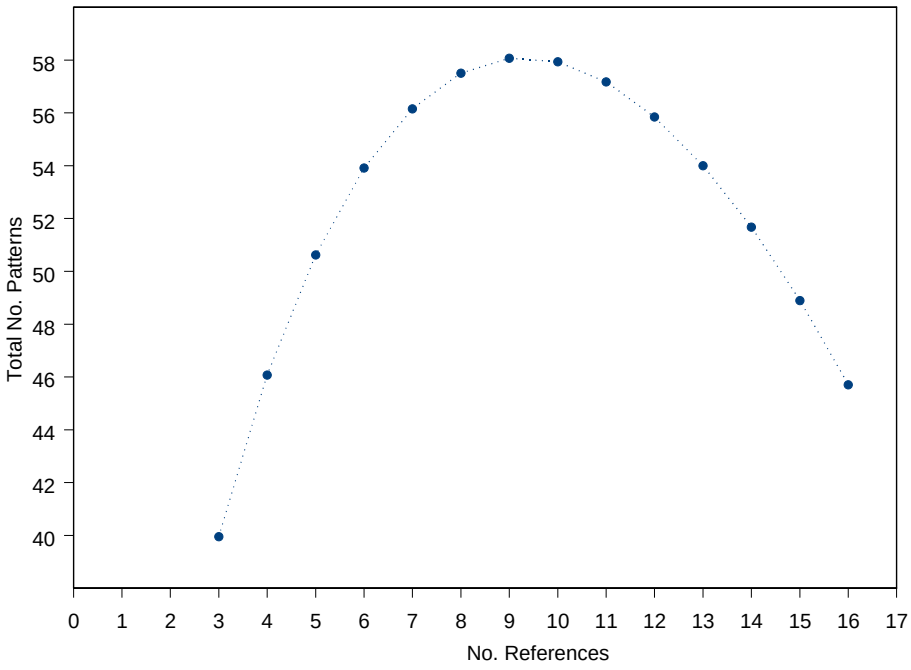

Figure 7.4: Using equation 7.7, which was derived from the data in figure 7.3, a theoretical curve can be found showing the maximum number of patterns as a function of the number of references (simply by multiplying the best-fit equation with the number of references). This gives an inverted-"U" curve indicating that a single maximum (optimal) capacity exists for the entire network which in the present case is found for 9 references.

of 0.7, this non-linearity could best be fitted using an equation of the the following form:

$$y_{0.7} = A \cdot \log_{10}(x) + B \tag{7.7}$$

where x corresponds to the number of references and $y_{0.7}(x)$ is the maximum number of patterns pr. reference that may be allowed if a performance level better than 0.7 is to be attained. Best fit was obtained for $A = -14.22$ and $B = 20.1$. This "best-fit" equation has also been plotted on figure 7.3. Using this equation we may find, for example, that at most 8 patterns pr. reference can be recalled with a performance level of 0.7 if 7 references are being used, thus yielding a total pattern capacity for the network of 56. The corresponding limit for 13 references is close to 4 patterns pr. reference, giving a total pattern capacity of 52. A plot showing the total pattern capacity of the network as a function of the number of references may thus be obtained by multiplying equation 7.7 times the number of references in question (i.e., total pattern capacity, z, is given by $z = x \cdot (A \cdot \log_{10}(x) + B)$). This is shown in figure 7.4, where it is clear that a maximum capacity exists for the present network when using 9-10 references with 6 patterns pr. reference (z is maximized at $x \approx 9.53$, for which $dz/dx = A \cdot \log_{10}(x) + x \cdot A \cdot (x \cdot \ln(10))^{-1} + B = 0$). Admittedly, a total capacity of ~ 56 patterns might seem rather low for a network of this size if compared with results obtained using state of the art learning algorithms such as back-propagation. In an application oriented framework, it would be perfectly acceptable to use state of the art learning algorithms to train each synaptic subset, thus further increasing the capacity of the network beyond what was attained here. Since this work aims at elucidating biological mechanisms, such a route was not further pursued at present.

Given the evidence, it seems that creating independently trainable synaptic subsets does not degrade overall network performance *per se*, and at least in one sense it actually improves it: the total pattern capacity is increased even if the cost is shorter sequences. The inverted-"U" curve on figure 7.4 thus allows for the following conclusion: parcellation of the synaptic population into smaller synaptic subsets affects network capacity in such a way that total pattern capacity may be maximized beyond what would be possible otherwise in a densely recurrent network, simply by finding the optimal number of references corresponding to a given network configuration. Such an interpretation nicely ties in with earlier findings which show that increasing sparseness may increase network capacity up to a certain point only to decrease again when patterns become too sparse[106]. In the present case however, the reduction of interference between patterns, which is one of the consequences of sparseness, is achieved by limiting the number of synapses that are available for learning and recall (which varies in proportion to $1/n_{ref}$), and not as is usually the case by using increasingly sparse patterns.

7.4.2 Experiment no. 5: Overlap of References

In a biological context it does not seem appropriate to assume a complete segregation between active an non-active hot-spots. Such a complete segregation (the ideal situation) was accomplished in the present work by assuming that reference afferents could only attain values of 1 (for active hot-spots) or 0 (for

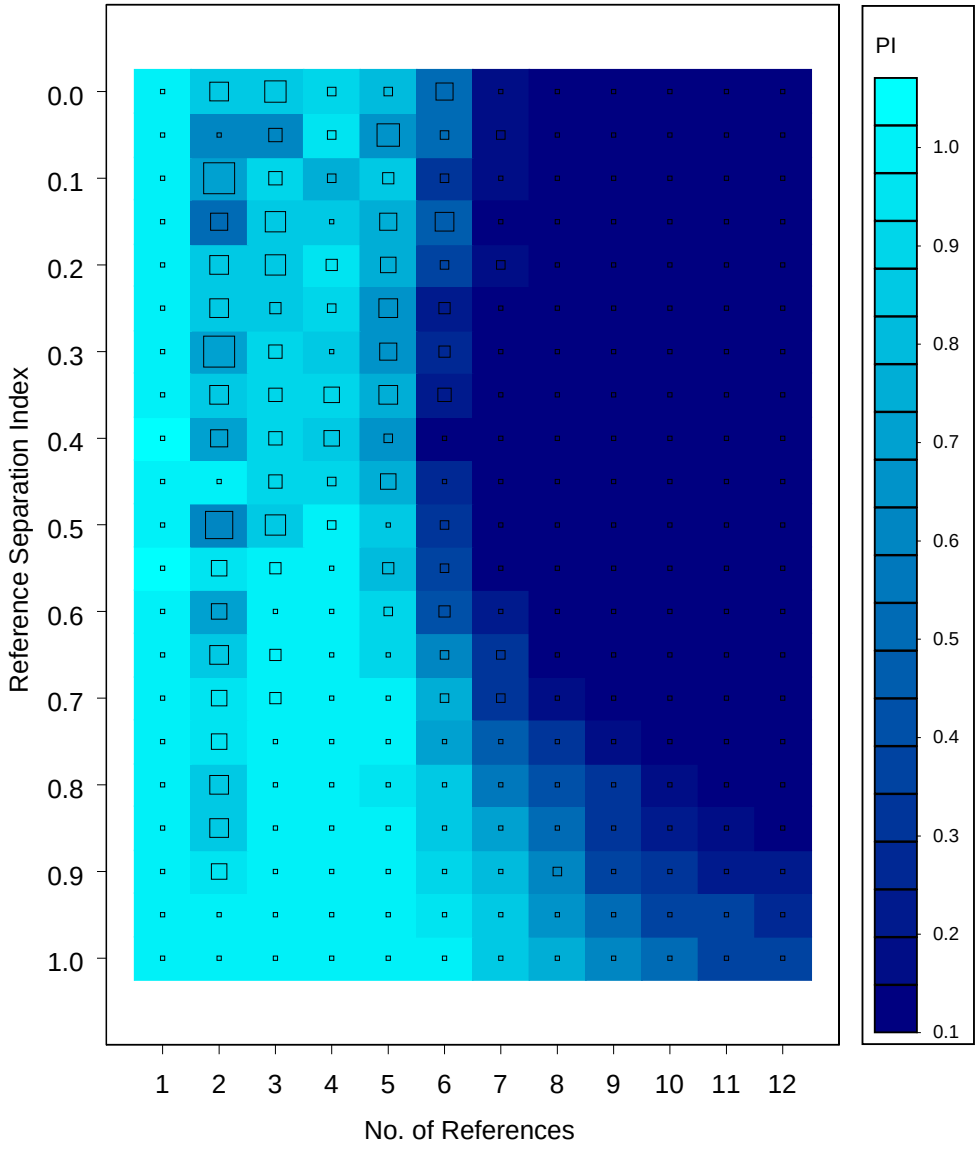

Figure 7.5: Performance as a function of the number of references (abscissa) and separation index (inverted ordinate) in a network with 400 neurons and 4 patterns pr. reference. The performance index is indicated by the colour code at right in the figure (PI). The small squares of varying size indicate the variance of the data resulting from 4 simulation trials, with the smallest squares corresponding to zero variance, and the largest squares to the maximum variance of 0.17. Note especially the robustness of performance when using 4 references, where performance is almost perfect and with low variance down to a separation index of 0.5, and the performance level still remains significantly above 0.6 even for completely randomized values in the reference arrays (compare with figure 7.6).

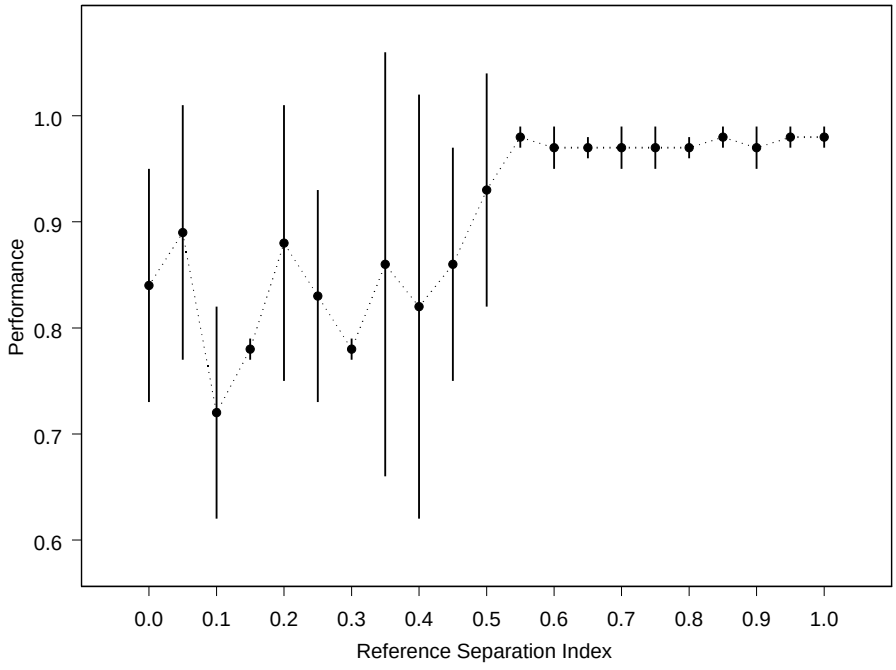

Figure 7.6: This figure shows the level of performance as a function of the overlap between references in a network with 400 neurons trained using 4 references and 4 patterns pr. reference. These data are identical to the data column corresponding to 4 references in figure 7.5. It should be noted that the network actually performs very well even with a reference separation index as low as 0.55, below which the performance degrades only little and stays significantly above 0.6 all the way down to a separation index of zero (the vertical bars show the standard deviation of the sample).

inactive). By permitting intermediate values for the reference afferents it is possible to evaluate whether any degradation of performance occurs when the synaptic subsets overlap to varying degrees. Subset overlap can be continuously varied by permitting the reference afferents to have random values between a lower and an upper limit which is specified independently for the different populations of references. For example, active hot-spots may be given random values within the interval $R_{active} \in [r_{min}, 1]$ while the non-active hot-spots have values within the interval $R_{inactive} \in [0, r_{max}]$. For simplicity the following relationship is given for the interval limits: $r_{max} = 1 - r_{min}$, in which case a single scalar value may be specified for the overlap between subsets, namely r_{min}, which has the value $r_{min} = 1$ for complete segregation ($R_{active} \in [1, 1] \Rightarrow R_{active} = 1$ and $R_{inactive} \in [0, 0] \Rightarrow R_{active} = 0$) and $r_{min} = 0$ for completely random reference values ($R_{active} \in [0, 1]$ and $R_{inactive} \in [0, 1]$).

Performance as a function of the number of references and the reference separation index was calculated for a network with 400 neurons trained on a protocol where the number of references varied from 1 to 12 with a step-size of 1 (and 4 patterns pr. reference), and the reference separation index varied from 0 to 1 with a step-size of 0.05. The resulting performance array is shown in figure 7.5, where the performance index has been colour coded. The empty squares within each coloured square indicate the variance (from 0 to 0.17) of the sampled data resulting from 4 independent trials. As expected, best performance is obtained for r_{min} close to 1 (i.e., total separation of synaptic subsets). Surprisingly, it can be observed that when using 3 or 4 references performance is also remarkably robust to changes in the separation index, to the extent that performance is virtually perfect down to a separation index of 0.5, and remains above a PI of 0.7 all the way down to a separation index of zero. As mentioned before, a separation index equal to zero implies that the values in a reference array essentially consists of random numbers between 0 and 1, and are therefore a far cry from the nice "binary" reference arrays used earlier. This evidence strongly supports the notion that reference activities do not necessarily have to be nicely segregated, but that they may have a considerable overlap amongst each other without seriously affecting network behaviour, a case in point if the methods presented here are to have any relevance in a biological context.

7.5 On the usefulness of synaptic subsets

In order to ensure safe storage and fast retrieval of a multiplicity of spatiotemporal patterns in a neural network, it is proposed in this work that dendritically based regional differences in synaptic plasticity are required, and that such regions can be individually accessed through activation of a "reference" input. Specifically, it is suggested that the NMDA receptor's voltage dependence may be used to keep track of dendritic sites with high activity, so that subsets of synapses can be kept functionally separated at those highly activated dendritic branches, especially if those branches are activated independently by means of a reference activity. Each synaptic subset can then be used as a learning locus which could contain a memory trace (e.g., one sequence), so that as many independent memory traces (sequences) as there are reference afferents can be coded into the network.

In addition to being a possible solution to the stability-plasticity dilemma in the context of sequence learning, a further advantage of using a reference-based memory access architecture is simply the speed with which a complex memory trace (such as a sequence) can be recalled from the network. As an example of this, see figure 7.2c, where the shift from one sequence to the other occurred almost immediately upon changing the reference signal. Also the method permits a tremendous economy of neurons in the sense that the same group of neurons may be involved in many different tasks (sequences) just by changing the reference, the alternative of course being to have a specialized group of neurons for each task. This suggests that the reference-based memory access architecture presented here will be most useful in cases where good recall with fast task transitions has to be accomplished with maximal economy of neural network size. Given these constraints, invertebrates and lower vertebrates would presumably have much to gain from such an architecture, and indeed there is some evidence that natural selection converged on such a solution at least at the organizational level. A case in point is the existence (in invertebrates) of so-called *command neurons* whose activity influences a *motor pattern generator* network in such a way that a particular sequential and stereotypical behavioural response is elicited which corresponds uniquely to the activated command neuron [143]. Activation of a different command neuron elicits a different action pattern. The relationship between the command neuron(s) and the motor pattern generator seems very similar to the relationship between the reference matrix and the sequence storage network, and is therefore a biologically valid example of a reference-based memory access architecture as the one advocated in this work.

Training a subset of synapses to perform some task, instead of using the full synaptic population, might at first seem counterproductive since one would expect a corresponding reduction in task performance. To address this issue directly, a computer simulation experiment was set up in which performance of a network was gauged as a function of the number of references and the number of patterns pr. reference (see section 7.4.1). The results of this experiment indicate that, although the pattern capacity pr. sequence is reduced when more sequences are to be learnt, the *total capacity* of the network (i.e. the number of sequences times the number of patterns pr. sequence) is actually *increased* up to a maximum which is 5 times larger (56 patterns) than the maximum number of patterns permissible when only one reference was used (10-12 patterns), as can be inferred from figures 7.3 and 7.4. If for no other reason, this manyfold increase in capacity should at least warrant using this kind of approach for densely connected recurrent networks.

It should also be noted, that the reduction in pattern capacity for individual sequences poses no problem if the references are controlled from outside the network: longer sequences corresponding to a composition of short sequences may be generated simply by activating the relevant references in the right order, for example by giving control of the references to a different recurrent network, which again might be influenced by another set of references controlled from yet another network, and so on *ad infinitum*. A modular system composed of such networks which sequentially code the references of subsequent networks can potentially be trained to generate sequences of *any* length while maintaining good accessibility to the memory contents (not unlike the easily addressable tracks of a record compared to the difficulty of finding storage positions on a tape). In lack of further evidence, I shall resist the temptation of relating

this reference based modular architecture to the language areas of the human brain, where one might suspect that references representing whole words activate sequences of patterns in a different area corresponding to phonemes, each of which subsequently serves as a reference to some other region responsible for generating a sound producing muscular sequence.

Binary reference activity arrays as those used for experiments 1 to 4 are simply not directly acceptable from a biological perspective, in particular because references must be assumed to be the consequence of synaptic activation which to all intents and purposes is a probabilistic and noisy process [254] whose effects depend on the weighted average of several consecutive activations giving rise to a post synaptic potential. A final experiment was performed (see section 7.4.2), in which the performance of a network was evaluated when varying the degree to which the reference arrays contained non-binary values. In the limit (minimum separation between reference arrays), the components of the reference arrays were random numbers between 0 and 1. Even in the limiting case with random valued reference arrays the network was able to perform surprisingly well (PI$\sim$ 0.7) when 4 references were used (see figure 7.5). This result is presented as evidence that the method is quite robust with respect to noise and overlapping/randomized reference arrays, and gives more credence to its proposed relevance for biological neural systems.

From a technical point of view, the learning strategy presented in this work might prove useful in the implementation of neural networks intended for learning of motor control strategies, in continuously behaving agents such as robots or software-based artificial autonomous agents: Once a motor sequence has been identified as not belonging to the already-learned repertoire, either by lack of recognition or by the influence from a teacher, this new sequence is appropriately assigned to a new subset of synapses within the motor effector area and learned there. If that same motor sequence is required at a later time, the control plant needs only to activate the appropriate reference activity to immediately recall the full sequence from the motor effector area. Such a functional architecture appears to be present in frogs, where modulators affecting the tectum can change the action repertoire of the animal [37]. Efforts in this direction are currently being pursued in combination with some recent ideas [45,46,47] regarding involvement of motor output in the generation of conscious perception and control, efference copy being the source of the reference signal.

It is still a matter of debate whether "hot-spots" like those found experimentally by Schiller et al. (2000) are of any use to the nervous system. The present work aims at specifying one of the possible uses that the nervous system may find for such "hot-spots", but it would not be surprising if other applications existed for differentially activated dendrites (such as those proposed in Segev [241], Mel [177], Agmon-Snir et al. [4]), perhaps even simultaneously. Also, it should be noted that the method presented here for synaptic parcellation invoking the NMDA receptor and dendritic anisopotentiality does not exhaust the ways in which parcellation could be realized in nervous systems, such as one-to-one modulation of synapses (perhaps requiring formation of synapses on the stalks of dendritic spines, like those observed in the basal-ganglia's neostriatal spiny cells [273]), some kind of inhibitory shunting [271] or highly localized Ca^{2+} transients (like those observed in branches and spines of Purkinje cell dendrites [54,55]). Any of these methods could thus in principle also be used to subdivide the synaptic population into individually trainable subsets.

This is work in progress and thus some outstanding questions still remain, but most importantly it remains to be investigated whether the reference activity as presented in this work has any relevance to real neurobiological systems. It is clear that some areas of the brain are exquisitely context sensitive even to the point that it becomes difficult to identify which factors actually make the difference[258]. Such context sensitivity may arise from neurons which are highly attuned to specific cues (be they internal cues as in efference copy, or external cues as in sensory stimuli), and it is this kind of neurons that to some extent are envisioned to be responsible for the reference signal in the present work (especially if assuming that a reference based architecture exists also in higher vertebrates). Other recent models[249,151] have invoked context neurons to allow for sequence disambiguation in the hippocampus. The present work differs from these other models in that it gives an alternative solution to the same class of problems, by invoking different neuronal properties expressed at the dendritic and synaptic level rather than at the whole-neuron level. Further studies will of course be necessary to decide whether sequence separation occurs at the synaptic level or at the single-neuronal level, but given the existence of command neurons and similar structures in invertebrates and lower vertebrates, these animals would seem to be particularly well suited candidates in which to search for the nitty-gritty details of reference-based memory access architectures.

The aim of this work has been to show that subdividing the synaptic population at the level of the dendritic branches can have some useful computational properties, and might even have some biological plausibility. It is hoped that this approach might give some insight into the workings of real nervous systems, particularly when selecting and encoding motor programs during continuous behaviour.

Chapter 8

Corticospinal Networks

Chapter Summary

A few of the most important anatomical features of the spinal cord will be reviewed, the purpose being to specify a realistic (although numerically reduced) model of spinal connectivity which may be incorporated into the computer model that is being developed. In the context of voluntary muscle control of the human arm, only the ventral spinal networks at the cervical segments need to be considered (as a first approximation). Some of the properties of the main corticospinal projections originating from corticomotoneuronal cells will also be reviewed and incorporated into the model.

A defining feature of animals belonging to the *phylum chordata* is the presence of a notochord†, the existence of a dorsal tubular nerve cord† and the presence at some point in their lifetime of pharyngeal gill slits†. In vertebrates the notochord is replaced by a vertebral column†, a feature which humans share with more than 43000 different species across 7 classes[250]: Agnatha (jawless fish), Chondrichthyes (sharks and rays), Osteichthyes (bony fish), Amphibia (frogs, toads and salamanders), Reptilia (lizards, snakes, turtles and alligators), Aves (birds) and Mammalia (mammals). The large success of all these animals in adapting to the enormous variety of environments in which they live must, to a large extent, be attributable to the excellent integrative properties of a centralized nervous system.

With such a wide range of applicability, it is no wonder that much research has been directed at studying the spinal cord (see Gordon[92], Burke[31], Purves et al.[217] for an overview), and indeed some of the earliest and foundational discoveries in neuroscience actually are related to this region of the nervous system[48]. It is probably also one of the best understood areas of the nervous system simply because neurons here have direct causal relationships with muscle activations or raw sensory input, both of which are easily measurable and

quantifiable[a].

8.1 Basic anatomy of the spinal cord

The spinal cord is a long tube with thick walls which runs inside the vertebral canal. The tube, or central canal, is filled with cerebrospinal fluid and its walls are an external layer of white matter and an internal core of gray matter (in a spinal cross-section, the gray matter resembles a butterfly). Functionally, the spinal cord is subdivided longitudinally into segments, each segment corresponding to a vertebrae and providing two dorsal and two ventral nerve-bundles called roots. Each of these roots corresponds to a particular set of muscles (motor efference through ventral roots only) and a specific band of sensory surface (sensory afference through dorsal roots only, including type Ia and type II spindle afference from a particular set of muscles). There is a very logical correspondence between the position of the segment along the cord and the corresponding muscles/sensory band: Segments at the cervical vertebrae are associated with arm muscles/sensory systems, while segments at the lumbar vertebrae are associated with the legs.

Another functionally important subdivision of the spinal cord is best appreciated in cross-section. The dorsal horns are the main target of the dorsal roots and are consequently mainly concerned with processing and relaying sensory related information. The ventral horns are mainly concerned with processing and relaying motor output related information, and are thus the source of the ventral root projecting efferent fibers to muscles and spindles. There are some complex interconnections between the neurons residing in the dorsal and ventral horns [92], mostly mediated via interneurons. A large proportion of these connections are directed from the dorsal to the ventral horns, and it is fair to say that via these connections the motoneurons in the ventral horn are very well informed with respect to exteroceptive† and proprioceptive† input (see below).

By placing retrograde tracers in a muscle, it is possible to observe the distribution within the spinal cord of all the motor neurons innervating the muscle. Typically such a motor neuron pool will contain approximately in the order of 10^2 large motoneurons [280], organized as narrow columns or rods running longitudinally within the ventral horn, and often spanning a few segments [217,34]. These columns are arranged so that the proximal muscles' motoneurons are arranged medially while the distal muscles have columns in lateral regions of the ventral horns. A detailed model of the motor neuron pool will be developed in chapter 9.

8.2 Connectivity and Neuron populations in the ventral horn

On first inspection, the neural connectivity within the ventral horn might appear bewilderingly complex. Fortunately, there are some very simple organizational principles which make it possible to make some progress nevertheless, as they

[a] Contrast this to the situation in the human association cortices which are far removed both from sensory input and motor output, and whose activity is far more difficult to interpret

reveal that the complexity by and large is caused by a repetition of the same basic circuits.

One very important organizing principle has to do with the activation of muscular synergies, i.e. groups of muscles that are functionally linked and hence are, more often than not, activated together. An example could be the synergy between the biceps, and the brachialis, both of which will cause elbow flexion. Under this principle, interneurons can often be trusted to have a projection field centered at neurons corresponding to a particular muscle but spreading also to neurons corresponding to other muscles in the same synergy or to neurons that inhibit an antagonistic synergy. This principle is so important, in fact, that it is not unreasonable to use it to define a canonical spinal circuit

8.2.1 Motoneurons

Motoneurons have the distinctive characteristic that they are the only neurons in the CNS which directly innervate non-neural cells[82,217], their main function being to stimulate contraction in muscle tissue. There are three classes of motoneurons in the ventral horn: α, β and γ, which are distinguished by the specific kind of muscle fibers that they innervate. Histochemically these motoneurons are rather similar, however there are quite significant size differences between them[105] (see also chapter 9). Anatomically they are all located within Rexed's lamina XI[222,31].

α-motoneurons

The best understood and functionally transparent neuron type in the whole central nervous system is certainly the α-motoneuron. The function of this neuron type is simply and solely to activate extrafusal muscle tissue to a level determined by a weighted evaluation of its input. This apparent simplicity completely vanishes when one considers the inputs to the cell because afference to α-motoneurons is complex and multimodal. Just to mention a few sources of afference (for review see Burke[31]): Type Ia spindle afference, type II spindle afference, type Ib GTO afference, Renshaw cells, IaIN, corticomotoneuronal, rubromotoneuronal, vestibulospinal tract, skin sensory neurons, joint sensory neurons, intersegmental connections. It is estimated that each α-motoneuron receives 50000+ synapses from about 10000 such neurons[281,31], however the exact numerical contribution from each source has yet to be elucidated in most cases (but see table 8.1).

It should be mentioned that the axons of α-motoneurons belong to the $A\alpha$ fiber class[51,202], and have conduction velocities in the range from 70 to 120m/s. Thus a conduction delay of 5ms may be assumed between spinal cord and distal arm muscles. The axon of a given α-motoneuron has ACh based synaptic terminations (neuromuscular junctions) on a number of extrafusal muscle fibers. This collection of muscle fibers together with the α-motoneuron responsible for their innervation is known as the motor unit (see chapter 9). A complex interaction between the motoneuron and the innervated muscle fibers takes place upon the arrival of a spike, the main outcome of which is the sudden contraction of the muscle fibers, a twitch. A model of this process is provided in section 9.3. α motoneurons come in a variety of sizes, and there are several important features which seem systematically correlated with the conduction velocity (size) of the

particular motoneuron[105,186,189]: Larger motoneurons are part of stronger and faster motor units than the corresponding units associated with smaller neurons (see chapter 9).

Via an axon collateral the α-motoneurons also innervate a number of Renshaw cells (see below), thus providing feedback inhibition to the synergic motoneuron pool. According to some accounts[31] there are also some size-related correlations in this connection in that larger motoneurons produce larger PSP's in the target Renshaw cells than do the smaller motoneurons. Perhaps surprisingly, the inhibitory effect of Renshaw cells on the larger motoneurons is less than on smaller motoneurons.

γ-motoneurons

The immediate function of this cell type is also very well defined, it is simply to activate the contractile element of the muscle spindles. Its precise role in movement, however, has been (and still is) the source of much controversy[95,214], as it touches upon some central issues related to motor control theory (see chapters 10 and 11). The afference to this type of neuron is little known, although it seems to be much the same as for the α-motoneurons, albeit with at least one important exception: There are no type Ia afferents to γ-motoneurons (probably to avoid instability due to strong positive feedback), however there is some evidence that they receive type II afferents[127]. The axon from γ-motoneurons belongs to the $A\beta$ fiber classification[202], with conduction velocities in the range from 30 to 80m/s. A conduction delay of approximately 5-10 ms should therefore be assumed between spinal cord and distal arm muscles.

Considering that intrafusal fibers may be dynamic or static giving rise to type Ia and type II spindle afference respectively (see chapter 10), a distinction should at least be made between γ-motoneurons which innervate dynamic bag fibers (γ_d) and those which connect to the static bags and chains (γ_s). The spinal connectivity patterns of both species are very similar, although there might be differences in the particular sources projecting to each group.

β-motoneurons

This neuron type innervates extrafusal and intrafusal muscle fibers alike, making it an intermediate between α and γ-motoneurons. Its role in motor control is complicated by the fact that this type of neuron does receive type Ia spindle afference, creating strong positive feedback loops.

8.2.2 Interneurons

Strictly speaking, an interneuron is any neuron which only has neuronal afferents and only innervates other neurons. Such a broad definition is really not very useful as it includes the vast majority of neurons in the CNS, so instead it is often used in a more regional sense, i.e. a neuron mediating communication within a restricted area of the nervous system. There are various classes of interneurons in the spinal cord, many of which have been studied extensively [113,276,31]. Functionally, the best characterized are the Renshaw cells, the Ia inhibitory interneurons and the Ib inhibitory interneurons.

Renshaw cells (R)

These cells are located in Rexed's lamina VII, and are primarily characterized by their connectivity pattern: Renshaw cells provide inhibition to the same group of α-motoneurons from which they receive excitatory inputs. As is common for inhibitory neurons, Renshaw cells can attain very high firing frequencies ($\sim$ 1000Hz). It is hypothesized[31] that there are two populations of these cells which have the same connectivity but use different inhibitory neurotransmitters (GABA and Glycine) for the task (although there is also evidence that GABA and Glycine may coexist in the nerve terminals on motoneurons[209]). As mentioned earlier, the inhibitory effects of Renshaw cells on large motoneurons seem to less than those on small motoneurons, however larger motoneurons produce larger EPSP's on Renshaw cells than do small motoneurons[116,115]. Finally, it has been reported that Renshaw cells may inhibit each other[231], and that they also inhibit IaIN cells acting on the antagonist muscle. An extensive review of the form and function of Renshaw cell connectivity is given in Windhorst[277].

Ia Inhibitory Interneurons (IaIN)

One of the targets for type Ia spindle afferents is a class of interneurons which primarily inhibit the motoneurons of antagonist muscle groups. These interneurons are sometimes referred to as IaIN, and certainly form an important class of neurons in the spinal cord. They receive input from many different neuron systems, most importantly from Ia afferents, Renshaw cells, and antagonist IaIN, but also from a wide variety of tracts (vestibulospinal, corticospinal, rubrospinal) as well as from cutaneous and joint afferents. Reciprocal inhibition seems to be the most prominent function of these neurons[276,31], but the exact functional role of IaIN will be influenced by which set of afferents to the IaIN that are most prominently active. For example during a stretch reflex, the firing rate of Ia afferents from the stretched muscle will increase, causing a reflex contraction of the stretched muscle, while simultaneously inhibiting the antagonist muscle via the IaIN. In a similar vein, a descending tract which excites or inhibits a particular motoneuron also sends collaterals to IaIN thereby inhibiting or exciting the motoneurons of the antagonistic muscle respectively[92].

Ib Inhibitory Interneurons (IbIN)

As their name indicates, these neurons receive their main inputs from type Ib sensory afferents, but other systems also contribute, such as EIns mediating cutaneous and joint sensory afference, and Ia afference. Ib inhibitory interneurons provide strong inhibitory input to homonymous motoneurons, and form part of an important mechanism to avoid muscle damage by reducing force production in overtensed muscle. A role in muscle force regulation during mechanical contact between a limb and the environment has also been suggested[92].

Excitatory Interneurons (EIn)

The existence of polysynaptic excitatory pathways in the spinal cord has been inferred by observing the delays between the time when a certain fiber system was activated, and the appearance of EPSP's in the presumed targets[31]. Very short delays indicate the presence of a monosynaptic connection whereas longer

delays might be attributable to polysynaptic connections characterized by the existence of interceding interneurons. Many excitatory interneurons have thus been identified, primarily in connection with sensory afferent systems which always seems to have synapses on EIns. There is thus a polysynaptic excitatory connection mediating cutaneous and joint afference which affects IbIN cells[92]. There is also a polysynaptic excitatory connection linking type Ib afferents to antagonist motoneurons[92]. And finally, there is a very important polysynaptic excitatory connection between type Ia and II afferents and the α motoneurons[31]. Most descending pathways will likewise activate polysynaptic circuits, but the details of these are less well known due to the difficulties inherent in identifying this neuron types[93,31].

PAD interneurons

Primary afference is subjected to cortical modulation via presynaptic inhibition of Ia terminals on motoneurons[53,182](for an extensive review of this subject, see Rudomin and Schmidt[229]). Presynaptic inhibition is usually accompanied by primary afferent depolarization (PAD), and is probably mediated via populations of GABA-ergic interneurons that have axo-axonal synapses on the primary afferents at their junctions with motoneurons[229,182]. Collectively, the interneurons responsible for this type of inhibition are sometimes referred to as PAD interneurons. Stimulation of the sensorimotor cortex (in cat) decreases this kind of presynaptic inhibition[163,228], an effect that under normal conditions is centrally programmed and observable roughly 50ms prior to the beginning contractions of the activated motor units[205]. There seems to be evidence pointing to a differential cortical effect on presynaptic inhibition depending on the functional role of the activated muscles[182]: in leg muscles motor cortical activity decreases presynaptic inhibition, thus facilitating the reflex pathways, whereas the opposite apparently is the case for the wrist muscles. Hultborn et al.[117] have reported that presynaptic inhibition is decreased in voluntarily activated muscles, but simultaneously increased in the non-active ones. Overall this activation pattern increases the gain of the monosynaptic reflex in the active muscles, perhaps enabling improved load compensation[229]. Flexor reflex afferents (FRA) also modulate the PAD pathways, and it has been surmised that appropriate cutaneous stimulation will reduce presynaptic inhibition, so that the gain of primary afference dependent reflexes becomes automatically increased during limb contact with the environment[182].

8.2.3 Sensory Afferents

A distinction is made between exteroceptive and proprioceptive afferents. The difference is related, respectively, to whether the information they carry is caused by events in the environment (mediated through touch, pain, pressure and temperature sensors), or whether the afference is associated with actual movements of the body (spindles, golgi-tendon organs, joint sensors, etc.). Thus, sensory information arriving at the ventral horn is highly multimodal, as would be expected of a system which has to produce fast and contextually appropriate responses independently from any central control. Simple reflexes, and locomotion are good examples of such responses. In the present case only proprioceptive afference will be considered as it is the most directly linked to the

control of movement, and emphasis will be mainly on those sensory inputs generated by the muscle stretch receptors which are mediated via type Ia and type II fibers.

Type Ia fibers

A stretch sensitive annulospiral innervation surrounds the central regions of dynamic bag and static chain fiber elements of the intrafusal fiber system in muscle[93,36] (see chapter 10). When the intrafusal fiber is subjected to a change in length, the innervated region will also change its length, but at a different rate, depending on the mechanical properties of the particular fiber (see section 10.1), which results in a stereotypical firing pattern, that for the type Ia fibers is highly correlated with the rate of change of length of the whole muscle. Firing rates in this type of fiber go from approximately 20 Hz at rest to over 150 when maximally stretched[93,31,259]. These fibers are among the fastest conducting fibers in the nervous system as they belong to the $A\alpha$ fiber class[51,202], with conduction velocities in the range 70 to 120m/s. The maximal conduction delay from a spindle in distal arm muscles to spinal cord will seldom exceed 5ms (assuming a distance of 50cm).

At the afferent side, type Ia fibers synapse directly onto α and *beta* motoneurons that are associated with the same muscle, and less densely on motoneurons of synergistic muscles. Type Ia fibers are also the principal input to type Ia inhibitory interneurons. The synapse is excitatory as it uses glutamate as transmitter in connection with AMPA type receptors postsynaptically[31]. On average there are about 10 synapses from a single Ia afferent onto any of its motoneuronal targets, making a very powerful connection. To a first approximation, it may be assumed that a muscle with n motor units, will have roughly $0.1n$ type Ia fibers, which means that a given motor neuron would be receiving at least n synapses associated with homonymous Ia afference. This assumption is based on numerical estimates of the number of Ia synapses on motoneurons (1000 approximately)[31], synaptic redundancy (10 synapses from the same Ia fiber)[31] and the typical size of a motor unit (10-2000 according to some accounts)[82]). However, some reports seem to favour a slightly denser connectivity where each Ia afferent contacts all motor neurons of the homonymous muscle plus a large fraction of the motor neurons of synergist muscles[179,92].

Type II fibers

In many respects this type of fiber is similar to the type Ia fiber, as it also conveys information from the spindles to the motoneurons. However, there are some very important differences. In particular, type II fibers solely innervate chain fibers in the spindle, and therefore only are responsive to the actual length of the muscle. Other important differences are that it has a much lower conduction velocity, a weaker connection to α motoneurons[31,127], and a monosynaptic but weak connection to γ motoneurons[127]. Like the Ia fibers, type II fibers also have excitatory effects on the Ia inhibitory interneurons. These fibers are slightly slower than Ia afferents, as they belong to the $A\beta$ fiber classification[202] with conduction velocities in the range from 30 to 80m/s. From a distal hand muscle to the spinal cord a conduction delay of 5-10ms should be assumed.

Origin	Class	Destination	Transmitter	E_{RP}
α	RS	Extrafusal	ACh	0mV
α	RS	Renshaw (H)	ACh	0mV
β	RS	Extra- and Intrafusal	ACh	0mV
γ	RS	Intrafusal	ACh	0mV
Ia	FS	α (H)	Glu	0mV
Ia	FS	EIn(H)	Glu	0mV
Ia	FS	IaIN(A)	Glu	0mV
Ia	FS	IbIN(H)[93]	Glu	0mV
II	FS	α(H), γ(H), EIn(H) (IaIN(A))	Glu	0mV
Ib	FS	IbIN(H)	Glu	0mV
Ib	FS	EIn(A)	Glu	0mV
IaIN	FS	α(H), IaIN(A) and γ(H)	Gly	-70mV
Renshaw	FS	α(H),γ(H)	GABA Gly	-70mV
Renshaw	FS	IaIN(A)	GABA Gly	-70mV
Renshaw	FS	Renshaw(A)	GABA Gly	-70mV
EIn	RS	IbIN,α	Glu	0mV

Table 8.1: Overview of spinal neuron types. Compiled from Jankowska and Gladden[127], Gordon and Ghez[93], Gordon[92], Burke[31, 32]

Type Ib fibers

Golgi tendon organs (GTOs) are specialized structures in muscle tendons which are well suited to measure a muscle's absolute tension especially during contraction. They are innervated by type Ib fibers which thus bring tension related information to both agonist (disynaptic inhibition via type Ib inhibitory interneurons) and antagonist motor neurons (disynaptic excitation via excitatory interneurons of the antagonist muscle). The GTO is highly sensitive to tension changes: the twitch of a single motor unit in a muscle is sufficient to increase the firing frequency of Ib afferents[92]. These fibers are as fast at the Ia afferents (70-120m/s is the normal range)[202], with similar conduction delays from distal hand muscles to spinal cord (5ms).

8.3 The Myotactic Unit

Due to the fact that muscles can only produce pulling forces, movement about any joint necessarily requires at least two counteracting muscles, usually termed the agonist muscle and the antagonist muscle. From the anatomy reviewed before, it seems that the whole motor system in the spinal cord is organized around this fundamental principle: The direct or indirect effect of any spinal neuron on the agonist muscle will be exactly opposite the effect on the antagonist muscle. Consider the following example:

1. Renshaw cells receive excitatory connections from α-motoneurons innervating a particular (agonist) muscle and provide inhibitory feedback to the α-motoneurons, dynamic and static γ-motoneurons, and inhibitory Ia interneurons.

2. Renshaw cells inhibit Renshaw cells that innervate the same cell groups

corresponding to the antagonist muscle

All in all, these points indicate that whenever a Renshaw cell is activated by the agonist muscle's motoneuron pool, it tends to inhibit all neurons that would directly or indirectly increase force production in the agonist muscle (point 1), and it would simultaneously be disinhibiting all neurons that increase force production in the antagonist muscle (point 2). A similar analysis of all the other neuron types in the spinal motor system reveals a similar pattern: If a neuron's net effect on the agonist motor neuron pool is excitatory, then it will be inhibitory on the antagonist motor neuron pool. And vice versa.

Thus a very simple organizational principle seems to apply, permitting the clear delimitation of a functional unit that controls movement around a single joint. This has sometimes been referred to as the Myotactic Unit[92,159], which corresponds to the minimal spinal circuitry that is involved in regulating joint stiffness and torque. Figure 8.1 presents a numerically reduced version of just such a myotactic unit for a two muscle joint, which includes all the major neuron groups and their interconnections (described in sections 8.2.1 to 8.2.3). In association with the specifications in table 8.1, figure 8.1 shows the basic connectivity patterns that will form the basis for the spinal networks used for the simulations of human arm movement presented in chapter 11.

8.4 The cortical connection

Experimentally based investigations into the functional localization of areas in the cortex began in 1870 with the work by Fritsch and Hitzig on the motor cortex of dogs. They showed that stimulation of the dog's cortex elicited contralateral limb movements. Later work by Leyton and Sherrington[150] demonstrated that the motor cortex is topographically organized in a relatively simple way, giving rise to the idea of a motor-homunculus. The simplicity of the "homuncular" motor cortex belies the underlying organizational complexity, where it becomes evident that at small length scales, the homunculus disappears. For example it has been demonstrated that individual neurons in the arm area of primary motor cortex do indeed influence multiple arm muscles, even to the extent that they innervate combinations between proximal and distal muscles (McKiernan et al 1998). Indeed, in later years it has become increasingly clear that the motor cortex has a much more complex, modifiable and distributed organization than what was previously assumed[235,236,232].

In a thorough review of cortical architectonics, Braitenberg and Schüz[28] provide much of the necessary statistics and geometry to build a general model of a cortical network. For our present purposes it will not be necessary to implement a cortical network in full detail because focus will be directed mainly at only a small subset population of cortical neurons commonly known as cortico-motoneuronal cells. These cortical neurons have descending projections which enter the spinal cord mainly via the corticospinal tract, and are thus primarily associated with the activation of distal muscles[147,148]. A technique known as "spike-triggered averaging of rectified EMG activity" was developed by Fetz and Cheney[65] for identifying *in vivo* cortical cells with direct connections to motoneurons. This technique is based on the idea that the firing probability of motor units (and hence the EMG) must be influenced directly by monosynaptic cortical connections. The influence of a cortical neuron on motor unit

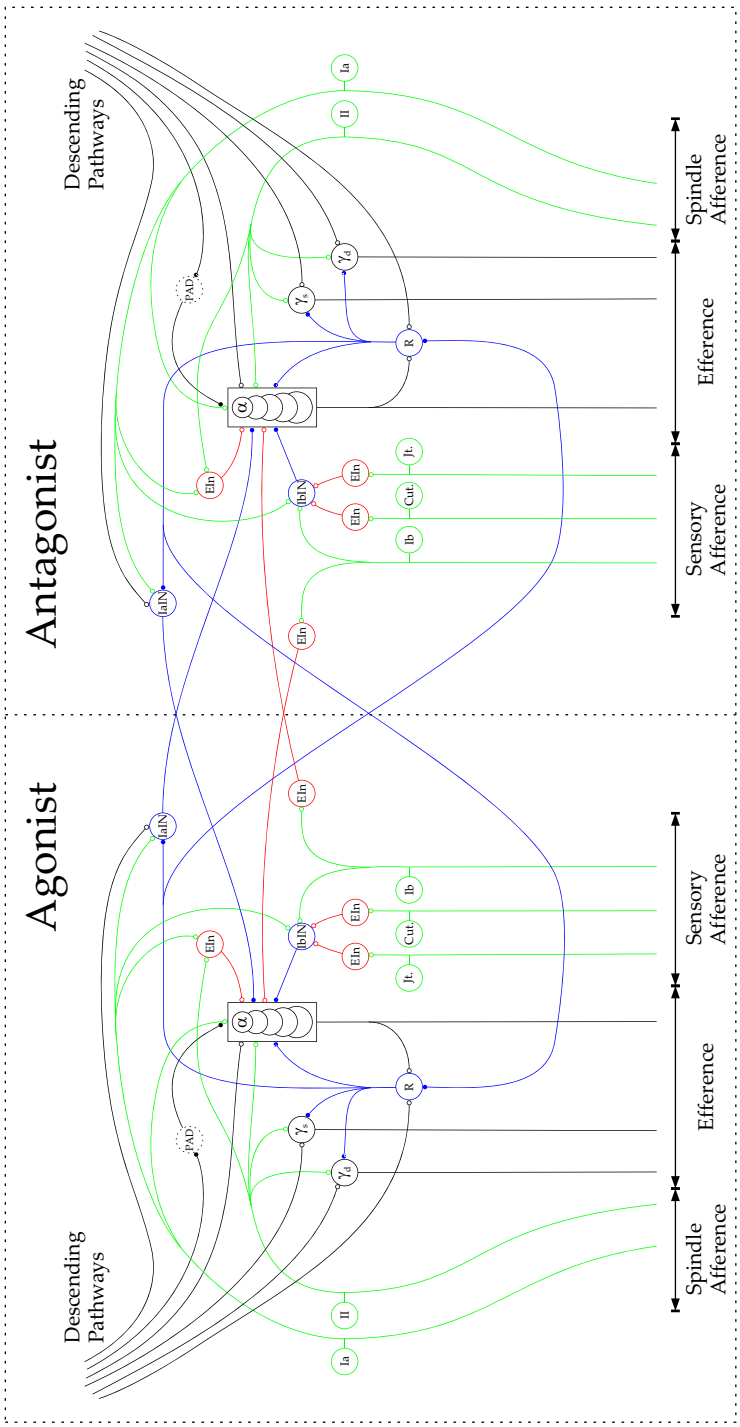

Figure 8.1: Basic motor circuitry in the spinal cord represented by a bi-muscular myotactic unit. Any number of motor units may be added to the myotactic unit. Nomenclature: α=α-motoneuron, R=Renshaw cell, γ_s=static γ-motoneuron, γ_d=dynamic γ-motoneuron, Ia=primary spindle afferent, II=secondary spindle afferent, EIn=Excitatory Interneuron, IaIN=Ia Inhibitory Neurons, IbIN=Ib Inhibitory Neuron, Jt.=Joint receptor, Cut.=Cutaneous fiber, Ib=Golgi tendon organ afference, PAD=PAD interneurons.

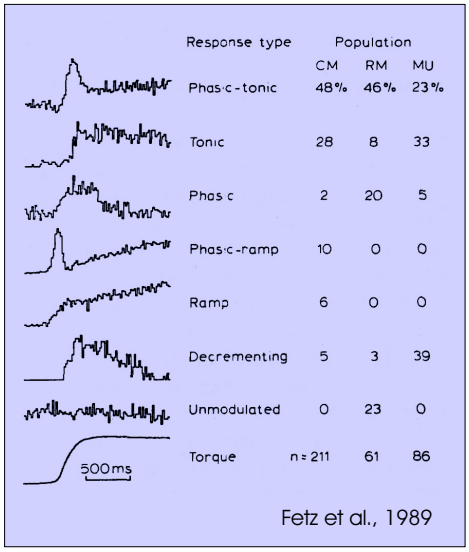

Figure 8.2: Response patterns of CM cells during ramp-and-hold wrist movements (figure from Fetz et al.[67]). See text for details.

activity may be deduced by aligning EMG traces with respect to the firing of that particular neuron[65,67,40]. In an elegant series of experiments Cheney and Fetz[39] have identified several functional classes of cortical cells under a variety of circumstances have strong *correlations* to EMG's, and hence to movement. Such cells are commonly referred to as "corticomotoneuronal" (CM) cells and their- activity patterns during various movement tasks have been classified[67] into six basic response patterns which seem to be prevalent among CM cells, as shown in figure 8.2, which also shows the relative percentage of each activity class (from Fetz et al.[67]).

As can be seen in figure 8.2, the two most common response patterns of CM cells are the phasic-tonic (48%), and the tonic (28%), and consequently these have received most attention as to their putative roles in motor control. It has thus been suggested[66] that the phasic component might be necessary for overcoming the inhibition of inactive agonist motor units and for inhibiting antagonist motor units via the corticospinal projections to IaIN cells. However, it should be emphasized that corticomotoneuronal EPSP's on spinal motoneurons are relatively small, and are probably not able to fully recruit the motoneuronal pools[66,31] (other descending systems are required for effective recruitment, such as the rubrospinal, the vestibulospinal and the reticulospinal). Furthermore, there are several instances in which the CM cells are active without observable EMG's in the innervated motor unit, or where they are inactive during the presence of strong EMG's. Various such situations are listed in Fetz and Cheney[66]:

- During ramp-and-hold movements CM cells increase their firing rates at various times before and after EMG onset in target muscles (-71 ms for phasic-tonic, -63 for phasic-ramp, +5ms for tonic and +101 for ramp)[40]
- At low muscle force levels, CM cells may be active (tonically) without an

accompanying activation of their target motor units.

- CM cells are recruited during passive (imposed) movements of the limbs when the target muscles are stretched, and thus these cells must almost certainly be responding to primary and secondary afferent activity (and even cutaneous stimuli).

- A few CM cells are recruited at higher force levels than what recruited the target motor units.

- CM cells are surprisingly inactive during forceful movements (such as rapid shaking) or in general when large forces are required (power grip).

All these observations lend support to the notion that CM cells are strongly correlated with movement, but not necessarily causing it, and in fact may have more a role of modulating voluntary movements requiring high precision. It is well known that descending tracts innervate several distinct cell populations in the spinal cord (see figure 8.1), and in particular it is common to observe that projections targeting motoneurons in fact target both the α and the γ variety, if not directly then certainly via local interneurons[83]. So what might then be the exact role of such cells, given their wide variability in pattern responses? An intriguing possibility will be explored in chapters 10 and 11, namely that CM cells might be involved in the cancellation or modulation of expected afference coming through primary and secondary fibers. The basis for this supposition resides in the observation that there are some similarities between the CM response patterns and those γ-motoneuronal activity patterns that would produce complete afference cancellation. These similarities extend also to the early onset activation of the phasic-tonic CM cells and to the late onset activation of the tonic CM cells.

8.4.1 Cortical functional topology

On first inspection, it might seem compelling to think that the introduction of lateral connectivity in the cortex will produce a sheet that only allows 2-dimensional mapping functions. Let us say the cortex is aligned to the xy-plane, then a given position in this plane, $\boldsymbol{r} \in \mathbb{R}^2$, will uniquely represent some piece of information. If the cortical plane is further subdivided into specialized regions then the nature of the information represented by $\boldsymbol{r}$ will be determined by the regional specialization. Thus, neural activity at a position inside the ocular dominance region corresponding to the left eye and inside the subregion corresponding to red coloring might represent the degree to which there are any red-tainted lines within the receptive field of the retinal ganglionic cell.

The existence of horizontal projections which spread out tangentially to the cortical surface posits a situation where lateral spreading of activity in the cortical mantle is a possibility. From being a concatenation of separate columns functioning independently and in parallel, a cortical region now becomes a self-contained dynamical structure capable of sustaining various attractor states[73]. In chapter 2 the notion was introduced that cortical networks might use lateral spreading of activity for computational tasks. Some simulations were reviewed where it was found that local lateral connectivity could be used for complex computations[86]. But this was under the assumption that the cortex functioned

as a 2 dimensional diffusion network, where each dimension corresponded to a parameter in the motor control problem (in that case it was the joint angles θ_1 and θ_2). Constraints can be imposed in such a system by blocking out connections, essentially limiting the routes through which activity diffusion might occur.

There is the question of cortical dimensionality: Connectivity within the cortical mantle produces a topological network which has been estimated [234] to be of at least 8 dimensions (based on the estimation of the *kissing number* of dense sphere packing). This should probably be seen as a lower estimate, because in more densely interconnected areas, the dimensionality would increase proportionately. This would mean that direct parametrization of the cortical dimensions leads to a situation where at most 8 degrees of freedom may be controlled with a given area of the motor cortex. How does this relate to the problem of controlling the body? The mobility of the human body is approximately 244 (see chapter 3), requiring an equivalent number of cortical dimensions. The first impression is that such a high mobility would be impossible to control with an 8-dimensional cortex. However, it is well known that the motor cortex is subdivided into several regions, each specialized in the control of one part of the body [150]. Kinematically, the most difficult single limb to position would be the arm with its 7 DOF's, and indeed it has its own partition in the motor cortex, as does each individual finger (4 DOF's each), each leg (6 DOF's). It seems, therefore, that each distinct area of the motor cortex is dedicated to controlling a system of lower dimensionality than 8, thus in principle leaving plenty DOF's unused.

This idea, that horizontal connections in the cortex might be involved in computations by constrained activity diffusion (or percolation) in a high dimensional network is very compelling, and in fact warrants much more investigation than what will be dedicated to it in this thesis. Assuming there is some truth in this hypothesis, the major problem really is to find what are the parameters that are controlled by the cortical network. It can certainly not be expected that the cortex specifies joint angles alone (as required in the model by Glasius et al. [86]). Identifying some of these parameters will be an important component in the rest of this work.

Chapter 9

The Motor Unit

Chapter Summary

In this chapter, a brief review of the different motor unit types will be given. Also a theoretical model of muscle fiber activation is provided, and compared with experimental data. The importance of scaling factors in the context of muscle modelling is emphasized and a model is derived which provides quantitatively accurate results even for simulations with only very few motor units, and which accounts for many of the experimentally observable properties of motor units during whole muscle activations. Finally, a full model of the *biceps caput breve* is tested as an example of all other muscles that are included in the arm model (chapter 11).

Once again, Sherrington has provided the first clues, and a name, to a very important concept that has certainly had a major influence in the study of vertebrate movement, namely the , which is the basic unit of motor control in vertebrates. It is well established [155,217,31] that a given motoneuron (of the α or β types) innervates a number of extrafusal muscle fibers within the muscle to which it projects. A one to one innervation ratio (one muscle fiber is innervated by a single motoneuron) may be found in certain muscles required for extremely precise movements (fingers, eyeball) [8]. However, the innervation ratio of a motor unit typically depends on overall muscle size and on motor unit type (see below), and ranges from 10 fibers pr. motoneuron in the smallest units (e.g. in human extraocular muscles) to 2000 fibers pr. motoneuron in very large motor units (e.g. in gastrocnemius muscle) [82,280]. These fibers are evenly (and randomly) spread out among other muscle fibers, so that the force produced by activation of a given motor unit is well distributed, and in the case of failure it does not affect muscle function significantly.

9.1 Motor unit types

Histochemically it is possible to identify three different fiber types in muscle each of which is characterized by the dominance of one of the three different isoforms of the myosin heavy chain (MHC) molecule. These are known as isoform I, isoform IIA and isoform IIB[32,8], and confer different contractile properties to the fibers [a]. The three fiber types vary with respect to their fatigability, contraction speed and maximum attainable tension[8,280]. In a given motor unit all fibers will usually be of the same type[217,57,82], so the contractile properties of a motor unit will be directly dependent on the identity of the constituent muscle fibers. In this context, the following physiologically based classification scheme of motor units has proven very useful[32,8,280,82]:

S : Slow motor unit fibers ("red meat") contract slowly but can maintain a constant tension for more than an hour of continuous activation. S-type motor unit fibers contain the type I isoform of the myosin heavy chain.

FR : Fast fatigue-Resistant motor unit fibers contract rapidly, generate intermediate tension levels and can maintain tension almost as long as the slow muscle fibers. FR-type motor unit fibers contain the IIA isoform of myosin.

FF : Fast Fatigable motor unit fibers ("white meat") contract rapidly but fatigue within minutes of continuous activation. These fibers contain the IIB isoform of myosin.

It should be noted that hybrid muscle fibers containing varying amounts of the different myosin isoforms also exist, creating a continuous spectrum of fiber properties (and thus of motor units). It has been reported[8] that conversions between fiber types can occur naturally as a consequence of training or aging, further complicating the picture. Finally, it should also be noted, that the proportion in which these fiber types are present within different muscles depends on the biomechanical requirements normally imposed on the muscle. Thus posture holding muscles will typically have a larger proportion of slow fibers[8].

There are at least three other properties of the motor unit which seem to coincide with the histochemical classification of its fibers: The motoneuron's activation threshold (neuron size), the innervation ratio and the cross-sectional area of individual fibers. Thus it has been observed, that large motoneurons have high innervation ratios to wide FF-type fibers while small motoneurons have low innervation ratios to narrow S-type fibers. Medium sized motoneurons have, not surprisingly, intermediate properties[8,217,57,82]. Functionally, this turns out to be a very important property of motor units, and is the basis for the production of precisely controlled movements as will become clear in the next section.

9.2 Orderly recruitment – The size principle

Finely graded changes in muscle tension may be produced by recruiting motor units in a very orderly and logical fashion. This was first discovered by

[a] Yet another isoform has been identified recently, known as IIx, and has properties in common with types IIA and IIB. For review and references concerning this and other myosin isoforms see Burke[32], Andersen et al.[8]

Henneman[105], who observed that by gradually increasing the afferent activity to a given motor pool, a gradual increase in force was obtained. It was found that motor neurons were recruited according to their axonal conduction velocity (and hence in proportion to their size), with slow (small) neurons being recruited first. This recruitment order is now known as the size principle of motoneuron recruitment. The gradual tension increase is a consequence of the fact that small motor neurons innervate type S fibers, medium sized neurons innervate FR fibers while the largest neurons innervate FF fibers. So, in other words, the first fibers that are recruited are the S fibers, which are the most fatigue resistant and produce the smallest tension, shortly followed by the much faster and stronger FR fibers, until finally the very strong and fast FF fibers are recruited.

If, as seems to be the case, the spectrum of motor unit sizes, twitch forces and excitabilities is continuous[186,189,279], a very smooth recruitment of units should be possible. According to some accounts[186,189], the number of motor units producing a given twitch force is best described by an exponential distribution (with an overabundance of small twitch forces). Exactly how this exponential distribution comes about is not entirely clear as it is a mixture of various factors: 1) the true distribution of motoneuron radii in the spinal cord [105], 2) the form of the proportionality between absolute motoneuron size and the end-plate potential (affecting twitch duration and amplitude)[279], 3) the form of the proportionality between motoneuron size and fiber cross-sectional area [82,8], 4) the exact relationship between motoneuron size and fiber composition of myosin isoforms[32,8]. In the following simulations it will be assumed that motoneuron radii follow an exponential distribution in league with the motor unit distribution.[b]

9.3 Neuromuscular junctions and their muscle fibers

The synapse linking motoneurons to muscle fibers is known as the neuromuscular junction, and is in may respects an archetypical directly gated synapse (see chapter 6). As such it has played an important role in the elucidation of synaptic mechanisms of transmission, and many models have been forwarded to yield up important information regarding the causal links involved (reviewed in Kandel and Siegelbaum[132]). Superficially, the activation dynamics observed at the muscle fiber do resemble the dynamics of a facilitatory synapse during short stimulations, with the addition of depressive dynamics during long stimulations (see chapter 6). This superficial similarity should not be taken too far without further study, simply because muscle activation is not only related to synaptic dynamics. After the arrival of an action potential with its resulting end-plate potential, it is well known that the final event causing contraction in muscle

[b] At least one other possible scenario seems to be discarded on a first inspection, namely that the radii of motoneurons within a motor neuron pool should conform to a normal distribution (i.e. mostly containing middle sized neurons with a few very large and a few very small neurons). Such a distribution would imply that the middle sized neurons would be required to form most of the slow/weak motor units (to account for the numerical superiority of this kind of motor unit), contrary to experiments showing a direct proportionality between neuron size and motor unit force (for review see Ghez[82]).

is the release of Ca^{2+} ions from the internal Ca^{2+} stores in the sarcoplasmic reticulum[176,82] and into the intracellular regions at the sarcomere where the myosin and actin filaments are located. As mentioned in chapter 4, intracellular Ca^{2+} is necessary to move the tropomyosin-troponin complex away from the actin binding site, and thus permitting the formation of cross-bridges[176,57]. Released Ca^{2+} will slowly be sequestered back into the sarcoplasmic reticulum, and with the lowered Ca^{2+} concentration, the tropomyosin-troponin complex will again conceal the actin binding sites. In a sense, the sarcoplasmic reticulum may be likened to a very slow "internal" synapse using Ca^{2+} as its transmitter in response to the arrival of an end-plate potential.

In the present case, the specific details of neuromuscular synaptic transmission and subsequent activation of the sarcoplasmic reticulum are not considered, but are instead subsumed into a simplified model of muscle fiber activation. The motivation for doing this is that sufficient data is available concerning the spike to force response properties of the muscle fibers (reviewed in Ghez[82]). In particular, it is well known that the twitch force of a muscle fiber (or motor unit) will have a sharp increase shortly after the arrival of a motoneuronal spike, and that after this initial rise, the force will slowly decay back to zero with a time constant in the order of 100 to 200 milliseconds. At low motoneuron spike frequencies the individual twitches are readily observable. However, if the frequency is increased, the individual twitches will begin to overlap each other (unfused tetanus) until at very high frequencies the twitches coalesce so the force produced is almost constant (fused tetanus)[82]. If high levels of activation are maintained for longer periods of time (minutes or hours), then some of the muscle fibers will fatigue, starting with the MHC IIB fibers, and then followed by the MHC IIA fibers[8], and the MHC I fibers will outlast all other fiber types[c].

A model of muscle activation levels should also include the "catch-like" effect that has been observed in many muscle preparations[33,82], which consists of a prolonged increase in twitch force following the insertion of an extra spike into an otherwise regular spike-train. The catch-like effect is frequency dependent, and also motor-unit type dependent, and in vertebrates it was initially observed in the medial gastrocnemius of the cat[33]. At least one model has been proposed earlier to account for this effect[103], but was dependent on using a particular muscle force model (a Voigt element) to provide a non-zero internal muscle node velocity during isometric contractions. Although maybe a matter of personal opinion, it seems to be more useful to keep the force producing mechanisms separate from the activation dynamics, at least until compelling evidence points to a strong link between the two. As pointed out earlier, muscle twitch activation dynamics could well be based on purely electrochemical processes resembling those in a central synapse (albeit with slower dynamics). The following is an empirical "synaptic-like" model which attempts to capture the twitch dynamics and the catch-like effect of muscle but purely based on a transmitter and ion release/reuptake type of mechanism (thus without reference to any particular muscle model). The main output from the model is the i^{th} muscle's activation level, $\mathcal{A}_i \in [0, 1]$, which via equation 4.34 in section 4.7 directly affects the number of force producing cross-bridges in the sarcomere. Assuming the arrival of an action potential to the neuromuscular junction at time t_{AP}, the activation

[c]None of the simulations presented in this thesis will exceed a time frame of 5 seconds, so muscle fatigue will not be an issue in the present work.

level obeys the following set of equations:

$$\begin{aligned}
\frac{d\alpha}{dt} &= -\frac{\alpha}{\tau_\alpha} + (\beta - a)\cdot(1-\alpha)\cdot\delta(t-t_{AP}) \\
\frac{d\beta}{dt} &= -\frac{\beta - b}{\tau_\beta} + \gamma\cdot(1-\beta)\cdot\delta(t-t_{AP}) \\
\frac{d\gamma}{dt} &= -\frac{\gamma}{\tau_\gamma} + \beta\cdot(1-\gamma)\cdot\delta(t-t_{AP}) \\
\frac{d\mathcal{A}_i}{dt} &= \frac{1}{\tau_\mathcal{A}}\cdot(-\mathcal{A}_i + c\cdot(1-\mathcal{A}_i)\cdot\alpha)
\end{aligned} \tag{9.1}$$

where $\delta(t-t_{AP})$ is the delta function, α, β and γ are rate variables which determine the activation increments, τ_α, τ_β, τ_γ and $\tau_\mathcal{A}$ are the decay time constants for the different parts of the process, and finally a, b and c are arbitrary constants determining equilibrium positions for the relevant rate variables. This model has been specifically designed to fit some of the available experimental data (particularly as reported by Burke et al.[33]), and as such no special physical significance should yet be attached to the different constants/parameters in the model[d].

Figure 9.1 shows the muscle activation level as it varies in time during stimulation at various frequencies. In all cases the larger amplitude traces were obtained by inserting an an extra action potential 10 ms after the beginning of the spike train, which was otherwise held constant during the experiment (the same activation protocol was used in Burke et al.[33]). A clearly defined "catch-like" effect is observed with maximum efficacy at a stimulation frequency of approximately 80Hz: The extra inserted spike causes the muscle to be in a heightened level of activation, which slowly converges back to the unperturbed situation at a frequency dependent rate. A similar scenario was observed in fast muscle fibers, except that the "catch-like" effect was much less pronounced and only consisted of a short-term increase in the perturbed fiber's activation level. A simulation of the fast fiber's activation levels is shown in figure 9.2.

9.4 Muscle force in the motor unit

The force that is produced by a whole muscle depends on many factors. One of these factors is of course the sarcomeric tension which in chapter 4 was expressed by equation 4.28, encompassing the hypothesis that entropic elasticity at the cross-bridge is the source of this force. In order to get the total force of a muscle, this sarcomeric tension has to be scaled up accordingly, and it is therefore necessary to consider some of the anatomical details which determine the scaling factors. In particular it is necessary to find out how many sarcomeres act in parallel during a muscular contraction.

As has been mentioned in the previous section, whenever an α-motoneuron fires, it will cause a twitch in all the muscle fibers which it innervates. The total isometric force that a motor-unit may generate is thus the product of the innervation ratio times the number of sarcomeres (or myofibrils) arranged in parallel

[d] This is work in progress, and a future model should most certainly include more direct links to measurable parameters. For the present purposes, this model will be perfectly adequate as long as its input/output ranges are not extended beyond the experimental values to which it was designed.

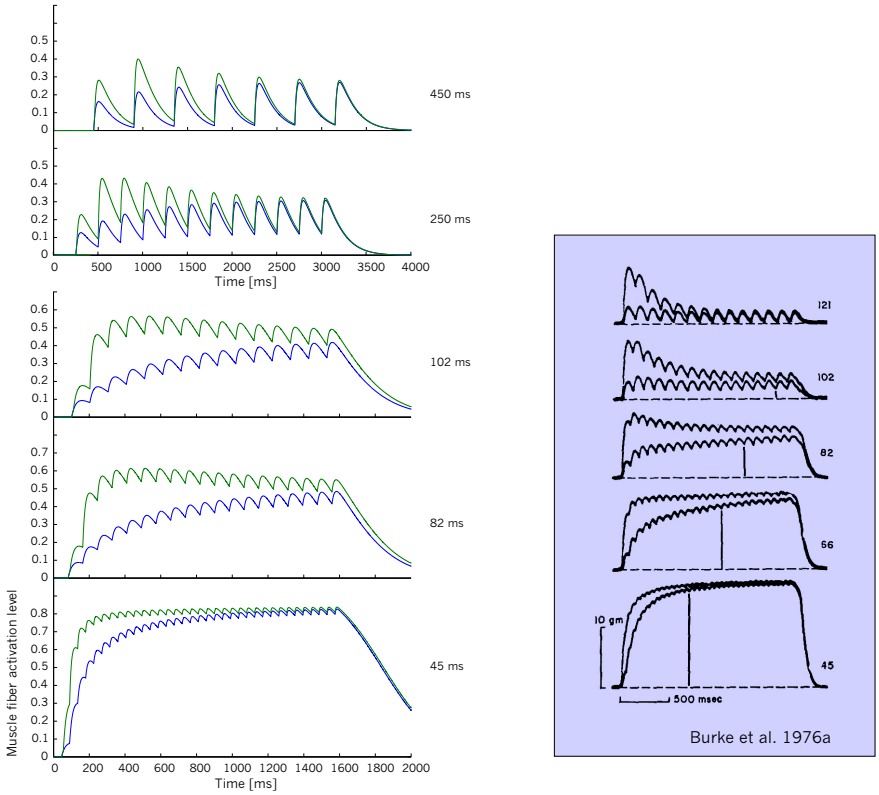

Figure 9.1: Simulation of slow fiber activation dynamics using model in equation 9.1. Inserts at right are modified from Burke et al.[33], figure 5.

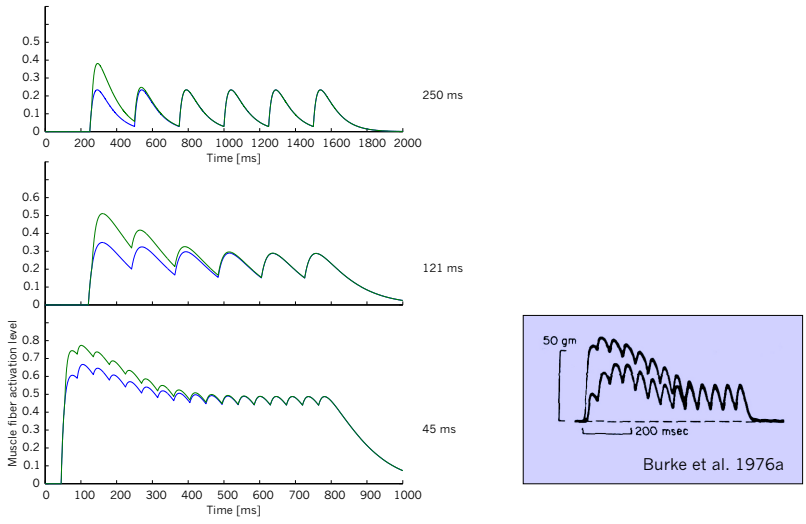

Figure 9.2: Simulation of fast fiber activation dynamics using model in equation 9.1. Insert at right modified from Burke et al.[33], figure 7.

within each muscle fiber times the force produced by an individual sarcomere. Given that a muscle fiber measures from 5 to 20μm in radius, while a myofibril is 0.5μm in radius, there must be from 100 to approximately 1600 myofibrils within a single muscle fiber. The maximal isometric tension in a single sarcomere was found to be $T_0 = 3.5 \cdot 10^{-7}$N in section 4.5.2, which means that the isometric force of a single fully activated muscle fiber will range from $3.5 \cdot 10^{-5}$N to $5.6 \cdot 10^{-4}$N. Innervation ratios range from 1 to 2000. This means that the smallest motor units, in principle should be able to produce only $3.5 \cdot 10^{-5}$N, while the largest motor units will produce a force of 1.12N (in "physiological" terms, the forces range from 3μg to 114g). Published values for motor-unit isometric forces in various different muscles range from 1 to 130 grams [189,186,82,217], so this theoretical estimate nicely overlaps with the physiological range.

Persuasive as it may seem, there are too many sources of variability in this approach as to be of any practical use: The innervation ratios for the different motor units within a muscle are seldom known in much detail, nor are the muscle fiber diameter distributions well studied in most muscles. What *is* known, however, is that the motor-unit twitch forces in most muscles follows an exponential distribution (see section 9.2). As this type of distribution seems to be a general principle in muscle [186,189,279], it is much more useful to define a motor unit according to the fraction of the muscle's maximal isometric force, that the unit may produce. Given that the fundamental unit of muscle force employed in the present work is based on the sarcomere (see chapter 4), a practical approach to the twitch distribution problem was to define an "average" myofibril (i.e. using equation 4.28). Myofibrils are made up of sarcomeres positioned end to end along the entire length of a muscle fiber, so their number therefore depends directly on a muscle's PCSA and on the cross-sectional area of a sarcomere (and is thus easily computable). To recreate the twitch force distribution, a fraction of the total number of myofibrils in the muscle was assigned to every motor unit depending on the unit's size. This of course removes any differentiation between different fiber types (I, IIA, IIB, IIX), which is absorbed in the distribution factor. From a physiological point of view this is an acceptable approximation because the correct muscle twitch force distributions are attained, and because much of the force-related variability between motor units is based on fiber cross-sectional area [8]. Thus rather than having to design different muscle fiber types and innervation ratios for each and every motor unit in a muscle, all the motoneuron-size dependent variations can be absorbed into a single scalar value which helps determine the range of force produced by a given motor unit (all motor units thus become computationally identical except for the force modification factor).

Let n_{mf} be the total number of parallel myofibrils in a muscle composed of n_{mu} motor units. The fraction of myofibrils assigned to the i^{th} motor unit, φ_i, may be defined as follows:

$$\varphi_i = \frac{1}{\varphi_{norm} \cdot \beta_{mu}} \cdot \exp\left(-\frac{i}{\beta_{mu}}\right) \tag{9.2}$$

where φ_{norm} is a normalization factor selected so that $\sum_{i=1}^{n_{mu}} \varphi_i = 1$, and where β_{mu} is a function of the number of units in the muscle, and is defined as:

$$\beta_{mu} = \alpha_{mu} \cdot n_{mu} \tag{9.3}$$

Here α_{mu} is an arbitrary constant which is important for determining the range and position of the force-recruitment profiles of the muscle (more about this in section 9.4.1). The total force produced by the k^{th} muscle may then be calculated as:

$$\mathcal{F}_k = \sum_{i=1}^{n_{mu}} n_{mf} \cdot \varphi_i \cdot T_{sarc,i} \tag{9.4}$$

where $T_{sarc,i}$ is the sarcomeric force (from equation 4.28 but updated with equation 4.34) corresponding to the i^{th} motor unit given the current muscle's contraction velocity, $\mathcal{V}_k$, and absolute muscle length, $\mathcal{L}_k$. (These should be scaled down to correspond to sarcomeric velocity and length, using data in chapter 3 and 4). Equation 9.4 should be used in connection with equation 3.15 from section 3.2.2.

9.4.1 Automatic motor unit re-scaling

For simulation purposes it will sometimes be necessary to scale down the number of motor units without changing the overall force production characteristics of the simulated muscle. To this end, β_{mu} was defined as a function of the number of units so that the minimum and maximum twitch forces in a muscle change appropriately[e], while at the same time maintaining a good muscle force dependency on the percent of the pool that has been recruited[270]. In particular the total muscle force should depend on the percentage of motor units that have been recruited as a simple monotonically increasing function. Assuming that motor units produce full force right from the moment they are recruited, then when 50% of the motor units have been recruited, the muscle should produce approximately 20% of its maximal force[270,217], at least in some muscles [f]. Let $\mathcal{F}_n$ be the muscle force produced when motor units from 1 to n have been fully activated, and let $\mathcal{F}_{max}$ be the maximal force of that muscle. Then the force fraction $\mathcal{F}_n/\mathcal{F}_{max}$ as a function of recruited motor units, n, takes on the form shown in figure 9.3A. The various curves shown here are equal for any total number of motor units, n_{mu}, and correspond to using different values of α_{mu} in equation 9.3. Alternatively, one might plot the muscle force when exactly 50% of the motor units have been recruited, as a function of α_{mu}. This yields the graph shown in figure 9.3B, which is also invariant to the number of motor units.

The fact that these force-fraction curves are invariant with respect to the number of motor units indicates that the chosen scaling function is appropriate for the task. Since the proportion of slow and fast muscle fibers is directly affected by α_{mu}, it seems that a useful classification scheme for muscles would be to determine their α_{mu} values. Muscles with an overabundance of slow fibers would then be expected to have small α_{mu} values, whereas fast muscles would have larger α_{mu} values.

To see how this α_{mu} and β_{mu} re-scaling mechanism works it is useful to plot the *force-recruitment profile* for the muscle, which here will be defined as

[e] A 45N muscle with only 10 units requires a mean unit force of 4.5N, whereas if 1000 units are available, the mean unit force would be 0.045N

[f] In reality, however, motor units are not recruited with full force, and a large component of the gradual force increase in muscle is due to increased motor unit activation rates and not unit recruitment *per se*[185]. See also figure 9.8.

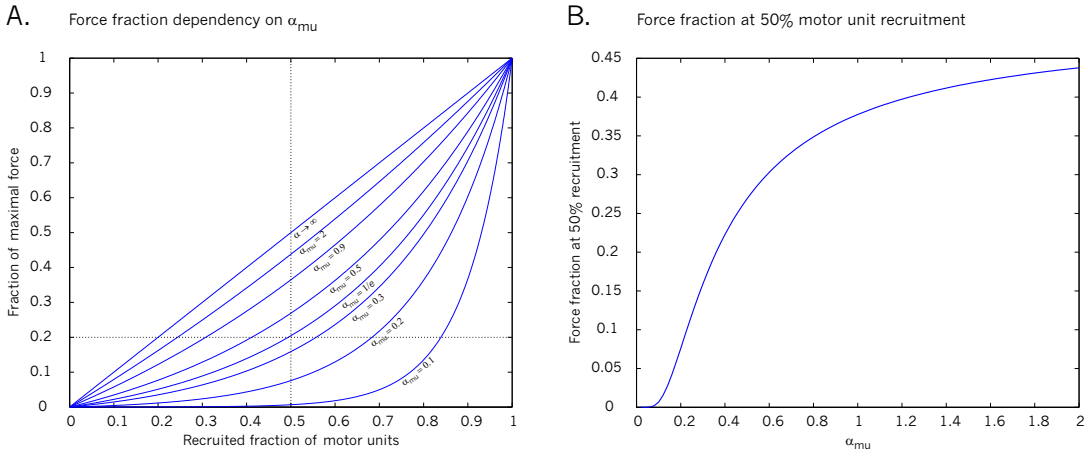

Figure 9.3: A. The force fraction $\mathcal{F}_n/\mathcal{F}_{max}$ as a function of recruited motor units, n. The various curves correspond to using different values of α_{mu} in equation 9.3; B. The force fraction when exactly 50% of the motor units have been recruited, plotted as a function of α_{mu}. See text for further details.

the twitch force of recruited units as a function of the total (voluntary) muscle force (e.g. by only letting equation 9.4 run to the largest recruited unit and plotting the force of that particular largest unit against the total resulting force up to that unit). This has been done as a log-log plot in figure 9.4, where the inserted graph shows a similar plot (same axis) with some experimental data from Milner-Brown et al.[186]. The numbers in parenthesis assigned to the individual curves indicate the number of motor units (left), the mean twitch force pr. unit in the muscle (middle) and the α_{mu} value (right). Even as the mean twitch force varied from 2.5g to 81.5g, in all cases did the muscle produce a maximal force of 4000g (corresponding to the maximal force of the first dorsal interosseus of hand)[186]. For some values of n_{mu} (~ 1200) the calculated graphs become virtually indistinguishable from the experimental graph. In these "best" graphs the calculated mean twitch forces ($\sim$ 3g) are well within range of the experimental results for at least one of the subjects (2.26 ± 2.8 grams) reported in Milner-Brown et al.[186]. The α_{mu} value for this muscle is approximately 0.15, indicating that it probably contains an overabundance of slow fibers compared to other muscles.

9.5 Modelling the motor neuron pool

All the ingredients have now been presented that are required to compose a relatively sophisticated model of a motor neuron pool innervating a muscle in the human arm. For the purpose of illustration the following model will be based on the *biceps caput brevi* muscle (BISH), but for the present project similar models have been implemented for the other arm muscles (those listed in chapter 3). Here is a recapitulation of some of the details that a model of the BISH muscle should include and/or account for:

- PSCA of 2.1cm^2 (chapter 3), corresponding to 2.7×10^8 myofibrils (sar-

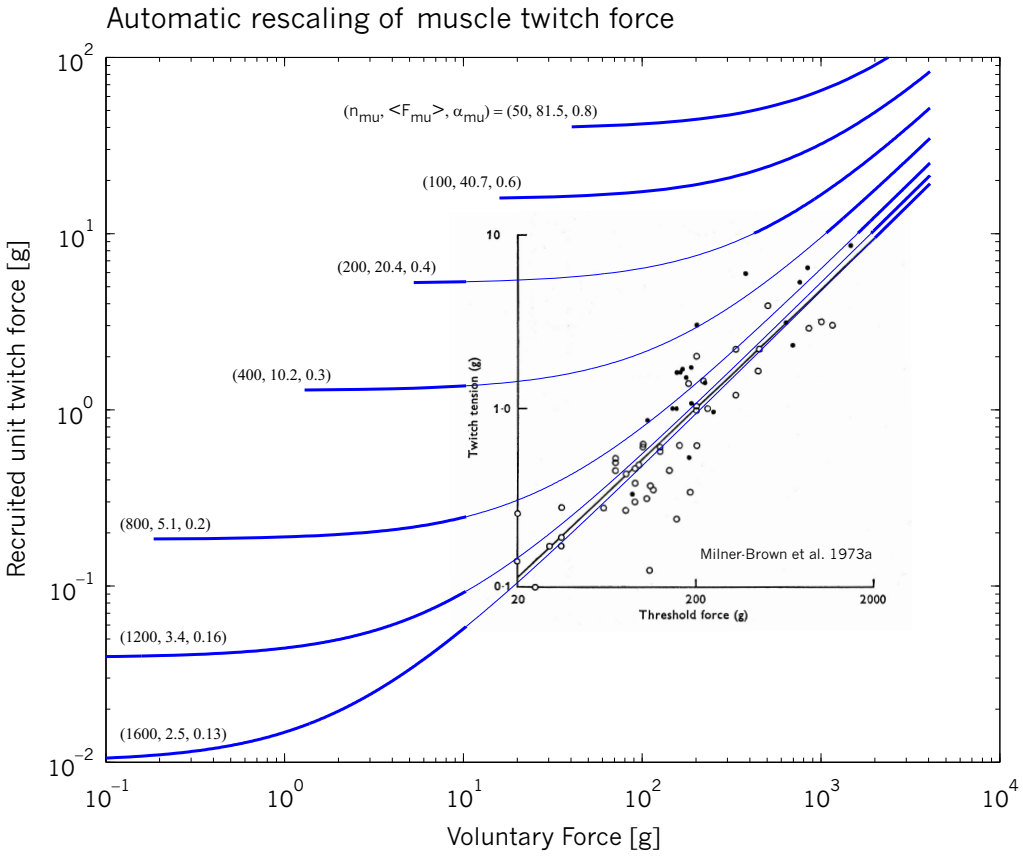

Figure 9.4: Twitch force of largest recruited unit as a function of the total (voluntary) muscle force. The inserted graph shows a similar plot (aligned to the same axis for data comparison) with some experimental data from Milner-Brown et al.[186]. There is a good fit between the simulation and the experimental data. The numbers in parenthesis assigned to the individual curves indicate the number of motor units (left), the mean twitch force pr. unit in the muscle (middle) and the α_{mu} value (right).

comeres) arranged in parallel (see table 4.1).

- Maximal isometric force pr. cross-sectional area should be within physiological range (i.e. 20-100N/cm^2 in striate muscle)[279], and thus close to the theoretically derived value of 45N/cm^2 (from section 4.5.2).
- >100 α-motoneurons pr. motor neuron pool.
- α-motoneurons have RS dynamics with a frequency range from 8 to 30 Hz.
- α-motoneurons are recruited in order according to size (chapter 5).
- Innervation ratio $\sim 10^2$.
- Proper muscle twitch activation responses such as tetanic fusion, and the "catch-like" effect, implemented in section 9.3.
- Motoneuron-size dependent motor-unit twitch force.
- Exponential distribution of motor-unit twitch force composition.
- Orderly recruitment of motor-units according to twitch force.
- Finely graded increases in force as response to a ramp increase in motoneuron afference (saturating at maximal isometric tension).

Within the computational framework that has been developed for this thesis, it is relatively easy to set up a simulation which exactly matches the specified requirements.

9.5.1 Simulation results for BISH

For the simulation of BISH, 800 RS neurons were modelled with size scaling factors, ϱ, ranging from 0.08 to 0.8 (see section 5.4.2) and following a simple exponential distribution of the neuron radii, r_i, as defined by the following equation:

$$r_i = a \cdot \exp(b \cdot i) \tag{9.5}$$

where a and b are arbitrary constants, and i is the index to the motor units. These neurons represent the α-motoneurons and were connected to the $2.73 \cdot 10^8$ myofibrils in BISH, distributed according to equation 9.2. The resulting twitch force distribution in the motor pool may be seen in figure 9.5.

In a series of experiments Monster and Chan[189] recorded the firing frequency of individual motor units at the extensor digitorum communis muscle as a function of total voluntary force during isometric contractions. Individual motor units would start firing at a low rate (~8Hz) and at a motor-unit specific minimum voluntary force. After recruitment, the firing rate for a motor unit increases gradually with the force produced and saturates at a maximum firing rate of 20-30Hz. These data are shown in figure 9.6a, as reproduced from Monster and Chan[189]. In a simulation of the biceps caput brevi (BISH) based on the models and parameters mentioned earlier, a similar set of data is obtained.

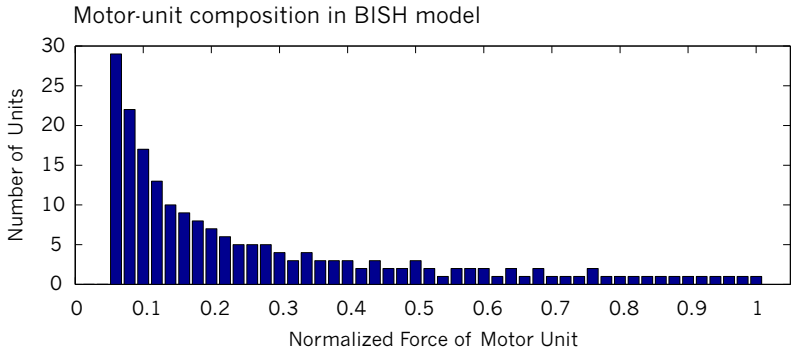

Figure 9.5: Motor unit composition in BISH muscle simulation. This exponential distribution of motor unit sizes corresponds very well with experimental data reported in Milner-Brown et al.[186] and Monster and Chan[189], who concluded that an exponential relation exists linking the number of motor units to the motor unit forces.

In this simulation, the motoneurons were subjected to a ramped increase of afference (similar to the one used in figure 5.2), which as expected, resulted in an orderly recruitment of the units. The spiking of each motoneuron activated a NMJ, which determined the activity level of the muscle fibers belonging to each unit. By plotting the activation frequency of each unit as a function of the total isometric force produced by the simulated muscle, a result very similar to that reported by Monster and Chan[189] was obtained, and is shown in figure 9.6b. Although a direct comparison is not entirely possible (due to the differences in total produced muscle force), the simulation results do show the same type of recruitment dynamics.

Another important relationship that must hold for the simulation to be biologically valid is that the twitch force of recruited fibers as a function of the total produced force in muscle should be approximately linear[186,189]. This is best evidenced by plotting both quantities on a log-log plot, as has been done in figure 9.7. By comparing the simulation data with the data from Milner-Brown et al.[186], Monster and Chan[189], it may be concluded that there is good correspondence between the experimental values and the BISH model. The best linear fit to the model output data has a slope of 0.004 while the corresponding experimental value is approximately 0.005 for the first dorsal interosseus muscle [186]. The model has a larger minimum recruitment force (approximately 0.01N in the model compared to 0.003N in Monster and Chan[189]) which is attributable to differences in muscle type (size) and to the fact that the BISH motor neuron pool was modelled with only 200 motor units.

A direct consequence of the muscle twitch force distribution presented in figure 9.5 in combination with the ordered recruitment of motor neurons, is that the total muscle force will increase only slightly (to 20%) until more than half of the motor units are recruited[270,217]. This property may be seen in figure 9.8, which is a plot of the instantaneous muscle force at the moment when a given motor becomes recruited. It should be noted that even when 100 percent of the motor units have been recruited, the BISH muscle is still only halfway towards its maximal isometric force of $\sim$ 90N. This is because there are two

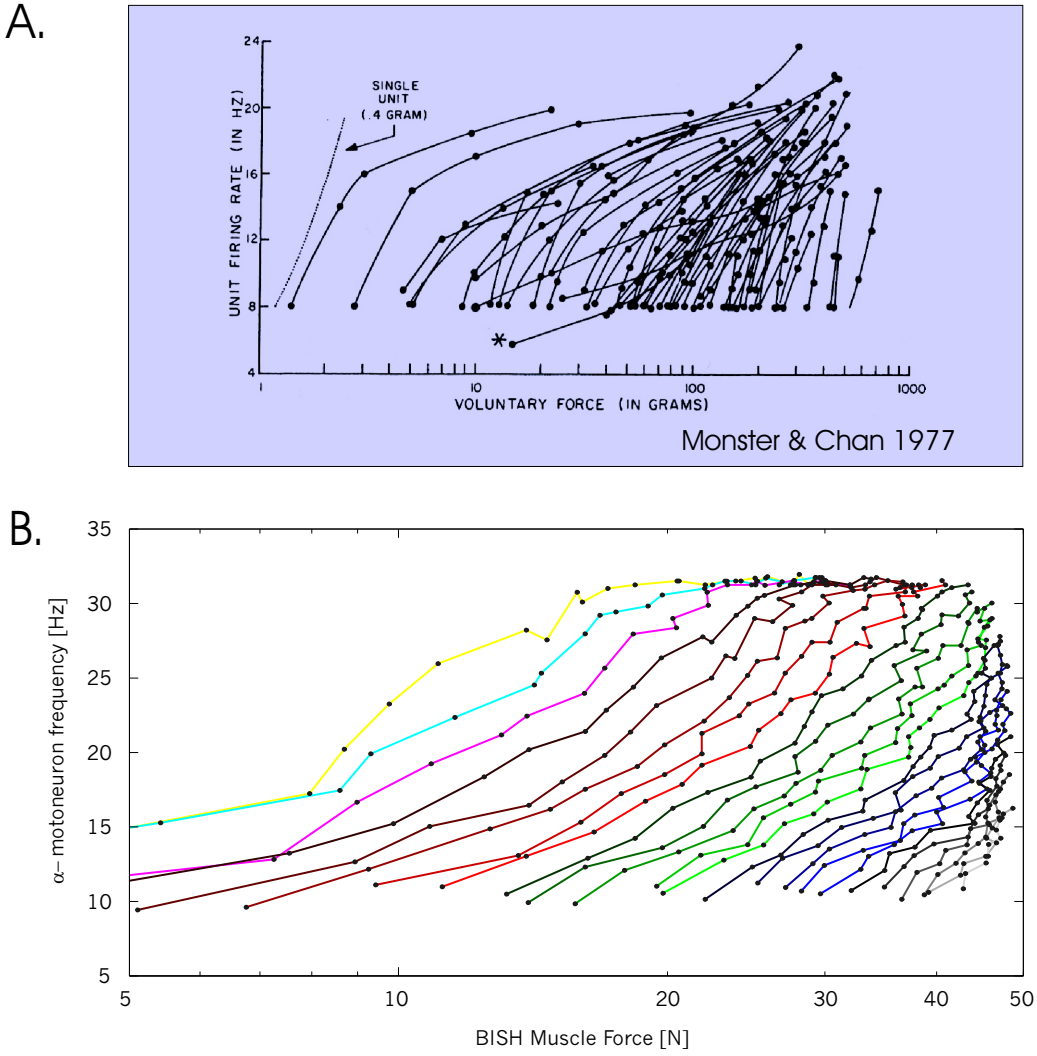

Figure 9.6: A. Data from[189] showing the firing frequency of individual motor units at the extensor digitorum communis muscle as a function of total voluntary force during isometric contractions; B. Firing frequency of individual motor units pertaining to the BISH muscle simulation. As can be seen, the simulation results are quite similar to experimental data in A.

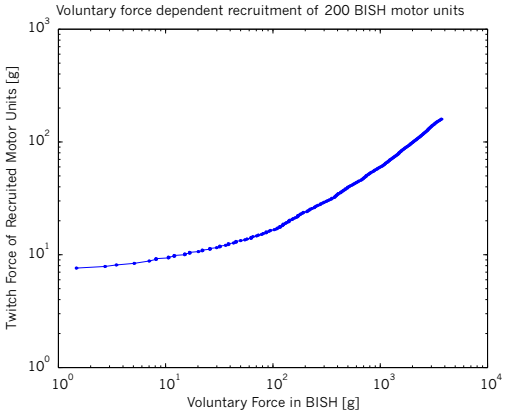

Figure 9.7: Twitch force of recruited fibers as a function of the total produced force in BISH muscle simulation.

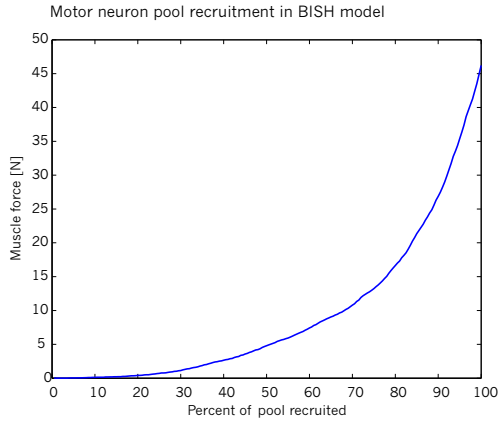

Figure 9.8: Total muscle force as a function of the percent of motor units that have been recruited.

major contributors to gradual force increase: Motor unit recruitment *and* motor unit activation frequency. Milner-Brown et al. [185] even conclude that motor unit recruitment only plays a role at low levels of muscle force, while increased firing rate is the main mechanism at higher force levels. Thus, even when all motor units have in fact been recruited, there is still plenty of reserve force left in the muscle, which can only be accessed by increasing the firing frequency of the motor neurons [185].

The modelled muscle eventually does reach the maximal isometric tension as shown in figure 9.9, which also shows that the force produced by the simulated BISH muscle increases gradually following a sigmoidal curve as the input current to the motor neurons increases.

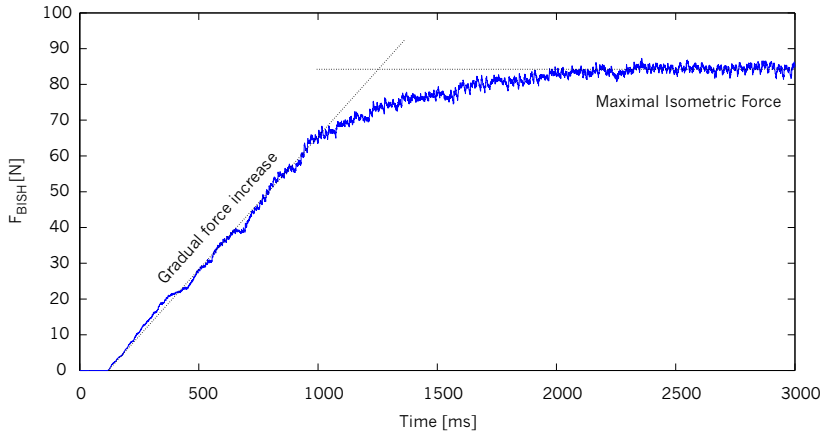

Figure 9.9: Gradual increase of BISH muscle force during a ramped increase in input current to the motor unit neurons.

Chapter 10

The Muscle Spindles

Chapter Summary

This chapter presents a brief review of muscle spindle physiology and function, but the main emphasis here is the presentation of a novel hypothesis regarding the function of γ-motoneuronal modulation of the muscle spindles. The functional importance of γ-motoneuronal activation during a simple movement task was explored using a computational model of a simplified neuromuscular system. Various schemes of γ-motoneuronal activation were tested under different task conditions. Analysis of the simulation data lend support to the idea that γ-motoneuron activity might be essential for cancelling *expected* stimuli rather than only for programming servo-controlled equilibrium positions of the limbs. It is concluded that the best performance of a movement is obtained when expected afference is cancelled by γ activity, thereby allowing for a relatively pure and "noise-free" detection of unexpected loads, which then may be compensated for correctly. This requires that the system learns the cancelling signals that are appropriate for different movements.

Note: Part of the work in this chapter will appear in Neurocomputing

The role of muscle spindles has had a long and controversial history in the field of motor control theory[95,259]. The muscle spindle is a specialized sensory organ which is intimately associated with striate muscle (for a thorough review of relevant spindle physiology see[93,36]). It is composed of a fusiform capsular sleeve measuring a couple of millimeters, whose endpoints are attached at different points to the muscle within which it is embedded. A distinction is usually made between *extrafusal* muscle fibers, which are the force producing muscle fibers *per se*, and the *intrafusal* muscle fibers, which are a series of specialized sensory fibers residing inside the muscle spindle. Three different types of intrafusal sensory fibers have been identified: the dynamic bag, b_1, the static bag, b_2, and

the static chain, c (see e.g. Taylor et al.[259] for a recent account). Each of these intrafusal muscle fibers is endowed with the following features:

- Cellular nucleus and mitochondria usually found in the central regions of the spindle.

- Contractile elements resembling ordinary sarcomeric tissue are found in the polar regions of the spindle. Each contractile element receives innervation from a γ-motoneuron in the spinal cord, and thus may be activated independently of the activity in the rest of the muscle.

- The stretch sensitive process from a sensory spinal neuron innervates the central region of the fiber, thus bringing sensory afference to the spinal cord.

The names of the intrafusal fibers derive from the characteristic response patterns of the sensory afferents originating in the different fibers: Dynamic fibers have activities which are correlated with velocity of contraction, whereas the activity in static fibers is directly correlated to the current extrafusal length. Ultimately, the differences in afferent response are caused by differences in the mechanical properties of the various intrafusal fibers. Essentially the stretch sensitive innervations will be stretched at different rates depending on the fiber in question.

In general, the function of the muscle spindle is to report to the nervous system about the current state of the muscle in which it is embedded. Within the context of motor control theory, several suggestions pertaining to the function of the intrafusal fibers have been forwarded, but the current consensus seems to indicate that one of the most important functions of these fibers is as a "servo-assist" mechanism[180,173,259]. In this view, α- and γ-motoneuron co-activation brings the innervated muscle to a certain state of contraction, as if moving towards an equilibrium point[62,146,23].

It should be noted that, contrary to other sensory systems like vision or hearing, proprioception due to type Ia and type II muscle spindle afference can be centrally modulated at the source via the γ-motoneuron system by changing the state of the contractile elements within the sensory organ itself. This means that the CNS in this case has an unique opportunity to modify the raw afferent data it receives, which hints at the existence of other possible functions for this kind of afference. Computationally, modulation of afference might be useful to set up an "early-warning" expectation based error correction system in which the CNS presets the tension levels of the intrafusal spindles via the γ-motoneurons according to expectations derived from an internal forward model of body biomechanics, loads, context, goals, etc. If the subsequent movements cause unexpected changes in the firing levels of the spindle system, then an error can be assumed to have occurred, and depending on the complexity of the error, different levels of the CNS are called upon to make up a new strategy. Such a function is more in lieu with the *forward internal model* hypotheses of motor-control proposed by some researchers[184,136].

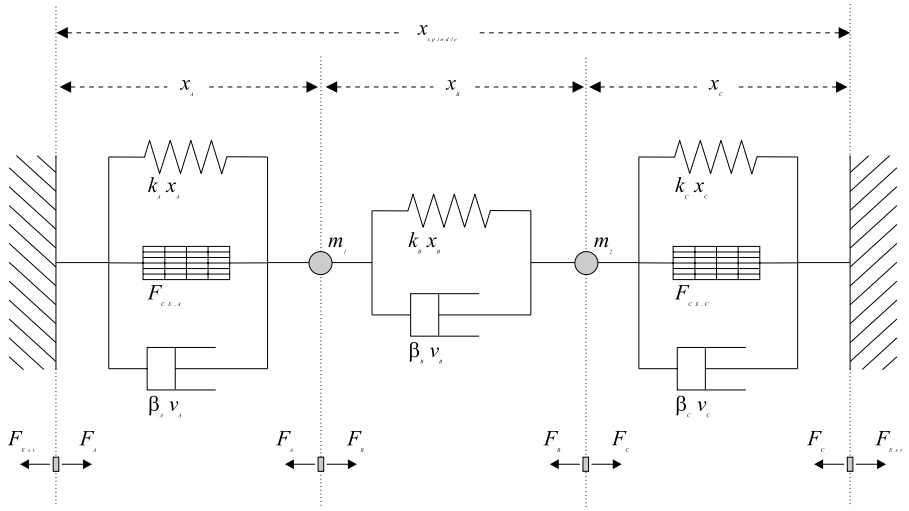

Figure 10.1: Spindle Model Diagram. This figure shows a simplified diagram of an intrafusal fiber. Emphasis has been given to the mechanical differences between different regions of the fibers. Static and dynamic fibers may be modelled by varying the parameters, in particular the damping coefficient of the primary region has importance in this respect.

10.1 Muscle Spindle Model

A simplified mechanical model of the muscle spindle can be derived by observing that the individual spindle consists of regions with different mechanical properties (for an introduction see e.g. Carpenter[36]). The central (primary) region of the spindle can be modelled as a Voigt body (i.e. a spring in parallel with a dashpot), while the polar regions consist of a contractile element in parallel with a Voigt body. The components of these three regions are arranged in series as shown in figure 10.1.

The forces produced individually by each of the three elements are described by the following equations (subindexes A, B and C indicating the element in question):

$$\begin{aligned} F_A &= F_{CE}(\gamma, x_A, \dot{x}_A) + k_A \cdot x_A + \beta_A \cdot \dot{x}_A \\ F_B &= k_B \cdot x_B + \beta_B \cdot \dot{x}_B \\ F_C &= F_{CE}(\gamma, x_C, \dot{x}_C) + k_C \cdot x_C + \beta_C \cdot \dot{x}_C \end{aligned} \tag{10.1}$$

where x indicates length of the elements, $\dot{x}$ is the rate of change of length, k is the spring constant, β is the damping coefficient, F_{CE} is the force produced by the contractile element of the spindle as a function of the fiber's length, rate of change of length and the γ-motoneuron activity, γ. In general F_{CE} may be any function which has a Hill type force-velocity profile with yielding at high stretching velocities and with a myosin-actin overlap dependent force-length relationship. In particular, F_{CE} will here be modelled using the muscle force relationship derived in chapter 4, namely equation 4.28 in combination with the neuromuscular activation function expressed in equation 9.1 as γ input.

The total forces acting on masses m_1 and m_2 are thus:

$$\begin{aligned} F_1 &= m_1 \cdot \ddot{x}_1 = F_B - F_A \\ F_2 &= m_2 \cdot \ddot{x}_2 = F_C - F_B \end{aligned} \tag{10.2}$$

where $\ddot{x}$ is the acceleration. It should be noted that the spindle's total length, x_{spin}, and contraction velocity, $\dot{x}_{spin}$, are imposed by the extrafusal fibers to which the spindle is connected (because the intrafusal force is much smaller than the extrafusal force). This means that the following constraints will apply to the system:

$$\begin{aligned} x_A = x_1 &\iff \dot{x}_A = \dot{x}_1 \\ x_B = x_2 - x_1 &\iff \dot{x}_B = \dot{x}_2 - \dot{x}_1 \\ x_C = x_{spin} - x_2 &\iff \dot{x}_C = \dot{x}_{spin} - \dot{x}_2 \end{aligned} \tag{10.3}$$

which if substituted into equation 10.2 yields:

$$\begin{aligned} m_1\ddot{x}_1 &= k_B \cdot (x_2 - x_1) + \beta_B \cdot (\dot{x}_2 - \dot{x}_1) - F_{CE}(\gamma, x_1) - k_A \cdot x_1 - \beta_A \cdot \dot{x}_1 \\ m_2\ddot{x}_2 &= F_{CE}(\gamma, x_{spin} - x_2) + k_C \cdot (x_{spin} - x_2) + \beta_C \cdot (\dot{x}_{spin} - \dot{x}_2) + \\ &\quad -k_B \cdot (x_2 - x_1) - \beta_B \cdot (\dot{x}_2 - \dot{x}_1) \end{aligned} \tag{10.4}$$

Using this set of equations it is possible to simulate the dynamical behaviour of the different types of intrafusal fibers during imposed length changes and varying γ-motoneuron activity. According to this model, it turns out that the critical parameter which distinguishes static fibers from dynamic fibers is the damping coefficient in the capsular region (β_B), which is much larger for the static fiber.

The results of a simulation of spindles using equation 10.4 are provided in figure 10.2, which shows the instantaneous firing frequency of type Ia and type II spindle afferents during a ramp increase (stretching), holding and ramp decrease (relaxation) of the total spindle length. Empirical data is provided for comparison (inset box). Spindle afference sensory neurons are here activated by scaling their input currents linearly with respect to the length of the capsular region, x_B. It should be noted that type Ia afferent sensory neurons receive input from dynamic and static intrafusal fibers, whereas type II fibers only receive input from the static intrafusal elements. In the present context it is considered more important to capture the muscle velocity and length sensitivities of primary and secondary fibers respectively, than to obtain an exact fit to a particular species' spindle afference frequencies. There is an ongoing discussion as to why spindle afference frequencies in non-human species seem to be significantly higher than in humans, as it has not been possible to base this difference on purely histological grounds[214]. Consensus now seems to be that the main culprit is a large difference in the performed experimental tasks[214], in which human data was obtained during slower movements than non-human data (primarily due to microelectrode fixation requirements). To emphasize the different velocity and length sensitivities of spindle afferents, figure 10.3 compares the activity in individual primary and secondary fibers during a stretch-hold task shortly followed by a sinusoidal variation of muscle length.

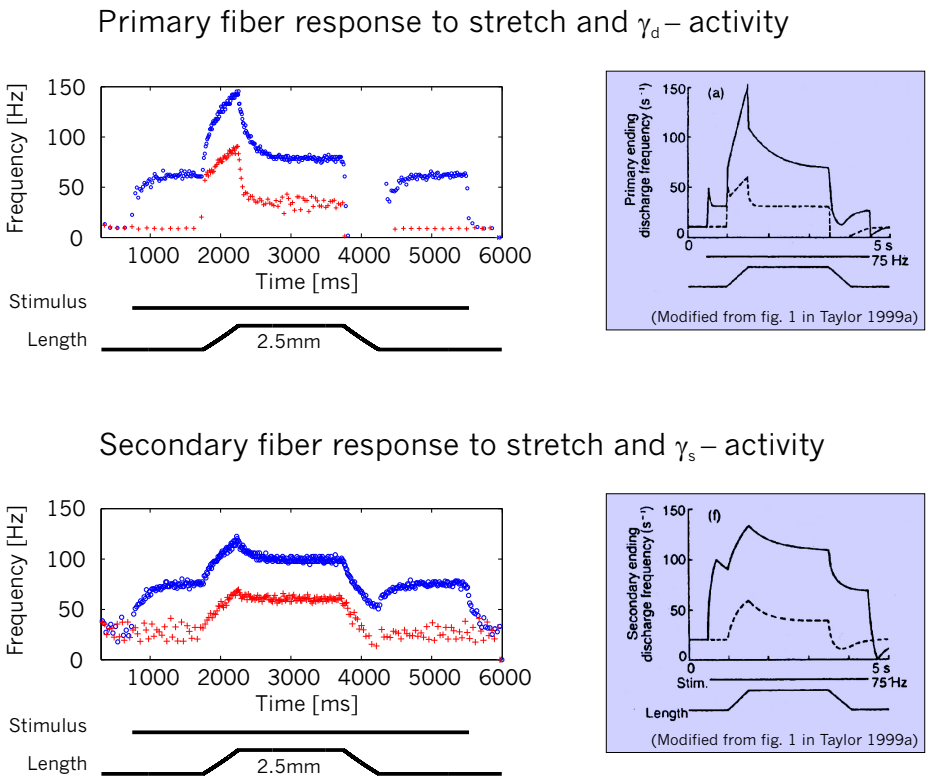

Figure 10.2: Simulation of muscle spindle afference. Instantaneous firing frequency in primary (Ia) and secondary (II) afferent fibers as a function of absolute spindle length with and without γ motoneuron activation.

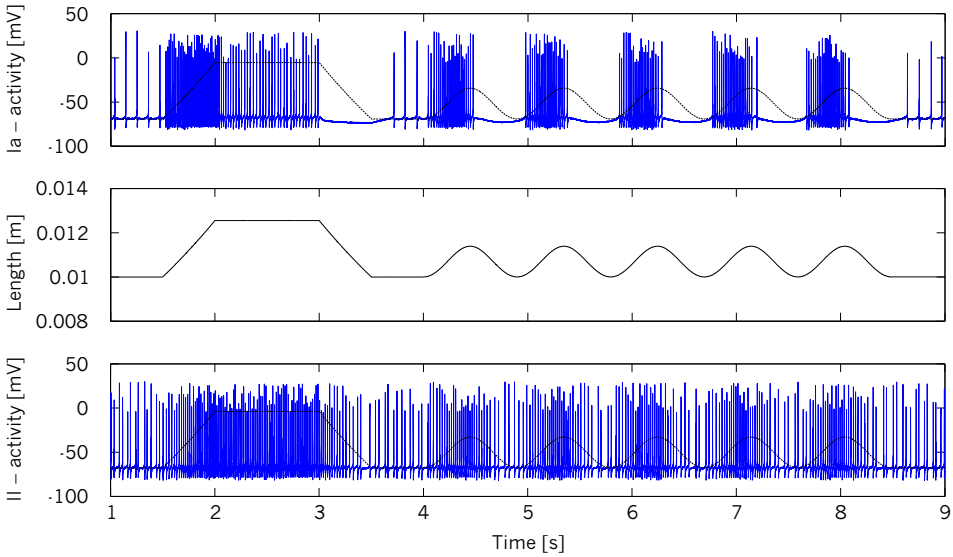

Figure 10.3: Simulation of the spiking behaviour of primary and secondary fibers during a stretch-hold task followed by a sinusoidal stretch-relaxation task. The upper diagram shows activity in type Ia fibers, the middle diagram shows the length variations and the lower diagram shows activity in type II fibers.

10.2 Spindle Afference Modulation and Cancellation

Activity in γ-motoneurons modulates spindle afference by varying the force produced in the intrafusal fiber's contractile element, and thus affecting the length of the fiber's central region (where type Ia and type II sensory fibers innervate the spindle). The main argument of the afference cancellation hypothesis presented here is that during well-learnt slow movements the γ-motoneuronal activity will have a form which completely compensates for the intrafusal length changes associated with such a movement so that the primary region of the spindle remains at constant length throughout. A consequence of this is that type Ia and II fibers will be firing at constant (low) rates during familiar well-learnt movements (see discussion).

It is relatively easy to show that complete afference cancellation may be achieved if the force in the contractile element of the intrafusal fibers has the following form (by letting $\ddot{x}_1 = \ddot{x}_2$):

$$F_{CE} = k_B \cdot x_B + \beta_B \cdot \dot{x}_B - \frac{1}{2} \cdot (k_A \cdot x_A + \beta_A \cdot \dot{x}_A + k_C \cdot x_C + \beta_C \cdot \dot{x}_C) \tag{10.5}$$

The γ-motoneuronal activity that is required to produce such a force may be calculated explicitly if it is assumed that force production in the contractile element of the spindle resembles force production in striate muscle (i.e. with a Hill-type force-velocity relationship and a myosin-actin overlap dependent force-length ratio, see figure 10.5). If it is further assumed that F_{CE} scales linearly

with the activation of the γ-motoneuron then the required γ efference may be found directly as:

$$\gamma = \frac{F_{CE}}{F_{imax}} \tag{10.6}$$

where F_{imax} is the maximal isometric force at a particular length (as calculated from the used muscle model), and F_{CE} is calculated from equation 10.5.

10.3 Simplified Neuromuscular Model System

To explore these issues quantitatively, a simplified model of neuromuscular control has been developed. For the sake of simplicity and conciseness this has been reduced to only consist of an antagonistic pair of muscles positioned vertically and with a mass m suspended between them (see figure 10.4). The mass can be moved up or down by varying the activation of the α-motoneurons which have a linear scaling effect on the force of muscles modelled using functions as those shown in figure 10.5. Four different scenarios are explored, distinguished by the presence or absence of modulatory spindle afference to the α-motoneurons, and by the presence or absence of a suddenly imposed doubling of the load. The simulation results are presented in figures 10.6 to 10.9, and further simulation details are given in the corresponding figures.

10.4 Discussion

The preliminary analysis of the simulation data lends support to the notion that γ-motoneuron activity could be concerned with cancelling expected spindle afference, the constancy of which thus indirectly informs the central nervous system that execution of a particular motor program is advancing as scheduled. Any performance errors as measured by tension discrepancies in the spindles will *immediately* be accessible to the CNS via the fast type Ia afferent connections, and positional errors will be available with a slight delay via the type II afferents. It is important to notice that the "afference cancelling γ activity" proposed herein is perfectly compatible with the role usually attributed to type Ia spindle afference, which is to reflexively correct for sudden changes of load. Actually this reflexive correction mechanism works even better when the γ-activity removes the influence of expected changes in muscle tension and length (as can be seen in the highlighted panel of figure 10.9. The γ-activity creates a constant "baseline" spindle activity during familiar well learnt movements, thereby improving the signal to noise ratio when unexpected events occur. This scenario of course requires that the appropriate γ-activation sequences must be learnt (in the example from figure 10.6 the optimal activation was calculated directly, stored, and then used in the remaining experiments as the "learnt" γ-activation corresponding to the task). Such learning would pose no problem for a neural system because even the error-signal required for optimal learning is provided in the afference.

Technically it has proven very difficult to identify γ-motoneurons *in vivo*, but if the idea presented here is true, that well learnt movements are associated with well learnt γ-responses, then neuromuscular models of simple tasks may

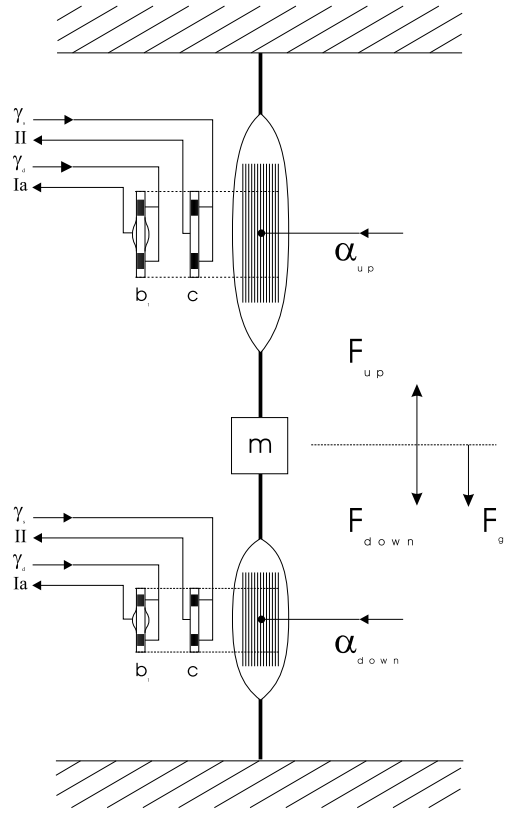

Figure 10.4: Simplified Neuromuscular System. A simplified neuromuscular system with extensor-flexor antagonism, where only two vertically positioned muscles are considered while pulling on a mass in opposite directions. Resulting simulations can be seen in figures 10.6 to 10.9.

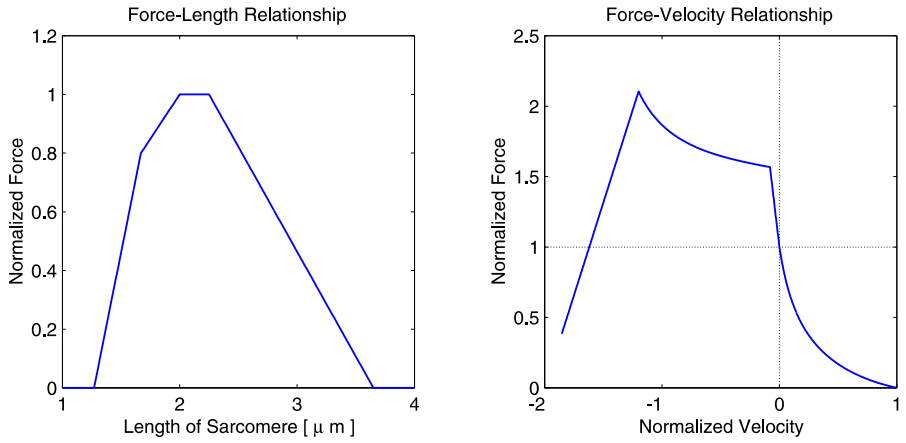

Figure 10.5: Canonical Muscle Model. For the development of structurally accurate models of striate muscle, the two most important features to be considered for modelling are the force-length (left panel) and force-velocity (right panel) relationships of muscle tissue.

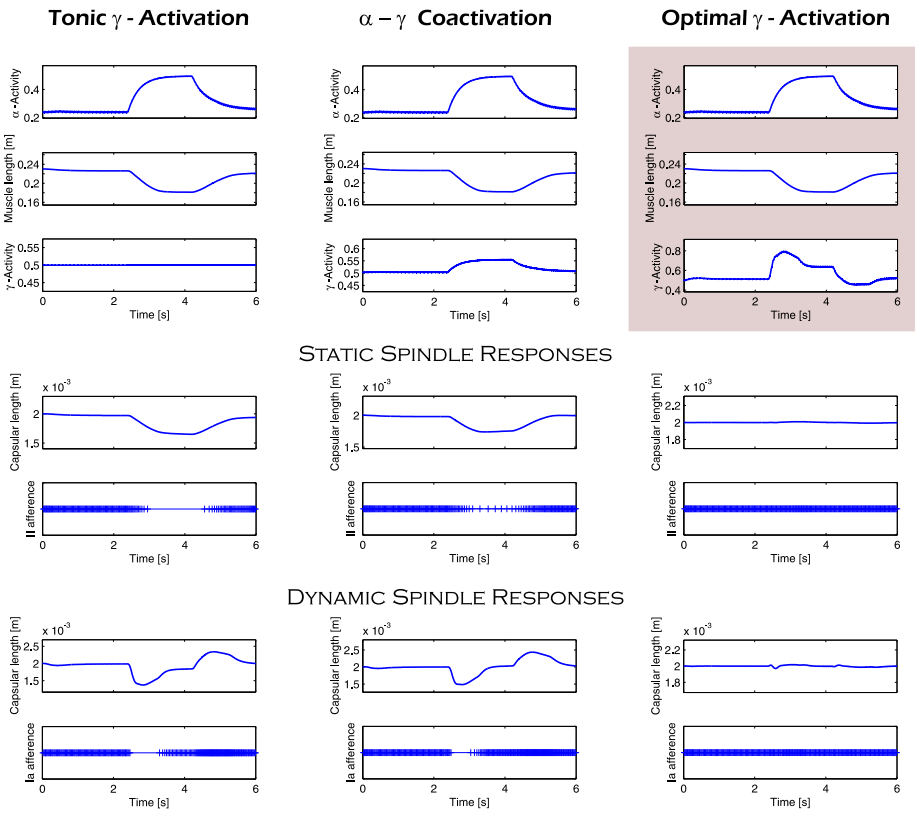

Figure 10.6: Deafferented and Unperturbed Muscle Contraction. This figure shows the variations in type Ia and II fiber afference during muscle contraction when different forms of γ-motoneuron activity are applied. In this simulation no spindle afference is provided to the α-motoneurons, and there are no sudden changes in the load (5kg). The task is to lift the suspended mass 5cm by changing the length of the lifting muscle from its resting length of 0.23m to a contracted length of 0.18m, and then to move the mass back again. This is done by activating and deactivating the α-motoneurons appropriately. The system is investigated during three different types of γ-motoneuron activity: tonic (constant firing frequency), $\alpha - \gamma$ coactivation (γ frequency closely linked to α frequency) and optimized γ-activation. Notice that with the optimized γ-activation there are no variations in the firing rate of Ia and II fibers because the primary regions of the spindles are kept at constant length. The optimized γ activation is calculated from equations 10.5 and 10.6, and the values are stored for later use (these values correspond to the "learnt" γ-activity which in this work is proposed to cancel afference during familiar movements).

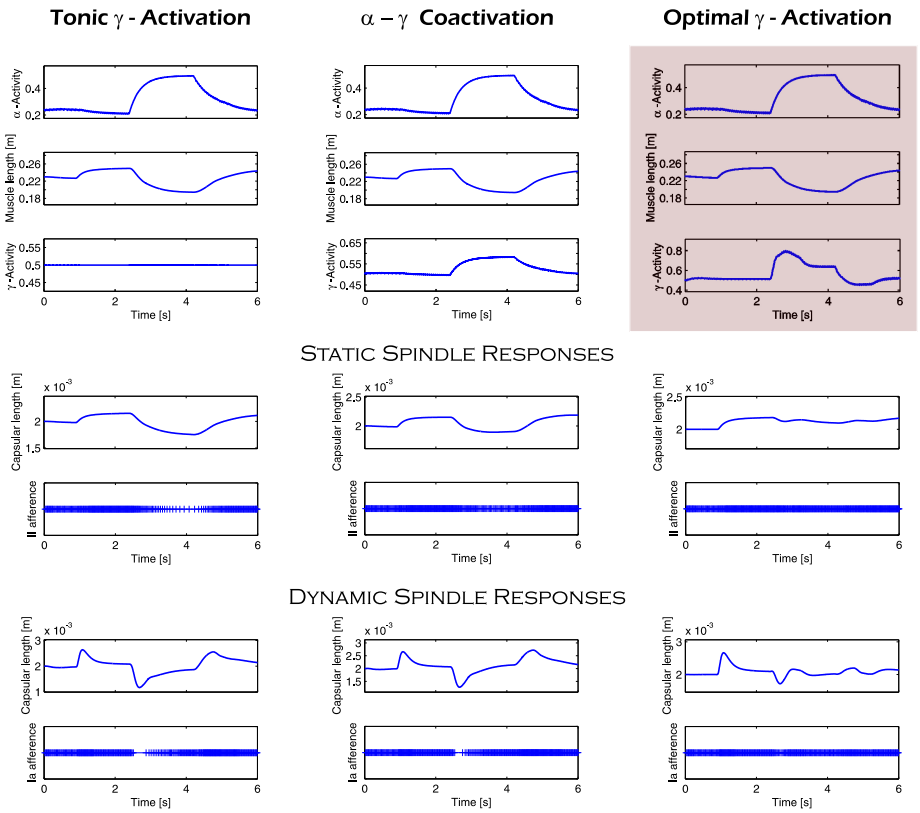

Figure 10.7: Deafferented and Perturbed Muscle Contraction. This figure shows the dynamic and static spindle responses during a perturbed muscle contraction. The task is as described in figure 10.6, except that the load is suddenly changed from 5 to 10 kg after 0.9 seconds. The change in load initially stretches the lifting muscle from 0.23m to a new resting length of 0.25m. As previously, α-motoneuronal activity starts after 2.4 seconds and the muscle contracts to 0.19m. Notice how the dynamic spindle closely indicates changes in the contraction velocity whereas the static spindle elements are more closely related to the actual length of the muscle. The previously stored ("learnt") optimal γ activation (from figure 10.6) is used in this simulation, but now notice that the change of load means that the optimal γ-activation is no longer able to cancel the afference completely, and actually the Ia afference seems to mark the points at which a "revision" of the previously learnt afference prediction model should occur. This corresponds to having a direct measure of the error between the planned execution vs. the resulting performance of a previously learnt movement. Strictly speaking, the lifting task (as defined in figure 10.6) has not been accomplished correctly because load compensation by afferently modulated α activity is lacking in this deafferented simulation.

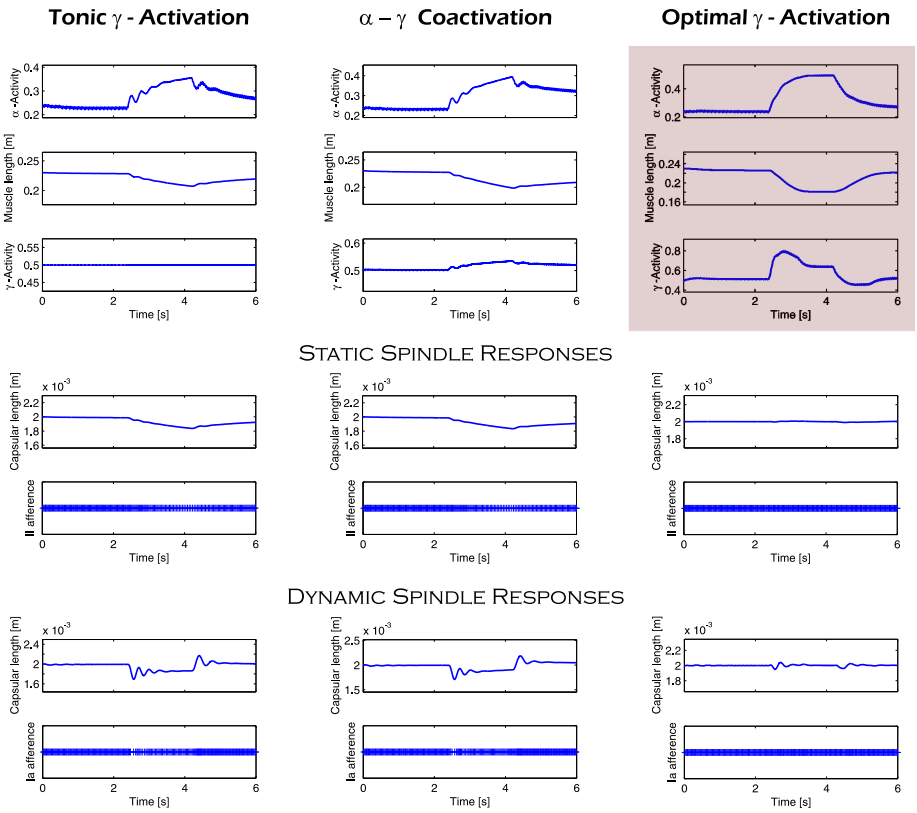

Figure 10.8: Afferented and Unperturbed Muscle Contraction. This figure is essentially identical to figure 10.6 except that now afference from the spindles is allowed to influence α-motoneuronal activity. The presence of a positive feedback loop can be observed by the appearance of small oscillations in the dynamical spindle's response. Best performance is obtained during optimal γ-activity, where the length of the primary region of the spindles is kept almost constant (except for some small oscillations), meaning tonic Ia and II afference.

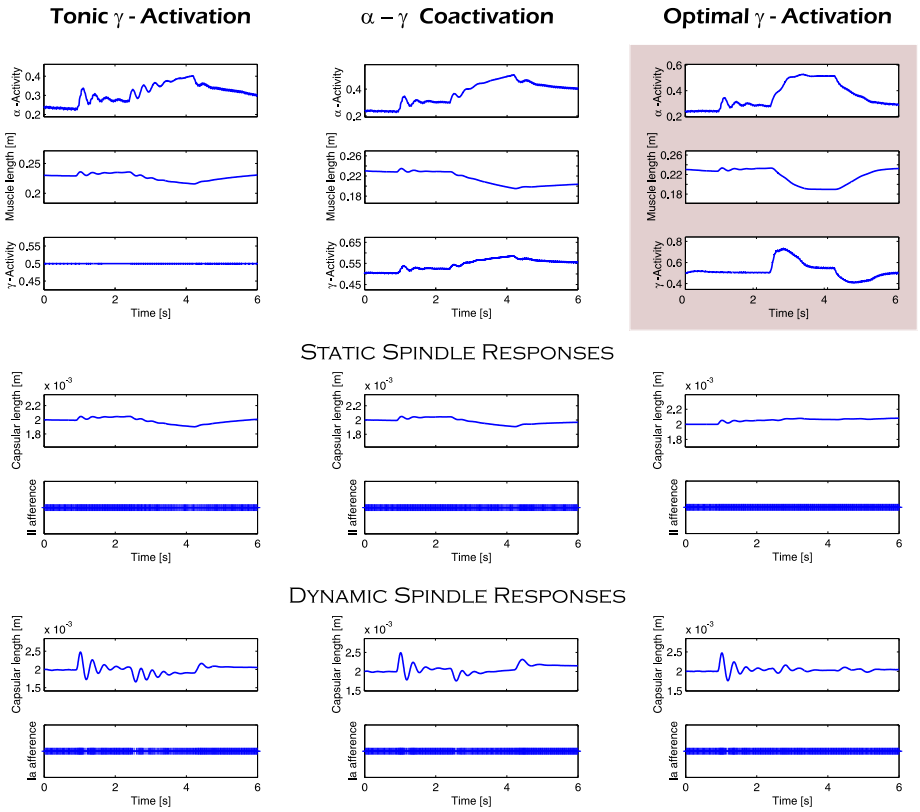

Figure 10.9: Afferented and Perturbed Muscle Contraction. In this simulation, load perturbations to the afferented system are compensated for by increased α-motoneuronal activity, regardless of the type of γ-activity that is imposed. But it is only during optimal γ-activation (taken from the simulation in figure 10.6) that the system is actually able to correctly perform the lifting task (see highlighted panel). It is therefore concluded that the best performance is obtained when expected afference is cancelled by γ activity, thereby allowing for a relatively pure and "noise-free" detection of unexpected loads, which then may be compensated for correctly.

help develop signature traces for these γ-neurons (see the γ traces presented in figures 10.6 to 10.9). These traces could then in theory be used to identify the neurons *in vivo* during similar tasks. Once identified, their activity during natural movement situations may be detected routinely.

Chapter 11

Human arm simulation

Chapter Summary

This chapter will build upon the concepts developed in all previous chapters in order to make a fully functional biologically realistic computer simulation of the systems (spinal, muscular and biomechanical) that are involved in human arm movement. Emphasis will be on identifying the differential role of α and γ motoneurons, particularly in connection with the hypothesized role of the muscle spindle and γ-motoneuronal system that was proposed in chapter 10.

In chapter 10, a "toy"-model of a neuromusculoskeletal system was used to argue that γ-motoneuronal activity could be associated with reafference cancellation. In that model, only two antagonistic muscles were considered and the task was to move a mass, hold it at the new position and then return it to start. There are many reasons for which that early setup may be considered too simplistic, but one major concern is that it does not accurately reflect arm biomechanics, where complex time-varying torques and forces may result when the arm moves from one position to another, giving rise to much more complicated reafference cancellation signals. Another major concern is, that it does not include a sufficiently developed model of the spinal circuitry, particularly of the motor neuron pool, so direct comparisons to experimental results are tentative at best. In this chapter, an attempt will be made to include all the missing elements so as to make the simulation as biologically realistic as possible by including most of the material presented in chapters 3 to 8, incorporating it all into a single computer program. To proceed, there are various unsettled issues which need attention first. In particular it is necessary to initialize the skeletomuscular model so that the operating range of different muscles correspond to experimental data. It is also necessary to rescale the spinal networks to a manageable size. Finally, it is necessary to ascertain that the completed model produces simulated arm movements which remain within realistic physiological bounds.

Myotactic Unit	Flexors	Extensors
$\mu_{shoulder}$	DELC and PMJC	DELA, DELS and TMAJ
μ_{elbow}	BILH, BISH, BRAD, BRAC, and PROT	TRIO, TRIA and TRIM
μ_{wrist}	FCUL and FCRD	ECUL and ECRD

Table 11.1: Muscle groups in the myotactic units of arm joints.

11.1 Setting up the human arm model

For modelling the human arm only three myotactic units need to be considered, one at the shoulder joint, $\mu_{shoulder}$, one at the elbow, μ_{elbow}, and one at the wrist, μ_{wrist}. Each myotactic unit is associated with several muscle groups acting around each of the joints, these are apportioned according to table 11.1. At present only arm movements in the sagittal plane will be considered as these correspond to the reaching task that will be investigated (see section 11.4). Physiological data such as PCSA and fiber lengths at rest as well as origin and insertion points for the different muscles has already been given in chapter 3. Approximate physical descriptions of the hand, forearm and upper arm are also given in chapter 3. Up to and including the simulation of the motor neuron pool it is relatively easy to find definitive experimental data which may be directly used for calibrating the simulations. The simulation results for the motor units presented in chapter 9 are thus quite reliable as they have been modelled directly after motor units in humans. This ideal situation changes somewhat when focus is directed towards spinal networks and the myotactic units, primarily because work in this area has mostly been done on non-human species (due to ethical as well as technical reasons).

11.1.1 Spinal connectivity matrix

A neural scripting language was developed for the simulation program, which makes it very easy to set up the connectivity matrix for any neural network architecture whatsoever. The only difficulty in setting up the simulation is now to find out what the neural architecture should be like. Chapter 8 presented a brief review of the main neuron populations involved in motor control which are present in the spinal cord. That chapter concludes with a summary diagram of putative spinal connections as they have been reported in the literature and corresponding to a two-muscle myotactic unit. In the present case, the three different myotactic units contain 4 motor units at the wrist, 5 motor units at the shoulder and 8 motor units at the elbow (see table 11.1), but the overall neural organization pertaining to an individual motor unit will remain the same as in the diagram, albeit with two important exceptions: 1) Agonist-antagonist interactions within a myotactic unit (particularly through IaIN and Renshaw cells) will be organized so that all flexor motor-units act on all extensor motor-units, and viceversa; 2) GTO's, joint receptors and skin afferents are not included in this model.

As a simplification, the number of α-motoneurons within a motor unit directly determines the number of other species of neurons in the myotactic unit

Neuron	α-ratio
Ia	0.1
II	0.1
γ_s	0.1
γ_d	0.1
IaIN	0.25
Renshaw	0.25
CM	1

Table 11.2: Network Ratios

and elsewhere. The exact ratios of α-motoneurons to other neuron types may vary, depending on the particular requirements of the simulation with respect to the task that is to be done, speed of simulation and statistical requirements. Table 11.2 lists an example of these ratios which was used for most simulations in this chapter. It should be mentioned, that a minimum of approx. 20 α-motoneurons pr. motor unit was found necessary to achieve a smooth force-recruitment profile for the unit, but most simulations were done with 40 α neurons pr. motor unit.

11.1.2 Skeletomuscular geometry and muscular operating range

Given the large variations in tension that must result from length changes in muscle due to the sarcomeric force-length relationship (see section 4.7), it is of the utmost importance to make sure that sarcomeric lengths during movements of the simulated arm remain within realistic bounds. Rather than simply guessing the extent of these bounds, it is highly fortunate that the necessary experimental data actually is available, and was reported very recently by Murray et al.[198] and by Lieber and Fridén[156], who studied the functional capacity of muscles at the elbow joint and the wrist, respectively. Murray et al.[198] report findings (from 10 human specimens) related to muscle fascicle length and sarcomeric length of elbow crossing muscles for different degrees of elbow flexion (some of these values are reproduced in table 3.4). They[198] found that when the arm was in full extension, the average sarcomere length in elbow flexor muscles ($\sim 2.91\mu$m) is significantly longer than for extensor muscles ($\sim 2.13\mu$m), data which in this thesis is used to initialize the muscle model (optimal sarcomeric length was set to 2.8μm, in accordance with Walker and Schrodt[269], see also section 4.7).

By using these data directly, the skeletomuscular model developed in this thesis accurately reproduces the experimental data, as may be verified by comparing figure 11.1 (modified fig. 5 from Murray et al.[198]) with figure 11.2. Furthermore, by using sarcomeric length specifications corresponding to flexor muscles of the elbow, the skeletomuscular model accurately predicts the operating ranges of wrist muscles, even if no attempt was made to specifically fit these data. This may be verified by comparing figure 11.3A (modified fig.3.11 from Lieber and Fridén[156]) with figure 11.3B, which shows the model results.

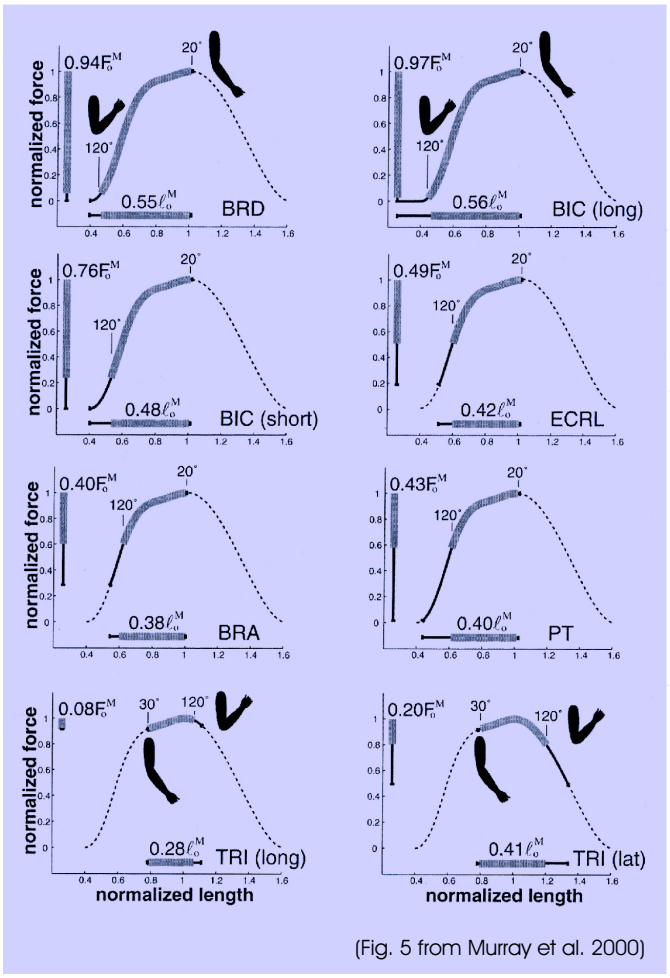

Figure 11.1: Experimentally identified operating ranges of elbow-crossing muscles[198]. The dashed part of the curves indicates the sarcomeric force-length relationship. The fine line indicates the maximal possible excursion of the individual muscles tested, and the bold line indicates the muscle excursion resulting from bending the arm from 20° to 120°. This figure was adapted from figure 5 in Murray et al.[198], and should be compared directly with figure 11.2. Key to equivalent muscle names: $BRD = BRAD$, $BIC(long) = BILH$, $BIC(short) = BISH$, $ECRL = ECRD$, $BRA = BRAC$, $PT = PROT$, $TRI(long) = TRIO$, $TRI(lat) = TRIA$

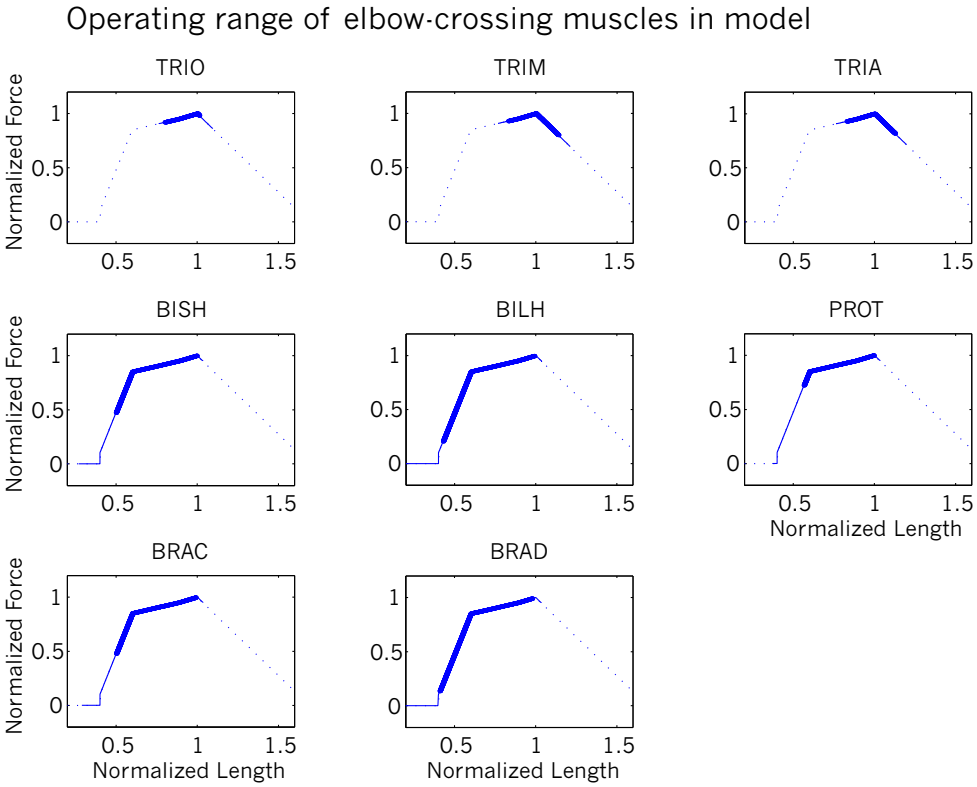

Figure 11.2: Operating ranges of elbow-crossing muscles according to the skeletomuscular model in this thesis. This figure was calculated directly from the human arm simulation during maximal isometric muscle activation by varying the angle between upper arm and forearm over 90°. The dashed part of the curves indicates the sarcomeric force-length relationship. The fine line indicates the maximal excursion of the individual muscles, and the bold line indicates the muscle excursion resulting from bending the arm from 30° to 120°. This figure should be compared with figure 11.2, using the following key to equivalent muscle names: $BRD = BRAD$, $BIC(long) = BILH$, $BIC(short) = BISH$, $ECRL = ECRD$, $BRA = BRAC$, $PT = PROT$, $TRI(long) = TRIO$, $TRI(lat) = TRIA$

A. Operating range of wrist muscles (Lieber and Fridén 2000)

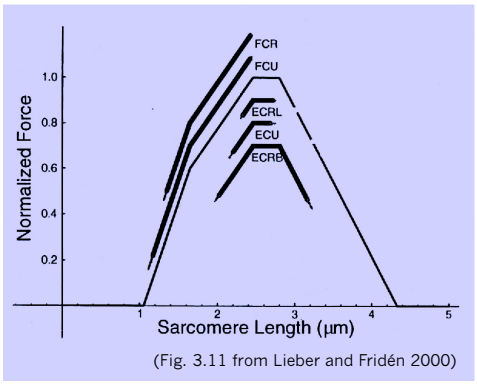

B. Operating range of wrist muscles in model

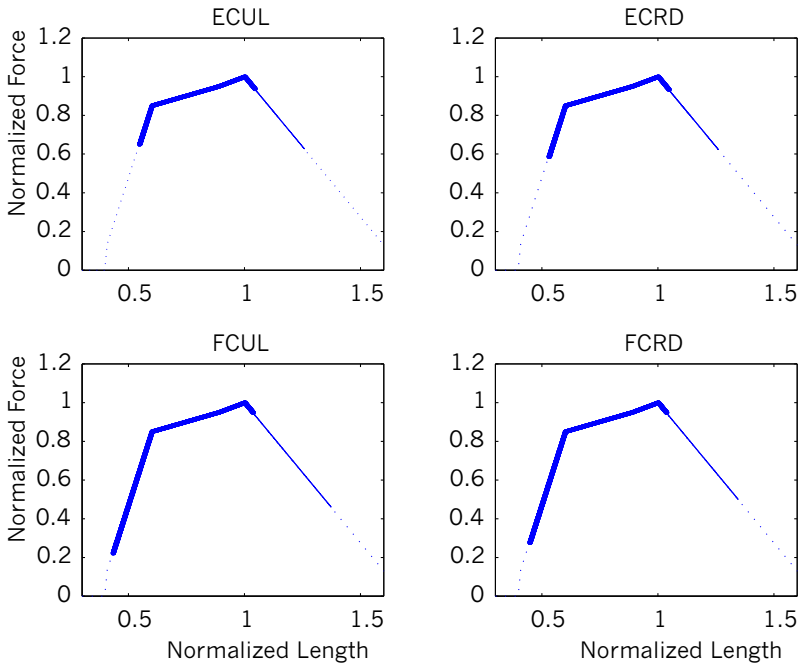

Figure 11.3: Comparison of operating ranges of wrist muscles between experiment and model. A. Experimental results obtained by Lieber and Fridén[156]. Figure adapted from fig. 3.11 in Lieber and Fridén[156]. B. Operating ranges of wrist muscles according to the skeletomuscular model in this thesis. The dashed part of the curves indicates the sarcomeric force-length relationship. The fine line indicates the maximal possible excursion of the individual muscles tested, and the bold line indicates the muscle excursion resulting from flexing or extending the wrist (over 180° from full flexion to full extension). This figure was calculated directly from the human arm simulation during maximal isometric muscle activation by varying the angle between forearm and hand. Key to equivalent muscle names: $FCR = FCRD$, $FCU = FCUL$, $(ECRL, ECRB) = ECRD$, $ECU = ECUL$.

11.1.3 Human benchmark test – Speed-drawing

The arm simulation must conform to certain restrictions with respect to the forces and hence the maximal hand transport velocities that it produces, so the question arises as to how fast humans are able to move their hands. In the work of Morasso[190] the hand movements along straight trajectories reached a peak velocity of ∼1 m/s (figure 3C in Morasso[190]), with subjects having received no particular instructions as to how fast the reaching movement should be made. To have a better set of limiting reference velocities upon which to base the arm simulations, it would be highly useful to have maximal hand velocity data for a variety of movements, straight as well as curved. In order to obtain these data an experimental paradigm was developed for this thesis, in which six human subjects were asked to draw as fast as possible along the lines representing a variety of figures with predefined path lengths[a].

Methods for speed-drawing benchmark test

Subjects were sitting at a table in a comfortable writing position, but were not allowed to rest their elbows on the table (in order to gain valid data for whole arm movements, rather than only movements involving the forearm pivoting around the elbow). They were asked to redraw each presented figure as many times as possible within a time frame of 30 seconds, while trying to follow the outline of the figure. Twelve different figure outlines (represented on paper) were used, including 4 circles of different diameter, 4 straight lines of different orientation, a triangle, 2 squares of different orientation and a 5 pointed star (see figure 11.4, where the different figures are represented).

There is a well known logarithmic speed-accuracy trade-off in human movement, famously quantified by Fitts' law[68], which of course also applies to the present task. Given that the current experiment was a speed-benchmark test, speed had obvious precedence over accuracy in this trade-off, and in some cases deviations from the intended path made it necessary to re-estimate the actually drawn path length rather than using the tabulated values for the figures (e.g. circles would be drawn slightly smaller or larger than the prototype, squares could be slightly skewed, etc.). However, subjects were not allowed to move so fast as to seriously affect accuracy, and in particular it was not allowed to "cut-corners", such as to start drawing a circle rather than a square. In trials where the figures had corners, each lap (defined as the completion of a figure after moving from starting hand position along the figure outline and back to start) was counted only if the hand had completed the circuit without jumping over any vertices.

Results of speed-drawing benchmark test

The results of this experiment are shown on figure 11.5. The upper graph shows the number of laps pr. second as an average of the six subjects' performance (± standard deviation). The lower graph shows the average hand velocity during a speed-drawing trial, and averaged across the six subjects. There are some quite clear performance differences related to the complexity of the traced figures.

[a]Three male and three female subjects volunteered for the experiment, age range from 19 to 30 years. All subjects were healthy and without any known history of neural or muscular diseases.

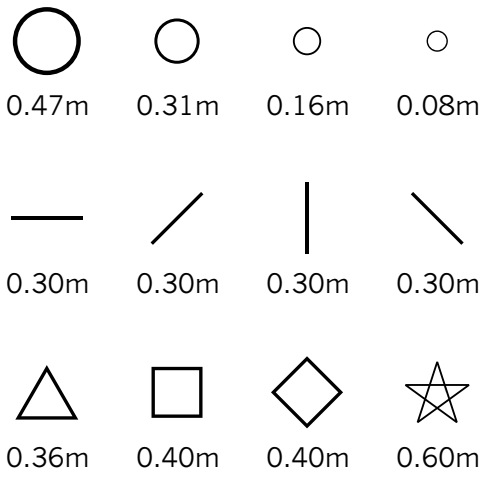

Figure 11.4: Figures used in the speed-drawing benchmark experiment. The number below each figure indicates the lap-length (in meters) for the trial figure, defined as the total distance traversed when moving from a starting position, along the figure, and back to the starting position (the actual length of the straight lines is thus half of what is indicated).

Note the significant difference in average hand velocity between trials using lines and trials using triangles, squares or stars ($p < 0.0005$, T-test). There is also a quite clear correlation between line orientation and average hand velocity. Note for example the significantly greater average hand velocity for lines drawn at 45° if compared to the other line orientations ($p < 0.005$, T-test). Finally, there are significant differences in average hand velocity related to the size of the traced circles (T-test for the two smallest circles gives $p < 0.025$). Thus even if the average number of laps pr. second increases for decreasing circle radius, this is not sufficient to compensate for the reduction in path length.

Overall, the maximal average hand velocity obtained is associated with the 45° line, and was found to be 1.6m/s ($\sigma = 0.2$). For all figures composed of straight lines it should be noted that the peak velocity must be much higher than what is reported in figure 11.5 because these are average velocities and thus include acceleration and deceleration of the hand in connection with changes in direction. The peak velocity for circular movements is equal to the average hand velocity, which is maximally 1m/s ($\sigma = 0.2$).

Some observations related to the speed-drawing task

It is interesting to note, that even though the last four objects (triangle, box, rhombus and star) are composed of simple straight lines, the average hand velocity when drawing these objects (0.4±0.02m/s averaged over trials) is significantly lower ($p < 0.0001$, T-test) than when drawing straight lines (1.2±0.3m/s averaged over trials). This difference (by a factor 3) cannot solely be attributed to the increased number of acceleration-deceleration events that are imposed by the increased number of vertices (2 for lines, 3 for triangles, 4 for the square and rhombus, and 5 for the star). To appreciate this, it is useful to multiply the number of vertices times the number of laps pr. second for each of the objects.

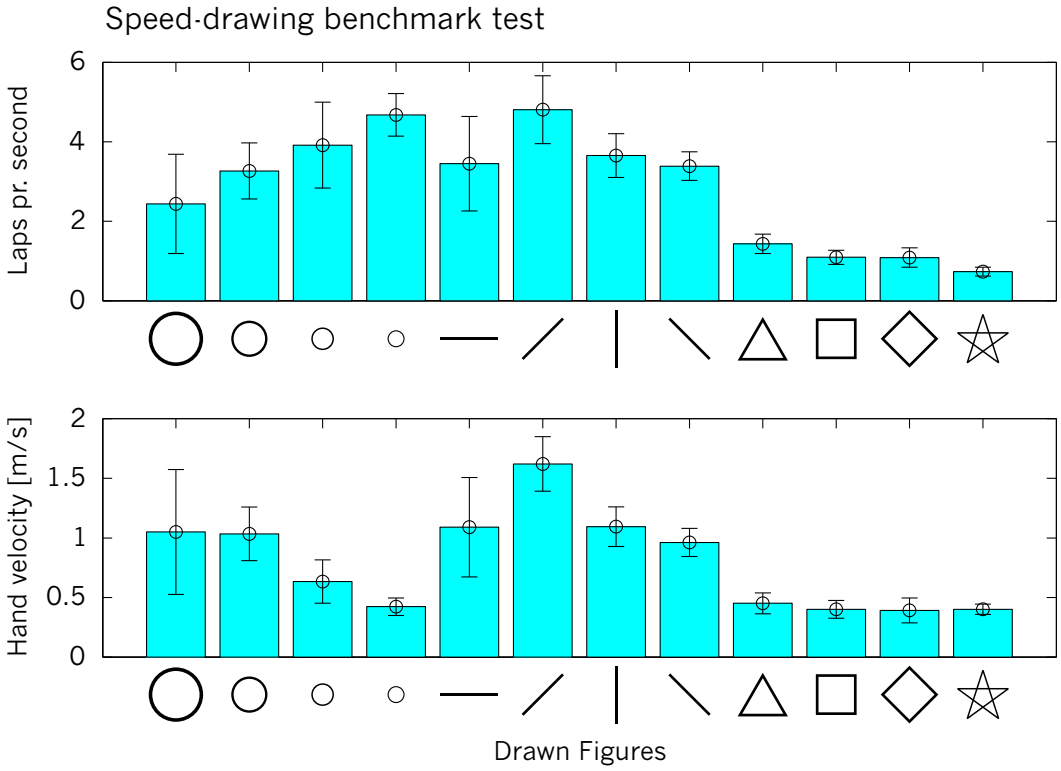

Figure 11.5: Main results of the speed-drawing experiment. See text for details.

This yields the number of vertices pr. second, i.e. the number of acceleration-deceleration events pr. second during a trial. For the simple straight lines one finds that the hand reaches from 7 to 9 vertices pr. second, whereas for the more complicated objects less than 4 vertices pr. second were reached. Thus there is more acceleration-deceleration taking place during simple straight line drawings than during complex object drawings.

Furthermore there appears to be very little difference in average hand velocity between trials with the four complex objects ($\sigma = 0.02$). Relating this observation to the previous discussion about vertices, it does seem as if there exists a fundamental neurophysiological difference between drawing objects with 2 vertices and drawing objects with more than 2 vertices, whereas all objects with more than 2 vertices are somehow related (the difference is probably not biomechanical because only straight lines are produced in these cases). Although curved objects are obviously different from the other two classes, there is a striking similarity between circles (at least the circles with diameters comparable to the line lengths) and simple straight lines when comparing the average hand velocities and the laps pr. second that were obtained during the trials with circles and lines. Can these observations be related to what is known about the neural organization in the spinal cord? At the risk of overinterpreting the data, the following suggestion is made nevertheless: Circles and lines are fundamental components of the spinal repertoire of movement patterns, and movements requiring such simple forms may therefore be relegated to the highly optimized central pattern generators and reflex systems in the spinal cord (associated with locomotion, grooming, reaching movements, etc.). The oscillatory activity patterns in the spinal cord are initiated and maintained active by the cerebral cortex based on an evaluation of figure form, size, type of task and need of corrections. This division of labour results in very high performance speeds. More complex figures, however, do not have direct spinal implementations and must be controlled directly by the motor cortex, resulting in a lower performance speed due to sensory delays and the necessary analysis of feedback. In the present trials figure complexity was only varied by increasing the number of vertices for objects otherwise composed of straight lines. But figure complexity can also be increased in purely curved objects by increasing the number of inflexion points and should give similar results as the complex straight line objects (drawing, e.g. bean or banana shaped objects is much slower than drawing circles).

11.2 Tests of the human arm simulation

With all the groundwork now behind us, the time has finally come to see the human arm simulation system in full function. Limb dynamics, muscles, spindles, spinal neurons and corticospinal connections have all been included in the model, but something essential is still missing: neural activation patterns[b]. In the simulation system developed here, there are at present no subsystems dedicated to automatically determining which spatiotemporal variations of activity profiles that the motor neurons should undergo for a given specified task. For some tasks it is certainly possible to set up optimization algorithms which by gradient descent (e.g. backpropagation of error, or reinforcement learning

[b]By now the arm simulation system is fully connected and ready to go, just like the warm and humming engine of a car waiting to be commandeered around the block by its driver.

methods) or by direct calculation can specify activation patterns for the motor neurons. In chapter 2 a brief review of such optimization strategies was given. It turns out, however, that for many simple tasks it is actually possible to make an estimate of the required activity patterns based on the EMG traces for various tasks. Alternatively, one may simply try to select by hand some suitable activation patterns which solve the requested problem.

11.2.1 Scheduling motor cortical activity

The methodology adopted here is essentially equivalent to selectively targeting corticospinal projections with microelectrodes inserted into the spinal cord. By activating the electrodes using different patterns and observing the resulting movements it essentially becomes possible to elucidate the input-output mapping functions that exist in the spinal cord. And since the model is completely transparent (we have access to all parameters), it also is possible to evaluate the functional relevance of different neuron populations. The activity patterns that must be imposed on the corticomotoneuronal cells of the network can be inferred and adapted from published EMG traces related to similar tasks (see e.g.[175]). This is of course a very crude method of gaining such information, but for our present purposes it turns out to be quite adequate as what we are after is not a specific set of instructions, but rather to identify some general rules that the system might use. In fact, for testing the system it does not really matter which task is performed, and it is even permissible to initially select a randomly but slowly fluctuating pattern. This we may do as long as it is always this very same pattern that is used consistently for all the remaining task related tests. The reason for this pattern selection liberty is that almost any structured cortical-muscular pattern could potentially be a learned pattern which is executed voluntarily, and is thus within the scope of this study. For the purpose of facilitating analysis, however, it is useful to settle on a very simple task, say a straightforward hand transportation task, implemented by using a relatively simple corticospinal activation pattern. Once a neural activation pattern has been selected and its corresponding task performs correctly, different perturbations may be imposed on the running system to evaluate the significance of the various components. Highly specific "damage" may be done on the system (e.g. removing the dorsal roots, or blocking PAD interneuron activity, or perhaps removing the Renshaw cells), or the arm simulation may be perturbed by controlled external forces.

11.3 Steady-state free hanging arm

Even when the arm is at rest, the primary and secondary spindle afferents remain active at low firing rates (see e.g. figure 10.2). Other neurons in the spinal cord will also always have low background firing rates, including the inhibitory interneurons. Before proceeding with pattern identification and model testing there is therefore one rather obvious criteria that the model must fulfill: Limbs at rest must remain at rest. The problem is essentially, that once in a while a group of neurons (say of primary afferents) will fire in close temporal proximity purely by chance. If these neurons have postsynaptic cells in common, the resulting PSPs will sum temporally, which may well bring the target cells

to threshold, perhaps even resulting in the twitch of a single motor unit if the target cell is an α-motoneuron. When this α-motoneuron fires it will increase the firing probability of the Renshaw cells which it innervates. This has the immediate effect of quenching further activity in that particular motor unit via feedback inhibition. But it also has the effect of increasing the firing probability of the antagonist motor unit through disinhibition because Renshaw cells actually inhibit those IaIN cells and Renshaw cells that normally would be keeping the antagonist motor unit below threshold. And because the initial twitch will have a tendency to stretch the antagonist muscle, the primary and secondary afference to the disinhibited antagonist muscle will have an increased excitatory effect. Eventually, this situation could lead to oscillations where first the agonist and then the antagonist muscle become activated intermittently. In a well balanced network, such a single twitch should not have great consequences. However, even if a single twitch is perhaps not a cause for concern, it still is a problem that the spinal circuitry seems to be in an unstable equilibrium and could begin oscillating spontaneously. The problem is of course enhanced if the limply hanging arm is suddenly perturbed by outside forces. Then the stretch receptors would become increasingly active and thus produce a higher incidence of reflex responses, a situation that is not compatible with our ability to render our limbs completely irresponsive to outside perturbations.

Within the spinal cord there are several mechanisms which might have a role to play in avoiding spontaneous generation of oscillatory muscle activations. One such mechanism could be the PAD pathway which exerts presynaptic inhibition on Ia afferent synapses. If presynaptic inhibition of Ia synapses is tonically effective while the limb is in a resting state, it would reduce the probability that random fluctuations in spindle afference could bring motoneurons to threshold. Effective presynaptic inhibition of Ia afferent synapses would also have the additional useful property of reducing or even removing any stretch reflexes even if the limp limb is moved by external forces. That presynaptic inhibition is the best strategy becomes obvious if one considers that the system needs to avoid stretch reflexes while still receiving proprioceptive information. It is thus not useful just to turn of the sensory neurons providing primary and secondary afferents as this would also shut down limb proprioception. It is also not very helpful simply to increase the rate of background activity in Renshaw cells and IaIN as this only postpones the instability, but does not remove it. Another possibility is to lower activity in the γ-motoneuron system during rest, which would relax the spindles, thereby reducing the firing frequency of primary and secondary afferents. This strategy is unacceptable on experimental grounds as it has been reported that some γ-motoneurons (in cat) have relatively high firing frequencies at rest ($\sim$ 70 impulses/s) and actually *decrease* their mean firing rates at different phases during movement[197]. Finally, although it does help simply to reduce the absolute synaptic efficacy of Ia synapses, this might severely disrupt performance in other situations where a strong link between primary afferents and motoneurons is required such as during rapid reflex enhanced movements. On these grounds, presynaptic inhibition seems to be the best way to attain resting-stability under a variety of circumstances.

To emphasize these points, the following three experiments were performed using the simulation system under different circumstances. In all cases the simulation starts with the arm model in a vertical position pointing down and without perturbations while the muscular system is fully connected to the spinal

and corticospinal networks using the wiring diagram in figure 8.1 except where otherwise noted. The resting firing rate of dynamic γ-motoneurons was set to 70 impulses/s and for static γ-motoneurons it was set to 16 impulses/s, in accordance with experiments reported by Murphy et al.[197]. Under these circumstances primary and secondary afferents will have an activity level of 10-20 impulses/s (see e.g. figure 10.2).

11.3.1 Immobilized arm with inactive PAD

This first simulation was done without presynaptic inhibition of the primary afferents. The arm model was immobilized so that there were no variations in the lengths of the muscles (they can only produce isometric forces). After a short stabilizing transient ($t < 350$ms), the network seems to have stabilized into a situation where excitation and inhibition are in balance. For some time there are only subthreshold fluctuations of the motoneuronal membrane potentials. At time $t \sim 500$ms a few of the smallest α-motoneurons become active (highlighted areas in figure 11.6)$^{\odot}$, which initiates a cascade of events leading to the oscillations seen for $t > 600$ms. It should be noted that in all the simulated muscles, the activity of joint flexor motoneurons is almost completely out of phase with respect to the joint extensor motoneurons. This oscillatory behaviour becomes even clearer if one plots the activity of Renshaw cells belonging to antagonist muscle pairs, as is done in figure 11.7, which yields an activity pattern that is very typical of spinal oscillators, especially those concerned with locomotion (see e.g. Orlovsky et al.[208]).

In the current simulation the oscillation has a periodicity of approximately 170ms, this means that the motor units are twitching at a frequency of close to 6Hz (a value which incidently is comparable to the 3-8Hz tremor in Parkinson's disease[252]). It is only the smallest motor units that are recruited so the isometric muscle forces produced by these tremors rarely exceed 5% of the maximal isometric force of the muscle, as may be seen in figure 11.8. And because the arm was immobilized, primary and secondary afferents maintain a constant low level of activity throughout the experiment (see figure 11.9). If the arm were free to move, the activity of primary and secondary afferents would also change strongly enhancing the oscillations.

11.3.2 Immobilized arm with active PAD

This simulation was set up to determine whether presynaptic inhibition of the primary afferent synapses on motoneurons could help reduce the amplitude of the intrinsic spinal oscillations to a level where muscle tremor was abolished. During this simulation PAD interneurons fired tonically at approximately 30 impulses/s, which in the model is adequate to strongly dampen the effects of primary afferents on the α-motoneurons. As before, the primary and secondary afferents were active at a resting level of 20Hz, so the α-motoneurons did receive excitatory input from the secondary fibers. As can be seen in figure 11.10$^{\odot}$ none of the α-motoneurons reached threshold, so tremor was effectively abolished. There is, however, still a tendency to oscillate in some of the cell populations, particularly the Renshaw cells which are tonically active and interconnected in flexor-extensor antagonism, just like a half-center oscillator[92]. These oscillations have exactly the same frequency as in the previous experiment (6Hz), which

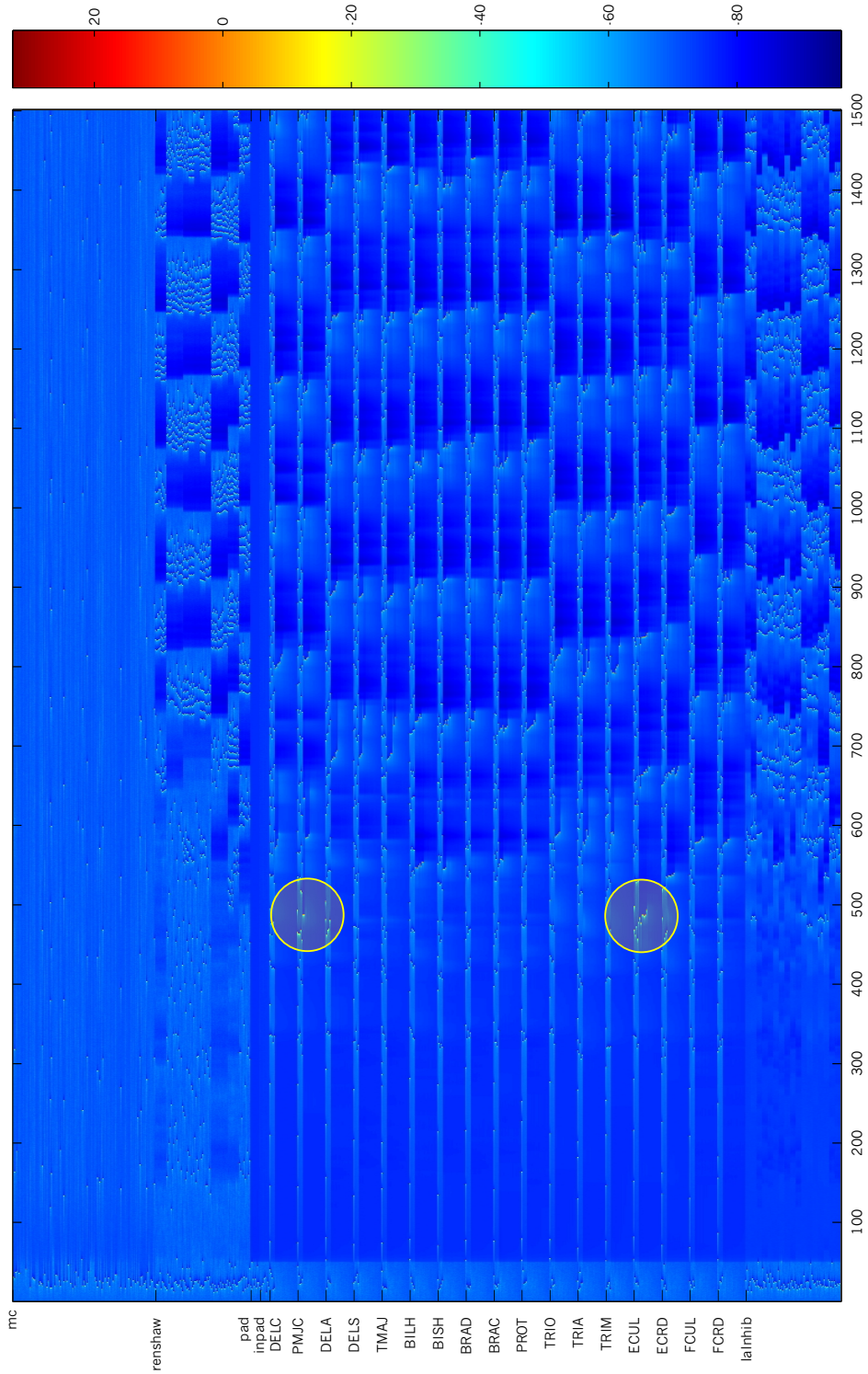

Figure 11.6: Neural membrane potentials of all neurons in the simulated network during experiment with immobilized arm and inactive PAD$^{\odot}$. This simulation was made with a network of 1582 neurons. Note that the activities of wrist flexor motor units (FCUL & FCRD) are completely out of phase with respect to wrist extensor motor units (ECUL & ECRD).

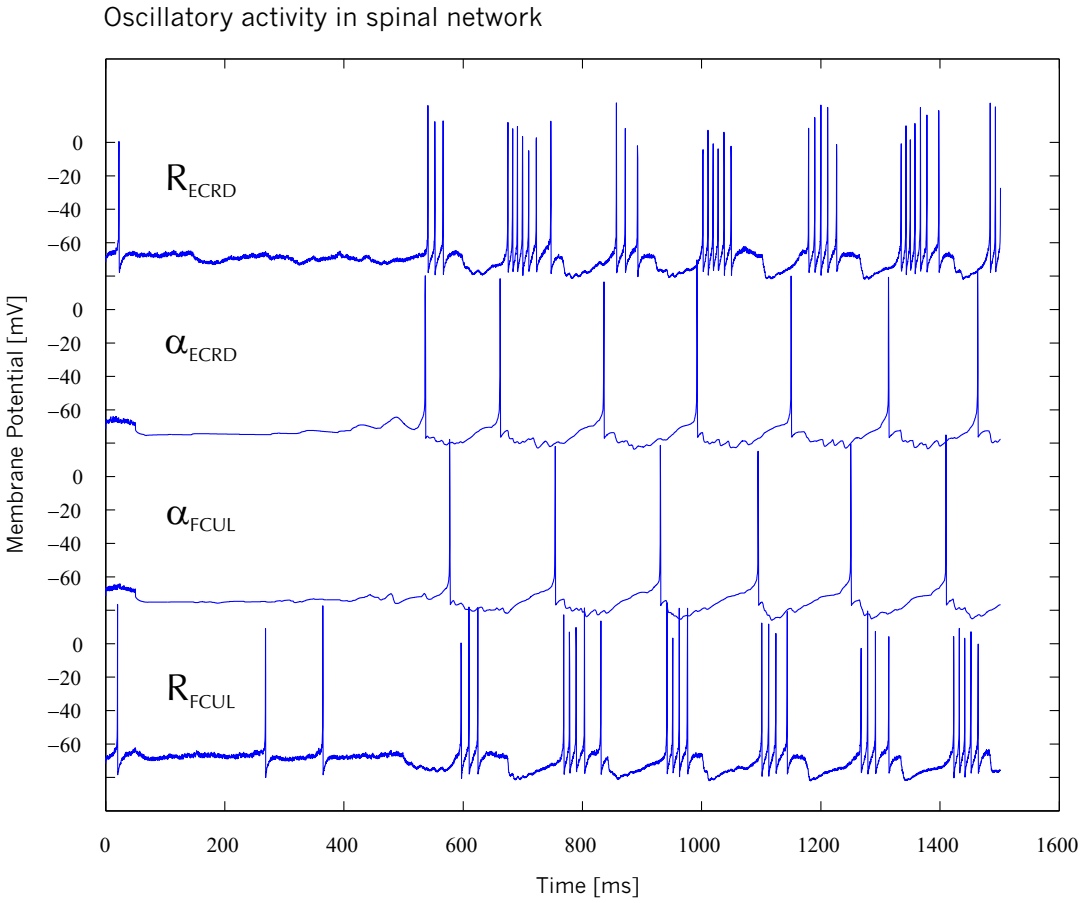

Figure 11.7: Two antagonist bursting Renshaw cells during immobilized arm simulation with inactive PAD.

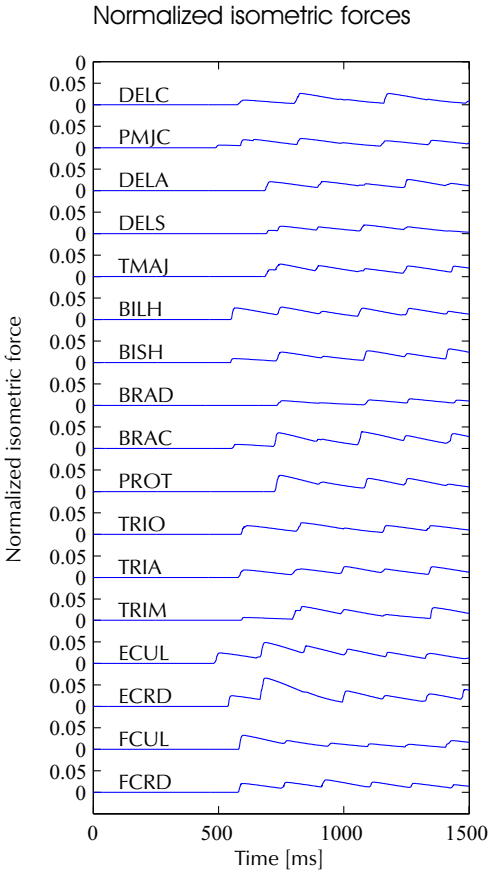

Figure 11.8: Normalized isometric muscle forces during immobilized arm experiment when PAD interneurons were inactive. Only 1-5% of the maximal isometric force is produced under these conditions (which is actually sufficient to produce small movements in the arm if it were released).

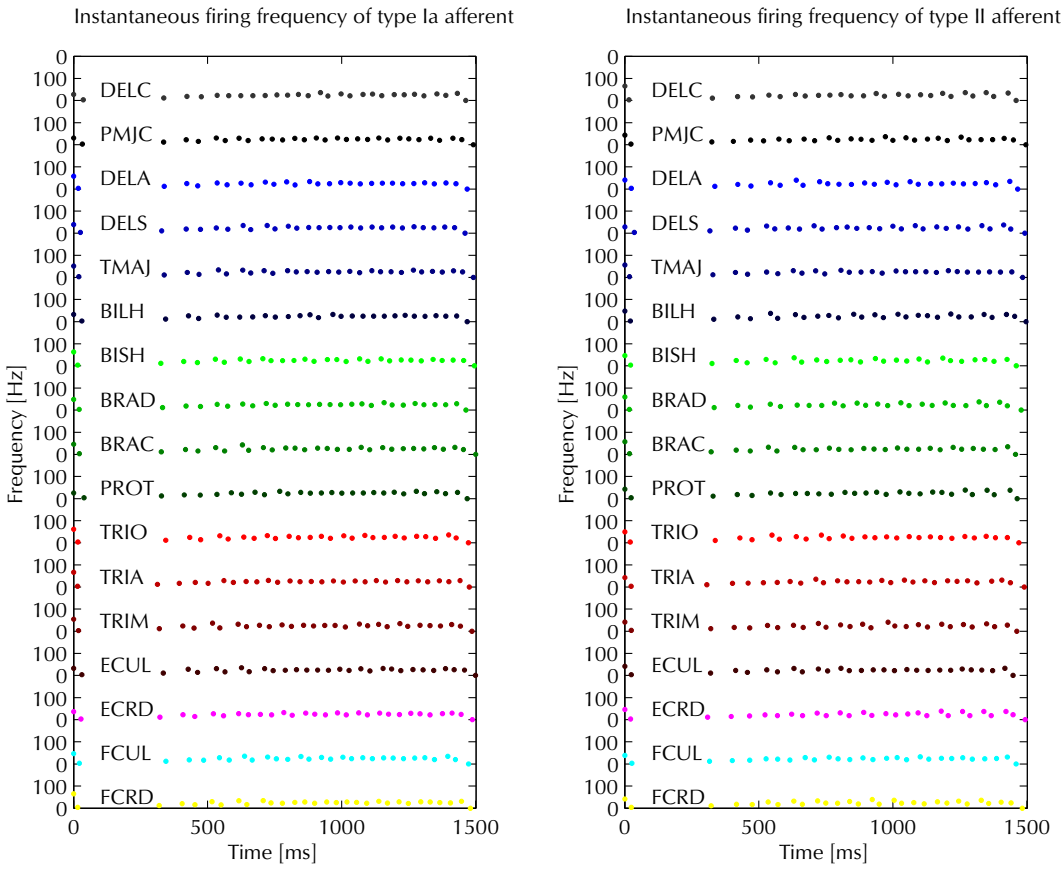

Figure 11.9: Primary and secondary afferent activity during immobilized arm experiment. Because the arm is immobilized, and the γ-motoneuron input is held constant, then there should be no time variations in the firing rate of primary and secondary afferents.

hints that it is the Renshaw cells that provide the driving frequency of the previously observed tremor.

11.3.3 External perturbation of free hanging arm with inactive PAD

A force of 16N was applied at the wrist for a duration of 350ms starting at time t=450ms (i.e. prior to the initiation of intrinsic oscillations). The force was applied in the sagittal plane in an anterior direction at 45°to horizontal. This results in an elbow flexion, thus stretching the elbow extensors and shortening the elbow flexors (during this simulation the elbow was flexed up to 40°). Under these circumstances the emerging neural activation patterns are fundamentally different from what was seen in the two previous experiments, as are also the mechanical properties of the arm (see figure 11.11). Shortly after the external perturbation force is applied, the primary and secondary afferents of the elbow extensor muscles increase their firing rates (see figure 11.12, thereby recruiting a larger fraction of the corresponding motor units. The total muscle forces are still rather modest, circa 10% of the maximal isometric force (see figure 11.13), but that is sufficient to cause a strong reflexive response to the perturbation.

11.3.4 External perturbation of free hanging arm with active PAD

If presynaptic inhibition is active, the arm simulation should essentially behave like a simple free swinging 3-link pendulum since no reflexes should be provoked by the perturbation. A force of 16N was applied at the wrist for a duration of 100ms, starting at $t = 450$ms. As expected the large increase of primary and secondary afference (see figure 11.14) had no influence on the activation levels of α-motoneurons and hence all muscle forces remained at zero (see figure 11.15).

11.4 Reaching from A to B – a typical task

The simplest non-trivial arm movement consists of transporting the hand along a smooth and straight trajectory with a single peaked velocity profile [190]. This task will form the basis for the rest of the arm simulations performed in this thesis, the selection being based on the following criteria: (1) It permits a straightforward evaluation of model performance, (2) EMG traces from similar tasks are available for comparison [175], (3) It has a relatively short duration and is therefore ideal for simulation, (4) It is a basic movement which nevertheless includes many important features such as joint angle inversion and triphasic activation of antagonist muscle pairs.

11.4.1 Deafferented arm simulations

Before setting up the appropriate neural activation patterns in the model, it is highly important to emphasize that simple movements of this kind may be performed even after partial or total deafferentiation [227,84]. In fact it has been found that some patients suffering from severe peripheral sensory neuropathy (leading to the deafferentiation) are nevertheless capable of a wide range of

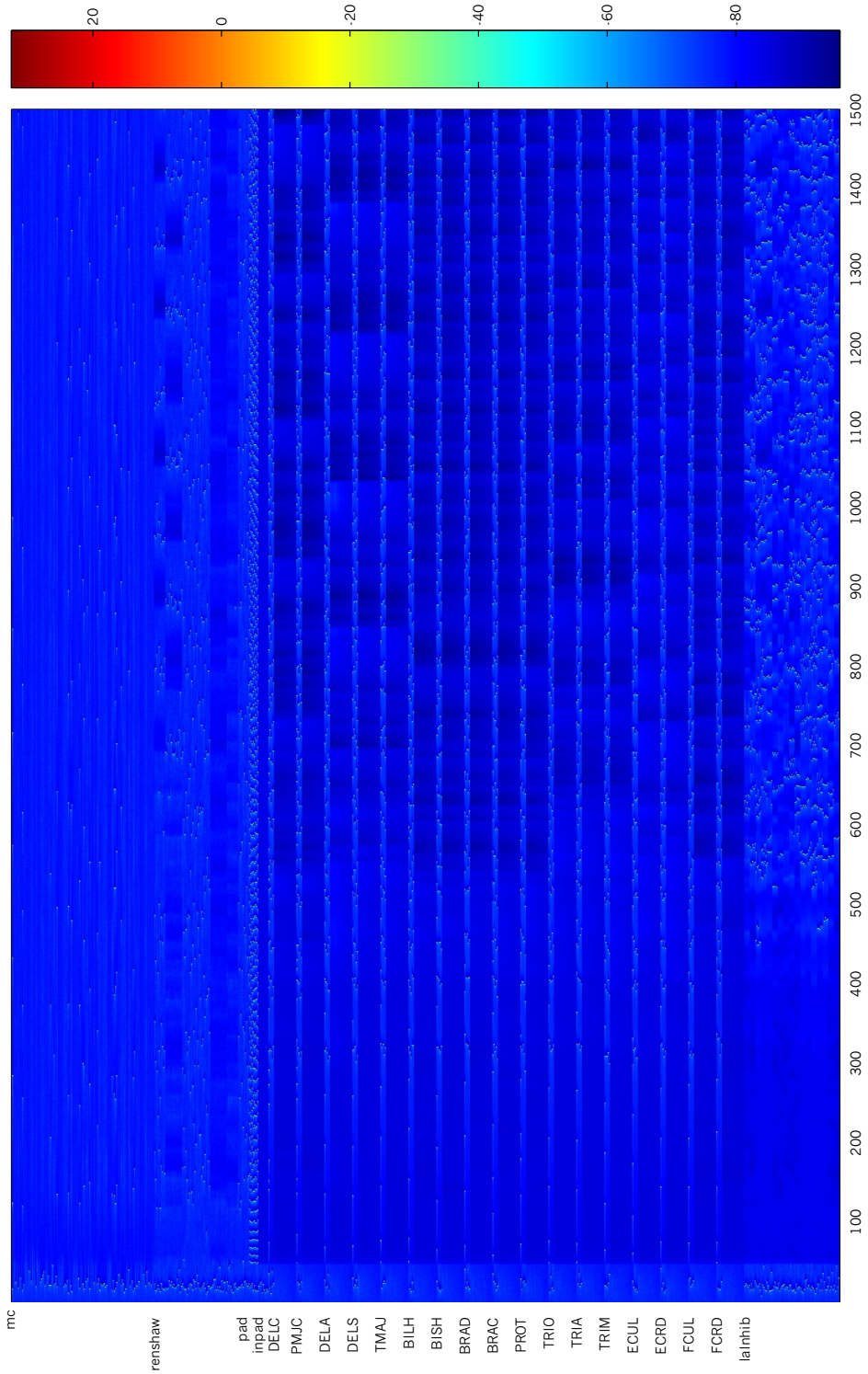

Figure 11.10: Neural membrane potentials of the 1582 neurons in the simulated network when the PAD based presynaptic inhibition is active$^{\odot}$. Notice that none of the α neurons reaches threshold.

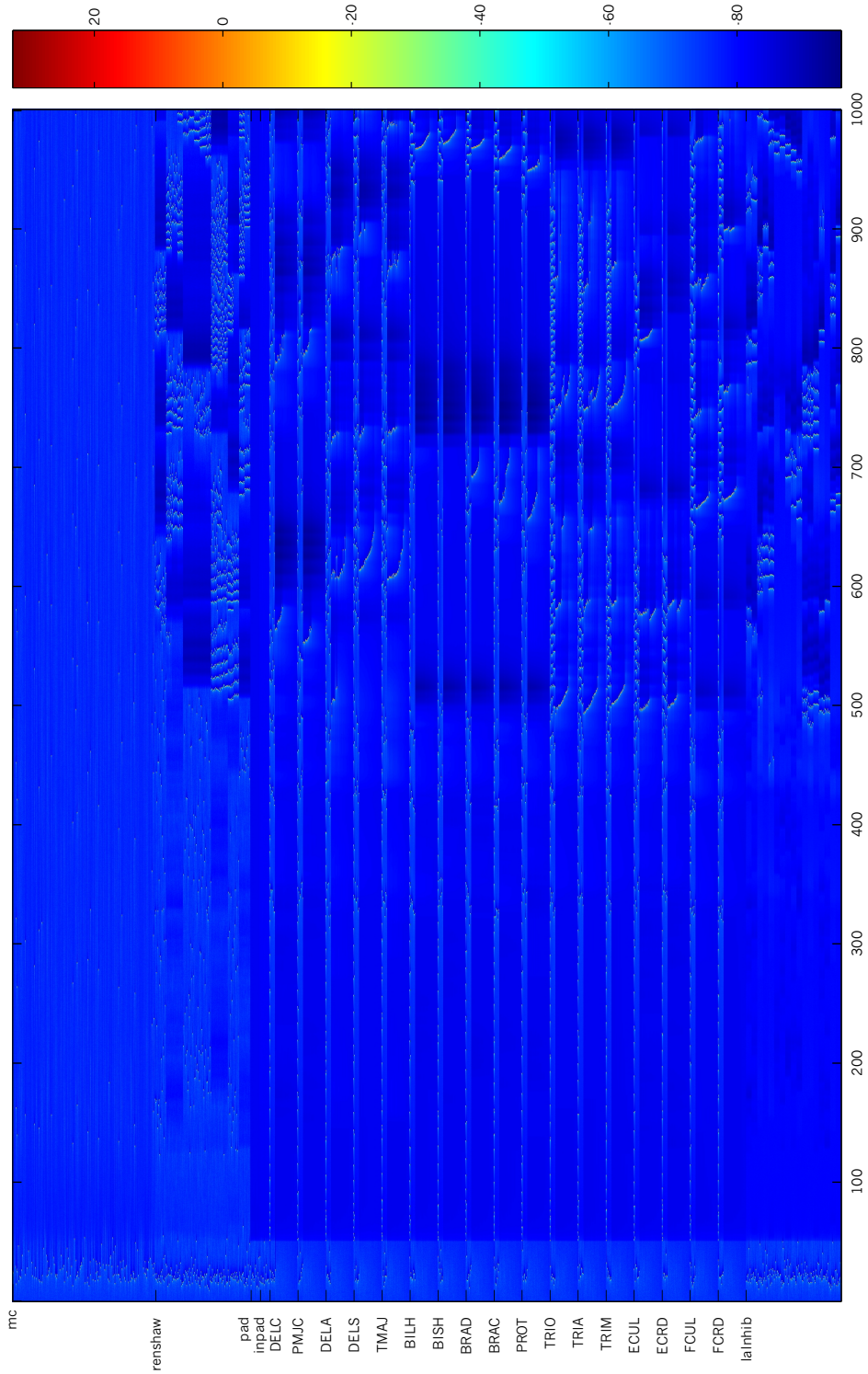

Figure 11.11: Neural activity profiles in the network when the freely hanging arm is perturbed$^{\odot}$. Arm extensor motor units are recruited by the primary and secondary afferents as a result of the suddenly imposed stretch.

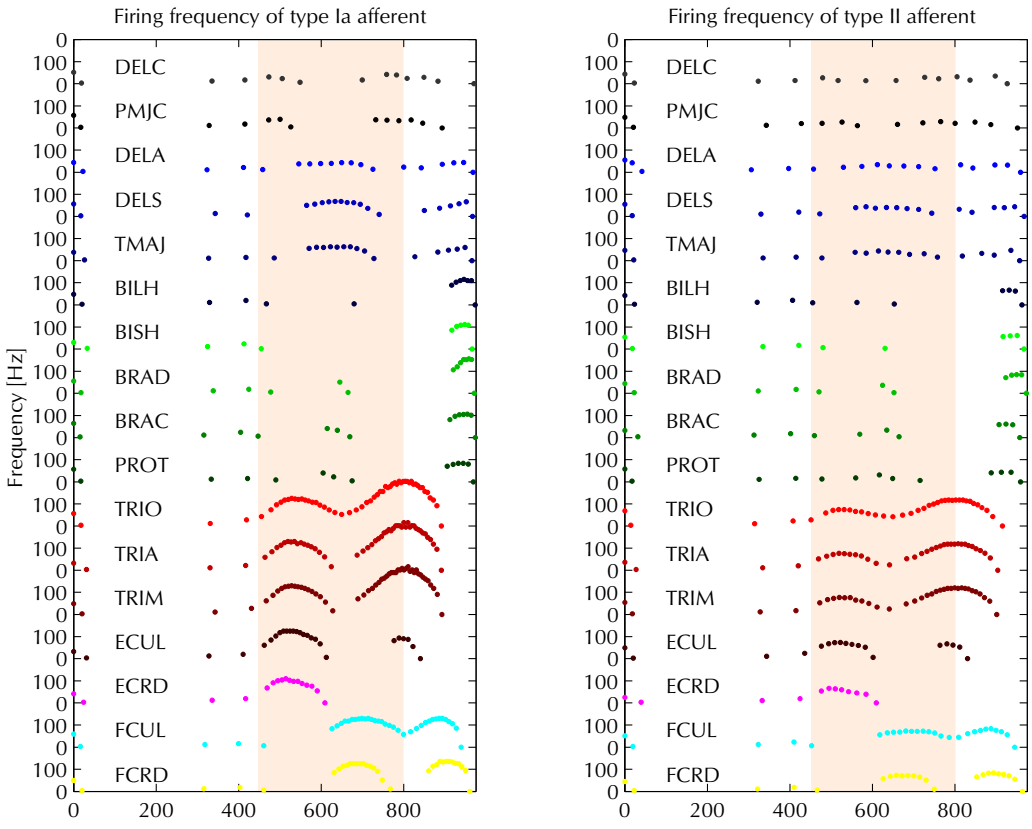

Figure 11.12: Primary and secondary afferent instantaneous firing rates during perturbation of free-hanging arm while synaptic inhibition was deactivated.

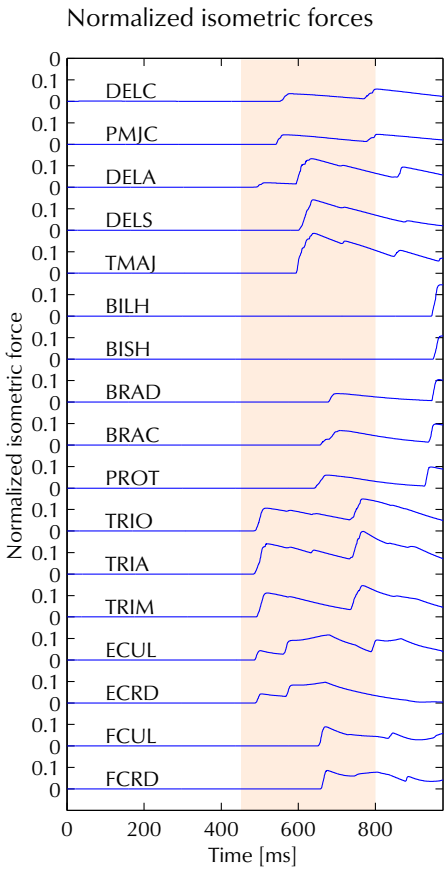

Figure 11.13: Normalized forces in all simulated arm muscles during perturbed free-hanging arm trial with inactive presynaptic inhibition. Note the sharp reflexive increase in force of the arm extensor muscles due to the increased primary afference.

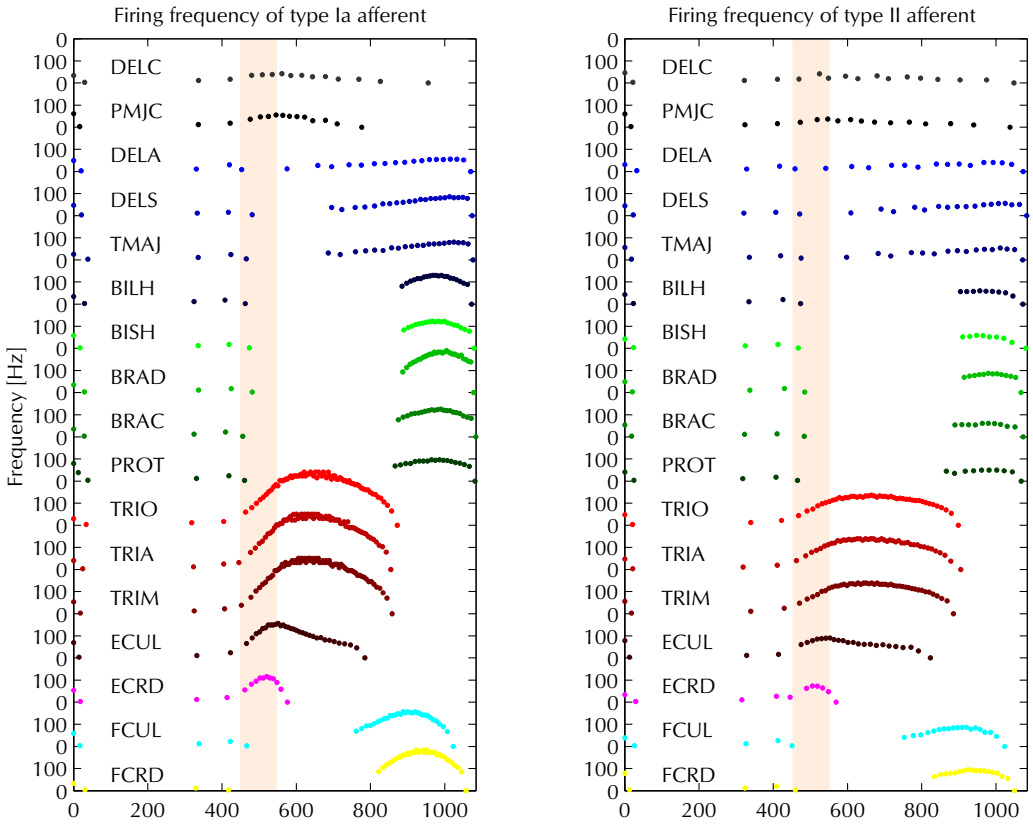

Figure 11.14: Instantaneous firing rate of primary and secondary afferents of perturbed (highlighted) free hanging arm with presynaptic inhibition.

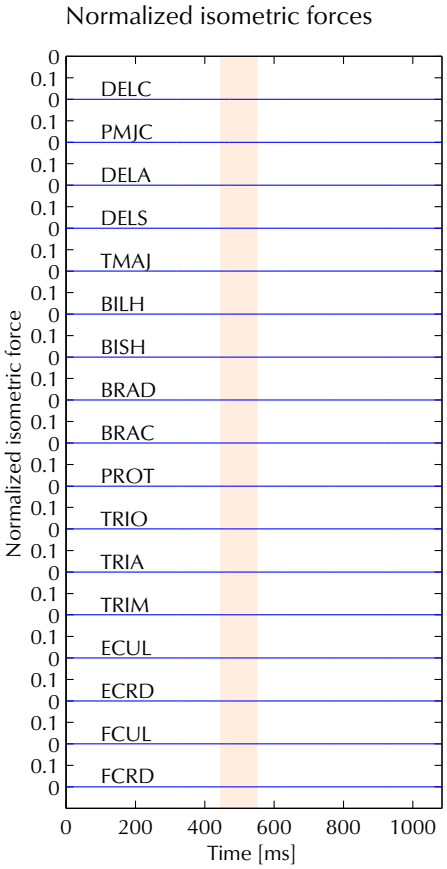

Figure 11.15: Normalized muscle forces of a free-hanging arm with active presynaptic inhibition during brief perturbation (highlighted). Presynaptic inhibition completely cancels the stretch reflex.

movements. In a very detailed report of just such a patient Rothwell et al.[227] observed that the patient was capable of drawing simple figures, tapping the fingers in predetermined sequences, moving the limbs at various specified speeds, and producing accurate matching forces. These movements were performed with a surprisingly high accuracy even though they involve complex muscle synergies of hand and forearm muscles. Pre- and post-movement EEG potentials were normal as were the bi/triphasic activation patterns of antagonist muscle pairs. All in all, during simple and short movements the patient seemed quite normal. However, if the patient was asked to maintain a given position or to continue a sequence, but without visual feedback, the movement deteriorated after a couple of seconds.

The reason that these observations are important in the present context is simply that they directly determine the type of activation patterns that should be imposed on the spinal simulation system. There are basically only two ways to go about this:

- Adapt the activation patterns to the spinal network. That is, to select the motor unit activation patterns in such a way as to perform the task with a fully connected (afferented) model, in which case the activation patterns will be precisely tailored only to the particular network at hand.

- Select activation patterns which correspond directly to the biomechanical task. That is, select motor-unit activation patterns that are directly related to the muscle forces that are required for the task.

Taken at face value, the data on deafferented patients presented before (see also Ghez et al.[84]) seems to indicate that "higher" brain areas (cerebellum, motor cortex, etc.) are perfectly capable of generating a full set of task specific instructions for the motor units based only on visual cues, and may thus control movement independently from the afferent circuits in the spinal cord.

When setting up the activation patterns for the arm simulation these facts should be taken into account, and consequently the network is temporarily deafferented during pattern specification. Good results were obtained by using the neural activation patterns shown in figure 11.16. These patterns were generated by scheduling step current "injections" at specified times and intensities for the CM cells (in the simulation each α-motoneuron receives projections from 10 CM cells). This manner of CM stimulation is of course a bit artificial, but it really just corresponds to letting the motor cortical networks perform a pre-learned spatiotemporal pattern sequence (like the ones presented in chapter 7, and perhaps using the same type of dynamics). The only difference being that the current spatiotemporal sequence was designed for the task rather than being truly learnt. During the scheduled activity the relevant muscles produce forces at predetermined times, thus producing the observed behaviour. The relevant muscle forces are shown in figure 11.17. As may be seen in figure 11.18, the simulation yields results which are in good agreement with the experimental results of Morasso[190], and with the experimental results reported in section 11.1.3. It should be noted that under these circumstances the simulation will functions in a purely feedforward manner.

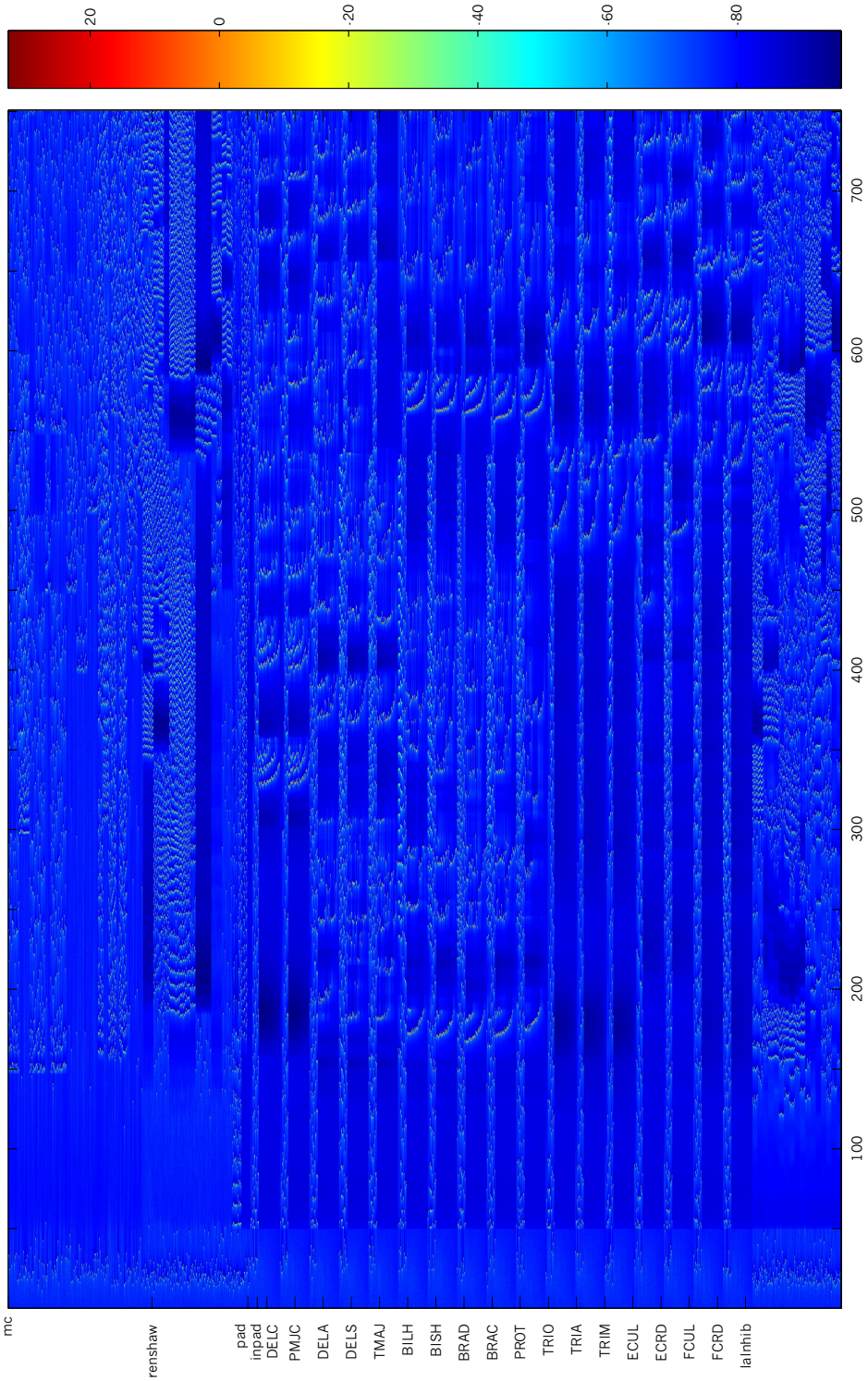

Figure 11.16: Neural activation patterns corresponding to straight hand movement$^{\odot}$. Scheduled current "injections" into CM cells of the motor cortex (mc) resulted in a stereotypical activation sequence leading to hand movement in a straight path.

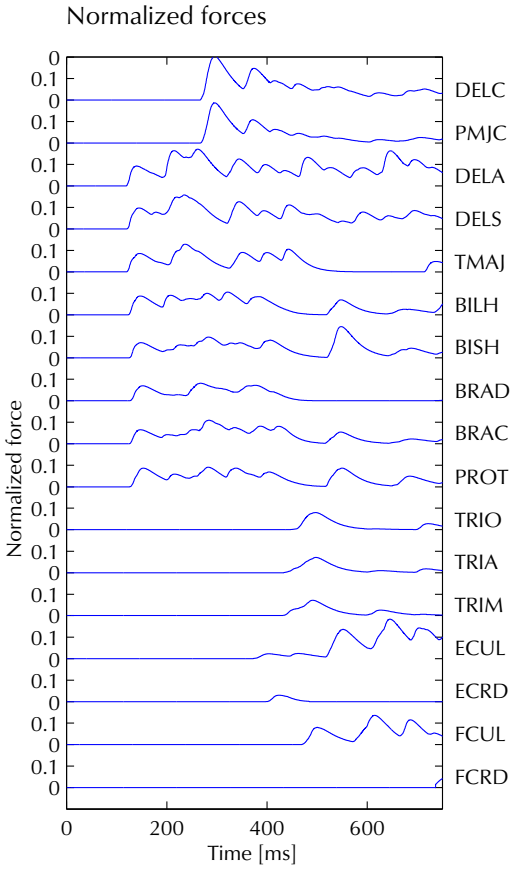

Figure 11.17: Normalized muscle forces during straight hand transportation task. Muscle forces reached at most 20% of maximum isometric force.

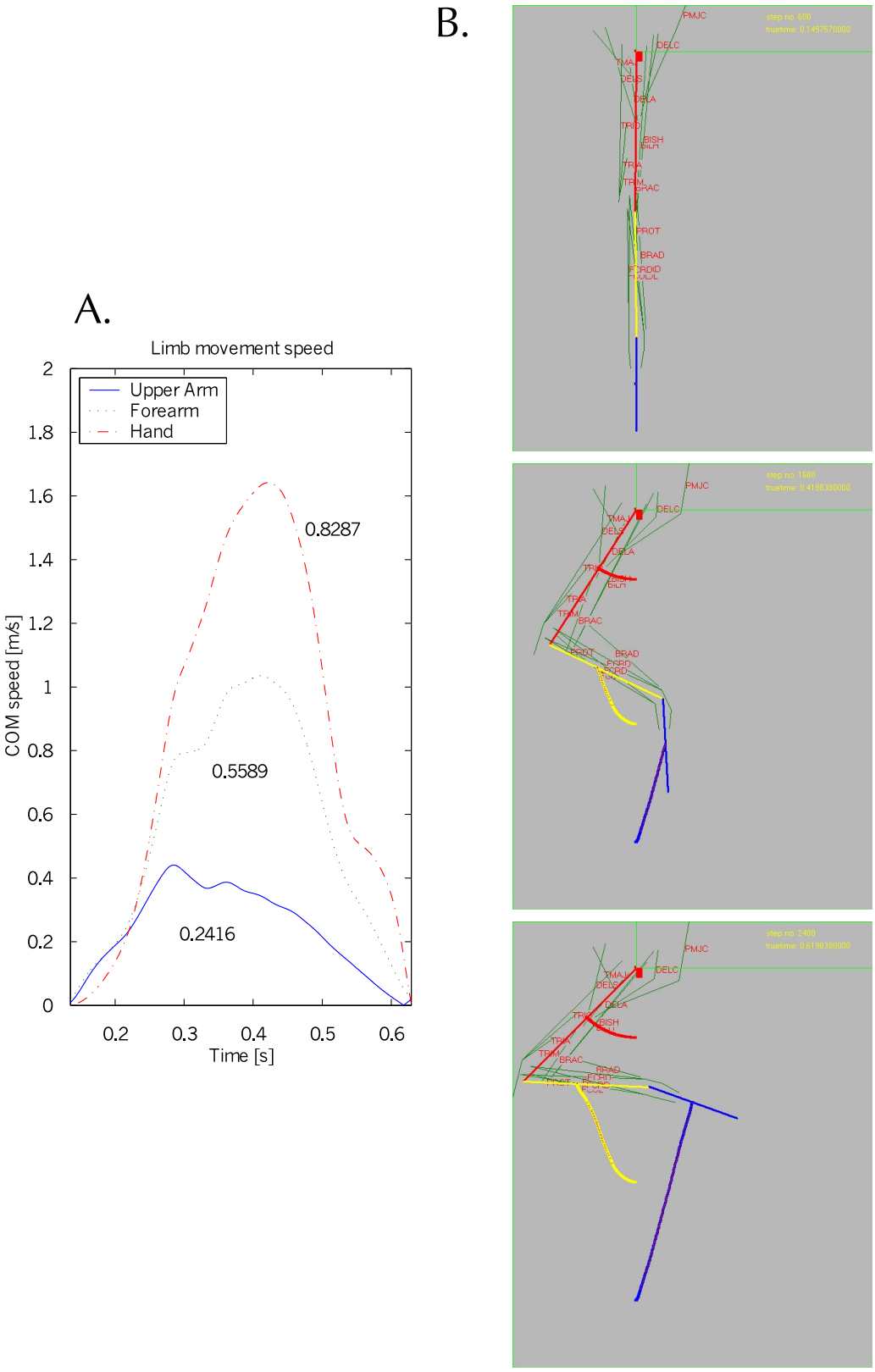

Figure 11.18: A. Velocity profiles of the different limbs during straight hand transportation task. Single peaked velocity profiles are observed during the task, with a maximum hand velocity $\sim$ 1.6m/s and an average hand velocity $\sim$ 0.8m/s. Both values are in agreement with experiment (see section 11.1.3). B. Three screenshots$^{\odot}$ corresponding to different phases of the task (time indicated in seconds)

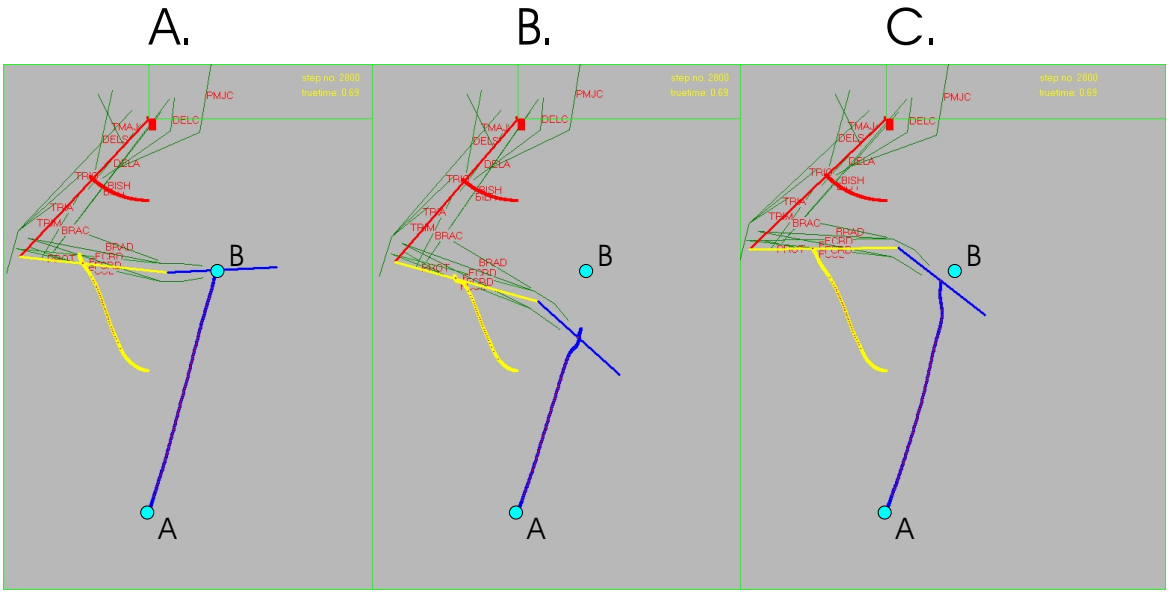

Figure 11.19: The effect of γ-motoneuronal activity on performance$^{\odot}$. (A). Deafferented arm simulation performing hand transportation task; (B). Afferented arm simulation performing hand transportation task, but with constant γ-motoneuronal activity. The unloading of spindles reduces the muscle force slightly, but sufficiently to affect performance; (C). Afferented arm simulation performing hand transport task with optimal γ-motoneuron activity.

11.4.2 Afferented arm simulations

According to the previous discussion, deafferented patients apparently are perfectly capable of producing normal movements as long as these movements are of a short duration and guided by visual cues. This essentially means that the spatiotemporal variations of EMG and EEG activities should be similar in afferented as well as deafferented persons. During inactivity, the increased excitatory input to α-neurons in the afferented case may be assumed (for simplicity) to be more or less balanced by the associated increase in the inhibitory IaIN input to these cells. This would result in a situation where the total resting input current to α-motoneurons is similar in the afferented and the deafferented situation.

If the fusimotor system is held at a constant level of activity during a task, the spindles will invariably become unloaded as a consequence of muscle shortening. This would cause variations in the total spindle afference. Such variations have not been taken into consideration during the original specification of α-motoneuronal activation levels as these were made in a deafferented arm. The predicted consequence of course being that the movement will be less forceful, and will probably not have sufficient force to reach the specified endpoint. This effect is seen in figure 11.19B.

Thus, under these conditions something extra is required for the model to work appropriately, namely to reduce the variations of primary and secondary afference so that the spindle related input to α-motoneurons again is held at a more or less constant level. To accomplish this, a strategy will be used which

is essentially identical to that followed in chapter 10, where spindle afference fluctuations were cancelled by pre-learned optimized fusimotor activity. The variations of spindle parameters that occurred during the simulations of a deafferented arm have been stored in a separate file (for all spindles). These data are then used to compute the optimal current input to γ-motoneurons by using equations 10.5 and 10.6. As before, this strategy corresponds to having stored a spatiotemporal sequence of neural activation patterns, corresponding to a learned fusimotor plan. During these experiments it was observed that the onset time of the fusimotor plan with respect to the actual motor plan, did actually influence the degree to which the γ-motoneurons were able to stabilize primary and secondary afference. By varying the fusimotor onset times for dynamic and static γ-motoneurons independently (γ_d and γ_s respectively), it was observed (see figure 11.20) that the optimal cancellation effect was obtained when γ_d initiated its fusimotor plan 100ms before the initiation of the CM activation patterns. For γ_s there was almost no difference for different onset times. The effect of including an appropriate fusimotor plan is seen in figure 11.19C. According to these results the primary and secondary afferent activity pertaining to the contracting muscles will maintain constant firing rates as long as the movement task is proceeding as planned. (The primary and secondary afferents associated with passively stretching muscles may safely be ignored because their contributions are cancelled more directly via presynaptic inhibition by the PAD system.) These results are perfectly equivalent to and compatible with the experimental observations made by Appenteng et al. [10], who stimulated fusimotor fibers to compensate for spindle unloading, thus avoiding silencing of the primary afferents.

11.4.3 A case of load correction

What happens when the movement is disturbed? For example if a load is applied to the forearm at some point while it is moving from A to B. In that case the flexion of the arm will occur at a reduced rate, which means that also the muscles will be shortening at a lower velocity. Assuming that the fusimotor plan is progressing at the normal pace, then at some point the capsular element of the muscle spindle will become overstretched, increasing primary and secondary afference, and thus leading to an increased firing probability of the α-motoneurons. The resultant increase in force should be able to compensate for the increased load, allowing the movement task to proceed according to plan. To test whether the model actually behaves in this way, the hand movement task was perturbed by applying a downward force of 4N at the wrist at time $t = 350$ms. The resulting hand trajectories, with and without a fusimotor plan, are shown in figure 11.21. Notice that it is only when the fusimotor plan is used, that the task is solved satisfactorily even in the presence of a load.

11.5 On the origin of the fusimotor plan

An important issue is to determine what is the actual *source* of this well learnt modulated γ-signal, that is, to determine which brain region is projecting to the spinal cord and explicitly telling the γ-motoneurons which signal is appropriate for cancelling fluctuations of the afference?. There are various candidates,

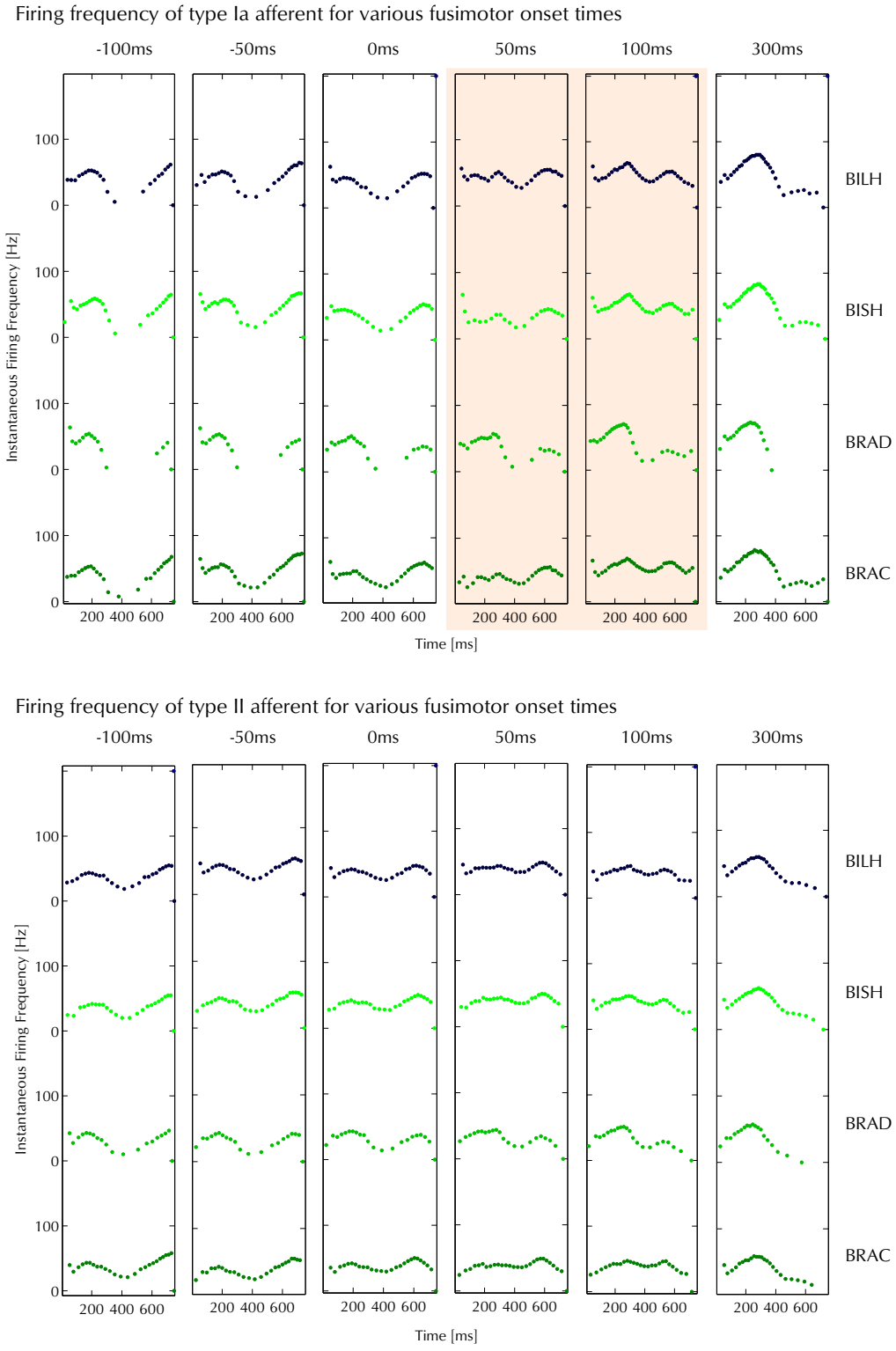

Figure 11.20: The effect of changing the onset time of the fusimotor plan during the straight hand transportation task. When γ_d-motoneurons become highly active 50-100 ms before motor unit recruitment, they are able to fully compensate for the unloading of the spindle that will occur as a consequence of the motor unit activity.

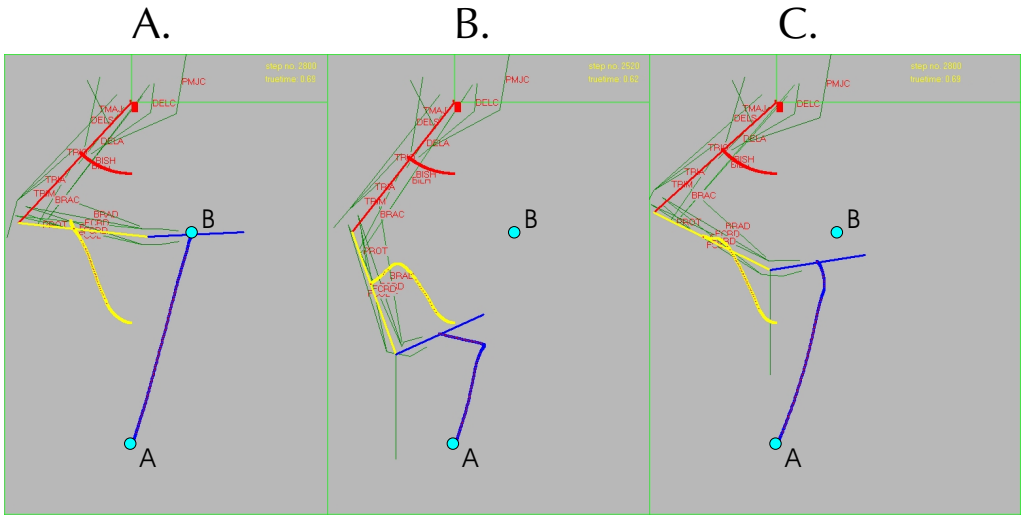

Figure 11.21: Perturbation of straight hand movement task$^{\odot}$. (A). Normal task performance (for comparison); (B). Perturbation of straight hand movement task when not stabilized by a fusimotor plan. The hand is deflected from its main trajectory, and ends up far away from the intended target. (C). Perturbation of straight hand movement task when accompanied by fusimotor plan. Even with the perturbation, the hand continues on the right track until target is reached.

spanning from intrinsic activity in the spinal cord itself, over sources in the brainstem and cerebellum, to the motor and premotor cortices.

The γ signatures that were calculated for the simulations in this chapter could, in principle, be used to identify γ-motoneurons directly *in vivo*, or perhaps to identify other neurons innervating the γ-motoneurons. But that would involve setting up an experimental paradigm which resembles the task used for the simulation, and with procedures aimed at sampling neural activities simultaneously in various parts of the CNS during a variety of specific and well learnt tasks. Fortunately, this type of approach has been pursued for some years now in a series of works by Cheney, Fetz and collaborators[67,39] where they investigated the activity of a population of neurons in the monkey motor cortex during a "ramp – hold" task. In particular they studied the activity of corticomotoneurons (CM) in primary motor cortex which project monosynaptically to the spinal cord. As reviewed in chapter 8, Fetz et al.[67] found various CM response patterns which were all well correlated with the investigated movement task, but which apparently did not have a direct causal link to the actual force production.

There are some intriguing points of similarity between the activation properties of CM cells and the optimal (reafference cancelling) activity profiles for γ-motoneurons. First of all there is the actual shape of the activation patterns: optimal γ_d activity somewhat resembles the activity in phasic-tonic CM cells, while optimal γ_s activity resembles tonic CM cell activity (see figure 11.22). Secondly, there is the observation that, to be optimal, γ_d activity had to have an early onset of activity ($50 - 100$ms prior to extrafusal activation, see figure 11.20), again corresponding to the phasic-tonic CM cells which on average

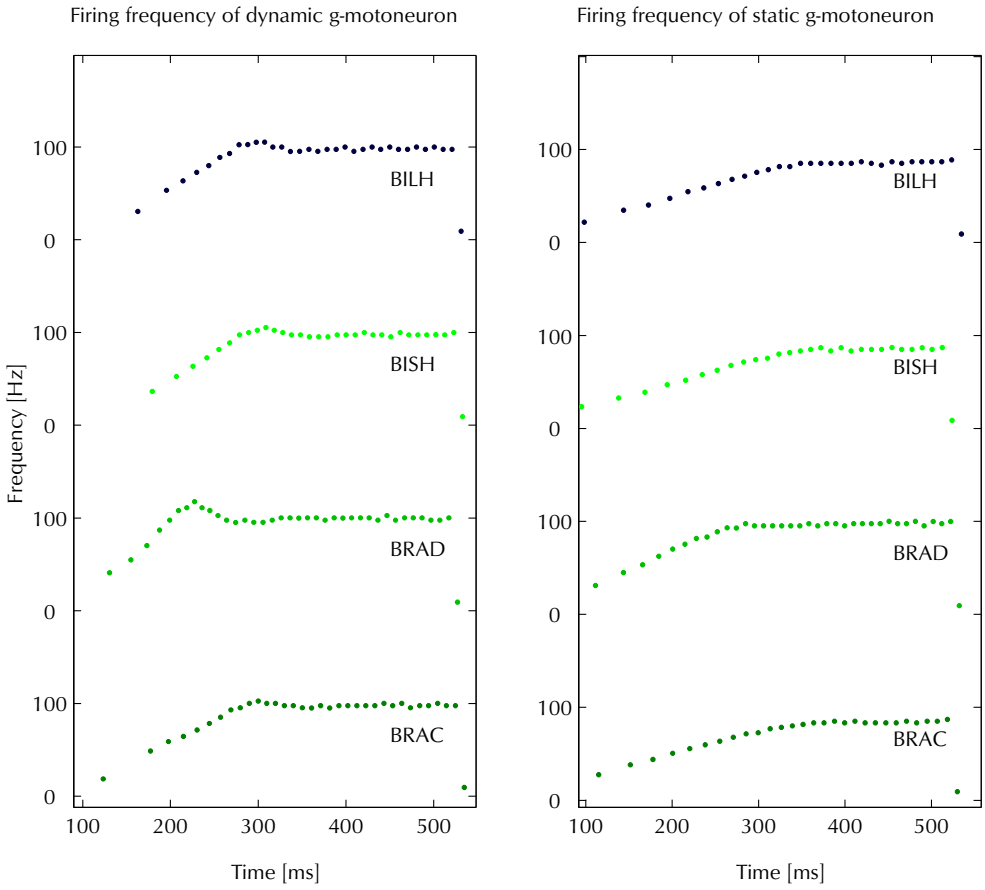

Figure 11.22: Typical optimal γ-motoneuron activity profiles pertaining to active muscles. Note that the γ_d profile is phasic-tonic, whereas the γ_s has a simple tonic activity profile.

started firing 71ms before EMG activity. Optimal γ_s activity could be obtained for various onset times, so it was left at zero displacement. Incidently, the tonic CM cells on average had onset times about 5ms after EMG activity. Thirdly, CM cells are responsive to muscle stretch, as evidenced by their increased firing rates during passive (imposed) movements, yielding yet another point of similarity to the γ-motoneurons' activity profiles which have been shown [215,93] to have high levels of activity during imposed movements and movements requiring high precision. Finally, due to their muscle stretch sensitivity, CM cells are ideally suited to update the fusimotor plan because this kind of updating necessarily requires current information about the state of the muscles. The dynamics of such updating could very well resemble the spatiotemporal attractor states of the abstract neural networks analyzed in chapter 7.

These, admittedly superficial, similarities may of course just be mere coincidences, but they do certainly warrant further investigation. Especially if one considers that if this hypothesis holds, it explains the activity of 76% of the total population of identified CM neurons (48% are phasic-tonic and 28% are

tonic)[67]. The crucial experiment now would be to verify that the *phasic-tonic* CM neurons and the *tonic* CM neurons respond predictably to other tasks. This could be done by setting up a completely different task, then monitor the same CM neurons during the new task (neurons initially identified in the ramp-hold task). A neuromuscular computer simulation of the new task is then set up (of course using the program developed in this thesis) from which the optimal γ_d-signature and γ_s-activities for the task may be calculated and subsequently compared to the experimental results.

It should be strongly emphasized that these similarities certainly do not constitute a solid proof of a functional link between CM cells and fusimotor activity. Especially not as long as they are only based on estimates derived from a computer simulation. The similarities do suggest, however, that there might be a linkage to be sought.

Chapter 12

General Conclusions – Towards the Motor Cortex and Beyond

Chapter Summary

This final chapter provides a brief discussion of the main results obtained in this thesis. Some future directions will also be outlined.

Eleven chapters it took to get to grips with only some of the most basic elements of neuromuscular control at the spinal level, and it would probably take another eleven to get a beginning feeling about what it is that the motor cortex tells the spinal cord to begin with. And even then, only the uppermost layer of paint will have been scratched away. Nevertheless, researchers all over the world are making great progress in unravelling the mysteries that the brain holds. It is my hope that this thesis may contribute positively to this endeavour.

12.1 Thesis Conclusion

There is an urgent need for highly accurate neuromusculoskeletal models which may be used to test ideas and suggest new venues for theorizing and experimentation. Motivated by this, an attempt has been made, within the scope of this thesis, to develop a highly detailed computational framework which may account for a large fraction of the existing experimental data. The resulting computational system necessarily covers many fields of study, and spans several orders of magnitude: From the molecular level where muscle proteins generate forces, to the macroscopic levels where overt arm movements are voluntarily controlled in an unsafe environment (which is full of sudden and unexpected

"loads"). Some of the most important features implemented into the system are the following:

- A computationally efficient general numerical solver for ordinary differential equations (variable time-step with Runge-Kutta's 4^{th}-order method) [144,213].
- A general mechanical physics simulation system for setting up dynamic simulations of limbs and joints (main emphasis on arm) [16].
- Realistic origin and insertion points for muscles (based on human data).
- Stable and flexible muscle and spindle models (also based on human data, see below).
- A neural scripting language which allows the user to produce almost any neural network architecture with just a few lines of text.
- Computationally efficient and interchangeable neuron models [274].
- Dynamic synapses [262].

Especial emphasis was given to creating a very detailed computational model of whole muscles, an endeavour which brought forth the following issues:

- The muscle model starts at the molecular level by invoking the conformational entropy of the myosin head group as the crucial factor determining the force produced by individual myosin filaments during a power stroke.
- Mathematical descriptions of the sliding filaments within the sarcomere are provided, and are used to develop a structurally accurate muscle force model which incorporates some important properties of single muscle fibers (primarily the force-velocity [107] and force-length [90,91] relationships).
- A simplified model of muscle-twitching is given in order to link neural activity to muscle activity via the neuromuscular junction. This model accounts for various phenomena such as the "catch-like" effect [33], tetanic fusion and the distinctions between fast and slow muscle fiber types [8].
- The muscle-twitch model is used in combination with the sarcomeric force model to create a muscle fiber model, which forms the basis of a whole-muscle model. Individual muscle fibers are joined into motor-units which are under the control of a single α-motoneuron. Many such motor-units functioning together make up the whole-muscle model, which accounts for many of the properties observed in individual motor units and whole muscles (including orderly recruitment [105], exponential motor-unit size distribution [189] and gradual force increase as a function of increasing input [185,270]).

As a final detail of the neuromusculoskeletal model developed herein, a mathematical model of the spindle was used to evaluate the dynamic range of such sensory organs. Theoretical analysis of this spindle model revealed that an explicit function may be derived which expresses the force that the spindle contractile elements must produce to exactly counter spindle unloading during muscle

shortening. If the fusimotor system is capable of having such a fine control over the intrafusal fiber contractions, then it could in principle maintain a close to constant (low) rate of primary and secondary afference during a wide variety of muscle tasks. Furthermore, if this fine control is based on the system having learnt certain task specific activation profiles which optimally down-modulate the naturally occurring afference during said task, then it is a clear example of reafference cancellation because it effectively removes the afference that otherwise results from self-generated voluntary planned movements.

These detailed computational models have been congealed into a single simulation program, which may serve as an ideal tool to explore some of the possible motor functional scenarios attributed to the motor cortex, cerebellum, basal ganglia, etc. However, only one such scenario was explored herein (in chapters 10 and 11), namely the proposition that the different firing patterns observed for corticomotoneuronal cells[67] might be involved in different aspects of fine tuning the control of otherwise strongly reflexive spinal networks by acting on the fusimotor plan. At present, the evidence in favour of this hypothesis is only indirect, based as it is on a computer simulation. But the similarities that were observed between CM cell activity and the activity of γ-motoneurons (listed in chapter 11) do certainly warrant the need for further investigations in this direction. It is quite well established that fusimotor activity modulates the activity in primary and secondary afferents, but so far it has not been entirely clear whether such modulation should be considered part of a servo-control system, or whether it is related simply to maintaining the spindle within a responsive dynamic range allowing for a more effective reflex mechanism, or more precisely to avoid silencing of the primary and secondary afferents due to unloading[10]. In this thesis a third view is maintained which falls somewhere in between the two other views, namely that fusimotor activity is concerned with maintaining the input from spindle afferents at a relatively constant level. According to some accounts[162,160,161] this is exactly what is observed *in vivo*, namely that the fusimotor activity varies in a task dependent manner so as to maintain spindle afference activity within a range from 50 to 200 impulses pr. second [162]. The purpose of this could be to obtain a spindle afference which only responds strongly to unexpected events, and not to self generated movements, thus greatly improving the signal-to-noise ratio. If for any reason the movement is not proceeding as planned, the fusimotor plan will to some extent be responsible for appropriately correcting the position discrepancies by increased recruitment of motor units in a servo-like manner. The important thing to note in this context is that, by using reafference cancellation, some of the problems associated with the presence of a long spinal delay loop may be somewhat avoided. This is because the only significant signals coming from the primary and secondary afferents are related to immediate positioning errors (delay $\sim$ 3ms from muscle to spinal cord).

12.2 Future directions

As already mentioned in chapter 11, the crucial experiment now would be to verify that the *phasic-tonic* CM neurons and the *tonic* CM neurons actually do respond predictably to other predefined tasks. To assay this, it would be necessary first to identify the relevant CM neurons by using the old task, af-

ter which a new task may be performed and the relevant neurons are sampled. Concurrently, a neuromuscular computer simulation of the new task is set up from which the optimal γ_d-signature and γ_s-activities for the task may be calculated and subsequently compared to the experimental results. If possible such signatures should be used to localize the γ-motoneurons within the spinal cord. If there still is a pattern similarity between CM cell activity and γ-motoneuron activity, even during longer experiments (at least 10s of seconds), a stronger case may be made that CM cells have a saying on the matter of fusimotor control.

There is also the question about the validity of the "entropic elasticity" model of muscle force that was presented in chapter 4. There are various tests which could be done to assay this hypothesis, requiring the use of optical tweezer technology in combination with fluorescent dyes. Also, a thermodynamic evaluation should be made of it, just to be sure that it does not violate any laws.

On a different note, it would be highly interesting to test various motor control theories using the neuromusculoskeletal model developed here. Several relevant issues were raised in earlier chapters (population coding, diffusion in topological networks, optimization strategies, etc.) which require just such a model to identify the relevant parameters, and to test whether the claims made for those hypothesis actually are realistic.

It would also be highly interesting to adapt this neuromusculoskeletal model to an actual robotic application. Perhaps it then would be necessary to produce specialized hardware to implement the model in real-time (rather than having to wait 20 minutes for every simulated second).

12.3 This is not the end

The optimism and elation that is felt after advancing a small step when it was the result of a huge effort, is somewhat tempered by the frustration of realizing that, indeed, it was only a small step. Few have captured this feeling as succinctly and eloquently as Sir Winston Churchill in a speech he gave at the Lord Mayor's Luncheon (Mansion House, London, November 10, 1942):

> This is not the end. It is not even the beginning of the end. But it is, perhaps, the end of the beginning.

Indeed...

Glossary

A-band : The A-(Anisotropic) band appears dark in the striation pattern.

Actin : Elongated protein which is the backbone of the thin filaments.

Agonist muscles : Muscles that cause joint movement in the same direction.

Antagonist muscles : Muscles that cause joint movements in opposite directions.

Dorsal tubular nerve cord : In chordate animals a hollow tube of nerve tissue spanning the animal's length along its dorsal aspect [250]. In some species it has a large anterior enlargement forming the brain and ventricular system. Posterior regions form the spinal cord *per se*. In vertebrates it is enclosed by the vertebral column.

Endomysium : Connective tissue surrounding a single muscle fiber (including sarcolemma), and interconnecting all the fibres in a fascicle.

Epimysium : Connective tissue surrounding a cluster of fascicles.

Exteroceptive input : Primarily related to skin sensations caused by events occurring in the environment (touch, pain, temperature) [31].

Fascia : Connective tissue surrounding complete muscle.

Fascicle : A small cluster of muscle fibers surrounded by a perimysium.

Fusiform muscle : Muscles in which the fibres are arranged parallel to longitudinal axis.

I-band : The I-(Isotropic)band appears light in the striation pattern.

Isometric contraction : A process wherein muscular tension is countered by a load to hold the stimulated muscle at a fixed length.

Isotonic contraction : Application of a constant load to a stimulated muscle.

Kissing number : Number of spheres touched by ("kissed by") a given sphere.

Monosynaptic reflex : Muscular contraction resulting from the direct activation of agonist α-motoneurons by the primary spindles (i.e. a monosynaptic connection between Ia afferents and α-motoneurons). In humans, these reflexes have a latency from 25 to 40 ms.

Motor unit : Consists of one α-neuron and all the muscle fibres it innervates. It is considered the smallest control unit of a muscle because all muscle fibres in a motor unit will act synchronously. Tetanic forces of single motor units range from 5 to over 100 grams (i.e. from 0.05N to over 1N).

Muscle fiber : Consists of an individual muscle cell surrounded by endomysium. Individual muscle fibers are surrounded by the sarcolemma. They measure from 1 to 40 mm in length and from 10 to 40 μm in width[102]. The maximal isometric tension in a single muscle fiber is therefore in the range from 3×10^{-5}N to 5×10^{-4}N (or from 0.003g to 0.05g).

Myofibril : These are bundles of parallel myofilaments. They are systematically arranged in the muscle and give rise to the microscopical striated appearance of skeletal muscles. They are as long as the muscle fiber, but only 1μm in width[102]. The maximal isometric tension of a myofibril is approximately 3.5×10^{-7}N (i.e. 3.5×10^{-5}g).

Myosin : Elongated protein with molecular weight of 500 kDa. It consists of a globular head (light meromyosin) connected to a long tail (heavy meromyosin). The globular head contains a binding site for actin and an enzymatic site causing hydrolysis of ATP. Myosin heads create cross-bridges between thin and thick filaments.

Notochord : Rod of firmly sheathed tissue which spans most of the chordate animal's length along the dorsal aspect[250]. Its primary function is supporting the body. In vertebrates the notochord is reinforced or substituted by a vertebral column.

Oligosynaptic reflex : Muscular contraction resulting from the indirect activation of agonist α-motoneurons by the primary spindles mediated through an interneuron (i.e. a bi- or trisynaptic connection between Ia afferents and α-motoneurons via interneurons).

Optimal Sarcomere Length : At this length the sarcomere produces maximal force. Typical values are: $2.1\mu m$ for frog, $2.4\mu m$ for cat and $2.7\mu m$ for human skeletal muscle[57].

PCSA : The Physiological Cross-Sectional Area is found as the ratio between muscle volume and muscle fibre length.

Pennate muscle : Muscle tissue in which the fibres are arranged at a distinct angle to the longitudinal axis. These can be unipennate (1 angle), bipennate (2 angles) or multipennate (more than 3 distinct angles).

Perimysium : Connective tissue surrounding an individual fascicle.

Pharyngeal gill slits : In chordate animal embryos these are grooves in the pharyngeal region of the body wall[250]. In aquatic chordates these grooves are completely perforated an become fully functional gill slits, but in terrestrial animals the grooves are modified to form other structures (such as the outer ear canal).

Phasic reflex : Occurs in response to a sudden change in the level of stimulation. This type of reflex is probably monosynaptic.

Proprioceptive input : Primarily related to sensory input caused by "own" movements. These are generated at specialized sensory organs in muscle (spindles and Golgi-tendon organs)[31].

Sarcolemma : Delicate membrane surrounding individual muscle fibers.

Sarcomere : The contractile unit of skeletal muscle, which is limited at its ends by the Z-lines (Zwischenscheiben). The sarcomere is made up of thick and thin filaments arranged in almost crystalline order.

Thick filament : These are located at the centre of the sarcomere, and consist of approximately 180 myosin molecules arranged so that the myosin heads protrude from the filament in opposite pairs, and in such a way that consecutive pairs along the filament are displaced by 14.3 nm, and rotated 60°.

Thin filament : These are bisected by the Z-lines and consist of two helically interwoven actin globule chains, two tropomyosin proteins lying along the grooves between the two actin chains, and a number of troponin protein units placed at 38.5nm intervals.

Tonic reflex : Sustained muscle contraction in response to the level of some stimulus. Tonic reflexes are polysynaptic.

Vertebral column : This is the skeletal axis of vertebrates, which encloses the nerve cord and gives support to the body[250]. It is made up of several segments of cartilagineous or bony tissue called vertebrae, which are linked together in a flexible and highly resistant construction.

Z-line : These are strands of protein oriented perpendicularly to the myofibrils.

Bibliography

1. L.F. Abbott and S.B. Nelson. Synaptic plasticity: taming the beast. *Nature Neuroscience Supplement*, 3:1178–1183, 2000.

2. L.F. Abbott, J.A. Varela, K. Sen, and S.B. Nelson. Synaptic depression and cortical gain control. *Science*, 275:220–224, 1997.

3. P.R. Adams. The platonic neuron gets the hots. *Current Biology*, 2:625–627, 1992.

4. H. Agmon-Snir, C.E. Carr, and J. Rinzel. The role of dendrites in auditory coincidence detection. *Nature*, 393:268–272, May 1998.

5. R.M. Alexander. *Exploring biomechanics - Animals in motion*. Scientific American Library, NY, 1992.

6. D.J. Amit. *Modelling brain function: the world of attractor neural networks*. Cambridge University Press, Cambridge, UK, 1989.

7. K. N. An, Hui F.C., Morrey B.F., Linscheid R.L., and Chao E.Y. Muscles across the elbow joint: A biomechanical analysis. *Journal of Biomechanics*, 14(10):659–669, 1981.

8. J.L. Andersen, P. Schjerling, and B. Saltin. Muscle, genes and athletic performance. *Scientific American*, 283(3):30–37, September 2000.

9. P. Andersen and A.F. Soleng. Long-term potentiation and spatial training are both associated with the generation of new excitatory synapses. *Brain Res Brain Res Rev*, 26(2-3):353–359, 1998.

10. K. Appenteng, A. Prochazka, U. Proske, and P. Wand. Effect of fusimotor stimulation on ia discharge during shortening of cat soleus muscle at different speeds. *Journal of Physiology*, 329:509–526, 1982.

11. M.A. Arbib, editor. *The Handbook of Brain Theory and Neural Networks*. MIT Press, Cambridge, MA, 1995.

12. A. Artola and W. Singer. Long-term depression of excitatory synaptic transmission and its relationship to long-term potentiation. *TINS*, 16(11): 480–487, 1993.

13. P. Ascher and L. Nowak. Electrophysiological studies of NMDA receptors. *TINS*, 10:284–288, 1987.

14. C.H. Bailey, D. Bartsch, and E.R. Kandel. Toward a molecular definition of long-term memory storage. *Proc. Natl. Acad. Sci. USA*, 93:13445–13452, 1996.

15. A. Bain. *Mind and body. The theories of their relation.* Henry King, London, 1873.

16. D. Baraff and A. Witkin. Physically based modeling: Principles and practice. *Siggraph '97 Course Notes*, 1997. Also available at: http://www.cs.cmu.edu/ ~baraff/ sigcourse.

17. G. Barrionuevo and T.H. Brown. Associative long-term potentiation in hippocampal slices. *Proc. Natl. Acad. Sci.*, 80:7347–7351, 1983. USA.

18. N.A. Bernstein. *The coordination and regulation of movement.* Pergamon, Oxford, 1967.

19. E.N. Best. Null space in the hodgkin-huxley equations. *Biophys. J.*, 27: 87–104, 1979.

20. E.L. Bienenstock, L.N. Cooper, and P.W. Munro. Theory for the development of neuron selectivity, orientation specificity and binocular interaction in visual cortex. *J. Neurosci.*, 2:32–48, 1982.

21. M.D. Binder, editor. *Peripheral and spinal mechanisms in the neural control of movement*, volume 123 of *Progress in Brain Research.* Elsevier, Amsterdam, The Netherlands, 1999.

22. E. Bizzi, N. Hogan, F.A. Mussa-Ivaldi, and S.F. Giszter. Does the nervous system use equilibrium-point control to guide single and multiple joint movements? *Behav. Brain Sci.*, 15:603–613, 1992.

23. E. Bizzi and F.A. Mussa-Ivaldi. Toward a neurobiology of coordinate transformations. In Gazzaniga[77], pages 495–506.

24. E. Bizzi, F.A. Mussa-Ivaldi, and S. Giszter. Computations underlying the execution of movement: A biological perspective. *Science*, 253:287–291, 1991.

25. E. Bizzi, A. Polit, and P. Morasso. Mechanisms underlying achievement of final head position. *J. Neurophysiol.*, 39:435–444, 1976.

26. T.V.P. Bliss and G.L. Collingridge. A synaptic model of memory: long-term potentiation in the hippocampus. *Nature*, 361:31–39, 1993.

27. T.V.P. Bliss and T. Lomø. Long-lasting potentiation of synaptic transmission in the dentate of the anesthetized rabbit following stimulation of the perforant path. *J.Physiol.*, 232:331–356, 1973.

28. V. Braitenberg and A. Schüz. *Anatomy of the Cortex: Statistics and Geometry.* Springer-Verlag, 1991.

29. I.E. Brown and G.E. Loeb. Measured and modeled properties of mammalian skeletal muscle. i. the effects of post-activation potentiation on the time course and velocity dependencies of force production. *Journal of Muscle Research and Cell Motility*, 20:443–456, 1999.

30. A. Browne, editor. *Neural network perspectives on cognition and adaptive robotics*. IOP Publishing, 1997.

31. R.E. Burke. Spinal cord: Ventral horn. In Shepherd[244], chapter 3, pages 77–120.

32. R.E. Burke. Revisiting the notion of 'motor unit types'. In Binder[21], chapter 15, pages 167–175.

33. R.E. Burke, P. Rudomin, and F.E. Zajac. The effect of activation history on tension production by individual muscle units. *Brain Research*, 109: 515–529, 1976.

34. R.E. Burke, P.L. Strick, K. Kanda, C.C. Kim, and B. Walmsley. Anatomy of medial gastrocnemius and soleus motor nuclei in cat spinal cord. *Journal of neurophysiology*, 40(3):667–680, 1977.

35. C. Bustamante, J.F. Marko, E.D. Siggia, and S. Smith. Entropic elasticity of lambda-phage DNA. *Science*, 265(5178):1599–1600, 1994.

36. R.H.S. Carpenter. *Neurophysiology*. Edward Arnold, London, 1996.

37. F. Cervantes-Pérez. Visuomotor Coordination in Frogs and Toads. In Arbib[11], pages 1036–1042.

38. P. Cesari, T. Shiratori, P. Olivato, and M. Duarte. Analysis of kinematically redundant reaching movements using the equilibrium-point hypothesis. *Biol. Cybern.*, 84:217–226, 2001.

39. P.D. Cheney and E.E. Fetz. Functional classes of primate corticomotoneuronal cells and their relation to active force. *Journal of Neurophysiology*, 44(4):773–791, 1980.

40. P.D. Cheney, E.E. Fetz, and K. Mewes. Neural mechanisms underlying corticospinal and rubrospinal control of limb movements. In G. Holstege, editor, *Progress in brain research*, volume 87, chapter 11, pages 213–252. Elsevier, 1991.

41. B.R. Christie, J.C. Magee, and D. Johnston. Dendritic calcium channels and hippocampal long-term depression. *Hippocampus*, 6:17–23, 1996.

42. G.L. Collingridge and T.V.P. Bliss. NMDA-receptors – their role in long-term potentiation. *TINS*, 10:288–293, 1987.

43. B.W. Connors and M.J. Gutnick. Intrinsic firing patterns of diverse neocortical neurons. *TINS*, 13(3):99–104, 1990.

44. J. Cooley, F. Dodge, and H. Cohen. Digital computer solutions for excitable membrane models. *J. Cell. Comp. Physiol.*, 66/supp. 2:99–101, 1965.

45. R.M.J. Cotterill. On the unity of conscious experience. *Journal of Consciousness Studies*, 2(4):290–312, 1995.

46. R.M.J. Cotterill. Prediction and internal feedback in conscious perception. *Journal of Consciousness Studies*, 3(2):245–266, 1996.

47. R.M.J. Cotterill. *Enchanted Looms: Conscious Networks in Brains and Computers*. Cambridge University Press, Cambridge, UK, 1998.

48. R.S. Creed, D. Denny-Brown, J.C. Eccles, E.G.T. Lidell, and C.S. Sherrington. *Reflex activity of the spinal cord*. Oxford University Press, Oxford, 1932.

49. F. Crepel, N. Hemart, D. Jaillard, and H. Daniel. Long-term depression in the cerebellum. In Arbib[11], pages 560–563.

50. R. Descartes. *L'Homme*. Charles Angot, Paris, 1664.

51. A. Despopoulus and S. Silbernagl. *Color atlas of physiology*. Thieme, 4th edition, 1991.

52. A. Destexhe, Z.F. Mainen, and T.J. Sejnowski. Kinetic models of synaptic transmission. In Koch and Segev[140], chapter 1, pages 1–25.

53. J.C. Eccles. *The physiology of synapses*. Springer, Berlin, 1964.

54. J. Eilers, G.J. Augustine, and A. Konnerth. Subthreshold synaptic Ca^{2+} signalling in fine dendrites and spines of cerebellar Purkinje neurons. *Nature*, 373(6510):155–158, 1995.

55. J. Eilers and A. Konnerth. Dendritic signal integration. *Current Opinion in Neurobiology*, 7:385–390, 1997.

56. E. Eldred, R. Granit, and P.A. Merton. Supraspinal control of the muscle spindles and its significance. *J. Physiol.*, 122:498–523, 1953.

57. M. Epstein and W. Herzog. *Theoretical Models of Skeletal Muscle: Biological and Mathematical Considerations*. John Wiley & Sons, West Sussex, UK, 1998.

58. B. Ermentrout. Neural networks as spatio-temporal pattern-forming systems. *Rep.Prog.Phys.*, 61:353–430, 1998.

59. P. Fatt and B. Katz. An analysis of the end-plate potential recorded with an intra-cellular electrode. *J. Physiol. (Lond.)*, 115:320–370, 1951.

60. P. Fatt and B. Katz. Spontaneous subthreshold activity at motor nerve endings. *J. Physiol. (Lond.)*, 117:107–128, 1952.

61. A.G. Feldman. Change of muscle length due to shift of the equilibrium point of the muscle-load system. *Biofizika*, 19:534–538, 1974.

62. A.G. Feldman. Once more on the equilibrium-point hypothesis (λ-model) for motor control. *J. Mot. Behav.*, 18:17–54, 1986.

63. A.G. Feldman, S.V. Adamovitch, D.J. Ostry, and J.R. Flanagan. The origin of electromyograms - explanations based on the equilibrium point hypothesis. In J.M. Winters and S.L. Woo, editors, *Multiple muscle systems. Biomechanics and movement organization*, pages 195–213. Springer-Verlag, 1990.

64. A.G. Feldman and G.N. Orlovsky. The influence of different descending systems on the tonic stretch reflex in the cat. *Exp. Neurol.*, 37:481–494, 1972.

65. E.E. Fetz and P.D. Cheney. Postspike facilitation of forelimb muscle activity by primate corticomotoneuronal cells. *J. Neurophysiol.*, 44:751–772, 1980.

66. E.E. Fetz and P.D. Cheney. Functional relations between primate motor cortex cells and muscles: fixed and flexible. In *Motor areas of the cerebral cortex*, volume 132 of *Ciba Foundation Symposium*, pages 98–117. Wiley, 1987.

67. E.E. Fetz, P.D. Cheney, K. Mewes, and S. Palmer. Control of forelimb muscle activity by populations of corticomotoneuronal and rubromotoneuronal cells. In J.H.J. Allum and M. Hulliger, editors, *Progress in Brain Research*, volume 80, chapter 36, pages 437–449. Elsevier Science, 1989.

68. P.M. Fitts. The information capacity of the human motor system in controlling the amplitude of movements. *J. Exp. Psychol.*, 47:381–391, 1954.

69. R. FitzHugh. Impulses and physiological states in models of nerve membrane. *Biophys. J.*, 1:445–466, 1961.

70. T. Flash and N. Hogan. The coordination of the arm movements: An experimentally confirmed mathematical model. *J. Neurosci.*, 7:1688–1703, 1985.

71. T. Flash and N. Hogan. Optimization principles in motor control. In Arbib[11], pages 682–685.

72. E. Fransén and A. Lansner. Low spiking rates in a population of mutually exciting pyramidal cells. *Network*, 6:271–288, 1995.

73. E. Fransén and A. Lansner. A model of cortical associative memory based on a horizontal network of connected columns. *Network*, 9(2):235–264, 1998.

74. J. Fridén and R.L. Lieber. Muscle architecture basis for neuromuscular control of the forearm and hand. In Wing et al.[278], chapter 4, pages 69–79.

75. A.A. Frolov, M. Dufossé, S. Řízek, and A. Kaladjian. On the possibility of linear modelling the human arm neuromuscular apparatus. *Biol. Cybern.*, 82:499–515, 2000.

76. J.M. Fuster. *Memory in the Cerebral Cortex*. MIT press, Cambridge,MA, 1995.

77. M.S. Gazzaniga, editor. *The Cognitive Neurosciences*. MIT Press, Cambridge, MA, 1st edition, 1997.

78. M.A. Geeves. The dynamics of actin and myosin association and the crossbridge model of muscle contraction. *Biochem. J.*, 274:1–14, 1991.

79. A.P. Georgopoulus, J.F. Kalaska, R. Caminiti, and J.T. Massey. On the relations between the direction of two-dimensional arm movements and cell discharge in primate motor control. *J. Neurosci.*, 2:1527–1537, 1982.

80. A.P. Georgopoulus, J.T. Lurito, M. Petrides, A.B. Schwartz, and J.T. Massey. Mental rotation of the neuronal population vector. *Science*, 243: 234–236, 1989.

81. A.P. Georgopoulus, A.B. Schwartz, and R.E. Kettner. Neuronal population coding of movement direction. *Science*, 233:1416–1419, 1986.

82. C. Ghez. Muscles: Effectors of the motor systems. In Kandel et al.[131], chapter 36, pages 548–563.

83. C. Ghez. Voluntary movement. In Kandel et al.[131], chapter 40, pages 609–625.

84. C. Ghez, J. Gordon, M.F. Ghilardi, and R. Sainburg. Contributions of vision and proprioception to accuracy in limb movements. In Gazzaniga[77], chapter 35, pages 549–564.

85. S.F. Giszter, F.A. Mussa-Ivaldi, and E. Bizzi. Convergent force fields organized in the frog spinal cord. *J. Neurosci.*, 13:467–491, 1993.

86. R. Glasius, A. Komoda, and S.C.A.M. Gielen. Neural network dynamics for path planning and obstacle avoidance. *Neural Networks*, 8(1):125–133, 1995.

87. R. Glasius, A. Komoda, and S.C.A.M Gielen. A biologically inspired neural net for trajectory formation and obstacle avoidance. *Biol. Cybern.*, 84:511–520, 1996.

88. M.S. Goldman, S.B. Nelson, and L.F. Abbott. Decorrelation of spike trains by synaptic depression. *Neurocomputing*, 26-27:147–153, 1999.

89. H. Gomi and M. Kawato. Human arm stiffness and equilibrium-point trajectory during multi-joint movement. *Biol. Cybern.*, 76:163–171, 1997.

90. A.M. Gordon, A.F. Huxley, and F.J. Julian. Tension development in highly stretched vertebrate muscle fibres. *J. Physiol.*, 184:143–169, 1966.

91. A.M. Gordon, A.F. Huxley, and F.J. Julian. The variation in isometric tension with sarcomere length in vertebrate muscle fibres. *J. Physiol.*, 184: 170–192, 1966.

92. J. Gordon. Spinal mechanisms of motor coordination. In Kandel et al.[131], chapter 38, pages 581–595.

93. J. Gordon and C. Ghez. Muscle receptors and spinal reflexes: The stretch reflex. In Kandel et al.[131], chapter 37, pages 564–580.

94. K.M. Van De Graaf and R.W. Rhees. *Theory and problems of human anatomy and physiology.* Schaum's Outline Series. McGraw-Hill, 1987.

95. R. Granit. The functional role of the muscle spindles - facts and hypotheses. *Brain*, 98:531–556, 1975.

96. C.M. Gray and D.A. McCormick. Chattering cells: Superficial pyramidal neurons contributing to the generation of synchronous oscillations in the visual cortex. *Science*, 274:109–113, 1996.

97. P.H. Greene. Why is it easy to control your arms? *Journal of motor behavior*, 14(4):260–286, 1982.

98. S. Grossberg. Adaptive pattern classification and universal recoding: I. parallel development and coding of neural feature detectors. *Biological Cybernetics*, 23:121–135, 1976.

99. S. Grossberg. Birth of a learning law. *Neural Networks*, 11(1), 1998. Newsletter.

100. J.M. Guccione, I. Motabarzadeh, and G.I. Zahalak. A distribution-moment model of deactivation in cardiac muscle. *Journal of Biomechanics*, 31: 1069–1073, 1998.

101. R. Guttman, S. Lewis, and J. Rinzel. Control or repetitive firing in squid axon membrane as a model for a neuroneoscillator. *J. Physiol.*, 305:377–395, 1980.

102. A.W. Ham. *Histology.* Lippincott-Blackwell, sixth edition, 1969.

103. B. Hannaford. A nonlinear model of the phasic dynamics of muscle activation. *IEEE Transactions on Biomedical Engineering*, 37(11):1067–1075, 1990.

104. D.O. Hebb. *Organization of behavior: A neuropsychological theory.* Wiley, New York, 1949.

105. E. Henneman, G. Somjen, and D.O. Carpenter. Excitability and inhibitibility of motoneurones of different sizes. *J. Neurophysiol.*, 28:599–620, 1965.

106. J. Hertz, A. Krogh, and R.G. Palmer. *Introduction to the Theory of Neural Computation*, volume I of *Santa Fe Institute Lecture Notes.* Addison-Wesley, Redwood City, CA, 1991.

107. A.V. Hill. The heat of shortening and the dynamic constants of muscle. *Proc. Roy. Soc. B*, 126:136–195, 1938.

108. A.L. Hodgkin and A.F. Huxley. A quantitative description of membrane current and its application to conduction and excitation in nerve. *J. Physiol.*, 117:500–544, 1952.

109. A.L. Hodgkin and B. Katz. The effect of sodium ions on the electrical activity of the giant axon of the squid. *J. Physiol. (Lond.)*, 108:37–77, 1949.

110. N. Hogan. An organizing principle for a class of voluntary movements. *J. Neurosci.*, 4:2745–2754, 1984.

111. K.C. Holmes. Muscle proteins - their actions and interactions. *Current Opinion in Structural Biology*, 6:781–789, 1996.

112. K.C. Holmes. The swinging lever-arm hypothesis of muscle contraction. *Current Biology*, 7:R112–R118, 1997.

113. G. Holstege. Descending motor pathways and the spinal motor system: Limbic and non-limbic components. In G. Holstege, editor, *Progress in Brain Research*, volume 87, chapter 14, pages 307–421. Elsevier, 1991.

114. A. Houdusse and H.L. Sweeney. Myosin motors: missing structures and hidden springs. *Current Opinion in Structural Biology*, 11:182–194, 2001.

115. H. Hultborn, R. Katz, and R. Mackel. Distribution of recurrent inhibition within a motor nucleus. ii. amount of recurrent inhibition in motoneurons to fast and slow units. *Acta Physiol. Scand.*, 134:363–374, 1988.

116. H. Hultborn, J. Lipski, R. Mackel, and H. Wigström. Distribution of recurrent inhibition within a motor nucleus. i. contribution from slow and fast motor units to the excitation of renshaw cells. *Acta Physiol. Scand.*, 134:347–361, 1988.

117. H. Hultborn, S. Meunier, E. Pierrot-Deseilligny, and M. Shindo. Changes in presynaptic inhibition of Ia fibres at the onset of voluntary contraction in man. *J. Physiol.*, 389:757–772, 1987.

118. A.F. Huxley. Muscle structure and theories of contraction. *Prog. Biophys. biophys. Chem*, 7:255–318, 1957.

119. A.F. Huxley. A note suggesting that the cross-bridge attachment during muscle contraction may take place in two stages. *Proc. Roy. Soc. B*, 183: 83–86, 1973.

120. A.F. Huxley and R. Niedergerke. Structural changes in muscle during contraction. interference microscopy of living muscle fibres. *Nature*, 173: 971–973, 1954.

121. A.F. Huxley and R.M. Simmons. Proposed mechanism of force generation in striated muscle. *Nature*, 233:533–538, 1971.

122. H.E. Huxley and J. Hanson. Changes in the cross-striations of muscle during contraction and stretch and their structural interpretation. *Nature*, 173:973–976, 1954.

123. M. Irving, T. St Claire Allen, C. Sabido-David, J.S. Craik, B. Brandmeier, J. Kendrick-Jones, J.E.T. Corrie, D.R. Trentham, and Y.E. Goldman. Tilting of the light-chain region of myosin during step length changes and active force generation in skeletal muscle. *Nature*, 375:688–691, 1995.

124. M. Ito, M. Sakurai, and P. Tongroach. Climbing fibre induced depression of both mossy fibre responsiveness and glutamate sensitivity of cerebellar purkinje cells. *J. Physiol. (Lond.)*, 324:113–134, 1982.

125. C.E. Jahr and C.F. Stevens. A quantitative description of NMDA receptor-channel kinetic behavior. *J. Neurosci.*, 10:1830–1837, 1990.

126. C.E. Jahr and C.F. Stevens. Voltage dependence of NMDA-activated macroscopic conductances predicted by single-channel kinetics. *J. Neurosci.*, 10:3176–3182, 1990.

127. E. Jankowska and M.H. Gladden. A positive feedback circuit involving muscle spindle secondaries and gamma motoneurons in the cat. In Binder[21], chapter 13, pages 149–156.

128. D. Johnston and S.M. Wu. *Foundations of Cellular Neurophysiology*. MIT press, Cambridge, MA, 1995.

129. M.I. Jordan and D.E. Rumelhart. Forward models: Supervised learning with a distal teacher. *Cognit. Sci.*, 16:307–354, 1992.

130. E.R. Kandel and J.H. Schwartz. Directly gated transmission at central synapses. In Kandel et al.[131], chapter 11, pages 153–172.

131. E.R. Kandel, J.H. Schwartz, and T.M. Jessell, editors. *Principles of Neural Science*. Appleton and Lange, Norwalk, Connecticut, 3rd edition, 1991.

132. E.R. Kandel and S.A. Siegelbaum. Directly gated transmission at the nerve-muscle synapse. In Kandel et al.[131], chapter 10, pages 135–152.

133. E.R. Kandel, S.A. Siegelbaum, and J.H. Schwartz. Synaptic transmission. In Kandel et al.[131], chapter 9, pages 123–134.

134. B. Katz. The relation between force and speed in muscular contraction. *J. Physiol.*, 96:45–64, 1939.

135. M. Kawato. Trajectory formation in arm movements: minimization principles and procedures. In H.N. Zelaznik, editor, *Advances in motor learning and control*, pages 225–259. Human Kinetics, Champaign, Illinois, 1996.

136. M. Kawato and D. Wolpert. Internal models for motor control. In G.R. Bock and J.A. Goode, editors, *Sensory Guidance of Movement*, Novartis Foundation Symposium 218, pages 291–304. John Wiley & Sons, Chichester, England, 1st. edition, 1998.

137. M.S.Z. Kellermayer, S.B. Smith, C. Bustamante, and H.L. Granzier. Complete unfolding of the titin molecule under external force. *Journal of Structural Biology*, 122:197–205, 1998.

138. M.S.Z. Kellermayer, S.B. Smith, H.L. Granzier, and C. Bustamante. Folding-unfolding transitions in sigle titin molecules characterized with laser tweezers. *Science*, 276:1112–1116, 1997.

139. K. Kitamura, M. Tokunaga, A.H. Iwane, and T. Yanagida. A single myosin head moves along an actin filament with regular steps of 5.3 nanometres. *Nature*, 397:129–134, 1999.

140. C. Koch and I. Segev, editors. *Methods in Neuronal Modeling: From Ions to Networks*. Computational Neuroscience Series. MIT Press, Cambridge, MA, 1998.

141. J. Koester. Membrane potential. In Kandel et al.[131], pages 81–94.

142. P.C. Krause, J.S. Choi, and T.A. McMahon. The force-velocity curve in passive whole muscle is asymmetric about zero velocity. *J. Biomechanics*, 28(9):1035–1043, 1995.

143. I. Kupfermann. Genetic determinants of behavior. In Kandel et al.[131], pages 987–996.

144. J.D. Lambert. *Numerical methods for ordinary differential systems: The initial value problem*. Wiley, 1993.

145. N. Lan. Analysis of an optimal control model of multi-joint arm movements. *Biol. Cybern.*, 76:107–117, 1997.

146. M.L. Latash. *Control of Human Movement*. Human Kinetics Publishers, Champaign, IL, 1993.

147. D.G. Lawrence and H.G.J.M. Kuypers. The functional organization of the motor system in the monkey. i. the effects of bilateral pyramidal tract lesions. *Brain*, 91:1–14, 1968.

148. D.G. Lawrence and H.G.J.M. Kuypers. The functional organization of the motor system in the monkey. ii. the effects of lesions of the descending brain-stem pathways. *Brain*, 91:15–36, 1968.

149. H. Lee and J.J. Kim. Amygdalar NMDA receptors are critical for new fear learning in previously fear-conditioned rats. *J Neurosci*, 18(20):8444–8454, 1998.

150. R. Lemon. The output map of the primate motor cortex. *TINS*, 11(11): 501–506, 1988.

151. W.B. Levy. A sequence predicting CA3 is a flexible associator that learns and uses context to solve hippocampal-like tasks. *Hippocampus*, 6(6):579–590, 1996.

152. W.B. Levy and O. Steward. Temporal contiguity requirements for long-term associative potentiation/depression in the hippocampus. *Neuroscience*, 8(4):791–797, 1983.

153. J. Liaw and T.W. Berger. Dynamic synapse: A new concept of neural representation and computation. *Hippocampus*, 6(591-600), 1996.

154. E.G.T. Liddell and C.S. Sherrington. Reflexes in response to stretch (myotactic reflexes). *Proc. Roy. Soc. London Ser. B*, 96:212–242, 1924.

155. E.G.T. Lidell and C.S. Sherrington. Recruitment and some other factors of reflex inhibition. *Proc. R. Soc. Lond. B Biol. Sci.*, 97:488–518, 1925.

156. R.L. Lieber and J. Fridén. Intraoperative sarcomere length measurements reveal musculoskeletal design principles. In Winters and Crago[281], chapter 3, pages 58–72.

157. D.J. Linden. The return of the spike: Postsynaptic action potentials and the induction of LTP and LTD. *Neuron*, 22:661–666, 1999.

158. R.R. Llinás. *I of the Vortex: From Neurons to Self*. MIT Press, Cambridge, MA, 2001.

159. D.P.C. Lloyd. Integrative pattern of excitation and inhibition in two-neuron reflex arcs. *J. Neurophysiol.*, 9:439–444, 1946.

160. G.E. Loeb and J.A. Hoffer. Activity of spindle afferents from cat anterior thigh muscles. ii. effects of fusimotor blockade. *Journal of neurophysiology*, 54(3):565–577, 1985.

161. G.E. Loeb, J.A. Hoffer, and W.B. Marks. Activity of spindle afferents from cat anterior thigh muscles. iii. effects of external stimuli. *Journal of neurophysiology*, 54(3):578–591, 1985.

162. G.E. Loeb, J.A. Hoffer, and C.A. Pratt. Activity of spindle afferents from cat anterior thigh muscles. i. identification and patterns during normal locomotion. *Journal of neurophysiology*, 54(3):549–564, 1985.

163. A. Lundberg and L. Vyklicky. Inhibitory interaction between spinal reflexes to primary afferents. *Experientia*, 19:247–248, 1963.

164. R.W. Lymn and E.W. Taylor. Mechanism of adenosine tri-phosphate hydrolysis of actomyosin. *Biochemistry*, 10:4617–4624, 1971.

165. G. Lynch. Memory and the brain: Unexpected chemistries and a new pharmacology. *Neurobiology of learning and memory*, 70:82–100, 1998.

166. W. Maass and E.D. Sontag. Neural systems as nonlinear filters. *Neural Computation*, 12:1743–1772, 2000.

167. S. Maren, G. Aharonov, D.L. Stote, and M.S. Fanselow. N-methyl-D-aspartate receptors in the basolateral amygdala are required for both acquisition and expression of conditional fear in rats. *Behav Neurosci*, 110 (6):1365–1374, 1996.

168. J.F. Marko and E.D. Siggia. Stretching DNA. *Macromolecules*, 28:8759–8770, 1995.

169. H. Markram, J. Lübke, M. Frotscher, and B. Sakmann. Regulation of synaptic efficacy by coincidence of postsynaptic APs and EPSPs. *Science*, 275:213–215, 1997.

170. H. Markram, D. Pikus, A. Gupta, and M. Tsodyks. Potential for multiple mechanisms, phenomena and algorithms for synaptic plasticity at single synapses. *Neuropharmacology*, 37:489–500, 1998.

171. P.E. Marszalek, H. Lu, H. Li, M. Carrion-Vazquez, A.F. Oberhauser, K. Schulten, and J.M. Fernandez. Mechanical unfolding intermediates in titin modules. *Nature*, 402:100–103, 1999. Authors present EMG data on reach to grab task.

172. P.B.C. Matthews. The dependence of tension upon extension in the stretch reflex of the soleus of the decerebrate cat. *J. Physiol.*, 47:521–549, 1959.

173. P.B.C. Matthews. Review lecture: evolving views on the internal operation and functional role of the muscle spindle. *J. Physiol. London*, 320:1–30, 1981.

174. J.L. McCulloch and W. Pitts. A logical calculus of ideas immanent in nervous activity. *Bulletin of Mathematical Biophysics*, 5:115–133, 1943.

175. B.J. McKiernan, J.K. Marcario, J.H. Karrer, and P.D. Cheney. Corticomotoneuronal postspike effects in shoulder, elbow, wrist, digit and intrinsic hand muscles during a reach and prehension task. *J. Neurophysiol.*, 80: 1961–1980, 1998.

176. T.A. McMahon. *Muscles, reflexes, and locomotion*. Princeton University Press, Princeton, New Jersey, 1st edition, 1984.

177. B.W. Mel. NMDA-based pattern discrimination in a modeled cortical neuron. *Neural Computation*, 4:502–517, 1992.

178. B.W. Mel. Information processing in dendritic trees. *Neural Computation*, 6:1031–1085, 1994.

179. L.M. Mendell and E. Henneman. Terminals of single Ia fibers: Location, density and distribution within a pool of 300 homonymous motoneurons. *J. Neurophysiol.*, 34:171–187, 1971.

180. P.A. Merton. Speculations on the servo-control of movements. In J.L. Malcolm, J.A.B. Gray, and G.E.W. Wolstenholm, editors, *The spinal cord*, pages 183–198. Little Brown, Boston, 1953.

181. Y. Metzger and D. Lehmann. Learning temporal sequences by local synaptic changes. *Network*, 1:169–188, 1990.

182. S. Meunier and E. Pierrot-Deseilligny. Cortical control of presynaptic inhibition of Ia afferents in humans. *Exp. Brain Res.*, 119:415–426, 1998.

183. R.C. Miall. Motor control, biological and theoretical. In Arbib[11], pages 597–600.

184. R.C. Miall and D.M. Wolpert. Forward models for physiological motor control. *Neural Networks*, 9(8):1265–1279, 1996.

185. H.S. Milner-Brown, R.B. Stein, and R. Yemm. Changes in firing rate of human motor units during linearly changing voluntary contractions. *J. Physiol.*, 230:371–390, 1973.

186. H.S. Milner-Brown, R.B. Stein, and R. Yemm. The orderly recruitment of human motor units during voluntary isometric contractions. *J. Physiol.*, 230:358–370, 1973.

187. M.J. Miserendino, C.B. Sananes, K.R. Melia, and M. Davis. Blocking of acquisition but not expression of conditioned fear-potentiated startle by NMDA antagonists in the amygdala. *Nature*, 345(6277):716–718, 1990.

188. J.E. Molloy, J.E. Burns, J. Kendrick-Jones, R.T. Tragear, and D.C.S. White. Movement and force produced by a single myosin head. *Nature*, 378:209–212, 1995.

189. A.W. Monster and H. Chan. Isometric force production by motor units of extensor digitorum communis muscle in man. *Journal of Neurophysiology*, 40(6):1432–1443, November 1977.

190. P. Morasso. Spatial control of arm movements. *Exp. Brain Res.*, 42:223–227, 1981.

191. P. Morasso. Three dimensional arm trajectories. *Biol Cybern*, 48:187–194, 1983.

192. P. Morasso and V. Sanguineti, editors. *Self-organization, computational maps, and motor control*, volume 119 of *Advances in psychology*. Elsevier, 1997.

193. J. Morel and N. D'Hahan. The myosin motor: muscle contraction and in vitro movement. *Biochimica et Biophysica Acta*, 1474:128–132, 2000.

194. C. Morris and H. Lecar. Voltage oscillations in the barnacle giant muscle fiber. *Biophys. J.*, 35:193–213, 1981.

195. R.G. Morris, E. Anderson, G.S. Lynch, and M. Baudry. Selective impairment of learning and blockade of long-term potentiation by an N-methyl-D-aspartate receptor antagonist, AP5. *Nature*, 319(6056):774–776, 1986.

196. V.B. Mountcastle. The columnar organization of the neocortex. *Brain*, 120:701–722, 1997. A thorough review.

197. P.R. Murphy, R.B. Stein, and J. Taylor. Phasic and tonic modulation of impulse rates in γ-motoneurons during locomotion in premammillary cats. *Journal of neurophysiology*, 52(2):228–243, 1984.

198. W.M. Murray, T.S. buchanan, and S.L. Delp. The isometric functional capacity of muscles that cross the elbow. *Journal of Biomechanics*, 33: 943–952, 2000.

199. F.A. Mussa-Ivaldi. How much coordination can be obtained without representing time? In Winters and Crago[281], chapter 24, pages 325–333.

200. J.S. Nagumo, S. Arimoto, and S. Yoshizawa. An active pulse transmission line simulating a nerve axon. *Proc. IRE*, 50:2061–2070, 1962.

201. K.S. Narendra. Adaptive control: Neural network applications. In Arbib[11], pages 69–73.

202. J.G. Nicholls, A.R. Martin, and B.G. Wallace. *From neuron to brain*. Sinauer, Sunderland, 3rd. edition, 1992.

203. B.G. Nielsen. Separability of spatiotemporal memory sequences through dynamic allocation of memory traces at distinct dendritic sites. *Consciousness Research Abstracts*, page p. 43, 1997. Abstracts from The Brain and Self Workshop: Toward a Science of Consciousness, August 21-24, Elsinore, Denmark.

204. B.G. Nielsen. Memory trace separation in dendrites. *Consciousness and Cognition*, 9(2):S99, June 2000.

205. J. Nielsen and Y. Kagamihara. The regulation of presynaptic inhibition during co-contraction of antagonistic muscles in man. *J. Physiol. (Lond.)*, 464:575–593, 1993.

206. E. Nijhof and E. Kouwenhoven. Simulation of multijoint arm movements. In Winters and Crago[281], chapter 28, pages 363–372.

207. A.F. Oberhauser, P.E. Marszalek, H.P. Erickson, and J.M. Fernandez. The molecular elasticity of the extracellular matrix protein tenascin. *Nature*, 393:181–185, 1998.

208. G.N. Orlovsky, T.G. Deliagina, and S. Grillner. *Neuronal control of locomotion: From mollusc to man*. Oxford University Press, 1999.

209. G. Örnung, O. Shupliakov, O.P. Ottersen, J. Storm-Mathisen, and S. Cullheim. Immunohistochemical evidence for coexistence of glycine and GABA in nerve terminals on cat spinal motoneurons: An ultrastructural study. *NeuroReport*, 5:889–892, 1994.

210. N. Otmakhov, A.M. Shirke, and R. Malinow. Measuring the impact of probabilistic transmission on neuronal output. *Neuron*, 10:1101–1111, 1993.

211. W. Penfield and T. Rasmussen. *The cerebral cortex of man: a clinical study of localization of function*. Macmillan, New York, 1950.

212. T.D. Pollard. Reflections on a quarter century of research on contractile systems. *TIBS*, 25:607–611, 2000.

213. W.H. Press, B.P. Flannery, S.A. Teukolsky, and W.T. Vetterling. *Numerical recipes in pascal: The art of scientific computing*. Cambridge University Press, 1996.

214. A. Prochazka and M. Hulliger. The continuing debate about CNS control of proprioception. *Journal of Physiology*, 513(2):315, 1998.

215. A. Prochazka, M. Hulliger, P. Trend, and N. Dürmüller. Dynamic and static fusimotor set in various behavioural contexts. In P. Hník, T. Soukup, R. Vejsada, and J. Zelena, editors, *Mechanoreceptors: Development, structure and function*, pages 417–430. Plenum, New York, 1988.

216. U. Proske and D.L. Morgan. Do cross-bridges contribute to the tension during stretch of passive muscle? *Journal of Muscle Research and Cell Motility*, 20:433–442, 1999.

217. D. Purves, G.J. Augustine, D. Fitzpatrick, L.C. Katz, A.S. LaMantia, and J.O. McNamara, editors. *Neuroscience*. Sinauer Associates, Sunderland:MA, 1997.

218. S. Ramón y Cajal. *New ideas on the structure of the nervous system in man and vertebrates*. MIT Press, Cambridge, MA, 1990. translation.

219. I. Rayment, H.M. Holden, M. Whittaker, C.B. Yohn, M. Lorenz, K.C. Holmes, and R.A. Milligan. Structure of the actin-myosin complex and its implications for muscle contraction. *Science*, 261:58–65, 1993.

220. I. Rayment, W.R. Rypniewski, K. Schmidt-Bäse, R. Smith, D.R. Tomchick, M.M. Benning, D.A. Winkelmann, G.Wesenberg, and H.M. Holden. Three-dimensional structure of myosin subfragment-1: A molecular motor. *Science*, 261:50–58, 1993.

221. L.A. Raymond, C.D. Blackstone, and R.L. Huganir. Phosphorylation of amino acid neurotransmitter receptors in synaptic plasticity. *TINS*, 16(4): 147–153, 1993.

222. B. Rexed. The cytoarchitectonic organization of the spinal cord in the cat. *J. Comp. Neurol.*, 96:415–496, 1952.

223. J. Rinzel. On repetitive activity in nerve. *Fed. Proc.*, 37:2793–2802, 1978.

224. J. Rinzel. Excitation dynamics: insights from simplified membrane models. *Fed. Proc.*, 44:2944–2946, 1985.

225. J. Rinzel and B. Ermentrout. Analysis of neural excitability and oscillations. In Koch and Segev[140].

226. S.P.R. Rose. How chicks make memories: the cellular cascade from c-fos to dendritic remodelling. *TINS*, 14(9):390–397, 1991.

227. J.C. Rothwell, M.M. Traub, B.L. Day, J.A. Obeso, P.K. Thomas, and C.D. Marsden. Manual motor performance in a deafferented man. *Brain*, 105: 515–542, 1982.

228. P. Rudomin, I. Jimenez, M. Solodkin, and S. Duenas. Sites of action of segmental and descending control of transmission on pathways mediating PAD of ia and ib afferent fibers in cat spinal cord. *J. Physiol.*, 50:743–769, 1983.

229. P. Rudomin and R.F. Schmidt. Presynaptic inhibition in the vertebrate spinal cord revisited. *Exp. Brain Res.*, 129:1–37, 1999.

230. D.E. Rumelhart and J.L. McClelland, editors. *Parallel Distributed Processing: Explorations in the microstructure of cognition.* MIT Press, Cambridge, MA, 1986.

231. R.W. Ryall, M.F. Piercey, and C. Polosa. Intersegmental and intrasegmental distribution of mutual inhibition of renshaw cells. *J. Neurophysiol.*, 34: 700–707, 1971.

232. J.N. Sanes and J.P. Donoghue. Plasticity and primary motor cortex. *Annu. Rev. Neurosci.*, 23:393–415, 2000.

233. T.D. Sanger. Theoretical considerations for the analysis of population coding in motor cortex. *Neural Computation*, 6(1):29–37, 1994.

234. V. Sanguineti, P. Morasso, and F. Frisone. Cortical maps of sensorimotor spaces. In Morasso and Sanguineti[192], pages 1–36.

235. M.H. Schieber. How might the motor cortex individuate movements? *TINS*, 13(11):440–445, 1990.

236. M.H. Schieber. New views of the primary motor cortex. *The Neuroscientist*, 6(5):380–389, 2000.

237. J. Schiller, G. Major, H.J. Koester, and Y. Schiller. NMDA spikes in basal dendrites of cortical pyramidal neurons. *Nature*, 404:285–289, March 2000.

238. A.C. Schouten, E. de Vlugt, F.C.T. van der Helm, and G.G. Brouwn. Optimal posture control of a musculo-skeletal arm model. *Biol. Cybern.*, 84:143–152, 2001.

239. S.H. Scott, I.E. Brown, and G.E. Loeb. Mechanics of feline soleus: I. effect of fascicle length and velocity on force output. *Journal of Muscle Research and Cell Motility*, 17:207–219, 1996.

240. T.W. Scutt and R.I. Damper. Designing a nervous system for an adaptive mobile robot. In Browne[30], chapter 11, pages 220–250.

241. I. Segev. Dendritic Processing. In Arbib[11], pages 282–289.

242. I. Segev, R.E. Burke, and M. Hines. Compartmental models of complex neurons. In Koch and Segev[140], pages 93–136.

243. R. Shadmehr. Equilibrium point hypothesis. In Arbib[11], pages 370–372.

244. G.M. Shepherd, editor. *The Synaptic Organization of the Brain.* Oxford University Press, 4th. edition, 1998.

245. G.M. Shepherd and S.D. Erulkar. Centenary of the synapse: from sherrington to the molecular biology of the synapse and beyond. *TINS*, 20(9): 385–392, 1997.

246. C.S. Sherrington. The central nervous system. In M. Foster, editor, *Textbook of physiology*, page 60. Macmillan, 1897.

247. D.A. Smith and S.E. Radford. Pulling back the frontiers. *Current Biology*, 10:R662–R664, 2000.

248. S.B. Smith, L. Finzi, and C. Bustamante. Direct mechanical measurements of the elasticity of single DNA molecules by using magnetic beads. *Science*, 258(5085):1122–1126, 1992.

249. V.S. Sohal and M.E. Hasselmo. $GABA_B$ modulation improves sequence disambiguation in computational models of hippocampal region CA3. *Hippocampus*, 8(2):171–193, 1998.

250. E.P. Solomon, L.R. Berg, D.W. Martin, and C. Villee. *Biology.* Saunders College Publishing, 3rd. edition, 1993.

251. H. Sompolinsky and I. Kanter. Temporal association in asymmetric neural networks. *Physical Review Letters*, 57:2861–2864, 1986.

252. S. Spieker, A. Boose, S. Breit, and J. Dichgans. Long-term measurement of tremor. *Mov. Disord.*, 13(Suppl. 3):81–84, 1998.

253. U. Staubli and G. Lynch. Stable hippocampal long-term potentiation elicited by 'theta' pattern stimulation. *Brain Research*, 435:227–234, 1987.

254. C.F. Stevens. Cooperativity of unreliable neurons. *Current Biology*, 4(3): 268–269, 1994.

255. K. Stratford, A. Mason, A. Larkman, G. Major, and J. Jack. The modeling of pyramidal neurons in visual cortex. In R. Durbin, C. Miall, and G. Mitchison, editors, *The Computing Neuron*, pages 296–321. Addison-Wesley, Workingham, England, 1990.

256. G. Stuart, N. Spruston, B. Sakmann, and M. Häusser. Action potential initiation and backpropagation in neurons of the mammalian CNS. *TINS*, 20:125–131, 1997.

257. G.J. Stuart and B Sakmann. Active propagation of somatic action potentials into neocortical pyramidal cell dendrites. *Nature*, 367:69–72, January 1994.

258. H. Tanila. Hippocampal place cells can develop distinct representations of two visually identical environments. *Hippocampus*, 9(3):235–246, 1999.

259. A. Taylor, P.H. Ellaway, and R. Durbaba. Why are there three types of intrafusal muscle fibers? In M.D. Binder, editor, *Peripheral and Spinal Mechanisms in the Neural Control of Movement*, volume 123 of *Progress in Brain Research*, pages 121–131. Elsevier, Amsterdam, The Netherlands, 1999.

260. E. Thiels, X. Xie, M.F. Yeckel, G. Barrionuevo, and T.W. Berger. NMDA receptor-dependent LTD in different subfields of hippocampus in vivo and in vitro. *Hippocampus*, 6:43–51, 1996.

261. P.A. Tipler. *Physics for Scientists and Engineers*. Worth Publishers, New York, NY, 3rd edition, 1991.

262. M. Tsodyks, K. Pawelzik, and H. Markram. Neural networks with dynamic synapses. *Neural Computation*, 10:821–835, 1998.

263. M.V. Tsodyks and H. Markram. The neural code between neocortical pyramidal neurons depends on neurotransmitter release probability. *Proc. Natl. Acad. Sci.*, 94:719–723, 1997.

264. Y. Uno, M. Kawato, and R. Suzuki. Formation and control of optimal trajectory in human multijoint arm movement: Minimum torque-change model. *Biol. Cybern.*, 61:89–101, 1989.

265. A.B. Vallbo. Basic patterns of muscle spindle discharge in man. In A. Taylor and A. Prochazka, editors, *Muscle receptors and movement*, pages 263–275. Macmillan, London, 1981.

266. F.C.T. van der Helm and A.J.K. van Soest. Planning of human motions: How simple must it be? In Winters and Crago[281], chapter 29, pages 373–381.

267. J.A. Varela, K. Sen, J. Gibson, J. Fost, L.F. Abbott, and S.B. Nelson. A quantitative description of short-term plasticity at excitatory synapses in layer 2/3 of rat primary visual cortex. *J. Neurosci.*, 17(20):7926–7940, 1997.

268. C. Veigel, L.M. Coluccio, J.D. Jontes, J.C. Sparrow, R.A. Milligan, and J.E. Molloy. The motor protein myosin-i produces its working stroke in two steps. *Nature*, 398:530–533, 1999.

269. S.M. Walker and G.R. Schrodt. I segment lengths and thin filament periods in skeletal muscle fibers of the rhesus monkey and humans. *Anat. Rec.*, 178:63–82, 1973.

270. B. Walmsley, J.A. Hodgson, and R.E Burke. Forces produced by medial gastrocnemius and soleus muscles during locomotion in freely moving cats. *Journal of Neurophysiology*, 41(5):1203–1216, 1978.

271. H. Wigström. A neuron model with learning capability and its relation to mechanisms of association. *Kybernetik*, 12(4):204–215, 1973.

272. A.L. Wilkes and N.J. Wade. Bain on neural networks. *Brain and Cognition*, 33:295–305, 1997.

273. C.J. Wilson. Basal ganglia. In G.M. Shepherd, editor, *The Synaptic Organization of the Brain*, chapter 9, pages 329–375. Oxford University Press, Oxford, UK, 4th edition, 1998.

274. H.R. Wilson. Simplified dynamics of human and mammalian neocortical neurons. *Journal of Theoretical Biology*, 200:375–388, 1999.

275. H.R. Wilson. *Spikes, Decisions and Actions, Dynamical Foundations of Neuroscience*. Oxford University Press, 1999.

276. U. Windhorst. On the role of recurrent inhibitory feedback in motor control. *Progress in Neurobiology*, 49:517–587, 1996.

277. U. Windhorst. The spinal cord and its brain: representations and models. to what extent do forebrain mechanisms appear at brainstem spinal cord levels? *Progress in Neurobiology*, 49:381–414, 1996.

278. A.M. Wing, P. Haggard, and J.R. Flanagan, editors. *Hand and brain: The neurophysiology and psychology of hand movements*. Academic Press, 1996.

279. D.A. Winter. *Biomechanics and motor control of human movement*. Wiley Interscience, 2nd edition, 1990.

280. J.M. Winters. Terminology and foundations of movement science. In Winters and Crago[281], chapter 1, pages 3–35.

281. J.M. Winters and P.E. Crago, editors. *Biomechanics and Neural Control of Posture and Movement*. Springer, 2000.

282. W.M. Yamada, C. Koch, and P.R. Adams. Multiple channels and calcium dynamics. In Koch and Segev[140], pages 137–170.

283. S.X. Yang and M. Meng. An efficient neural network approach to dynamic robot motion planning. *Neural Networks*, 13(2):143–148, 2000.

284. S.X. Yang and M. Meng. Real-time collision-free path planning of robot manipulators using neural network approaches. *Autonomous Robots*, 9: 27–39, 2000.

285. A. Zador, C. Koch, and T.H. Brown. Biophysical model of a hebbian synapse. *Proc. Natl. Acad. Sci. USA*, 87:6718–6721, 1990.

286. G.I. Zahalak. The two-state cross-bridge model of muscle is an asymptotic limit of multi-state models. *J. theor. Biol*, 204:67–82, 2000.

287. V.M. Zatsiorsky. *Kinematics of human motion*. Human Kinetics, 1998.

288. R.S. Zucker. Short-term synaptic plasticity. *Ann. Rev. Neurosci.*, 12:13–31, 1989.